Dynamics versus kinetics in complex liquids

Jukić, Ivo

University of Split
Faculty of Science
Doctoral Study of Biophysics

Sorbonne University
Doctoral School "Physique en Île-de-France"

Doctoral thesis

Dynamics versus kinetics in complex liquids

Ivo Jukić

Split, September 2023.

Sveučilište u Splitu, Prirodoslovno-matematički fakultet
Odjel za fiziku, Doktorski studij Biofizika

„Dinamika u sustavima s mikrosegregacijom“

Doktorski rad autora Ive Jukića, kao dio obaveza potrebnih da se dobije doktorat znanosti, izrađen je pod vodstvom mentora: dr. sc. Auréliena Perere i izv. prof. dr. sc. Bernarde Lovrinčević

Dobiveni akademski naziv i stupanj: doktor prirodnih znanosti iz polja fizike

Povjerenstvo za ocjenu i obranu doktorskog rada u sastavu:

1. prof. dr. sc. Jean-François Dufrêche, Institut za separativnu kemiju sveučilišta u Montpellieru, ocjenjivač
2. izv. prof. dr. sc. Jean-Marc Simon, Interdisciplinarni laboratorij Carnot sveučilišta u Burgundiji, ocjenjivač
3. prof. dr. sc. Helene Gerard, Laboratorij za teorijsku kemiju sveučilišta Sorbonne u Parizu, predsjednica povjerenstva
4. prof. dr. sc. Leandra Vranješ-Markić, Prirodoslovno-matematički fakultet u Splitu, ispitivačica
5. izv. prof. dr. sc. Bernarda Lovrinčević, Prirodoslovno-matematički fakultet u Splitu, mentorica
6. dr. sc. Aurelien Perera, Laboratorij za teorijsku fiziku kondenzirane materije sveučilišta Sorbonne u Parizu, mentor

Potvrđuje da je disertacije obranjena dana 8. rujna 2023.

Zamjenik voditelja studija: izv. prof. dr. sc. Damir Kovačić

_____

Dekan: prof. dr. sc. Mile Dželalija

_____

TEMELJNA DOKUMENTACIJSKA KARTICA

Sveučilište u Splitu
Prirodoslovno-matematički fakultet Doktorski rad

Dinamika u sustavima s mikrosegregacijom

Ivo Jukić

Rad je izrađen u: Prirodoslovno-matematičkom fakultetu Sveučilišta u Splitu i Laboratoriju za teorijsku fiziku kondenzirane materije (LPTMC) Sveučilišta Sorbonne u Parizu

Sažetak

Mikro - heterogene tekućine karakterizira specifična heterogena mikro - struktura, koja sadrži labilne supra - molekularne agregate. Tipični primjeri takvih tekućina su alkoholi, ionske tekućine i razne tekućine meke tvari. Osim uobičajene molekularne dinamike, zajedničke svim tekućinama, dinamiku ovih sustava karakterizira i kinetički aspekt, koji je povezan s dinamikom labilnih supra - molekularnih agregata, uz uobičajenu dinamiku individualnih atoma i molekula. Cilj ovog rada je otkriti specifičnosti u dinamici mikro - heterogenih tekućina, vezane upravo uz spomenuti kinetički aspekt. Dinamika se proučava analizom različitih dinamičkih veličina dobivenih simulacijama molekularne dinamike, kao što je van Hove korelacijska funkcija $G(r,t)$, funkcija raspršenja $F(k,t)$ i dinamički strukturni faktor $S(k,\omega)$. Pokazat će se da heterogena mikro-struktura ostavlja trag u ovim dinamičkim veličinama, što omogućuje direktno razlikovanje dinamike i kinetike u istim sustavima. Pokazat će se i da je, za razliku od dinamike, kinetika pod jakim utjecajem prisustva neutralnih atomskih grupa i veličinom istih grupa. Istraživanje se provodi za različite vrste tekućina, uključujući jednostavne tekućine, kao što je aceton, te složene tekućine, kao što su voda i mali monoli. Svrha rada je razviti teorijski i računalni okvir za istraživanje složenosti u tekućinama.

(151 stranica, 70 slika, 3 tablice, 191 literaturni navod, jezik izvornika: engleski)

Rad je pohranjen u:
- Nacionalnoj sveučilišnoj knjižnici u Zagrebu
- Sveučilišnoj knjižnici u Splitu
- knjižnici Prirodoslovno-matematičkog fakulteta, Sveučilišta u Splitu

Ključne riječi: dinamika, kinetika, kompleksne tekućine, mikrosegregacija, vodikova veza

Mentori: dr. sc. Aurelien Perera i izv. prof. dr. sc. Bernarda Lovrinčević

Ocjenjivači:

1. prof. dr. sc. Jean-François Dufrêche
2. izv. prof. dr. sc. Jean-Marc Simon
3. prof. dr. sc. Helene Gerard
4. prof. dr. sc. Leandra Vranješ-Markić

Rad prihvaćen dana 16.08.2023.

BASIC DOCUMENTATION CARD

University of Split
Faculty of Science

Ph.D. thesis

Dynamics versus kinetics in complex liquids

Ivo Jukić

Thesis performed at Faculty of Science, University of Split and Laboratory for Theoretical Physics of Condensed Matter, Sorbonne University in Paris

Abstract

Micro - heterogeneous liquids are characterized by particular heterogeneous micro - structure, which contains labile bonded supra - molecular aggregates. Typical examples of such liquids are alcohols, ionic liquids and various soft - matter liquids. In addition to the usual molecular dynamics, common to all liquids, the dynamics of these systems is characterized by kinetic aspect, which is related to the dynamics of labile supra - molecular aggregates, instead of individual atoms or molecules. The aim of the thesis is to reveal the specificities in the dynamics of micro - heterogeneous liquids, which are attributed precisely to this kinetic aspect. Particularly, dynamics will be studied by extraction of various dynamical quantities from computer simulations, such as the van Hove correlation function $G(r,t)$, the associated scattering function $F(k,t)$ and the dynamical structure factor $S(k,\omega)$. It will be shown that heterogeneous micro - structure leaves marked signature in these observables, which enables to directly distinguish between dynamics and kinetics in these systems. While dynamics is shown to be governed by the time evolution of charge order, which determines the arrangement of charged species in the system, kinetics is governed by the existence of neutral species and their size. Study is performed for several types of liquids, ranging from simple disordered liquids, such as carbon tetrachloride or acetone, and complex disordered liquids, such as water and small monols. The purpose of the thesis is to elaborate the theoretical and computational framework for exploring complexity in liquids.

(151 pages, 70 figures, 3 tables, 191 references, original in English)

Thesis deposited in:
- National and University Library in Zagreb
- University Library in Split
- Library of the Faculty of Science, University of Split

Keywords: dynamics, complex liquids, hydrogen bond, kinetics, micro-heterogeneity

Supervisors: Dr. Aurelien Perera and Assoc. Prof. Bernarda Lovrinčević

Reviewers:
1. Prof. Jean-François Dufrêche
2. Assoc. Prof. Jean-Marc Simon
3. Prof. Helene Gerard
4. Prof. Leandra Vranješ-Markić

Thesis accepted on 16.08.2023.

Acknowledgments

Most of the doctoral students will agree that doing Ph.D. and writing thesis is a unique and special journey. Luckily, I was not alone on this journey. There are many people who accompanied me on this adventure and supported me in many ways, both from professional and personal point of view. This section will be devoted to each of them.

First, I would like to thank both of my supervisors, Bernarda Lovrinčević and Aurélien Perera, for enormous help during this period of 4 years. This thesis would not be possible without them. Their knowledge, creativity and passion for science are really unique and I am extremely grateful that they shared them with me all along. I am extremely grateful also to Martina Požar, important member of our group, who has always been perceived as the third supervisor from my part. Her help and advices cannot be appreciated enough.

I would also like to express my gratitude to Laboratoire de Physique Théorique de la Matière Condensée (LPTMC) at Sorbonne Université, led by the current director Bertrand Delamotte, for receiving me as a member of this laboratory during my Ph.D. program.

Special thanks also go to both Doctoral School of Biophysics in Split and École doctorale "Physique en Île-de-France" in Paris. The assistance provided by Prof. Mile Dželalija and Dr. Irena Bitunjac in Split, together with the help from Prof. Maria Chamarro and Nadine Yassine in Paris, will always be appreciated.

I am also especially grateful to Prof. Jean-François Dufrêche, Assoc. Prof. Jean-Marc Simon, Prof. Hélène Gerard and Prof. Leandra Vranješ-Markić for taking part in jury for my thesis defense.

This journey would have been impossible without the enormous help and support of my entire family, specially my parents, Vesna and Damir, and my sister Lucija, who have always been there for me. I want to give thanks also to all my friends, specially Krešo, for huge support during whole this period. Finally, enormous thank you goes to my dearest Celia, whose motivational words and encouragements are out of this world.

This work has been supported in part by the Croatian Science Foundation under the project UIP-2017-05-1863 "Dynamics in micro-segregated systems".
Additional fundings were provided by the French Government Grant, for the period of 13 months spent at Sorbonne Université in Paris. I wish to thank both organizations for the financial support.

Contents

Introduction

1

1 Introduction

The main goal of this thesis is to study the dynamics of liquids and mixtures which exhibit micro-heterogeneities [144, 6, 178, 128, 134]. The main problem which will be adressed is how micro - heterogeneities evolve in time, and how this evolution is manifested through the van Hove function $G(r,t)$, the intermediate scattering function $F(k,t)$ and the dynamical structure factor $S(k,\omega)$. All mentioned functions describe the microscopic structure of the system from pair correlation point of view. Since the term "micro - heterogeneity" represents the key point of this research, we will discuss this point in more details, in order to further clarify the principal motivation behind this work.

1.1 Duality of fluctuations and micro - heterogeneity

Micro-heterogeneities in neat liquids can be seen as particular case of fluctuations in density, while, in mixtures, these fluctuations are related to the concentrations of each molecular component. Fluctuations in density are characteristic for any liquid. For example, they arise even in the hard sphere toy model, where the interaction is purely repulsive, and the origin of fluctuations is purely entropic. In simple Lennard – Jones liquid, where particles interact both repulsively (at small inter-particle separations) and attractively (at larger inter-particle separations), the origin of these fluctuations is both entropic and energetic, since particles mutually attract in this case. The complexity of fluctuations increases as the complexity of interparticle interactions in the system grows. In an ionic liquid, such as NaCl at sufficiently large temperatures ($\sim$ 3000 K), a special form of local order appears, which is called charge order [163, 77, 132, 137, 57, 55]. This order is particularly characteristic for molten salts [153, 163, 77] and is realized through the alternation of + and – charges, caused by the fact that $(+,+)$ and $(-,-)$ charges mutually repel, while $(+,-)$ charges attract each other. Although the alternation of charges in the liquid state is not as perfect as in a crystal, it is still visible, as in a simulation snapshot shown in Figure 1, where two simulation boxes of equal sizes are compared, consisting of red and blue soft spheres of equal diameters. In the left simulation box, both red and blue spheres are neutral, while, in the right simulation box, red spheres are positively charged (+1), while blue spheres are negatively charged (-1).

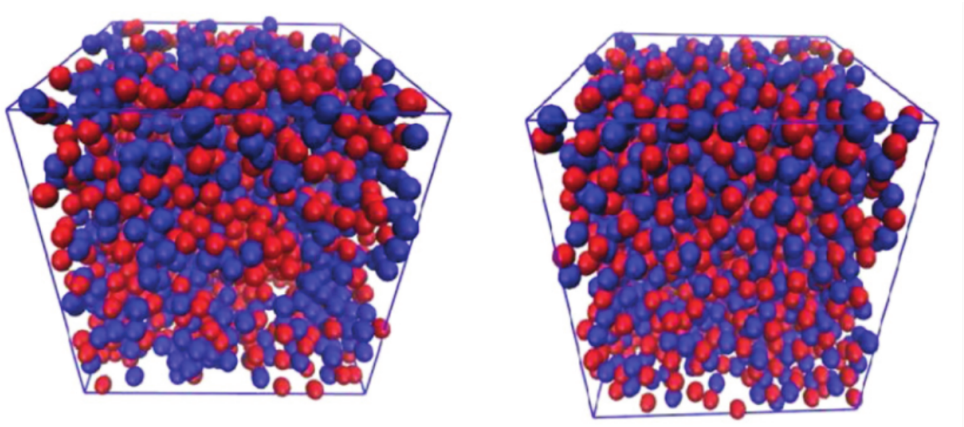

Figure 1: Simulation snapshots showing one microstate of simple Lennard - Jones binary mixture (left panel) and one microstate of charged soft sphere model (right panel). Both red and blue spheres have the same diameters. In the case presented in left panel, both red and blue spheres are neutral, while, in the case presented in right panel, red spheres are positively charged $(+1)$, while blue spheres are negatively charged (-1).

One can note that the right simulation box appears to be "more ordered" through the alternation of charges. This form of order affects significantly the pair correlation functions, as is shown in Figure 2, where $g_{AA}(r)$, $g_{AB}(r)$ and $g_{BB}(r)$ functions are shown (A - red spheres, B - blue spheres) in black, red and green colors respectively for the case of LJ binary mixture (left panel) and charged soft sphere model (right panel). Corresponding $S(k)$ functions are shown in the insets.

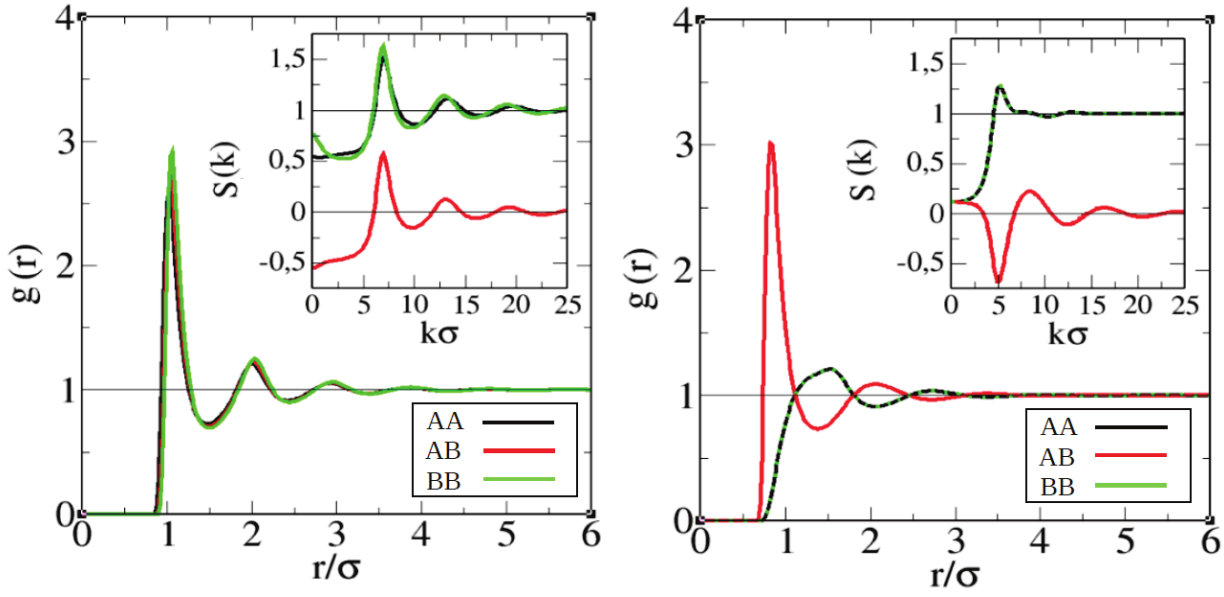

Figure 2: Radial distribution functions $g_{AA}(r)$, $g_{AB}(r)$ and $g_{BB}(r)$ of simple LJ binary mixture (left panel) and charged soft sphere model (right panel). Insets show corresponding structure factors $S(k)$. Particles A represent red spheres, while B represent blue spheres from Figure 1.

While, in the left panel of Figure 2, correlations *AA*, *AB* and *BB* are all in phase, in the right panel we see that *AB* correlations are out of phase with *AA* and *BB* correlations, due to alternation of charges. In addition, the structure factors in the right inset show the peak and anti-peak, which correspond to the dephasing of the spatial correlations.

Interactions in liquids with higher structural complexity, such as water, alcohols, amines or amides, are, within classical description, described as the combination of LJ interaction and Coulomb interaction between atoms in molecules. Coulomb interaction is governed by partial charges which each atom bear. Therefore, the total interaction between molecule A (formed of atoms $i = 1,...,N$) and molecule B (formed of atoms $j = 1,...,M$) is given with [56]:

$$V_{AB} = \sum_{i=1}^{N} \sum_{j=1}^{M} \left\{ 4\varepsilon_{ij} \left[\left(\frac{\sigma_{ij}}{r_{ij}} \right)^{12} - \left(\frac{\sigma_{ij}}{r_{ij}} \right)^{6} \right] - L \frac{Z_i Z_j}{r_{ij}} \right\} \tag{1}$$

where σ_{ij} is obtained with Lorentz rule, $\sigma_{ij} = \frac{\sigma_i + \sigma_j}{2}$, where σ_i and σ_j are diameters of atoms i and j respectively. ε_{ij} is obtained with Bertholet rule, $\varepsilon_{ij} = \sqrt{\varepsilon_i \varepsilon_j}$, with ε_i and ε_j representing the depth of the LJ potential wells of atomic species i and j respectively. Constant L is given with $L = \frac{e^2}{4\pi\varepsilon_0}$, while Z_i and Z_j represent the valences of atoms i and j.

Since the fundamental inter-molecular interactions, in all liquids mentioned above, can be described with equation 1, all these liquids will be governed by the same fluctuations mentioned earlier, regardless of their chemical specificity. To further discuss this problem, let us compare the simulation box of a simple LJ liquid with that of neat octanol, shown in the left and right panels of Figure 3 respectively. We note that the simulation box of octanol is characterized by clustering of hydroxil OH groups (O - red spheres, H - white spheres) in chain - like clusters by charge - order mechanism. Clustering of OH groups in one place results in the deficiency of OH groups in the close neighbourhood of formed aggregate. This creates a local heterogeneity in density of O atoms, with the density being high along the OH chain, and low around the chain. We refer to this type of heterogeneities as micro - heterogeneities [144, 6, 178, 128, 134].

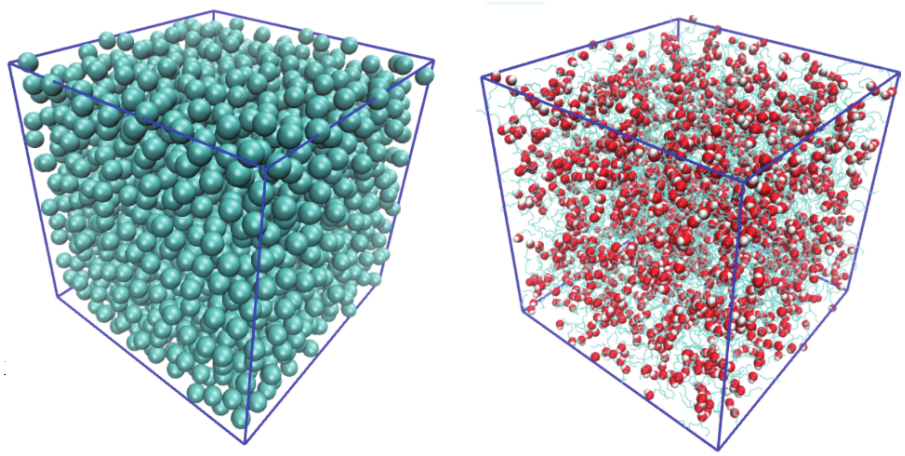

Figure 3: Snapshots of simulation boxes of simple LJ liquid (left panel) and octanol (right panel), each representing one microstate of the system. In the right panel, oxygen atoms are shown in red, hydrogen atoms in white and alkyl groups in cyan color.

We note that the formation of such heterogeneities is possible also in simple LJ liquid, where all charges are equal to 0. Similarly like in the case of OH groups in octanol, gathering of LJ particles in one place is likely to result in deficiency of the same particles in the close neighbourhood of the formed "cluster". However, the origin of the formed heterogeneities will not be the same for the two liquids, since, in octanol, their origin is mostly related to the attractive Coulomb potential between $(+,-)$ pairs, which is significantly stronger than attractive part of LJ potential. Hence, density fluctuations in octanol are closer to the self-assembly mechanism [182, 33, 51, 170], which forms "molecular objects", which can perform "tasks". For example, micelles and vesicles are such objects. Through this example, we see that fluctuations have a dual aspect, one corresponding to a random gathering of particles (as in LJ liquid), and the other being closer to the formation of supra - molecular object (as in octanol). We note that the supra - molecular object is itself subject to local fluctuations in density.

Supra - molecular objects are mostly found in soft-matter, but also in biological liquids [28, 24]. The Life itself is closely related to self-assembly, with organic molecules, such as lipids, peptides or nucleic acids, being self - assembled to form constitutional structures of the cell, including membranes, proteins or the genome [33]. Since the mechanism of formation of supramolecular entities in soft matter is similar to the formation of the same entities in smaller systems, such as alcohols, understanding kinetics of these smaller systems is essential for understanding kinetics of larger and complex biological systems. Therefore, the study of kinetics of alcohols and acqueous mixtures of alcohols represents the bridge between understanding simple liquids and complex biological liquids.

This situation could be analogous to the spontaneous emergence of elementary particles from the quantum fluctuations in vacuum. This analogy is interesting if we suppose that specific types of fluctuations, those that accompany the emergence of self-assembled objects, have the potential to create a situation where information is stored in some of these objects, and that their interactions allow them to use this information to reach a completely new physical state. The analogy between fluctuations in molecular liquids and quantum fluctuations has already been introduced by Pierre - Gilles de Gennes, in the context of liquid crystals, who showed the analogy between phase transitions from nematic to smectic phase of crystal with the phase transition from metal to superconductor [36], which is a purely quantum mechanical concept. This analogy is materialized mathematically into the Landau – de Gennes free energy [149].

It is possible that only specific solvents (e.g. water), mixed with other appropriate molecular objects, may give rise to specific types of fluctuations, accompanied with the formation of self - assembled meta - molecular objects, which would create conditions precursor to Life. In order to test this hypothesis, it is necessary to start first with simple aqueous mixtures and explore the various types of results obtained, while keeping this goal in mind. Although the aim of this thesis is not to answer all the questions posed herein, it is clear that this type of research works could have significant impact on understanding the important biological processes. In this work, the study of dynamics will be performed on the basis of the past work of the research group, related to the analysis of micro-heterogeneity from static point of view, by extending it to the dynamical point of view.

To conclude this section, the study of dynamics in this work will be based on the analysis of dynamical correlation functions, which represent dynamic equivalents of static radial distribution function and structure factor. These functions are expected to clarify the specificities in dynamics of micro - heterogeneous liquids, which we are particularly interested herein. In section 2, we present fundamental mathematical formalism behind these functions and their relationship with Theory of Liquids.

Theory

2

2 Elements of the Theory of Dynamics in Liquids

The aim of this chapter is to briefly introduce the way how the theory of dynamics in molecular liquids can be constructed from atom - atom interactions, in relation with molecular simulations and statistical physics. Since the main observables of this thesis are dynamical correlation functions, special focus is put on the relationship between those functions with their static equivalents. The understanding of this relationship is important for understanding how charge order, together with micro - heterogeneity, manifests in dynamical correlation functions. In addition, we introduce difficulties encountered in the development of coherent formalism, which are expected to be solved numerically in the future.

2.1 Introduction

In statistical physics, dynamics in liquids can be conveniently studied in phase space [38, 109, 191], which represents all possible states $(\mathbf{r}^N, \mathbf{p}^N)$ which specific system can occupy, with $\mathbf{r}^N = (\mathbf{r}_1, \mathbf{r}_2, ..., \mathbf{r}_N)$ and $\mathbf{p}^N = (\mathbf{p}_1, \mathbf{p}_2, ..., \mathbf{p}_N)$ representing positions and momenta of all N particles in the system. A Hamiltonian of such system is given with [183, 56, 191, 17]:

$$H = \sum_{i=1}^{N} \frac{\mathbf{p}_i^2}{2m_i} + V_N(\mathbf{r}_N) \tag{2}$$

,with the first term being the total kinetic energy of the system, whereas the second term is the total potential energy. We note that this form of equation (2) does not specify whether particles i are bound within molecules or not, or whether there are many species or only one single specie.

The equations of motions (as the ones used in typical simulation) are given with equations (3) and (4):[56, 191, 17]

$$\dot{\mathbf{r}}_i = \frac{\partial H}{\partial \mathbf{p}_i} \tag{3}$$

$$\dot{\mathbf{p}}_i = -\frac{\partial H}{\partial \mathbf{r}_i} \tag{4}$$

These equations describe the dynamics of N particles in 3D space. In a specific state, a 6 - dimensional vector, $(r_{ix}, r_{iy}, r_{iz}, p_{ix}, p_{iy}, p_{iz})$, can be attributed to each particle i, describing its total position $(\mathbf{r}_i)$ and momentum $(\mathbf{p}_i)$. Therefore, one state of the entire system, composed of N particles, can be described with a point in $6N$ - dimensional space. The dynamics of this "point" occurs in sub - space of the total phase space, with the sub - space being determined with the choice of ensemble. We remind that an ensemble represents a collection of microstates for which certain thermodynamic quantities are kept constant. For example, in microcanonical ensemble, N, V, and E (number of particles, volume and energy respectively) are constant, while in canonical ensemble, N, V and T are constant (with T denoting the temperature).

[191, 56, 17] The analogy between dynamics in three - dimensional space (used in simulations with periodic boundary conditions (PBC)) and the dynamics in 6N - dimensional NVT sub - space is illustrated in Figure 4. As shown in the right panel, each configuration in phase space is represented with a point inside $6N$ - dimensional space. Points t_1 and t_2 represent the states of the system at times t_1 and t_2 respectively.

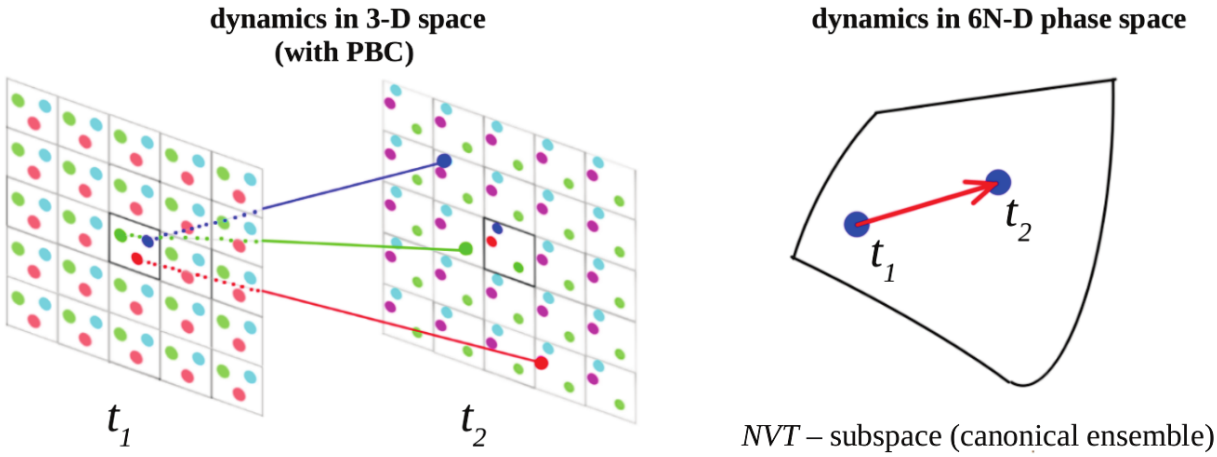

Figure 4: Visualization of relationship between dynamics in real 3-D space (left panel) and dynamics in $6N$-D phase - space (right panel). In phase - space, each microstate is represented with a point in $6N$-D space.

The probability of each $(\mathbf{r}^N, \mathbf{p}^N, t)$ state is given with $f^{[N]}(\mathbf{r}^N, \mathbf{p}^N, t)\mathrm{d}\mathbf{r}^N\mathrm{d}\mathbf{p}^N$, with $f^{[N]}(\mathbf{r}^N, \mathbf{p}^N, t)$ being phase - space probability density [56, 191, 17], which satisfies:

$$\int_{\mathbf{r}^N}\int_{p^N} f^{[N]}(\mathbf{r}^N, \mathbf{p}^N, t)\mathrm{d}\mathbf{r}^N\mathrm{d}\mathbf{p}^N = 1 \tag{5}$$

for all times t. Since the states $(\mathbf{r}^N, \mathbf{p}^N)$ are not being created or destroyed as time t changes, distribution $f^{[N]}(\mathbf{r}^N, \mathbf{p}^N, t)$ is stationary and its time evolution can be described with Louville equation:[56]

$$\frac{\mathrm{d}f^{[\mathrm{N}]}(\mathbf{r}^{\mathrm{N}}, \mathbf{p}^{\mathrm{N}}, \mathrm{t})}{\mathrm{d}t} = 0 \tag{6}$$

Since both positions and momenta are functions of t, the total time derivative in equation (6) can be rewritten in more explicit form:

$$\frac{\partial f^{[N]}}{\partial t} + \sum_{i=1}^{N}\left\{\frac{\partial f^{[N]}}{\partial \mathbf{r}_i}\cdot\frac{\partial \mathbf{r}_i}{\partial t} + \frac{\partial f^{[N]}}{\partial \mathbf{p}_i}\cdot\frac{\partial \mathbf{p}_i}{\partial t}\right\} = 0 \tag{7}$$

,which, by using equations (3) and (4), can be written as:

$$\frac{\partial f^{[N]}}{\partial t} + \sum_{i=1}^{N}\left\{\frac{\partial f^{[N]}}{\partial \mathbf{r}_i}\cdot\frac{\partial H}{\partial \mathbf{p}_i} - \frac{\partial f^{[N]}}{\partial \mathbf{p}_i}\cdot\frac{\partial H}{\partial \mathbf{r}_i}\right\} = \frac{\partial f^{[N]}}{\partial t} + \left\{H, f^{[N]}\right\} = 0 \tag{8}$$

where we have introduced the Poisson bracket [38], defined as:

$$\{H,f\} = \sum_{i=1}^{N} \frac{\partial H}{\partial \mathbf{r}_i}\frac{\partial f}{\partial \mathbf{p}_i} - \frac{\partial H}{\partial \mathbf{p}_i}\frac{\partial f}{\partial \mathbf{r}_i} \tag{9}$$

By introducing Louville operator [183, 119] $L = i\{H,\ \}$, we can write equation (8) in form:

$$\frac{\partial f^{[N]}}{\partial t} = -iLf^{[N]} \tag{10}$$

The formal solution of equation (10) is given with:

$$f^{[N]}(\mathbf{r}^N,\mathbf{p}^N,t) = \exp(-iLt)\cdot f^{[N]}(\mathbf{r}^N,\mathbf{p}^N,0) \tag{11}$$

and it describes the time evolution of the phase - space probability density.
Similarly, in the case of general phase - space variable $A(\mathbf{r}^N,\mathbf{p}^N)$, we can write [38, 109, 17, 56]:

$$\frac{dA}{\mathrm{d}t} = iLA \tag{12}$$

with $\frac{\partial A}{\partial t}$ term being omitted, since $A(\mathbf{r}^N,\mathbf{p}^N)$ does not depend explicitly on time, but only through positions and momenta. Equation (12) has formal solution in form:

$$A(t) = \exp(iLt)\cdot A(0) \tag{13}$$

In this work, we will be particularly interested in microscopic density ρ. The most general form of microscopic density, dependent of both positions and momenta, is given with [38]:

$$\rho(\mathbf{r},\mathbf{p},t) = \sum_{i=0}^{N} \delta(\mathbf{r}-\mathbf{r}_i(t))\delta(\mathbf{p}-\mathbf{p}_i(t)) \tag{14}$$

Configurational density $\rho(\mathbf{r},t)$ [63, 56, 17] can be obtained by integrating $\rho(\mathbf{r},\mathbf{p},t)$ over all possible momenta in phase - space:

$$\rho(\mathbf{r},t) = \int \rho(\mathbf{r},\mathbf{p},t)\mathrm{d}\mathbf{p} = \sum_{i=0}^{N} \delta(\mathbf{r}-\mathbf{r}_i(t)) \tag{15}$$

Similarly, the microscopic flux $j(\mathbf{r},t)$ is given with [17]:

$$j(\mathbf{r},t) = \frac{1}{m}\int \rho(\mathbf{r},\mathbf{p},t)\mathbf{p}\mathrm{d}\mathbf{p} \tag{16}$$

,while microscopic kinetic energy $e(\mathbf{r},t)$ is given with [17]:

$$e(\mathbf{r},t) = \frac{1}{2m}\int \rho(\mathbf{r},\mathbf{p},t)\mathbf{p}^2\mathrm{d}\mathbf{p} \tag{17}$$

Theoretical developments under Kinetic Theory of Liquids [17, 56, 191, 2], are quite involved, since they couple both positions and momenta. However, in this work, we will consider only (r,t) functions, in particular the Van Hove and related functions. This operation is possible in Classical Mechanics, since the momentum part can be decoupled from the configurational part, as can be seen from equations (14) and (15).

For any microscopic variable $A(\mathbf{r}^N,\mathbf{p}^N,t)$, it is possible to define average in terms of the phase space probability density $f^{[N]}(\mathbf{r}^N,\mathbf{p}^N,t)$ [38, 119]:

$$< A(\mathbf{r}^N,\mathbf{p}^N,t) >= \int_{r^N}\int_{p^N} A(\mathbf{r}^N,\mathbf{p}^N,t) f^{[N]}(\mathbf{r}^N,\mathbf{p}^N,t)\mathrm{d}\mathbf{r}^N\mathrm{d}\mathbf{p}^N \tag{18}$$

or equivalently [38, 119]:

$$< A(\mathbf{r}^N,\mathbf{p}^N,t) >= \int_{r^N}\int_{p^N} A_0(\mathbf{r}^N,\mathbf{p}^N) f_0^{[N]}(\mathbf{r}^N,\mathbf{p}^N)\mathrm{d}\mathbf{r}^N\mathrm{d}\mathbf{p}^N \tag{19}$$

In the case of particularly microscopic density ρ, defined with equation (15), it can be shown that:[56]

$$< \rho(\mathbf{r},t) >= \frac{N}{V} \tag{20}$$

with N representing the total number of particles in volume V.

2.2 Dynamical correlation functions

For given microscopic density $\rho(\mathbf{r},t)$, density autocorrelation function between points $(\mathbf{r}_1,\tau)$ and $(\mathbf{r}_2,\tau+t)$ is given with:[63, 56, 17]

$$C_{\rho\rho}(\mathbf{r}_1,\mathbf{r}_2;t) =< \rho(\mathbf{r}_1,\tau)\rho(\mathbf{r}_2,t+\tau) >= \rho^{(2)}(\mathbf{r}_1,\mathbf{r}_2;t) \tag{21}$$

with τ representing the time origin. Since we are considering liquids in equilibrium, the choice of the time origin is arbitrary and we can set $\tau = 0$. In addition, function $\rho^{(2)}(\mathbf{r}_1,\mathbf{r}_2;t)$ is even [56, 17]:

$$\rho^{(2)}(\mathbf{r}_1,\mathbf{r}_2;t) = \rho^{(2)}(\mathbf{r}_1,\mathbf{r}_2;-t) \tag{22}$$

,which means that its time derivative is zero in time origin:

$$\frac{\mathrm{d}}{\mathrm{d}t}\rho^{(2)}(\mathbf{r}_1,\mathbf{r}_2;t=0) = 0 \tag{23}$$

2.2.1 Van Hove correlation functions

We note that, in spatially homogeneous and isotropic liquids, the correlation functions depend only on the modulus of the relative distance. We introduce here a more general density correlation function between atoms, whether or not they are part of molecules, and subsequently consider molecular liquids as mixtures of atoms. The intra-molecular correlations should then account for the molecular nature, as we show below.
Correlation between density ρ_a of atoms a in point $(\mathbf{r}_1, 0)$ and density ρ_b of atoms b in point $(\mathbf{r}_2, t)$ is given with:[63, 56]

$$\rho_{ab}^{(2)}(\mathbf{r}_1, \mathbf{r}_2; t) = < \rho_a(\mathbf{r}_1, 0)\rho_b(\mathbf{r}_2, t) > \tag{24}$$

In the limit when the relative distance $r_{12} = |\mathbf{r}_1 - \mathbf{r}_2|$ is large enough, densities $\rho_a(\mathbf{r}_1, 0)$ and $\rho_b(\mathbf{r}_2, t)$ will be decorrelated:

$$\lim_{r_{12}\to\infty} \rho_{ab}^{(2)}(\mathbf{r}_1, \mathbf{r}_2; t) = < \rho_a(\mathbf{r}_1, 0) >< \rho_b(\mathbf{r}_2, t) >= \rho_a\rho_b \tag{25}$$

,where the last equality follows from equation (20).
Equation (24) allows us to define Van Hove correlation function:[56, 37, 17]

$$\begin{aligned} G_{ab}(\mathbf{r}_1, \mathbf{r}_2, t) &= \frac{1}{\rho_a\rho_b V} \int \rho_{ab}^{(2)}(\mathbf{r}_1, \mathbf{r}_2, t) \mathrm{d}\mathbf{r}_1 \\ &= \frac{1}{\rho_a\rho_b V} < \sum_{a_i} \sum_{b_j} \int \delta\left[\mathbf{r}_1 - \mathbf{r}_{a_i}(0)\right] \delta\left[\mathbf{r}_2 - \mathbf{r}_{b_j}(t)\right] \mathrm{d}\mathbf{r}_1 > \end{aligned} \tag{26}$$

with $\sum_{a_i}$ and $\sum_{b_j}$ representing sums over all atoms $a_1, a_2, ..., a_n$ and $b_1, b_2, ..., b_m$ respectively, with a and b denoting atomic species. In homogenous and isotropic liquids, correlations will be dependent only of the relative distance $\mathbf{r} = \mathbf{r}_2 - \mathbf{r}_1$. If we apply the substitution $\mathbf{r}_2 = \mathbf{r}_1 + \mathbf{r}$, it follows:

$$G_{ab}(\mathbf{r}, t) = \frac{1}{\rho_a\rho_b V} < \sum_{a_i} \sum_{b_j} \delta\left[\mathbf{r} - \left(\mathbf{r}_{b_j}(t) - \mathbf{r}_{a_i}(0)\right)\right] > \tag{27}$$

From equations (26) and (25), it follows:

$$\lim_{r_{12}\to\infty} G_{ab}(\mathbf{r}_1, \mathbf{r}_2, t) = 1 \tag{28}$$

The sum $\sum_{ab}$ in equation (27) is over all possible (a_i, b_j) atomic pairs and, therefore, encompasses both the cases when pairs belong to the same molecule and when pairs belong to different molecules. Hence, the total sum can be written as:

$$\sum_{a_i, b_j} = \sum_{a_i, b_j}^{(s)} + \sum_{a_i, b_j}^{(d)} \tag{29}$$

with sum $\sum_{a_i,b_j}^{(s)}$ representing the sum over all pairs (a_i,b_j) which belong to the same molecule, while $\sum_{a_i,b_j}^{(d)}$ representing all pairs (a_i,b_j) which belong to different molecules. Therefore, the total Van Hove function from equation (27) can be written as:

$$G_{ab}(\mathbf{r},t) = G_{ab}^{(s)}(\mathbf{r},t) + G_{ab}^{(d)}(\mathbf{r},t) \tag{30}$$

with self Van Hove function $G_{ab}^{(s)}(\mathbf{r},t)$ and distinct Van Hove function $G_{ab}^{(d)}(\mathbf{r},t)$ defined with following equations:

$$G_{ab}^{(s)}(\mathbf{r},t) = \frac{1}{\rho_a \rho_b V} < \sum_{a_i,b_j}^{(s)} \delta\left[\mathbf{r} - \left(\mathbf{r}_{b_j}(t) - \mathbf{r}_{a_i}(0)\right)\right] > \tag{31}$$

$$G_{ab}^{(d)}(\mathbf{r},t) = \frac{1}{\rho_a \rho_b V} < \sum_{a_i,b_j}^{(d)} \delta\left[\mathbf{r} - \left(\mathbf{r}_{b_j}(t) - \mathbf{r}_{a_i}(0)\right)\right] > \tag{32}$$

Self Van Hove function represents intramolecular contribution to the total density correlations between atoms a and b, while distinct Van Hove functions represents intermolecular contribution. We note that these definitions of Van Hove functions are not the same as in the literature [56, 17, 63], and differs by a factor ρ_b^{-1}. Our definition is compatible with the standard definition of the $t = 0$ static pair correlation function $g_{ab}(r)$, since we have:

$$G_{ab}^{(d)}(\mathbf{r},t=0) = g_{ab}(\mathbf{r}) \tag{33}$$

We note that equation (27) can be rewritten in form:

$$\sqrt{\rho_a \rho_b} G_{ab}(\mathbf{r},t) = \frac{1}{\sqrt{N_a N_b}} < \sum_{a_i} \sum_{b_j} \delta\left[\mathbf{r} - \left(\mathbf{r}_{b_j}(t) - \mathbf{r}_{a_i}(0)\right)\right] > \tag{34}$$

,which will be used in the section 2.2.2, in context of the definition of intermediate scattering function $F_{ab}(\mathbf{k},t)$.

2.2.2 Intermediate scattering function and dynamical structure factor

Van Hove functions, presented in section 2.2.1, cannot be measured experimentally, which means that experiments cannot directly provide information about the distribution of atoms and molecules in space. This information can be obtained only by computer simulations, which are a convenient way to mimic matter, but through a model representation, which distorts reality to some extent. However, this information can be obtained experimentally by probing liquids with different forms of radiation in scattering experiments, such as X - ray or neutron scattering. In quantum mechanical representation, radiation is described with plane waves $\exp(i\mathbf{kr})$, where

$\mathbf{k}$ is the wave vector describing spatial periodicity of the wave. It is known that the spatial distribution of molecules in $\mathbf{k}$ - space (with $\mathbf{k}$ now being related to the difference in momentum of scattered radiation and incident radiation, $\mathbf{k} = \mathbf{k}_2 - \mathbf{k}_1$), accessible by experiments, is related to the distribution in $\mathbf{r}$ - space (with $\mathbf{r}$ denoting the inter-particle separation, $\mathbf{r} = \mathbf{r_2} - \mathbf{r_1}$) by simple Fourier transformation [56]. Following this, one can measure the structure factor $S_{ab}(k)$, which is the Fourier transform of the static correlation function $g_{ab}(r)$. The corresponding dynamical equivalent of the static structure factor is called the intermediate scattering function $F_{ab}(k,t)$, which is formally defined as:[56, 63, 37, 17]

$$F_{ab}(\mathbf{k},t) = \frac{1}{\sqrt{N_a N_b}} < \rho_a(\mathbf{k},0)\rho_b(-\mathbf{k},t) > \tag{35}$$

where $\rho_a(\mathbf{k},t)$ represents the Fourier transform of microscopic density $\rho_a(\mathbf{r},t)$:

$$\rho_a(\mathbf{k},t) = \sum_{a_i} \exp(i\mathbf{k}(\mathbf{r}_{a_i}(t)) \tag{36}$$

Then we can write:

$$F_{ab}(\mathbf{k},t) = \frac{1}{\sqrt{N_a N_b}} < \sum_{a_i,b_j} \exp(-i\mathbf{k}(\mathbf{r}_{b_j}(t) - \mathbf{r}_{a_i}(0)) > \tag{37}$$

If we rewrite the last equation in slightly different form:

$$F_{ab}(\mathbf{k},t) = \frac{1}{\sqrt{N_a N_b}} < \sum_{a_i,b_j} \int \mathrm{d}\mathbf{r}\delta\left[\mathbf{r} - \left(\mathbf{r}_{b_j}(t) - \mathbf{r}_{a_i}(0)\right)\right] \exp(-i\mathbf{k}\mathbf{r}) > \tag{38}$$

then, by using the definition (34), it can be easily shown:

$$F_{ab}(\mathbf{k},t) = \sqrt{\rho_a \rho_b} \int \mathrm{d}\mathbf{r} \exp(-i\mathbf{k}\mathbf{r}) G_{ab}(\mathbf{r},t) \tag{39}$$

meaning that $F_{ab}(\mathbf{k},t)$ is indeed the spatial Fourier transform of $G_{ab}(\mathbf{r},t)$. The power spectrum of $F_{ab}(\mathbf{k},t)$ is called dynamical structure factor $S(\mathbf{k},\omega)$ and represents the time Fourier transform of $F_{ab}(\mathbf{k},t)$: [56, 17]

$$S(\mathbf{k},\omega) = \int \mathrm{d}t \exp(-i\omega t) F_{ab}(\mathbf{k},t) = \tag{40}$$

In addition, this quantity is measurable in scattering experiments.

2.2.3 Relationship with the RISM theory and W - matrix

The description of the microscopic structure of molecular liquids can be done in two different manners, through orientational description or through atom - atom description [15, 56]. The first description requires a large set of rotational invariants in order to account for correlations between molecules, while the second method requires to properly take into account all atom - atom correlations, including both intramolecular and intermolecular part. In this work, we choose the second description, and clarify the relation between the intra - molecular correlations and the self-part of the van Hove function. The atom - atom van Hove function is then the appropriate correlation function to describe molecular liquids.

In section 2.2.1, we discussed density correlations between atoms a and b and showed that total correlations are, in fact, superposition of intramolecular and intermolecular contributions. Particularly, in the special case when atomic species a and b are identical (i.e. $a = b$), it follows from equation (31) that self Van Hove function $G_{aa}^{(s)}(\mathbf{r},0)$ is simply delta function $\delta(\mathbf{r})$, centered at the origin in this case. As time increases, this function spreads over entire $\mathbf{r}$ - domain. Ultimately, in large t limit, we have:

$$\lim_{t\to\infty} G_{aa}^{(s)}(\mathbf{r},t) = 0\,; \quad \forall \mathbf{r} \tag{41}$$

In the case when $a \neq b$, self Van Hove function $G_{ab}^{(s)}(\mathbf{r},0)$ will be a delta function centered at specific intramolecular distance $\mathbf{d}_{ab}$ between atoms a and b, i.e. $\delta(\mathbf{r}-\mathbf{d}_{ab})$.
It is interesting to compare this situation with the Reference Interaction Site Model (RISM) [23, 17, 56, 67, 167, 40, 64] in the static theory of liquids. In this theory, molecules are modeled as hard objects, composed of spheres (representing atoms), whose distribution is determined with chemical structure of each molecule. The total static density correlations between atoms a and b, denoted with $g_{ab}^{(total)}(r)$, then can be written as the sum of intramolecular part $w_{ab}(r)$ and the usual intermolecular part $g_{ab}(r)$:

$$g_{ab}^{(total)}(r) = w_{ab}(r) + \rho g_{ab}(r) \tag{42}$$

where the intramolecular part $w_{ab}(r)$ is equivalent to the self Van Hove function introduced earlier, with $w_{ab}(r) = \rho G_{ab}^{(s)}(r,0)$, while $g_{ab}(r)$ is usual radial distribution function, equal to the distinct Van Hove function $G_d(r,0)$. With $W_{ab}(k)$, $H_{ab}(k)$ and $S_{ab}(k)$ we denote spatial Fourier transforms of functions $w_{ab}(r)$, $g_{ab}(r)$ and $g_{ab}^{(total)}(r)$ respectively. Following equation (42), we have:

$$S_{ab}(k) = W_{ab}(k) + \rho H_{ab}(k) \tag{43}$$

Now we recall that the Ornstein - Zernike (OZ) equation [23, 56, 17, 11, 22, 40, 64] of a mixture of atoms can be written in matrix form as:

$$\hat{\mathrm{S}}(k)\hat{\Gamma}(k) = \hat{\mathrm{I}} \tag{44}$$

where $\hat{\mathrm{S}}$ is the structure factor matrix, composed of elements $S_{ab}(k)$, $\hat{\mathrm{I}}$ is the identity matrix, and $\hat{\Gamma}$is given with:

$$\hat{\Gamma}(k) = \hat{\mathrm{W}}^{-1}(k) - \rho\hat{\mathrm{C}}(k) \tag{45}$$

with $\hat{\mathrm{C}}(k)$ representing the direct correlation matrix [56, 23, 17]. Intramolecular matrix elements $W_{ab}(k)$ are given with: [23]

$$W_{ab}(k) = \delta_{ab} + (1-\delta_{ab})\int w_{ab}(r)\cdot\exp(-i\mathbf{kr})\mathrm{d}\mathbf{r} \tag{46}$$

with δ_{ab} representing Kronecker delta. Elements $H_{ab}(k)$ are defined with Fourier transform of $g_{ab}(r)$ as:

$$H_{ab}(\mathbf{k}) = \int d\mathbf{r}\exp(-i\mathbf{kr})\left[g_{ab}(r)-1\right] \tag{47}$$

Eq.(44) is formally referred to as the OZ equation for a mixture of atoms [23, 56], and the $\hat{\Gamma}$ matrix is simply the inverse of $\hat{\mathrm{S}}$ matrix, i.e. $\hat{\Gamma} = \hat{\mathrm{S}}^{-1}$. We immediately note that the SSOZ equation (44) has strong formal resemblance with the Mori - Zwanzig (MZ) equation, which will be described in section 2.3.1. This resemblance between the two equations indicates that the MZ equation could represent the dynamical equivalent of the SSOZ equation.

2.2.4 Relationship with Kirkwood - Buff integrals

The Kirkwood-Buff integrals are usually defined as: [8, 9, 130, 82, 35, 34]

$$K_{ab} = \int_0^\infty d\mathbf{r}\left[g_{ab}(r)-1\right] \tag{48}$$

The importance of these integrals lies in the fact that they relate microscopic properties of liquids with thermodynamic properties, such as molar volume, isothermal compressibility or chemical potential. For example, in the simplest case of one - component system, containing only atomic species a, we have: [8, 9]

$$K_{aa} = \frac{\kappa_T}{\beta} - \frac{1}{\rho_a} \tag{49}$$

where κ_T is isothermal compressibility and $\beta = \frac{1}{k_B T}$, where T is the temperature of the system, while k_B is Boltzmann factor. However, the last equation is valid only in the thermodynamic

limit of systems with infinite size. In addition, in large r limit, we have:[9, 35]

$$\lim_{r\to\infty} g_{aa}(r) = 1 - \frac{\rho}{\beta N}\kappa_T \tag{50}$$

where we note that $\lim_{r\to\infty} g_{aa}(r) = 1$ when $N \to \infty$. Therefore, in finite size simulations, the asymptote of $g(r)$ will clearly depend on the size of simulation box. [35, 82]

It is interesting adress what would be the KBI corresponding to the integrals of the dynamical correlation functions, which we call here D-KBI (for dynamical KBI). We first note that there are 2 such D-KBI integrals, one from the integral of the self part and one from the distinct part of Van Hove function. Formally, the D-KBI should concern only the distinct part because of the definition (48), which accounts only for distinct part of Van Hove function.

In one component system, the D-KBI of the self part is proportional to the molar volume $V^{(m)}$and is independent of time in the large R limit:

$$\lim_{R\to\infty} K_{ab}^{(s)}(R,t) = \lim_{R\to\infty} \int_0^R d\mathbf{r} G_{ab}^{(s)}(r,t) = \frac{1}{\rho} = \frac{V}{N} = \frac{V^{(m)}}{N_A} \tag{51}$$

where $N_A = 6.022 \cdot 10^{23}\text{mol}^{-1}$ is the Avogadro constant. This is intuitively reasonable, since $G_{ab}^{(s)}(r,t)$ is proportional to the probability density that atom b at time t is found at the distance r from the origin (i.e. position of reference atom a at $t = 0$), with ρ^{-1} representing the proportionality constant. Hence, $G_{ab}^{(s)}(r,t)$ integrated over entire volume gives precisely ρ^{-1}, since the probability of finding the particle anywhere inside the volume of integration is sure event, with probability equal to 1.

The D - KBI of the distinct part is also independent of time in the large R limit:

$$\lim_{R\to\infty} K_{ab}^{(d)}(R,t) = \lim_{R\to\infty} \int_0^R d\mathbf{r} \left[G_{ab}^{(d)}(r,t) - 1 \right] = K_{ab} \tag{52}$$

since the average number of particles within the integrated volume is fixed for all t. We note that, for one - component systems, the KBI is equal to the isothermal compressibility, shifted by the molar volume ($K = \frac{\kappa_T}{\beta} - \frac{V_m}{N_A}$).

Self and distinct KBI integrals for neat ethanol, for the case of the oxygen (OO) and carbon - oxygen (OC_1) correlations, are shown in Figure 5, where we illustrate the convergence of integrals in large R limit for all time values. The direction of increasing time is indicated with arrows in Figure 5.

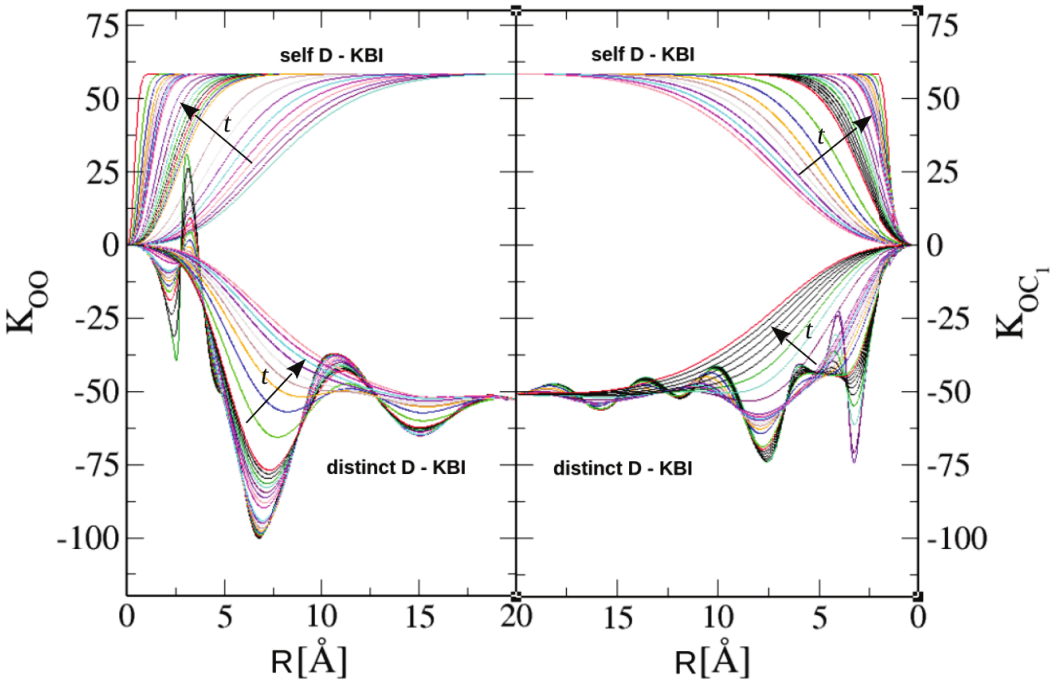

Figure 5: D - KBI integrals of neat ethanol, for the case of OO (left panels) and OC (right panels) correlations. The direction of increasing t is indicated with arrows on each panel.

2.3 Dynamical evolution of Van Hove function

Dynamical evolution of Van Hove function can be addressed from the context of Mori - Zwanzig formalism. This formalism is applicable to any type of dynamical variable $A(r,t)$ or its autocorrelation function $C_{AA}(r,t)$, as it will be shown in the next section. There, we introduce the basis of Mori - Zwanzig approach.

2.3.1 Mori - Zwanzig formalism

In order to introduce the basis of Mori - Zwanzig formalism [62, 56, 89, 191], let us consider a phase - space dynamical variable $A(t)$. We have shown earlier that the time evolution of A is described with Louville equation, $A(t) = \exp(-iLt)A(0)$, suggesting that $A(t)$ can be seen as vector in phase - space, obtained by "rotation" of vector $A(0)$ by "angle" Lt. By using this analogy with vectors, one can consider the projection of $A(t)$ "parallel" to the vector $A(0)$, together with projection "perpendicular" to $A(0)$. Parallel projection can be written in terms of linear projection operator P:

$$PA(t) = \frac{< A(t)A(0) >}{< A(0)A(0) >} A(0) \tag{53}$$

where one can immediately note that the factor in front of $A(t)$ corresponds to normalized autocorrelation function $C_{AA}(t)$ of variable A. Therefore, we can write:

$$PA(t) = C_{AA}(t)A(0) \tag{54}$$

The perpendicular projection, denoted with $A^{'}(t)$, can be written in terms of projector Q:

$$A^{'}(t) = QA(t) \tag{55}$$

which satisfies:

$$< A^{'}(t)A(0) >= 0 \tag{56}$$

Now, if we consider dynamical variable A in Laplace space, denoted with $\widetilde{A}(z)$, we can write Louville equation in form:

$$(z+L)\widetilde{A}(z) = iA \tag{57}$$

Since $P+Q=I$ [38, 56], we can write:

$$(z+L)(P+Q)\widetilde{A}(z) = iA \tag{58}$$

The last equation can be projected in directions parallel and perpendicular to $A(0)$, by the application of projectors P and Q respectively. Then, by using fundamental properties of operators

P and Q ($P^2 = P$, $Q^2 = Q$ and $PQ = 0$), one can obtain equations for the time evolutions of projections $C_{AA}(t)$ and $A^{'}(t)$ [109, 191]:

$$\frac{\partial}{\partial t}C_{AA}(t) - i\Omega C_{AA}(t) + \int_0^t dsM(t-s)C_{AA}(s) = 0 \tag{59}$$

$$\frac{\partial A^{'}(t)}{\partial t} - i\Omega A^{'}(t) + \int_0^t dsM(t-s)A^{'}(s) = R(t) \tag{60}$$

The time evolution of total $A(t)$ is described with [109, 191, 56, 114, 2, 90]:

$$\frac{\partial A(t)}{\partial t} - i\Omega A(t) + \int_0^t dsM(t-s)A(s) = R(t) \tag{61}$$

The term $R(t)$ in the last equation is called the random force, while the term $M(t)$ is the memory function, which is the autocorrelation of the random force:

$$M(t) = \frac{< R(t)R(0) >}{< A(0)A(0) >} \tag{62}$$

The frequency term Ω is given by

$$i\Omega = \frac{< \dot{A}(0)A(0) >}{< A(0)A(0) >} \tag{63}$$

Since, in the considered systems, autocorrelation functions are even functions of time, it follows $i\Omega = 0$.

Mori - Zwanzig equation (61) has identical form as generalized Langevin equation [126, 113, 99, 56, 4], which describes the time evolution of brownian particle's velocity in a liquid bath composed of other particles. In a specific case when brownian particle is much larger than surrounding particles, Langevin assumed that the net force on brownian particle consists of two parts: a frictional (drag) force proportional to the velocity $\mathbf{v}(t)$ of the particle and a random force $\mathbf{R}(t)$ which rises from the collisions with surrounding particles. Therefore, the equation of motion of the brownian particle can be written as:[126, 113, 99, 56, 4]

$$m\frac{d\mathbf{v}(t)}{dt} = -\xi\mathbf{v}(t) + \mathbf{R}(t) \tag{64}$$

with $\mathbf{R}(t)$ representing the random force, equivalent to the one from Mori - Zwanzig approach, while ξ is friction coefficient. One of the assumptions taken in the Langevin equation (64) is that the frictional force at time t is proportional only to velocity $\mathbf{v}$ at the same time t, which means that the diffusing particle adapts instantaneously to changes in surrounding medium and that the history of the system doesn't affect particle's motion in the present time. This assumption is reasonable when diffusing particle is much bigger that the particles of the surrounding

bath. However, when the dimensions of the diffusing particle are similar to the dimensions of the surrounding particles, more generalized assumptions need to be taken into consideration. Clearly, it would be more realistic to suppose that the frictional force depends on the history of the system in times earlier than t, which means that certain "memory" is associated with the motion of the particle. Mathematically, this can be achieved by introducing friction coefficient $\xi(t-s)$ which is non-local in time and represents the contribution to the total friction force at time t that is coming from the state of the system at earlier time $t-s$. Then, by writing frictional force in the form of convolution in time, we obtain more generalized form of Langevin equation [56, 17, 191, 4]:

$$m\frac{d\mathbf{v}(t)}{dt} = -\int_0^t \xi(t-s)\mathbf{v}(s)ds + \mathbf{R}(t) \tag{65}$$

We note that the form of generalized Langevin equation (65) is identical to the form of Mori - Zwanzig equation (61). Therefore, memory function $M(t-s)$ from Mori - Zwanzig approach is analogous to the time - dependent friction force $\xi(t-s)$ from generalized Langevin equation. In addition, both equations have analogous random force terms.

We note that, if we multiply equation (65) and take the average $<>$, we obtain:

$$m\frac{dZ(t)}{dt} = -\int_0^t \xi(t-s)Z(s)ds \tag{66}$$

with $Z(t)$ representing velocity autocorrelation function $Z(t) =< \mathbf{v}(t)\mathbf{v}(0) >$[191, 56]. In the last equation, we used the fact that $< \mathbf{R}(t)\mathbf{v}(0) >= 0$, which reflects the nature of random force $\mathbf{R}(t)$, which is uncorrelated to the initial velocity $\mathbf{v}(0)$ [99, 56]. We note that form of equation (66) is identical to the equation (59) for the time evolution of autocorrelation function $C_{AA}(t)$ of random variable $A(t)$. This shows that Mori - Zwanzig equation (61) represents generalization of equation (65) to any dynamical random variable $A(t)$.

Since the memory function is formal, one must rely to approximations of it. The simplest approximation is exactly that of the initial Langevin equation (64), namely to set the memory function as independent of time:

$$M(t) = \xi_0\delta(t) \tag{67}$$

We will show in the section 3.4.7 that this approximation is not valid for realistic liquids.

2.3.2 Application to Van Hove correlation functions

Since Mori - Zwanzig formalism can be applied to any dynamical variable (equation 61) or its autocorrelation function (equation 59), it can be applied to microscopic density $\rho(\mathbf{r},t)$ or Van Hove function $G(\mathbf{r},t)$. We remind that the van Hove correlation function is the auto - correlation of the microscopic density, which allows us to directly apply the Mori - Zwanzig formalism to it. However, Fourier - Laplace transform is required instead of the simple Laplace transform (the Fourier transform concerns the position variable $\mathbf{r}$, while the Laplace transform concerns the time variable t).

This formalism can be applied to the microscopic density of specific atomic specie ($\rho_a(\mathbf{r},t) = \sum_{a_i} \delta(\mathbf{r}-\mathbf{r}_{a_i})$) or to the total microscopic density ($\rho(\mathbf{r},t) = \sum_a \rho_a(\mathbf{r},t)$). Since this formalism is very general, it can also be applied to the *vector* microscopic variable [56] $\hat{\rho} = \left[\rho_a(\mathbf{r},t), \rho_b(\mathbf{r},t), ..., \rho_f(\mathbf{r},t)\right]$. In addition, more general full phase space variables, including both positions and momenta, can be equally used.

The auto - correlation of $\rho_a(\mathbf{r},t)$ is the self Van Hove function $G^{(s)}_{aa}(\mathbf{r},t)$. The auto - correlation of the total $\rho(\mathbf{r},t)$ is the full van Hove function $G(\mathbf{r},t)$. For a system in which there are totally n atoms belonging to specie a, one can define matrix $\hat{\rho}_a(\mathbf{r},t)$:

$$\hat{\rho}_a(\mathbf{r},t) = \begin{pmatrix} \rho_{a_1}(\mathbf{r},t) \\ \vdots \\ \rho_{a_n}(\mathbf{r},t) \end{pmatrix} \tag{68}$$

where $\rho_{a_i}(\mathbf{r},t)$ represents the microscopic density of atom i of specie a: $\rho_{a_i}(\mathbf{r},t) = \delta(\mathbf{r}-\mathbf{r}_{a_i}(t))$.

The correlation function becomes then a correlation matrix :

$$\hat{\mathrm{P}}_a(\mathbf{r},t) = \{\mathrm{P}_{a;ij} = G^{(s)}_{a;ij}(\mathbf{r},t)\} \tag{69}$$

Similarly, for the total density in a system composed of totally f different atomic species, the vector density is:

$$\hat{\rho}(\mathbf{r},t) = \begin{pmatrix} \rho_a(\mathbf{r},t) \\ \vdots \\ \rho_f(\mathbf{r},t) \end{pmatrix} \tag{70}$$

and the corresponding correlation matrix of the total van Hove functions:

$$\hat{\mathrm{P}}(\mathbf{r},t) = \{\mathrm{P}_{ab} = G_{ab}(\mathbf{r},t)\} \tag{71}$$

In order to deal with the Mori - Zwanzig formalism, one requires the Fourier - Laplace transform of these matrices. Spatial Fourier transform ($\mathbf{r} \rightarrow \mathbf{k}$) of $P_{ab}(\mathbf{r},t)$, denoted with $P_{ab}(\mathbf{k},t)$, is equivalent to intermediate scattering function $F_{ab}(\mathbf{k},t)$:

$$P_{ab}(\mathbf{k},t) = F_{ab}(\mathbf{k},t) \tag{72}$$

,while the time Fourier transform ($t \rightarrow \omega$) of $P_{ab}(\mathbf{k},t)$, denoted with $P_{ab}(\mathbf{k},\omega)$, gives the dynamical structure factor $S_{ab}(\mathbf{k},\omega)$:

$$P_{ab}(\mathbf{k},\omega) = S_{ab}(\mathbf{k},\omega) \tag{73}$$

The MZ equation for $\hat{\mathrm{P}}(\mathbf{k},t)$ is given with:

$$\frac{\partial}{\partial t}\hat{\mathrm{P}}(\mathbf{k},t) = -\int_0^t \mathrm{d}s\hat{\mathrm{M}}(\mathbf{k},t-s)\hat{\mathrm{P}}(\mathbf{k},s) \tag{74}$$

while time - Laplace transform ($t \rightarrow z$) of the same equation gives:

$$\hat{\mathrm{P}}(k,z)\left[iz\hat{\mathrm{I}} - \hat{\mathrm{M}}(\mathbf{k},z)\right] = \mathrm{P}(\mathbf{k},t=0) \tag{75}$$

We note that $P_{ab}(\mathbf{k},t=0) = S_{ab}(\mathbf{k})$, while one can define a dynamical structure factor matrix $\hat{\mathrm{S}}(\mathbf{k},z)$ as time - Laplace transform of $\hat{\mathrm{P}}(\mathbf{k},t)$, instead of usual time Fourier transform $\hat{\mathrm{S}}(\mathbf{k},\omega)$. Using these analogies and the SSOZ equation (44), we can rewrite the Mori - Zwanzig equation above as:

$$\hat{\mathrm{S}}(\mathbf{k},z)\hat{\mathrm{T}}(\mathbf{k},z) = \hat{\mathrm{I}} \tag{76}$$

with

$$\hat{\mathrm{T}}(\mathbf{k},z) = \left[iz\hat{\mathrm{I}} - \hat{\mathrm{M}}(\mathbf{k},z)\right]\hat{\mathrm{S}}^{-1}(\mathbf{k}) = \left[iz\hat{\mathrm{I}} - \hat{\mathrm{M}}(\mathbf{k},z)\right]\hat{\Gamma}(\mathbf{k}) \tag{77}$$

This equation suggests that the memory function $\hat{\mathrm{M}}(\mathbf{k},z)$ could represent a dynamical equivalent of the atom - atom direct correlation matrix $\hat{\mathrm{C}}(k)$, which is part of the $\hat{\Gamma}$ matrix as in Eq.(45), similarly like $\hat{\mathrm{M}}(\mathbf{k},z)$ is contained in $\hat{\mathrm{T}}(\mathbf{k},z)$ matrix. Matrix $\hat{\mathrm{T}}(\mathbf{k},z)$ is then supposed to be obtained by the inversion of $\hat{\mathrm{S}}(\mathbf{k},z)$ matrix, which is related to $\hat{\mathrm{S}}(\mathbf{k},\omega)$ with known relation:[56]

$$\hat{\mathrm{S}}(\mathbf{k},\omega) = \lim_{\varepsilon\rightarrow 0}\frac{1}{\pi}\mathrm{Re}\left[\hat{\mathrm{S}}(\mathbf{k},z=\omega+i\varepsilon)\right] \tag{78}$$

2.3.3 Approximations of dynamical correlation functions

We will demonstrate that the self van Hove function can be approximated with a simple Gaussian function. However, it is important to keep in mind that this approximation is valid only in diffusive regime, when $t \to \infty$. The origin of this approximation comes from microscopic diffusion equation, which has identical form as Fick's equation, which describes the dynamics of liquids in hydrodynamic regime. This equation is, in microscopic case, given with: [56]

$$\frac{\partial}{\partial t}\rho^{(s)}(\mathbf{r},t) + \nabla \mathbf{j}^{(s)}(\mathbf{r},t) = 0 \tag{79}$$

,with $\mathbf{j}^{(s)}(\mathbf{r},t)$ being the flux associated with microscopic density $\rho^{(s)}(\mathbf{r},t)$. The solution of equation (79) is given with:[56]

$$\mathbf{j}^{(s)}(\mathbf{r},t) = -D\nabla\rho^{(s)}(\mathbf{r},t) \tag{80}$$

where D is the self-diffusion coefficient. Combining both equations (79) and (80) leads to:

$$\frac{\partial}{\partial t}\rho^{(s)}(\mathbf{r},t) = D\nabla^2\rho^{(s)}(\mathbf{r},t) \tag{81}$$

,which can be written in k-space as:

$$\frac{\partial}{\partial t}\rho^{(s)}(\mathbf{k},t) = -Dk^2\rho^{(s)}(\mathbf{k},t) \tag{82}$$

The solution of equation (82) is given with:

$$\rho^{(s)}(\mathbf{k},t) = \rho^{(s)}(\mathbf{k},t=0)\exp\left(-Dk^2t\right)$$

The autocorrelation function of $\rho^{(s)}(\mathbf{k},t)$ is then given with;

$$F^{(s)}(\mathbf{k},t) = \exp(-Dk^2t) \tag{83}$$

The corresponding van Hove function is given by the inverse Fourier transform of $F^{(s)}(\mathbf{k},t)$: [56]

$$G^{(s)}(r,t) = \frac{1}{(4\pi Dt)^{\frac{3}{2}}}\exp\left[-\frac{r^2}{4Dt}\right] \tag{84}$$

whose time Fourier transform gives the following form for the self dynamical structure factor: [56]

$$S^{(s)}(k,\omega) = \frac{1}{\pi}\frac{Dk^2}{\omega^2 + (Dk^2)^2} \tag{85}$$

In practice, none of these form fits properly the self dynamical correlation of realistic liquids, except in the $t \to \infty$ regime, or equivalently small $\omega \to 0$ limit.

In addition, if we approximate the memory function with:

$$M(k,t) = M(k)\delta(t) \tag{86}$$

we can write the Mori - Zwanzig equation for $F(k,t)$ in form:

$$\frac{\partial F(k,t)}{\partial t} = -M(k)\int_0^t \delta(t-s)F(k,s)\mathrm{d}s \tag{87}$$

which leads to simpler equation for the time evolution of $F(k,t)$:

$$\frac{\partial F(k,t)}{\partial t} = -M(k)\cdot F(k,t) \tag{88}$$

with the solution given with:

$$F(k,t) = F(k,t=0)\cdot \exp\left[-t\cdot M(k)\right] \tag{89}$$

In the section 3.4.7, we will demonstrate that this simple approximation of memory function fails to describe the dynamics in realistic liquids.

2.4 Molecular dynamics simulations

2.4.1 The basic theory of molecular dynamics

In order to start a molecular dynamics simulation of any liquid, it is necessary to have an initial configuration, which determines the starting coordinates and velocities of all atoms composing the liquid. First, atoms are put inside a simulation box of given dimensions, where dimensions are determined by the density of the liquid at desired temperature. Initial velocities are determined by Maxwell distribution at given temperature, such that the total momentum of the system is equal to zero. The time evolution of the system composed of N atoms is then determined with classical equations of motions [56]:

$$m_i \frac{\mathrm{d}^2 \mathbf{r}_i}{\mathrm{d}t^2} = \mathbf{F}_i \; ; \; i = 1, ..., N \tag{90}$$

where i denotes each atom in the system. In order to reach the equilibrium at given thermodynamic conditions, it is necessary to let the system run for a certain period of time [3]. In this work, typical equilibration time was 1 ns for all the system studied.
The force $\overrightarrow{F_i}$ on each atom i is obtained with [3]:

$$\mathbf{F}_i = -\nabla_i V(\mathbf{r}_1, \mathbf{r}_2, ..., \mathbf{r}_N) \; ; \; i = 1, ..., N \tag{91}$$

where the potential V of the system is the function of coordinates of all atoms. Potential V is composed of intramolecular and intermolecular contributions [3]. Intramolecular contribution comes from interactions of atoms inside ("intra") the same molecule, while intermolecular part comes from the interactions between ("inter") different molecules. Hence, intramolecular contribution is related to variations of covalent bond lengths (2 - body contribution), variations of angles between covalent bonds (3 - body contribution) and variations of dihedral angles (4 - body contribution) from equilibrium value.

Intramolecular potentials

The intramolecular contribution related to stretching of the covalent bond between atoms i and j, $V_{ij}^{(b)}$, is usually described with harmonic potential [1]:

$$V_{ij}^{(b)} = \frac{k_{ij}^{(b)}}{2} (r_{ij} - r_{ij}^{(0)})^2 \tag{92}$$

where r_{ij} represents the separation between bound atoms i and j, while $r_{ij}^{(0)}$ is the length of the bond in non - stretched state. Constant $k_{ij}^{(b)}$ depends of the model used. In addition to harmonic potential, anharmonic potentials can be used if necessary, like Morse potential or cubic bond stretching potential [1].

Similarly to $V_{ij}^{(b)}$, the intramolecular contribution $V_{ijk}^{(a)}$, related to vibrations of intramolecular angles, θ_{ijk}, enclosed by bonds between atoms ij and jk, is most commonly described with harmonic potential [1]:

$$V_{ijk}^{(a)} = \frac{1}{2} k_{ijk}^{(a)} (\theta_{ijk} - \theta_{ijk}^{(0)})^2 \tag{93}$$

where $\theta_{ijk}^{(0)}$ represents the angle enclosed by ij and jk bonds in equilibrium state.
Variations of dihedral angle between planes ijk and jkl are taken into account when molecules need to remain planar (like in the case of aromatic rings). The harmonic dihedral potential $V_{ijkl}^{(d)}$ is given with [1]:

$$V_{ijkl}^{(d)} = \frac{1}{2} k_{ijkl}^{(d)} (\xi_{ijkl} - \xi_{ijkl}^{(0)}) \tag{94}$$

where $\xi_{ijkl}^{(0)}$ represents the angle between ijk and jkl planes in equilibrium state. Constants $k_{ij}^{(b)}$, $k_{ij}^{(a)}$, $k_{ij}^{(d)}$, together with $r_{ij}^{(0)}$, $\theta_{ijk}^{(0)}$ and $\xi_{ijkl}^{(0)}$ are characteristic of each model. We note that we used models with rigid bonds in this work, where the length of covalent bonds remains fixed during the simulation.

Intermolecular potentials

Intermolecular potential is composed of Lennard - Jones component, describing Van der Waals interactions, and Coulomb component, as given by equation (1) in the Introduction. Equation for potential energy V, with parameters σ, ε, Z from equation (1), together with $k_{ij}^{(b)}$, $k_{ij}^{(a)}$, $k_{ij}^{(d)}$, $r_{ij}^{(0)}$, $\theta_{ijk}^{(0)}$ and $\xi_{ijkl}^{(0)}$ mentioned earlier in this section, collectively represent a force - field. Force - fields are usually obtained by fitting of the mentioned parameters to the experimental data, usually obtained by thermodynamic or spectroscopic measurements. In this work, SPC/E [189] model of water has been used, while OPLS (united - atom) models have been used to model methanol [71], ethanol [71], DMSO [175] and propylamine [150]. Hexane has been modeled with TraPPE model [104]. Force - field parameters water, methanol and ethanol are shown in Figures 6, 7 and 8 respectively, since these models have been used extensively in this work.

atom	σ / Å	ε / kJmol^{-1}	Z
O	3.16	0.65	- 0.848
H_1	0.0	0.0	0.424
H_2	0.0	0.0	0.424

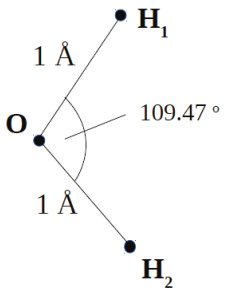

Figure 6: Force - field parameters of SPC/E model of water. Lennard - Jones parameters (σ and ε) and partial charges (Z) are listed in the table for each atom. The sketch on the right side shows the lengths of intramolecular bonds and angles.

atom	σ / Å	ε / kJmol^{-1}	Z
O	3.07	0.17	- 0.700
H	0.0	0.0	0.435
C	3.9	0.49	0.265

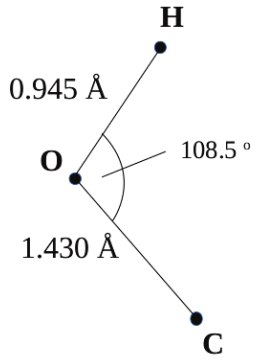

Figure 7: Force - field parameters of OPLS (united - atom) model of methanol. Lennard - Jones parameters (σ and ε) and partial charges (Z) are listed in the table for each atom. The sketch on the right side shows the lengths of intramolecular bonds and angles.

atom	σ / Å	ε / kJmol^{-1}	Z
O	3.07	0.17	- 0.700
H	0.0	0.0	0.435
C	3.9	0.49	0.265
M	3.77	0.87	0.000

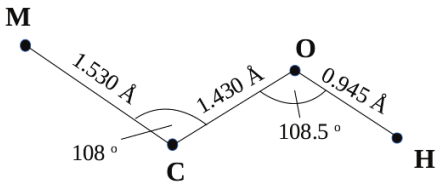

Figure 8: Force - field parameters of OPLS (united - atom) model of ethanol. Lennard - Jones parameters (σ and ε) and partial charges (Z) are listed in the table for each atom. The sketch on the right side shows the lengths of intramolecular bonds and angles.

Integration algorithms

When both intramolecular and intermolecular interactions are known, it is possible to solve equations of motions (90). These equations are commonly solved with the application of numerical algorithms, such as Verlet [173], velocity - Verlet [169], Leapfrog [65] or predictor - corrector algorithm [7]. Verlet algorithm is one of the most commonly used algorithms. If $r_i(t)$, $v_i(t)$ and $\mathbf{a}_i(t)$ represent the position, velocity and acceleration respectively of particle i at time t, it is possible to account for the position at $t+\Delta t$ by the application of Taylor expansion:

$$r_i(t \pm \Delta t) = r_i(t) \pm v_i(t)dt + \frac{1}{2}a_i(t)\Delta t^2 \pm O(\Delta t^3) \tag{95}$$

where $O(\Delta t^3)$ denotes the error in the estimation of the position at $t \pm \Delta t$. If one sums up the $+$ and $-$cases of equation (95), we obtain:

$$r_i(t+\Delta t) + r_i(t-\Delta t) = 2r_i(t) + a_i(t)\Delta t^2 \tag{96}$$

Similarly, if we subtract $-$ case from $+$ case, we obtain:

$$r_i(t+\Delta t) - r_i(t-\Delta t) = 2v_i(t)dt \tag{97}$$

We note that, in order to obtain positions of all particles at $t+\Delta t$, it is sufficient to know the forces ($a_i(t) = \frac{F_i(t)}{m_i}$) at time t on each particle and previous positions ($r_i(t)$ and $r_i(t-\Delta t)$), without knowing the velocities $v_i(t)$ at time t (see equation 96). However, the Verlet algorithm is not "self - starting", meaning that another algorithm should be used in order to obtain $r_i(\Delta t)$ and $r_i(2\Delta t)$.

One of the mathematically analogous variants of Verlet algorithm is known as "velocity - Verlet". In this algorithm, positions at $t+\Delta t$ are obtained with:

$$r_i(t+\Delta t) = r_i(t) + v_i(t)\Delta t + \frac{1}{2}a_i(t)\Delta t^2 \tag{98}$$

, while velocities at $t+\Delta t$ are obtained with:

$$v_i(t+\Delta t) = v_i(t) + \frac{\Delta t}{2}\left[a_i(t+\Delta t) + a_i(t)\right] \tag{99}$$

Although both Verlet (equations 96 and 97) and velocity - Verlet (equations 98 and 99) are mathematically equivalent, velocity - Verlet is self - starting and the involvement of additional algorithms is not neccessary. In addition, this algorithm minimizes roundoff errors. However, it is computationally more demanding, since the storage of velocities is required for each time step.

Finally, we will show the "leap - frog" Verlet's algorithm, which has been used in this work. In

this algorithm, positions at $t + \Delta t$ are calculated based on positions at time t and velocities at mid - step time $t + \frac{1}{2}\Delta t$:

$$r_i(t + \Delta t) = r_i(t) + v_i(t + \frac{1}{2}\Delta t)\Delta t \tag{100}$$

,while velocities are calculated with:

$$v_i(t + \frac{1}{2}\Delta t) = v_i(t - \frac{1}{2}\Delta t) + a_i(t)\Delta t \tag{101}$$

The algorithm is called “leap - frog” because calculation of velocities $v_i(t + \frac{1}{2}\Delta t)$ occurs before (“jumps ahead”) the calculation of positions $r_i(t)$. Similarly to the original Verlet, this algorithm is also not “self - starting”, since the term $v_i(\frac{1}{2}\Delta t)$ requires involvement of additional algorithms. However, this algorithm is time - reversible, which makes it different from previously mentioned algorithms. Time - reversibility is important because it guarantees the conservation of energy, angular momentum and other conserved quantities. For example, this algorithm is ideal for solving problems in orbital dynamics.

Since molecular dynamics simulations deal with systems of finite size (i.e. with certain number of particles put in simulation box of given size), it is necessary to minimize finite - size effects, in order to obtain results which resemble real macroscopic systems as much as possible. This can be conveniently done by the application of periodic boundary conditions [3] on selected integrational algorithm. Periodic boundary conditions imply the existence of infinite number of copies of the simulation box, as illustrated in Figure 9, where the simulation box is shown in the center (grey particles). As one particle leaves the box (indicated with the arrow), it re - enters the box from the other side. The positions and momenta of all particles are the same in all the boxes.

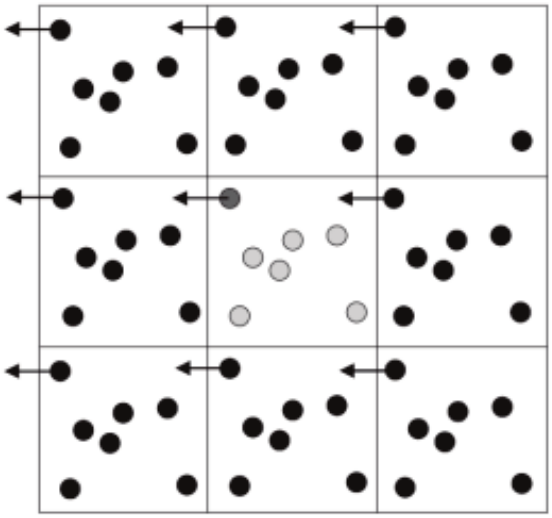

Figure 9: Visualization of periodic boundary conditions. Central box (filled with grey particles) represents the simulation box, while surrounding boxes (filled with black particles) represent copies of the central box. Positions and momenta of all particles are the same in all copies of the central box. Once a particle leaves the central box, it re - enters on the other side, as illustrated with black arrows.

When considering particularly interactions between particles, where inter-particle separation plays a key role, minimum image convention [3] needs to be applied, in order to prevent accounting for the same particle twice (once in the original box and once in the copy). Let us consider two particles, A and B, with respective coordinates (x_A, y_A, z_A) and (x_B, y_B, z_B), which are put in the simulation box of dimensions (L_x, L_y, L_z). The x - separation between the particles is $\Delta x = |x_A - x_B|$. If $\Delta x < \frac{L_x}{2}$, the Δx is taken into account for computation of inter-particle potential. However, if $\Delta x > \frac{L_x}{2}$, the Δx needs to be corrected, such that it represents the x - separation between nearest copies of particles A and B:

$$\Delta x^{'} = L_x - \Delta x \tag{102}$$

The same needs to be applied for Δy and Δz, if $\Delta y > \frac{L_y}{2}$ and $\Delta z > \frac{L_z}{2}$:

$$\Delta y^{'} = L_y - \Delta y \tag{103}$$

$$\Delta z^{'} = L_z - \Delta z \tag{104}$$

We note that minimum image convention is essential also for the computation of dynamical quantities, such as Van Hove functions, as it will be shown later on.

Temperature and pressure coupling

In order to calculate statistical quantities of a simulated system, simulations are run in different types of statistical ensembles. An ensemble represents the collection of all possible microstates for which certain thermodynamical properties are constant. For example, in canonical ensemble, N (number of particles), V (volume) and T (temperature) are kept constant. In isothermal - isobaric ensemble, N,T and p (pressure) are constant [48]. It is important to note that all ensembles are equivalent in the thermodynamic limit, so the thermodynamic properties of a system can be calculated as an average in any ensemble (or the most convenient one) [3].

In order to keep the temperature or pressure constant in simulation, we use different thermostat or barostat algorithms. Let us consider the most simple thermostat - velocity re-scaling thermostat [3]. In the system with $3N$ degrees of freedom, temperature at time t, $T(t)$,is related to the total kinetic energy K of the system with:

$$\frac{K}{3N} = \frac{k_{\mathrm{B}} T(t)}{2} \tag{105}$$

where the total kinetic energy K is defined with:

$$K = \sum_{i=1}^{3N} \frac{m v_i^2}{2} \tag{106}$$

which leads to the expression for temperature T:

$$T(t) = \frac{2}{3N k_{\mathrm{B}}} \sum_{i=1}^{3N} \frac{m v_i^2}{2} \tag{107}$$

If one wants to change the temperature of the system from $T(t)$ to T_0 (bath temperature), one possibility is to scale the velocities v_i with factor λ:

$$T_0 = \frac{2}{3N k_{\mathrm{B}}} \sum_{i=1}^{3N} \frac{m(\lambda v_i)^2}{2} = \lambda^2 T(t) \tag{108}$$

with λ being equal to:

$$\lambda = \sqrt{\frac{T_0}{T(t)}} \tag{109}$$

Another modification of velocity - re-scaling thermostat is Berendsen thermostat [10], where the deviation ΔT from from the bath temperature T_0 relaxes according to the equation:

$$\frac{\Delta T}{\mathrm{d}t} = \frac{T_0 - T(t)}{\tau_T} \tag{110}$$

where dt is equal to the time step in simulation, while τ_T is the time constant attributed to the thermostat. We note that, if we choose $\tau_T = \mathrm{d}t$, we obtain the thermostat analogous to simple velocity - re-scaling. If τ_T is too large, thermostat becomes inactive, since large amount of time is required to damp temperature deviations from the bath temperature. With τ_T being too small, system exhibits non - realistic temperature fluctuations. In molecular dynamics simulations of liquids, typical value of τ_T is 0.4 - 0.5 ps for equilibrium runs, while equilibration is usually performed with $\tau_T = \mathrm{d}t$. Finally, the velocity - re-scaling factor is, in the case of Berendsen thermostat, equal to:

$$\lambda = \sqrt{1 - \frac{\mathrm{d}t}{\tau_T}\left(\frac{T_0}{T(t - \frac{\mathrm{d}t}{2})} - 1\right)} \tag{111}$$

,with the temperature $T(t - \frac{\mathrm{d}t}{2})$ being calculated at $t - \frac{\mathrm{d}t}{2}$ due to the application of leap - frog algorithm. We note that both simple velocity - re-scaling and Berendsen thermostat affect fluctuations of kinetic energy. Therefore, rigorously speaking, this thermostat does not generate proper canonical ensemble. However, this error scales with $1/N$ and is, therefore, small in the case of very big systems. Hence, most of ensemble averages will remain unaffected for large systems. However, in order to reproduce canonical ensemble more accurately, Nose - Hoover thermostat [120][66] could be used.

The control of the system pressure can be achieved by application of Berendsen barostat [10], which is equivalent to its temperature counterpart:

$$\frac{\Delta P}{dt} = \frac{P_0 - P}{\tau_P} \tag{112}$$

,with τ_P being the time constant analogous to τ_T. Instead of velocity scaling, the scaling of coordinates and box sides is performed, with the scaling factor η:

$$\eta = 1 - \frac{\kappa_T \mathrm{d}t}{3\tau_P}(P_0 - P) \tag{113}$$

,with κ_T representing isothermal compressibility. Since κ_T affects only the time constant τ_P of the pressure relaxation, and not the average pressure itself, its value can be estimated. For example, many molecular dynamics program packages use the compressibility of water ($\kappa_T = 4.5 \cdot 10 - 5\ \mathrm{bar}^{-1}$) at ambient conditions [46]). However, this barostat does not account for pressure fluctuations accurately. This is why this barostat is ideal for equilibration purposes, while production runs can be performed with Parrinello-Rahman barostat [124, 125], analogously to previously mentioned Nose - Hoover thermostat, if precise pressure fluctuations need to be accounted for.

2.4.2 Liquidlib program package

In this work, modified version of Liquidlib program package [180] has been used for the calculation of Van Hove correlation functions. The modification has been done by our group and was needed because the original version of the program did not account for the asymptotes ($r \to \infty$) of the Van Hove function correctly, due to an error in the application of minimum image convention on the calculation of mentioned functions. Furthermore, the original package was able to perform calculations of Van Hove functions only for correlations between same atom types (e.g. OO correlations). However, for the purposes of this work, correlations between different atom types were also required (e.g. OH correlations) so we modified the code accordingly, such that it accounts for those correlations also. In the rest of this section, we will briefly outline the basics of how this program package operates.

In order to calculate Van Hove correlations, Liquidlib uses trajectories as the input, which can be in .trr, .xtc, .xyz or .dump format. Our trajectories were generated by Gromacs program package [61, 147, 172] so we used trajectories in .trr format. Trajectories contain positions and velocities of all particles in the system for the series of time frames from $t = 0$ until $t = T$, spaced by chosen Δt. For the purpose of this calculation, velocities were not required, but merely atomic positions.

In order to calculate the total Van Hove function at time $t = \tau$, $G(r, \tau)$, for the case of correlations between atoms X (reference atoms) and Y, program does the following. First, the time frame $t = 0$ is read from the trajectory and positions of all reference atoms (i.e. X atoms) are taken as origins. We denote those origins with $O_i^{(0)}$, with $i = 1, ..., N$, where N represents the number of X particles in the system, while superscript (0) indicates that origins are taken from the time frame $t = 0 \cdot \Delta t$. Then, the histogram $H_0(r)$ of number of Y particles from the time frame $t = \tau$ is made, where r represents the distance of Y particle from the origin:

$$H_0(r) = \sum_{O_i^{(0)}} n_i(r, r + \mathrm{d}r) \tag{114}$$

,where $n_i(r, r + \mathrm{d}r)$ represents the number of Y particles in a sphere shell of radius r and thickness dr, centered at the origin $O_i^{(0)}$.
After all origins $O_i^{(0)}$ from time frame $t = 0$ have been accounted for and histogram $H_0(r)$ is completed, program switches to the next time frame ($t = 1 \cdot \Delta t$) and makes histogram $H_1(r)$ of number of Y particles from the time frame $t = \tau + \Delta t$, with origins $O_i^{(1)}$ now corresponding to positions of X particles in time frame $t = 1 \cdot \Delta t$. The same procedure is done repetitively untill finally the histogram H_f is calculated, with f denoting the number of frames over which the

statistical average is performed. Ultimately, the total histogram H_{total} is equal to:

$$H_{total}(r) = H_1(r) + H_2(r) + ... + H_f(r) \tag{115}$$

Here, we are interested in averaged histogram:

$$\overline{H(r)} = \frac{H_{total}(r)}{Nf} \tag{116}$$

where $\overline{H(r)}$ represents the average number of Y particles at distance r from the origin at time τ, assuming that the density of X particles at the origin is non - zero at $t = 0$.
In order to obtain total Van Hove function, averaged histogram is normalized with the differential volume of the sphere shell:

$$G(r,\tau) = \frac{\overline{H(r)}}{4\pi\rho_Y r^2 \mathrm{d}r} \tag{117}$$

with ρ_Y representing the density of Y particles in bulk.
Self - Van Hove function, $G_s(r,\tau)$ is calculated in similar fashion, with the exception that $n_i(r, r+\mathrm{d}r)$ (see equation 114) now only accounts for the particle which was located at origin $O_i^{(k)}$ at $t = k \cdot \Delta t$. Hence, $n_i(r, r+\mathrm{d}r)$ can be either 0 or 1. Histogram $\overline{H(r)}$ obtained in this way can be seen as the probability that particle diffuses distance between r and $r+\mathrm{d}r$ during time interval τ. After $G_s(r,\tau)$ is obtained, distinct Van Hove function $G_d(r,\tau)$ can be obtained by simple subtraction: $G_d(r,\tau) = G(r,\tau) - G_s(r,\tau)$.

We noted earlier that the application of minimum image convention is required for the computation of Van Hove functions. Minimum image convention needs to be applied because the calculation of Van Hove functions is based on calculation of inter - atomic separations. For each separation, it is necessary to make sure that the distance between the nearest copies of atomic pairs is taken into account, such that same pairs are not accounted for multiple times into statistics.

After Van Hove functions are known, $F(k,t)$ and $S(k,\omega)$ can be obtained by simple space and time Fourier transformations, according to equations (118) and (119) [56]:

$$F(k,t) = \int_0^\infty G(r,t)\exp(-i\mathbf{kr})\mathrm{d}\mathbf{r} \tag{118}$$

$$S(k,\omega) = \int_{-\infty}^\infty F(k,t)\exp(-i\omega t)\mathrm{d}t \tag{119}$$

Results

3

3 Results and Discussion

3.1 Static structural properties of associative systems - the basics for dynamics

3.1.1 Water

The importance of water in our daily life and biological activity is very well-known. Water is known for numerous anomalies. [19, 21, 47, 49, 121, 156, 91] One such anomaly is the existence of a density maximum at 4^{o}C under ambient conditions. Naturally, this feature is absent from simple liquids, where the density monotonically decreases with increasing temperature. The existence of this density maximum causes the density of solid phase to have lower density than the liquid phase, which is visible simply in the fact that ice floats in the liquid. Moreover, thermodynamic response functions, such as specific heat capacity (c_P), isothermal compressibility (κ_T) and thermal expansion coefficient (α_P) also show anomalous behavior. While isothermal compressibility of simple liquids monotonically increases with increasing temperature, in the case of water, this occurs only for temperatures $t > 46^{o}$C, while, at lower temperatures, isothermal compressibility of water increases with decreasing temperature, exhibiting its minimum at $t = 46^{o}$C. Another specificity of water is hidden in the unusual behavior of it specific heat capacity (c_P), which increases with decreasing temperature when $t > 35^{o}$C. Normally, in simple liquids, specific heat monotonically decreases with decreasing temperature. Moreover, linear expansion coefficient (α_P) of water becomes negative at $t < 4^{o}$C, indicating that the volume increases with decreasing temperature, which is in accordance with the density anomaly mentioned earlier. The physical origin of these anomalies has not been completely understood yet. However, it is commonly accepted that anomalous behavior of various properties of water must be related to specificities in hydrogen bonding network of water.[19, 21, 47, 49, 121, 156, 91] This is precisely why water has been the subject of numerous studies recently. In this work, water is important because it is the simplest representative of hydrogen bonding species, consisting only of oxygen and hydrogen atoms. In this context, water can be seen as a crossover between simple liquids, which do not form hydrogen bonds, and more complex associative liquids, like alcohols, which consist of additional alkyl group of atoms covalently bound to hydrogen bonding hydroxil groups. Hence, understanding dynamics of water is a precursor for understanding dynamics of associative species in general.

In this subsection, well-known static structural properties of water, which are essential for understanding dynamics, will be presented and discussed. Structure factor, which is the main observable in experiments, will be taken as the starting point. Structure factors obtained by X-ray diffraction experiments and by SPC/E water model is presented on Figure 10 (taken from Ref.[131]). Since X-rays mostly interact with electron clouds around nuclei of atoms, hydrogen atom of water is nearly invisible in this type of experiments. [69] This means that

the total structure factor obtained by experiments (represented by circles on Figure 10) mainly describes structural arrangement of O atoms in the liquid. This explains why the experimental data shows fairly good agreement with OO partial structure factor (red line on Figure 10) obtained in computer simulations.

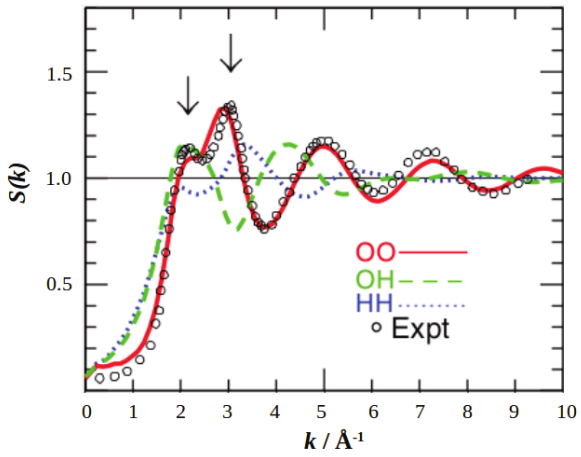

Figure 10: Structure factor of water obtained by experiments (circles) and partial structure factors of OO (red), OH (green) and HH (blue) contributions obtained by SPC/E model of water. Figure taken from Ref.[131]

Structure factor of water is characterized by the split-peak feature (indicated by the arrows in Figure 10), consisting of the inner (smaller) peak at $k \approx 2$ Å^{-1}, and the outer (taller) peak at $k \approx 3$ Å^{-1}. The inner peak, which would correspond to $r \approx 3.14$ Å, has been interpreted as the main diffraction peak. [127, 160, 158] Indeed, for simple liquids, like Lennard-Jones (LJ) liquid for example, the main diffraction peak is always centered at $k \approx \frac{2\pi}{\sigma}$, where σ is the atomic diameter of LJ particle [131]. However, the diffraction patterns of simple liquids do not exhibit split-peak feature, which poses the question about the nature of the split-peak found in structure factor of water. In order to further discuss the differences between simple liquids and water, it would be useful to compare the structures of these two systems by analyzing $g(r)$ and $S(k)$ functions. Figure 11 shows functions $g_{OO}(r)$ (main panel) and $S(k)$ (inset) of water (blue lines) and simple LJ liquid (red lines), where the value of LJ parameter σ is equal to 3.16 Å, the length of diameter of O atom in water.

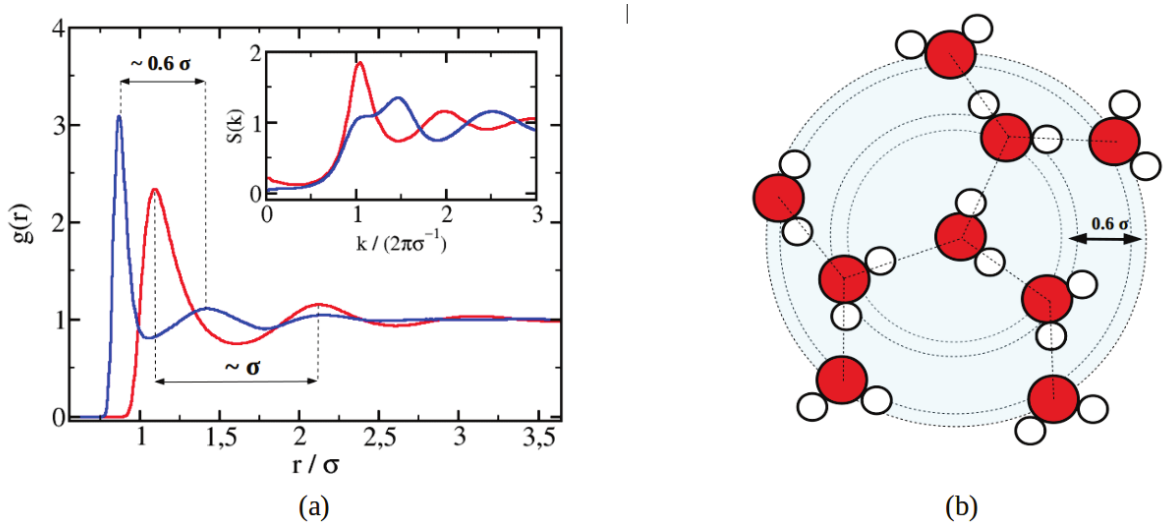

Figure 11: (a) Main panel: radial distribution functions $g_{OO}(r)$ of simple LJ liquid (red line) and water SPC/E (blue line) obtained by molecular dynamics simulations Inset: Structure factors $S_{OO}(k)$ of simple LJ liquid (red line) and water SPC/E (blue line) obtained by Fourier transformation of $g_{OO}(r)$ functions from the main panel. (b) 2D illustration of the shell structuring in water. The two-sided arrow indicates the separation between the first two maxima of radial distribution function $g_{OO}(r)$ of water.

The main panel of Figure 11 shows two marked differences between $g_{OO}(r)$ functions of LJ liquid and water. The first difference is related the r-position of the the first maximum of $g(r)$, which is shifted to smaller r-value for water. The second difference is related to the period of spatial oscillations of $g(r)$, which is smaller for water ($\sim 0.6\ \sigma$) than for LJ liquid ($\sim \sigma$), as shown in Figure 11. Let us discuss these differences in more details, starting from the observed shift of the first maximum. In LJ liquid, particles interact with LJ potential. This potential is strongly repulsive at distances shorter than atomic diameter σ, while it is attractive at higher distances. In such liquid, the characteristic separation between first neighbours is found at nearly 1.1 σ, as shown in Figure 12a. This separation corresponds exactly to the r-position of the first maximum of $g(r)$ for LJ case in Figure 11 a.

The distribution of $g(r)$ around $r \approx 1.1\ \sigma$ represents a measure of probability of finding first neighbours at some particular distance. Clearly, this probability is the highest for $r \approx 1.1\ \sigma$, meaning that the probability of particularly this separation between first neighbours is the highest. As slowly shifting from this distance to shorter distances, the probability gradually decreases until it finally reaches nearly zero value at $r \approx 0.9\ \sigma$. This is the critical separation at which repulsive LJ force becomes too strong, leading to great majority of particles being repelled from further approaching. However, in the case of water, this critical distance is somewhat shorter, being at $r \approx 0.75\ \sigma$ instead of $r \approx 0.9\ \sigma$. Moreover, the first maximum appears at $r \approx 0.85\ \sigma$ instead at $r \approx 1.1\ \sigma$, as in LJ case.

This shift of the first maximum towards smaller r-value is direct consequence of the fact that water is a polar molecule, with oxygen atom being negatively charged and hydrogen atom positively charged. Positively charged hydrogen atom and negatively charged oxygen atoms of distinct molecules interact with Coulomb interaction, the interaction which is absent in LJ liquid composed of non-polar particles. At distances $r \sim \sigma$, attractive Coulomb interaction between unlike charges dominates repulsive LJ potential, leading to the overall shift of first neighbours shell at shorter distances, as depicted in Figure 12b. Furthermore, we observe that the distribution of $g(r)$ of water around the first maximum is much narrower than the same distribution in LJ liquid. This feature demonstrates how Coulomb interaction reduces the possible distances between first neighbours inside very short interval around first maximum. This interval is much wider in case of LJ liquid, which is characterized by the absence of Coulomb potential.

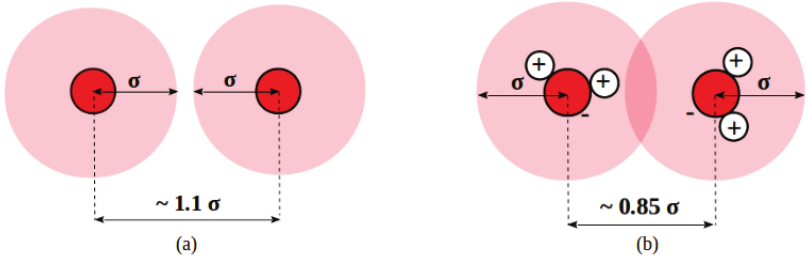

Figure 12: Illustration of the OO average separation between the first neighbours in simple LJ liquid (a) and water (b)

Let us now discuss the second major difference of $g_{OO}(r)$ functions illustrated in Figure 11, related to the period of spatial oscillations of these functions. As shown in the figure, $g_{OO}(r)$ of water is characterized by shorter oscillatory period ($\sim 0.6\,\sigma$) than LJ liquid ($\sim \sigma$), indicating that the separation between the centers of the first and second coordination shell is shorter in water than in LJ liquid. At this point, one potentially might ask how it is possible to have any oxygen atoms of water at separation as small as $0.6\,\sigma$. When the main features of the first maxima were discussed, we stated that the critical value at which first neighbours can be separated is found at $r \approx 0.75\,\sigma$ for water, indicating that shorter separations between the first neighbours, such as $0.6\,\sigma$, are highly unlikely. Hence, previous arguments might seem contradictory, since the separation between first and second neighbours seems to be precisely $0.6\,\sigma$.

The key point here is that the separation of $0.6\,\sigma$ does not correspond to the distance between first and second neighbours, but to the distance between first and second neighbours *shell*s. Separation of two atoms which are located in shells separated by distance d can be much bigger than d. Distance d is the minimum possible distance between the atoms, which realizes only in the case when both atoms are located along the same radial direction from the origin. This is illustrated in Figure 11b, where the 2D arrangement of water molecules is presented,

with the characteristic separation between first and second neighbours shell being 0.6 σ. In this example, the distance between any oxygen atom within the first shell and any oxygen atom of the second shell is clearly bigger than 0.6 σ. Although this is a 2D illustration, the same conclusions can be applied also for real 3D water, which is characterized by well-known tetrahedral arrangement of molecules, induced by hydrogen bonding. In this type of arrangement, tetrahedral angular restrictions lead to characteristic charge ordering of molecules into shells spaced by characteristic 0.6 σ distance. This arrangement is manifested as the successive appearance of peaks separated by 0.6 σ in radial distribution function $g_{OO}(r)$ of water. Conversely, LJ liquid is characterized by ordinary disorder characteristic to any simple liquid. In this type of packing, atoms are distributed in shells spaced by characteristic σ separation, which is manifested as the successive appearance of peaks separated by σ in radial distribution function $g_{OO}(r)$ of LJ liquid.

However, this analysis would be incomplete without discussing the tail details of both radial distribution functions shown in Figure 11 (left panel), since oscillatory features of the two functions are preserved even at distances larger than 3.5 σ, which was taken as the upper limit in the Figure 11. The details of these functions at larger r-values are shown in Figure 13. In the case of LJ liquid, we note the same spatial period of oscillations (σ) as in earlier analysis from Figure 11. However, $g(r)$ of water shows additional feature which was not obvious in Figure 11. On this scale, packing structure of water seems to oscillate with period σ, which is visible from the fact that both functions exhibit peaks at $k \approx 2.25\ \sigma$, $k \approx 3.25\ \sigma$ and $k \approx 4.25\ \sigma$, as seen from Figure 13. However, we note that the peak at $k \approx 3.25\ \sigma$ of $g(r)$ of water is split into two smaller peaks separated by approximately 0.6 σ, which corresponds to the spatial period deduced earlier by the analysis from Figure 11. Hence, packing structure of water seems to be dominated by two spatial frequencies, the first being determined with period σ, while the second one by period 0.6 σ. The latter seems to dominate the shape of radial distribution function at shorter distances (see Figure 11) , while the latter one at larger distances (see Figure 13). Conversely, radial distribution function of simple LJ liquid is dominated by one single spatial period, σ, at all distances (see 11).

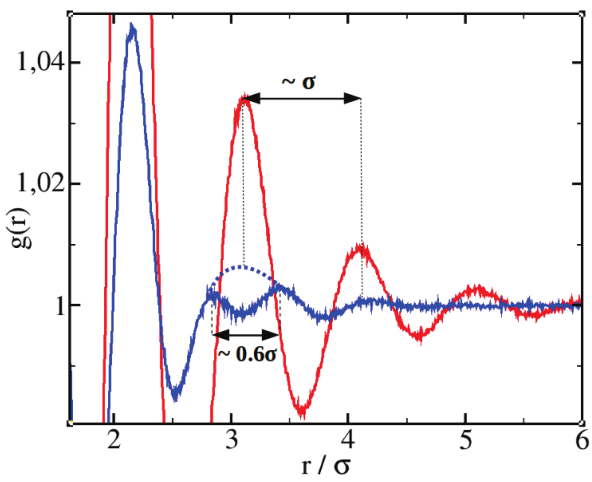

Figure 13: Zoomed view on $g(r)$ functions from the main panel of Figure 11a

At this point we are in good position to discuss the main properties of structure factors of simple LJ liquid and water, which are presented in the inset of Figure 11 (left panel). The main diffraction peak of simple LJ liquid is found at $k \approx 2\pi\sigma^{-1}$, while the structure factor of water exhibits split-peak feature mentioned earlier, consisting of the inner (smaller) peak at $k \approx 2\pi\sigma^{-1}$, and the outer (taller) peak at $k \approx 3\pi\sigma^{-1}$. This leads us to the already posed question about the origin of the split-peak feature. In reciprocal space, the value $k \approx 2\pi\sigma^{-1}$ corresponds to $r \approx \sigma$ in real space, while $k \approx 3\pi\sigma^{-1}$ corresponds nearly to $r \approx \frac{2}{3}\sigma$. One can immediately notice that the two r-values, σ and $\frac{2}{3}\sigma$, correspond to oscillatory periods of radial distribution functions discussed earlier. Hence, the split-peak feature of the structure factor of water appears as the consequence of the fact that $g(r)$ of water oscillates with 2 dominant spatial frequencies, while $g(r)$ of simple LJ liquid exhibits a single dominant spatial frequency. The description of water structure in terms of two fundamental spatial frequencies is in agreement with the general idea of water being a mixture of charge ordered tetrahedral liquid and ordinary disordered liquid found in the literature [131, 160]. In this context, charge order in water, which is induced by dominant Coulomb field, is manifested through the appearance of higher spatial frequency (i.e. lower spatial period 0.6 σ) in $g(r)$ correlations, whereas the ordinary disordered behavior is manifested through the lower spatial frequency (i.e. larger spatial period σ). The latter frequency is also present in $g(r)$ of simple liquids. Consequently, dual behavior of water is manifested as the split-peak feature of water structure factor.

In the literature, split-peak feature is commonly interpreted as a signature of tetrahedrality in water.[117, 159, 160] Indeed, the strong sensitivity of the two maxima to variation of temperature has been observed in various works. [127, 158, 117] There, it was shown that the amplitudes of the two diffraction peaks increase upon cooling, forming two well-defined distinct maxima in form of two distinct peaks, instead of being merged in almost one single peak as in higher temperatures. Since it is well-known that tetrahedrality of water structure enhances

upon decreasing temperature [127, 158, 117], the sensitivity of the split-peak structure on temperature change clearly demonstrates the relation with tetrahedrality and, consequently, with charge ordering. In our interpretation, the inner peak (IP) of the structure factor reflects the disordered nature of water structure similar to the structure of ordinary simple liquids, while the outer peak (OP) reflects the charge ordered nature of the structure, realized through strong tetrahedral ordering. Moreover, charge ordered structure could be seen as some type of substructure inside globally disordered structure of water. This interpretation is inspired by result presented in Figure 13, where we see that the peak at $r \approx 3\sigma$ appears in form of two distinct subpeaks separated by 0.6σ. Hence, these two sub-peaks represent two distinct sub-shells formed due to charge ordering. These two sub-shells can be seen as part of one big shell centered at $r \approx 3\sigma$ (shown with dotted blue lines in Figure 13), representing globally disordered structure of water. Interestingly, this big shell is centered at the same r-value as the one corresponding to simple LJ liquid, which further supports this argument. In this context, structure of water can be seen as superposition of charge ordered structure and disordered structure. As a consequence of this structure duality, the main diffraction peak appears in form of two sub-peaks, as shown earlier.

3.1.2 Alcohols

Structure of alcohols has been the subject of research for long time, primarly because scattering experiments of alcohols show interesting features in low-k interval of the structure factor. These features are related to the appearance of pre-peak in k-region 0.3 Å - 1.0 Å. Structure factors from literature obtained experimentally for linear monols are presented in Figure 14 [146].

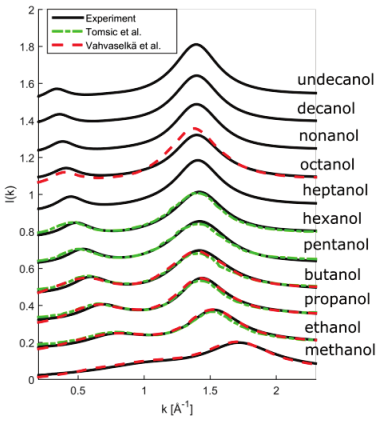

Figure 14: Structure factors of linear monols obtained experimentally. Figure taken from Ref. [143]

Figure 14 shows that the k-value at which pre-peak appears (k_P) decreases systematically when going from lower to higher alcohols [146]. We note that the structure factors presented in Figure

14 are the total structure factors, which means that they contain contributions of all atom-atom correlations in the liquid.

In order to interpret the shift of the pre-peak to lower k-values when going from lower to higher alcohols, it is useful to compare particularly $g(r)$ and $S(k)$ functions describing OO correlations in alcohols versus water. Radial distribution functions of water, methanol and ethanol are shown in the main panel of Figure 15 in black, red and green colors respectively. The insets show show the tail properties of $g(r)$ which are not visible in the scale of the main panel. RDF-s of alcohols show marked differences in comparison with the RDF of water, namely the first peak exhibits higher amplitude in case of alcohols, followed by depletion of the first minimum. The amplitude of the first peak increases as going from lower to higher alcohol. Higher amplitude of the first peak is the consequence of the fact that the bulk density ρ of oxygen atoms is lower in higher alcohols than in lower alcohols. In this context, it is useful to remind that $g(r)$ represents the ratio of local density at distance r from the origin ($\rho_L(r)$) with the bulk density (ρ). Hence, if $\rho_L(r)$ for specific r is the same for both alcohols, the peak corresponding to higher alcohol will have higher amplitude, since the denominator of the ratio $\frac{\rho_L(r)}{\rho}$ will be lower in the case of higher alcohol. Therefore, the large difference in the amplitudes of the first peaks observed in Figure 15 is mostly the consequence of the difference in bulk density ρ of the 3 systems. If the amplitude of the first peak happened to represent the measure of purely the number of first neighbours, the amplitude for water would be the highest, since water molecules form in average 3-4 hydrogen bonds, while methanol and ethanol form 2 [152, 141, 5].

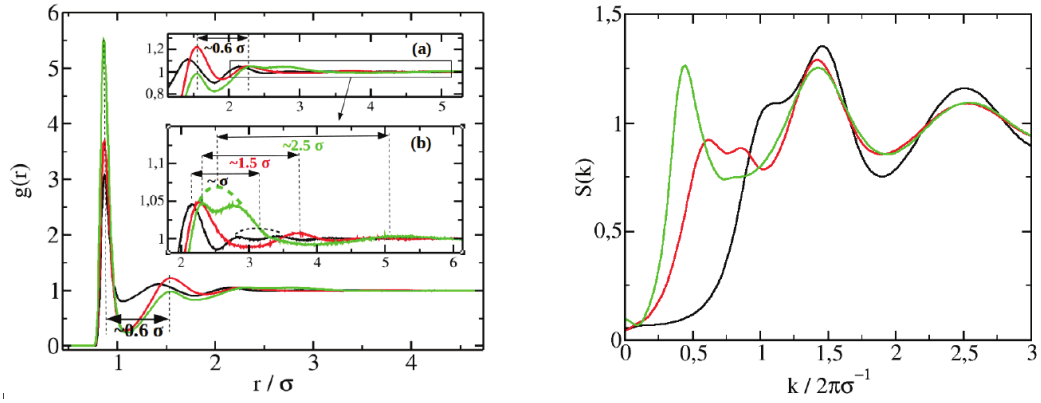

Figure 15: Radial distribution functions $g_{OO}(r)$ of water SPC/E (black line), methanol OPLS (red line) and ethanol OPLS (green line) obtained by molecular dynamics simulations. Insets (a) and (b) show zoomed views on the same functions.

Turning our attention now to the depletion of the first minimum in RDF of alcohols comparing to water, this feature reflects the nature of linear aggregation, which reduces the number of second neighbours in chain-like aggregate [133, 143]. This phenomenon is illustrated in Figure 16, where comparison of shell structuring in water (left panel) and ethanol (right panel) is presented. Clearly, structure of ethanol is characterized by reduced number of neighbours in

second coordination shell, which is manifested as depletion of the first minimum in RDF.

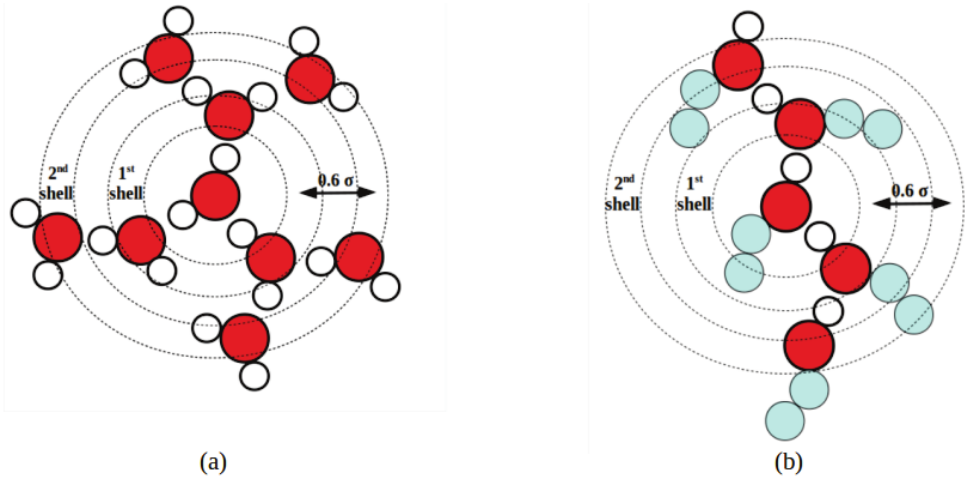

Figure 16: Illustration of the shell structuring in water (a) and ethanol (b)

Furthermore, we note that the distance between first and second neighbours shell (0.6 σ) is nearly the same for water and alcohols, as demonstrated in the main panel of Figure 15 and in Figure 16. In addition, the distance between second and third neighbours shell is also characterized by the same distance, as shown in the inset (a) of Figure 15. This indicates that short ranged correlations of both water and alcohols, which describe charge ordering, are characterized by the same spatial period of density correlations (0.6 σ), the value which in reciprocal space would correspond to $k \approx 3\pi\sigma^{-1}$. Indeed, all 3 systems exhibit a diffraction peak at precisely this $k-$value, as it will be shown later in the discussion.

Now we put focus on the inset (b) which shows long-ranged density correlations of all 3 systems. This inset illustrates how the period of the density correlations increases when moving from water (σ) to methanol (1.5σ) and ethanol (2.5σ), the values which in reciprocal space would correspond to k-values of $2\pi\sigma^{-1}$,$\frac{4}{3}\pi\sigma^{-1}$and $\frac{4}{5}\pi\sigma^{-1}$respectively. Let us now put our attention to OO partial structure factors of all three systems, which are presented in Figure 15b, with the same color convention as in the left panel. Starting from pre-peaks, we note that the pre-peaks of methanol and ethanol are centered at $k \approx \frac{4}{3}\pi\sigma^{-1}$ and $k \approx \frac{4}{5}\pi\sigma^{-1}$, which are exactly the $k-$values which correspond to the periods of long-ranged density correlations in methanol and ethanol, as presented in the inset (b) of Figure 15. Therefore, pre-peaks of the structure factor describe periodicity of long-ranged correlations in a specific system. Previous works of this group have shown that the period of long-range OO correlations increases when moving from lower to higher alcohols [143]. This is a reasonable result and can be explained as follows. Function $g_{OO}(r)$ can be seen as histogram (normalized with $4\pi\rho r^2$) of number of atoms O at specific distance r from the reference atom O. When r is small, $g_{OO}(r)$ is dominated by contribution of atoms which are part of the same cluster as the reference atom. This is the consequence of the fact that OH clusters are mutually separated by alkyl groups, as explained in

the Introduction. Hence, within close neighbourhood of the reference atom O, $g_{OO}(r)$ is dominated by neighbouring O atoms within the *same* aggregate. However, when r is sufficiently large, contribution of O atoms from neighbour*ing* aggregates becomes more significant. These atoms are not distributed around the reference atom like they would be in simple disordered liquid, but their distribution is governed by the existence of neutral alkyl groups, which form barriers between OH aggregates. The size of these barriers depends on the size of alkyl tails and, consequently, grows with the size of alcohol molecule. Hence, looking from the origin point of reference atom O, liquid at large distances will be seen as field of varying density of O atoms, where the density changes radially when going from smaller to larger distances from the origin.

It is important to note that even simple liquids can be interpreted in this fashion, since long-range density correlations of simple liquids also appear in form of oscillations around $g(r) = 1$. However, the period of these oscillations in simple liquids is governed by atomic diameter σ, while, in alcohols, it is governed by the size of alkyl tails. Therefore, the period of long-range OO correlations in alcohols can be interpreted as an average distance between OH aggregates in the liquid. Since pre-peaks of alcohols are centered exactly at k-value corresponding to the period of these oscillations, pre-peaks contain information about the average distance between aggregates in a liquid, which has been one of the proposed interpretations of the pre-peak in the literature [185].

Besides the pre-peak, structure factor of both alcohols exhibit the main peak centered at $k \approx 3\pi\sigma^{-1}$, similarly like water. The origin of this peak is similar to the one for water and is caused by the same short-range periodicity of density correlations in both methanol and ethanol, with the characteristic period 0.6 σ, as illustrated in the main panel of Figure 15 and in the inset (a) of the same figure. However, in addition to the pre-peak and the main peak, structure factors of both alcohols show an intriguing bump in correlations at $k \approx 2\pi\sigma^{-1}$, centered at the same k-position as the inner peak of water structure factor. In the context of water, this peak was interpreted in terms of σ periodicity of long-range density correlations in water. However, according to results presented in Figure 15, long-range density correlations of alcohols do not show such periodicity. In order to interpret this intriguing bump in correlations at $k \approx 2\pi\sigma^{-1}$ of both structure factors of alcohols, we will decompose the total $g(r)$ of both alcohols into 2 components, as presented in the main panels of Figure 17. The first component is sigmoidal step function, while the second component is oscillatory part. The sum of the two components gives the total $g(r)$ functions.

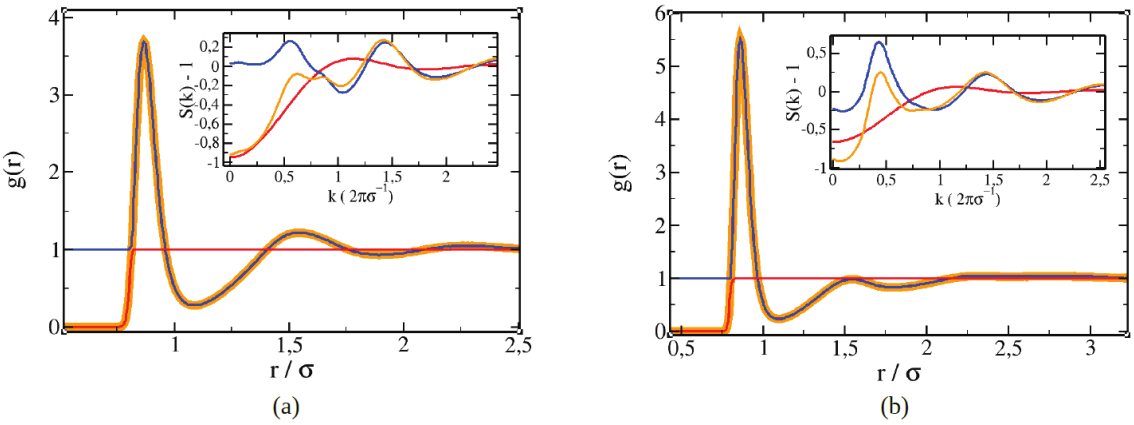

Figure 17: Main panels: Decomposition of the total $g_{OO}(r)$ functions (orange line) of methanol OPLS (a) and ethanol OPLS (b) into sigmoidal step function (red line) and oscillatory part (blue line). Insets: Fourier transformations of the functions from the main panels, with the same color convention.

The main panels of Figure 17 show $g(r)$ functions of methanol (left panel) and ethanol (right panel) in orange. The sigmoidal step parts are shown in red, while the oscillatory parts are shown in blue color convention. Fourier transforms of the functions from the main panel are shown in the insets by using the same color convention. We note that the FT of the step part produces a peak at $k \approx 2\pi\sigma^{-1}$ in both cases. In the case of methanol, this peak emerges in the total $S(k)$ function as small shoulder-peak at $k \approx 2\pi\sigma^{-1}$next to the pre-peak, whereas, in the case of ethanol, this peak emerges as plateau around the same k-value. Hence, the intriguing bumps at $k \approx 2\pi\sigma^{-1}$ of both structure factors are mathematical consequence of performing FT of the step function. This function describes sudden jump in density of neighbouring atoms when moving from close vicinity of the origin ($r < 0.75\ \sigma$), characterized by strong repulsive forces between interacting atoms, to larger distances. The jump of the step function occurs at r position which corresponds to the distance of the first coordination shell from the reference atom. Therefore, the bump at $k \approx 2\pi\sigma^{-1}$ of the structure factors describes first neighbours contact interactions, similarly like the small inner peak in the case of water which we discussed earlier.

The main message of this section is that structure of any liquid, usually described by radial distribution function, can be seen as superposition of density correlations of different spatial frequencies. High-frequency (i.e. small period) correlations describe the details in the liquid structure, whereas low-frequency correlations (i.e. large periods) describe the global features of the liquid. In reciprocal k-space, global trends are manifested as specific features of small-k part of the structure factor, whereas the details in the packing structure are hidden at higher k-values. We note that static functions discussed herein do not contain any information about changes in liquid structure over time. This the point where the importance of dynamics comes to light. Dynamics provides a direct answer on how long specific structural features are pre-

served, both globally and locally. In the context of kinetic time, global features of the density correlations are directly related to aggregation properties which we are particularly interested herein. Hence, including a temporal description of global static properties is expected to reveal the timescale of cluster formation and destruction in microheterogeneous liquids, which is one of the principal goals of this thesis.

3.2 Dynamics of neat associative liquids by classical hydrogen bonding model

3.2.1 Motivation

We have previously discussed structural properties of associative liquids through the analysis of correlations functions. Static density correlations, $g(r)$, statistically describe local density $\rho_{\mathrm{L}}(r)$ of neighbouring particles as the function of distance r from a reference particle located at the origin O (see $t = 0$ case of Figure 18). In Figure 18, the reference particle is, at $t = 0$, located at the origin O, while the other particles are distributed around the origin. Of course, $g(r)$ is a statistical quantity, meaning that it represents a distribution of particles obtained as an average over large number of reference particles (origins), and not only over one single origin.

The important point which should be noted is that the choice of origins, around which the distribution is being averaged, is obviously not *arbitrary*. One does not perform an average over a set of randomly chosen set of origins, but precisely around origins occupied by particles in the system. The obtained distribution of particles, described by $g(r)$, is greatly influenced by the choice of precisely this set of origins. Hence, one could interpret $g(r)$ as some type of *conditional density* of particles at distance r from the origin, *under the condition* that the density in origin point is non-zero. Therefore, one could say that the presence of a particle at the origin induces specific distribution of neighbouring particles around the origin. This distribution of particles around the origin is described with the radial distribution function $g(r)$.

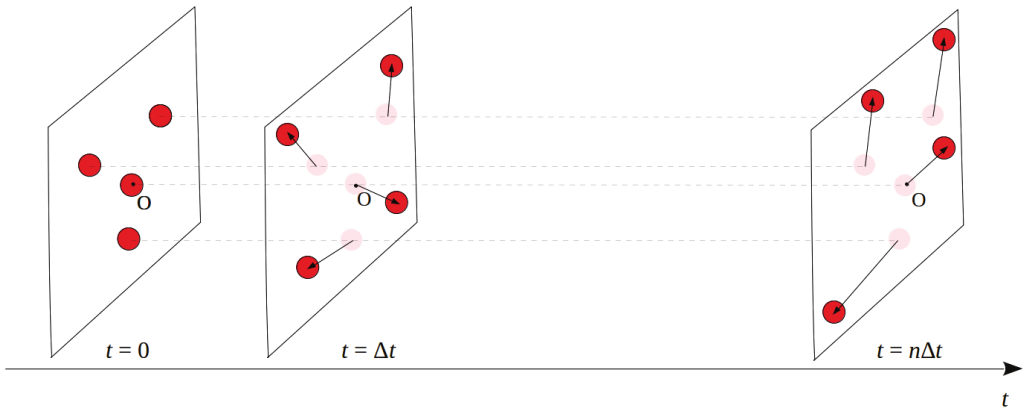

Figure 18: Illustration of temporal evolution of a microstate from $t = 0$ until $t = n\Delta t$. Microstates are represented with rectangular shapes filled with red circles, which represent particles.

Although the reference particle, located at the origin at $t = 0$, will move from the origin very quickly, the distribution of neighbouring particles, induced by the reference particle's presence at the origin at $t = 0$, will not vanish instantly, but some relaxation time will be required. The purpose of extending the static study into dynamic one is precisely to appreciate for the

timescale of this relaxation time. As already noted, dynamics of liquids in real space can be conveniently described with Van Hove function $G(r,t)$, which, in specific static case, satisfies $G_d(r,0) = \rho g(r)$. Hence, in $t = 0$ case, $G_d(r,t)$ is equivalent to $g(r)$ up to the density factor. In $t = \Delta t$ case, $G_d(r,t)$ represents a mean radial distribution of particles at time t, obtained as an average of distributions around *the same origins* as for $t = 0$ case, regardless of the density in those origin points being non-zero or not. We remind that this is not the case when static ($t = 0$) correlations are accounted for, when statistical average is performed exclusively over the set of origins characterized by non-zero density of particles. This is depicted in Figure 18, where we see that, when $t = \Delta t$, origin O (representing one of the origins included in statistical average) is not occupied by any of particles, meaning that the density of particles in origin point is zero in this case. Therefore, comparing $G(r,\Delta t)$ with $G(r,0)$ for specific r, describes how much of density correlations at $t = 0$, induced by non - zero density of particles at the origin, is preserved at $t = \Delta t$ in average.

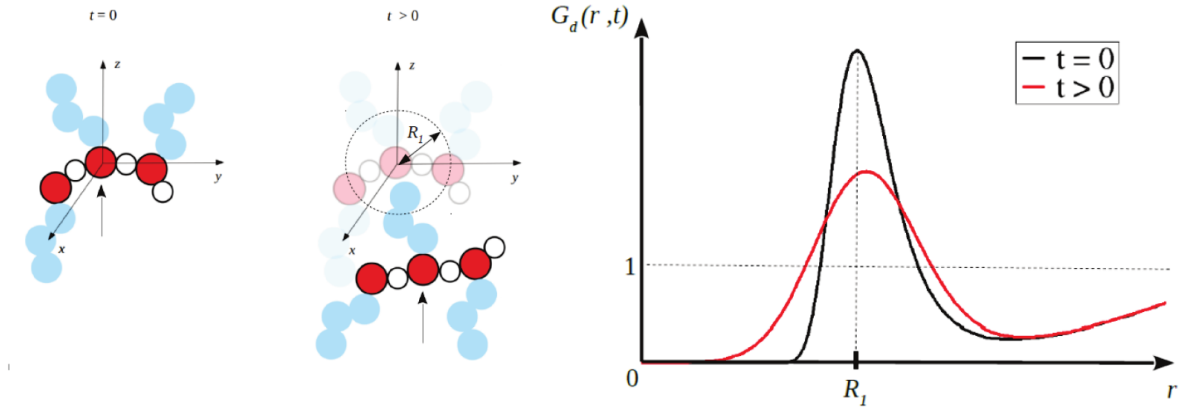

Figure 19: Illustration of dynamics of propanol cluster. In panels (a) and (b), red circles represent oxygen atoms, white circles represent hydrogen atoms, and light blue circles represent atoms within alkyl tails. The reference atom (in the origin at $t = 0$) is marked with black arrow. Panel (c) shows $G_d(r,t)$ correlations between O atoms at $t = 0$ and $t > 0$.

Let us consider a particular case of G_d correlations between O atoms (represented by red circles in Figure 19a and Figure 19b), when selected r corresponds to the position of the first peak (marked with R_1 in Figure 19c). In static $t = 0$ case, the first peak of $G_d(r,0)$, centered around $r = R_1$, is caused by hydrogen bonded O neighbours being distributed around reference O atom at distance around $r = R_1$. In dynamic $t > 0$ case, $G_d(r,t > 0)$ is characterized by decrement of correlations around $r = R_1$, compared to $G_d(r,0)$. Although the first peak of $G_d(r,0)$ is a clear indication of hydrogen bonding, the decrement of G_d correlations around $r = R_1$ at larger t is not the consequence of only hydrogen bond breaking, but also of the collective diffusion of hydrogen bonded pairs away from their starting position at $t = 0$. Therefore, the t - decay of the first peak is not dependent only of the lifetime of typical hydrogen bond, but also of diffusion.

This is shown in Figures 19a and 19b, which illustrate dynamics of a propanol cluster, centered at the origin at $t = 0$ (Figure 19a). In the context of this illustration, the first maximum of $G_d(r,0)$ would be a consequence of 2 hydrogen bonded O neighbours, distributed around the reference O atom (indicated with arrows in Figure 19a and 19b). At $t > 0$ (Figure 19b), the reference atom may be dislocated from the origin, without breaking hydrogen bonds with its neighbours. In Figure 19b, the dislocated cluster at $t > 0$ is shown in high-contrasted colors, while the cluster shown in low-contrasted colors is the same cluster at $t = 0$. The decrement of correlations at $r \approx R_1$ in $G_d(r,t > 0)$, compared to $G_d(r,0)$, is then not manifestation of hydrogen bond breaking, but simply of the fact that reference atom is not located at the origin anymore when $t > 0$. In general, the decrement of correlations at $r \approx R_1$ in $G_d(r,t > 0)$, compared to $G_d(r,0)$, is then combined effect of both hydrogen bond breakings and diffusion. However, if one wants to study the timescale related to the lifetimes of hydrogen bonded pairs exclusively, more convenient mathematical tools than density correlations functions should be used.

In the context of associative liquids, dynamics of hydrogen bonded pairs in classical systems has been appreciated through, among others, the extensive studies of probability distribution of hydrogen bonding lifetimes [105, 84, 95, 101, 176, 96, 122]. In classical modeling, hydrogen bonding is described as attractive electrostatic interaction between intermolecular pair of positively charged hydrogen atom, covalently bound to a donor atom, and negatively charged acceptor atom [60]. In the context of pure hydrogen bonding analysis, it is well-known that classical models have a very limited value in describing fundamental hydrogen bonding properties, which are much better described in quantum mechanical context. For example, the length of majority of hydrogen bonds are shorter than the sum of van der Waals radii of the hydrogen bonding atoms, indicating that there must be some orbital overlap and, therefore, covalent character of the bond [60]. Even quantum-mechanical Hartree-Fock calculations, which neglect electron-electron correlations, overestimate the lengths of hydrogen bonds [60]. These realizations led to addition of empirical terms to purely electrostatic models in order to better capture hydrogen bonding energies and lengths [60]. The need for adding additional restraints to purely electrostatic model indicates that hydrogen bonding can hardly be considered as purely electrostatic interaction, highlighting the importance of its strong quantum - mechanical character.

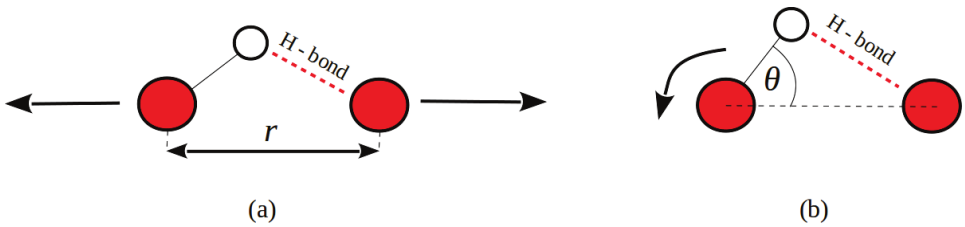

Figure 20: Illustration of stretching vibrations of donor and acceptor atoms (a) and librations of hydrogen atom (b). Donor and acceptor atoms are represented with red circles, while hydrogen atom is represented with white circles.

However, from dynamical point of view, the analysis of properties of hydrogen bonding lifetimes in classical systems provides information about two timescales which are particularly interesting for dynamics. Taken a water molecule as an example, the first timescale would be related to stretching vibrations of oxygen donor and acceptor atoms (illustrated in Figure 20a), while the second timescale would be related to librational dynamics of hydrogen atoms (illustrated in Figure 20b). Both stretching vibrations and librations are the result of interactions of hydrogen bonded pair of molecules with surrounding liquid. In the case presented in Figure 20a, the increment of O - O distance (denoted with r in Figure 20a) results in weakening of attractive electrostatic interaction (i.e. hydrogen bond) between O and H atoms, represented with red dashed lines in Figures 20a and 20b. In Figure 20b, the same weakening of electrostatic interaction occurs due to the increment of H - O - O angle (denoted with θ). In classical modeling, the weakening of electrostatic O - H attraction is equivalent to weakening of hydrogen bond strength. Therefore, since the strength of hydrogen bond in time depends of O stretching vibrations and H librations, it is expected that the average lifetime of hydrogen bond will also be influenced by the same two types of dynamics. Hence, distribution of hydrogen bonding lifetimes is expected to contain signatures of dynamics of O and H atoms. In addition, this distribution is expected to provide complementary dynamical information about already known static picture, accessible through the analysis of static $g(r)$ density correlations functions. However, we emphasize that the dynamical information accessible through this distribution of lifetimes is different from the information accessible by dynamic density correlations functions $G_d(r,t)$ because, as explained earlier, the latter functions are dependent of diffusion. Lifetime distributions (considered in this work) are not dependent of diffusion in sense that the distribution is not affected by the displacement of hydrogen bonded pair at time t relative to the position at time origin. Lifetime distributions are affected only by the fact if a selected pair of molecules is hydrogen bonded at time t or not, regardless of how far from the origin the pair diffused.

3.2.2 On the coupling between hydrogen bonding kinetics and diffusion

In previous works [122, 96, 95], lifetime distributions of hydrogen bonds were mainly discussed in the context of kinetic relaxation of collective hydrogen bonding network. In order to mathematically describe a hydrogen bond between pair of molecules (i, j), Luzar and Chandler [96, 95] introduced a hydrogen bonding population operator, h_{ij}. Operator h_{ij} is equal to 1 if pair of molecules (i, j) is hydrogen bonded and 0 otherwise. In an associative system composed of N molecules, the average value of the population operator is given by equation (120),

$$< h >= \frac{\sum_{i=1}^{N-1} \sum_{j=i+1}^{N} h_{ij}}{\frac{1}{2}N(N-1)} \tag{120}$$

where the double sum $\sum_{i=1}^{N-1} \sum_{j=i+1}^{N}$ takes into account all possible pairs of molecules in the system, and $\frac{1}{2}N(N-1)$ is the total number of those pairs. Hence, the average number of hydrogen bonded pairs in the system can be estimated with $\frac{1}{2}N(N-1) < h >$, where $< h >$ represents the probability that a random pair of molecules in the system is hydrogen bonded. In the dynamic equilibrium, hydrogen bonds fluctuate in time and these fluctuations can be described with correlation function $C(t)$:

$$C(t) = \frac{\sum_{i=1}^{N-1} \sum_{j=i+1}^{N} h_{ij}(0) \cdot h_{ij}(t)}{\sum_{i=1}^{N-1} \sum_{j=i+1}^{N} h_{ij}(0) \cdot h_{ij}(0)} = \frac{< h(0)h(t) >}{< h(0)h(0) >} = \frac{< h(0)h(t) >}{< h >} \tag{121}$$

For a tagged pair of molecules (i, j), the product $h_{ij}(0) \cdot h_{ij}(t)$ will be non-zero only if molecules i and j are hydrogen bonded both at times 0 and t. Therefore, correlation function $C(t)$ represents the conditional probability that a random pair of molecules is hydrogen bonded at time t, given the condition that the bond was formed at $t = 0$, after not existing previously. Therefore, correlation function $C(t)$ describes relaxation of collective hydrogen bonding network in the system. Taken a sample of N_0 selected hydrogen bonds, just formed at $t = 0$, function $C(t)$ can be expressed with equation (122),

$$C(t) = \frac{N(t)}{N_0} \tag{122}$$

where $N(t)$ represents number of hydrogen bonds still existing at time t. We note that equation (121) is equivalent to equation (122). As explained in work by Luzar [95], there are two different approaches to account for $C(t)$. One can account for $C(t)$ such that:
(i) Number $N(t)$ includes only the bonds which were uninterrupted in the time interval between 0 and t. This means that those hydrogen bonds did not break and re-form again within this time interval, but they existed continuously from 0 till t. The negative time derivative of $C(t)$ defined in this way represents probability distribution of hydrogen bonding lifetimes, $L(t)$, as given by equation (123). This physical quantity will be addressed in more details later on.

$$L(t) = -\frac{\mathrm{d}C(t)}{\mathrm{d}t} \tag{123}$$

However, one can also account for $C(t)$ such that:
(ii) Number $N(t)$ includes all bonds which broke at time t, regardless of them being previously interrupted between 0 and t or not. Obviously, the time derivative of $C(t)$ defined in such way does not represent the distribution of lifetimes, since $N(t) - N(t + \Delta t)$ does not represent number of bonds with the lifetime between t and $t + \Delta t$ because, in this case, $N(t)$ includes also bonds with the lifetime shorter than t. Within definition (ii), number of hydrogen bonds at time t, $N(t)$ is governed with hydrogen bond breaking and reforming events. This process can be conveniently described with reaction (124) [95],

$$A \underset{K'}{\overset{K}{\leftrightarrows}} B \tag{124}$$

where A represents reactants (pairs) which are hydrogen bonded, while B represents products for which the bond is broken. K and $K^{'}$ are forward and backward rate constants respectively (of dimension ps^{-1}), which describe the rate of change from reactants A to products B and vice versa. At $t = 0$, population A consists of N_0 hydrogen bonds, while population B is empty. As time increases, population B slowly grows, as bonds from population A are being broken. However, bonds from population B can reform and return to population A. Number of hydrogen bonds at time t, represented with $C(t)$ and $N(t)$ in equation (122), is dependent of both breaking and reforming processes. Temporal distribution of breaking probabilities (K direction in reaction 124) is described with $L(t)$. In order to describe events related to reforming of hydrogen bonds ($K^{'}$ direction in reaction 124), Luzar introduced probability distribution of death times (denoted with $Q(t)$ in ref [95]), which represents probability that hydrogen bond reforms after being "dead" for time t. Functions $Q(t)$ and $L(t)$ obtained by Luzar are presented in the main panel and the inset of Figure 21 respectively. While the t-decay of $L(t)$ is shown to be nearly exponential, the t-decay of $Q(t)$ exhibits non-exponential behavior [95]. Since $C(t)$ (in the type (ii) definition) depends both of $L(t)$ and $Q(t)$, the t-decay of $C(t)$ is non-exponential (see $k(t)$ function in Figure 21, which represents the negative time derivative of $C(t)$: $k(t) = -\frac{\mathrm{d}C(t)}{\mathrm{d}t}$).

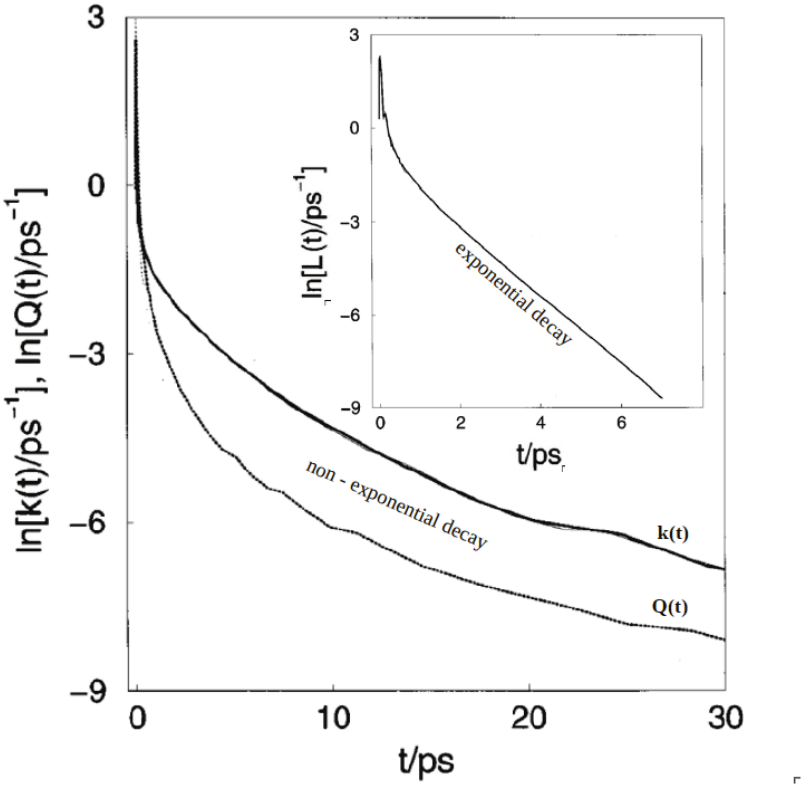

Figure 21: Functions $k(t)$, $L(t)$ and $Q(t)$ obtained by Luzar for SPC/E model of water. Figure taken from Ref. [95] and adjusted to the current discussion. Function $L(t)$ represents probability distribution of hydrogen bonding lifetimes, $Q(t)$ represents the distribution of death times, while $k(t) = -\frac{dC(t)}{dt}$.

The source of non-exponential kinetics of $C(t)$, when definition of type (ii) is considered, was discussed in the famous work of Luzar and Chandler [96] on hydrogen bonding dynamics in liquid water. Authors suggested that the origin of this non-exponential kinetics is related to the coupling between hydrogen bonding dynamics and diffusion dynamics, implying that both dynamics occur in the same timescale. Therefore, if $C(t)$ depends of $L(t)$ and $Q(t)$, clearly one of the two latter quantities are affected by diffusion. Non-exponential kinetics of $Q(t)$, in addition to exponential kinetics of $L(t)$, implies that $Q(t)$ is coupled with diffusion. Since $Q(t)$ represents the probability of reforming of hydrogen bond after time t, it is reasonable that this probability is governed by diffusion. Hydrogen bond will reform at time t only if the previously bonded pair of molecules did not diffuse from each other at separation bigger than 3.5 Å during the time interval between 0 and t, while the bond between the pair of molecules was broken. Therefore, diffusion influences the kinetic relaxation of hydrogen bonding network by affecting the probability of hydrogen bond reforming events. In the liquid characterized by faster diffusion, probability of hydrogen bond reforming events generally decreases.

However, in our work, we put focus on solely $L(t)$, which is characterized by nearly exponential kinetics above transient regime, as it will be demonstrated later on. Function $L(t)$ considered

in this work is not affected by diffusion because the impact of hydrogen bond reforming events has no impact on this distribution. The lifetime of hydrogen bond in this work represents the time interval between the formation and breaking of the bond. Hence, the distribution is not affected with events after the bond breaking, which are governed by diffusion.

3.2.3 Hydrogen bonding criteria in classical simulations

In order to analyze quantitative properties of hydrogen bonding network by computer simulations, it is necessary to choose a criterion which determines whether a random pair of molecules is hydrogen bonded or not. It is important to understand that, for a hydrogen bonded dimer, all possible diagnostics of hydrogen bonding (like binding energies, charge transfer or geometrical properties) are continuous [84, 168, 181, 122]. This means that there is no sharp boundary between hydrogen bonded and non-hydrogen bonded state. Therefore, the choice of hydrogen bonding criteria is somewhat arbitrary. The most commonly used criteria to check if a random pair of molecules is hydrogen bonded are energetic criterion, various geometric criteria or combinations of both [84, 168, 181, 122].

Energetic criterion states that a pair of molecules (i, j) is hydrogen bonded if the interaction energy between the pair, E_{ij}, is lower than chosen critical value E_{C}:

$$E_{ij} \leq E_{\mathrm{C}} \tag{125}$$

The choice of critical value E_{C} is usually inspired by the shape of probability distribution of pair interaction energies, which appears to be bimodal [84, 168]. This distribution consists of two peaks: lower peak centered around $E \approx -20$ kJmol^{-1} and higher peak centered around $E \approx 0$. The lower peak represents the contribution of hydrogen bonded pairs, while the higher peak represents the remaining pairs of molecules which are not hydrogen bonded [84, 168]. The two peaks are separated by a minimum around $E \approx -10$ kJmol^{-1}, and the position of this minimum appears to be independent of temperature variation [168]. This position of minimum thus can be regarded as natural boundary (E_{C}) between energies corresponding to hydrogen bonded population and non-hydrogen bonded population [84, 168].
The energetic criterion chosen this way is shown not to be completely efficient, since it does not account for O-H...O alignment. Hence, by using this criterion, it is possible to mistakingly account for a pair of molecules as hydrogen bonded, even though the H atom is improperly oriented [168]. This effect is much more enhanced at high temperatures, where it has been shown that, at $T = 573$ K, the total hydrogen bonding population, selected by energetic criterion, contained 17% of pairs with improper relative orientation [168]. However, at ambient temperatures, only 4% of pairs was mistakingly selected [168]. Therefore, the efficiency of energetic criterion depends strongly of thermodynamic conditions.

Now we turn our attention to various geometric critera. Geometric critera can be single - conditioned or multi - conditioned. They are based on geometric properties (distances and/or angles) enclosed by hydrogen, donor and acceptor atoms. The most commonly used geometric parameters, r_{OO}, r_{OH} and θ_{HOO} are depicted in Figure 22, where hydrogen, donor and acceptor atoms are denoted with H, A and B respectively .

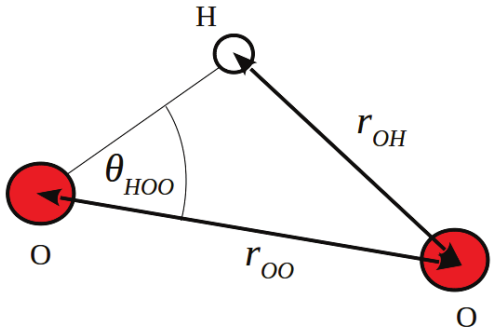

Figure 22: Illustration of geometric parameters (r_{OO}, r_{OH} and θ_{HOO}) commonly involved in various hydrogen bonding criteria. Donor and acceptor atoms (A and B) are represented with red circles. Hydrogen atom (H) is represented with white circle.

The simplest example of single - conditioned geometric criterion is based on the distance r_{OO} between donor and acceptor atoms. Within this criterion, a pair of molecules is considered as hydrogen bonded if the distance between O donor and acceptor atoms is smaller than selected critical distance $r_{OO}^{(C)}$ [168]:

$$r_{OO} \leq r_{OO}^{(C)} \tag{126}$$

where the choice of $r_{OO}^{(C)}$ usually corresponds to the center of the first minimum of radial distribution function $g_{OO}(r)$, with the value of 3.5 Å. This minimum represents the natural boundary between first and second coordination shell. Another single - conditioned geometric criterion is based on the distance r_{OH} between donor hydrogen H and acceptor atom O [168]:

$$r_{OH} \leq r_{OH}^{(C)} \tag{127}$$

where, analogously to the previous case, the choice of $r_{OH}^{(C)}$ is determined by the first minimum of $g_{OH}(r)$ function. It has been shown that both criterion (126) and criterion (127) are not very accurate. At ambient temperatures, 16% of pairs selected by criterion (126) were interacting repulsively ($E_{ij} > 0$), while 28% of pairs had attractive interaction too weak for hydrogen bonding state ($E > -8$ kJmol^{-1}) [168]. Criterion (127) is shown to be more accurate than criterion (126), leading to 3% of selected pairs interacting repulsively and 12% of selected pairs interacting with weak attractive interaction [168]. Inaccuracies of both criteria are even more enhanced at higher temperatures [168]. Therefore, single criterions (126) and (127) may not be the best choice for quantitative analysis.

The rejection of non - bonded ($E_{ij} > 0$) and weakly bonded ($E > -8$ kJmol^{-1}) pairs can be significantly improved by imposing multi - conditioned geometric critera. One of the most commonly used set of criteria (containing 2 conditions) is given by equations (128) [84, 168, 181, 122],

$$r_{OO} \leq r_{OO}^{(\mathrm{C})}$$
$$\theta_{HOO} \leq \theta_{HOO}^{(\mathrm{C})} \tag{128}$$

where θ_{HOO} represents hydrogen - donor - acceptor angle. For highly - associated liquids, the commonly used value of $\theta_{HOO}^{(\mathrm{C})}$ is 30°[105, 103, 96, 95, 122], as suggested with neutron scattering data, which show disruption of hydrogen bond when θ_{HOO} exceeds 30° [157]. At ambient temperatures, only 1% of pairs selected by criteria (128) is shown to interact repulsively, and 6% was shown to interact with weak - attraction [168]. Clearly, this is significant improvement comparing to single - conditioned geometric criteria (126) and (127). Furthermore, applying more strict geometric criteria, with 3 conditions instead of 2, leads to similar results [168]. In those criteria, conditions (128) are combined with condition (127), forming a set of geometric criteria composed of totally 3 geometric conditions. More precise quantitative information than obtained by applying criteria (128) can be achieved by combination of energetic criterion (125) with geometric criteria (128). However, for the purposes of the analysis within this work, criteria (128) will be sufficient, since the emphasis is put more on qualitative differences in trends of hydrogen bonding dynamics across different associative liquids, than on precise quantitative information about hydrogen bonding lifetime.

In subsequent discussion, parameter $r_{OO}^{(\mathrm{C})}$ will be denoted with abbreviate form, r_{C}, because the specification of A and B is redundant, since donor and acceptor species are identical for all systems studied herein. The same will be applied in the case of θ_{HOO}, where the abbreviated form θ_{C} will be used.

3.2.4 Hydrogen bonding lifetimes in ethanol

Probability distributions of hydrogen bonding lifetimes for typical alcohol, ethanol, is presented in Figure 23. Lifetime distributions are calculated for different values of r_{C}, which are listed in the legend box. The selected range of r_{C} values corresponds to the range within the first peak of radial distribution function, $g_{OO}(r)$, for ethanol, representing all possible donor - acceptor distances in the liquid. In previous works [105, 84, 95, 101, 176, 96, 122], where the emphasis was put mainly on kinetic relaxation of hydrogen bonding network, these distributions were calculated only for $r_{\mathrm{C}} = 3.5$ Å, corresponding to the first minimum of $g_{OO}(r)$. Since here the focus is put on dynamics and the timescale of characteristic motions of atoms which are part of hydrogen bonding dynamics, namely oxygen and hydrogen atoms, the variation of critical r_{C} value will appear to be useful.

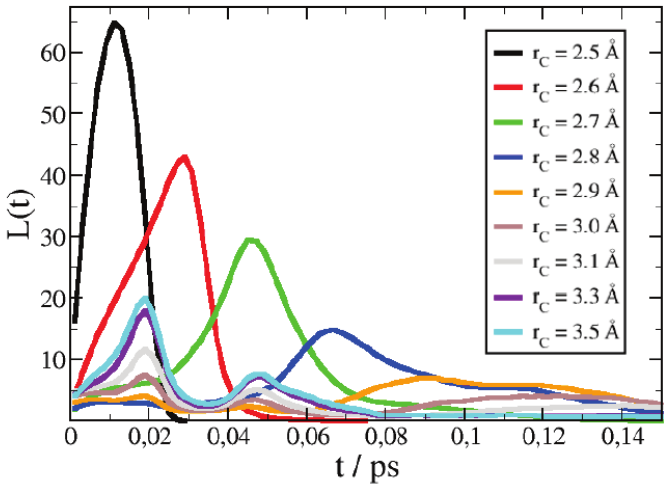

Figure 23: Probability distributions of hydrogen bonding lifetimes for various selected r_C values, obtained by molecular dynamics simulations with OPLS model of ethanol at ambient conditions.

Figure 23 shows that, for $r_C = 2.5$ Å (black curve), we obtain narrow-peaked distribution of lifetimes, centered at $t \approx 0.01$ ps. As we increase r_C value, the distribution shifts towards larger t values, followed by the appearance of two smaller peaks at $t \approx 0.02$ ps and $t \approx 0.05$ ps. In the rest of the discussion, the big peak which dominates the distribution for small values of r_C will be referred to as the *primary peak*, while the two peaks, at $t \approx 0.02$ ps and $t \approx 0.05$ ps, which appear for larger r_C values, will be referred to as *secondary peaks*. Clearly, lifetime distributions are characterized by 3 different timescales, corresponding to 3 different peaks. The first timescale, described with the main peak, is strongly sensitive on the variation of r_C, while the remaining two timescales, described with the two secondary peaks, are independent of variation of r_C. We have already stated that we expect timescales related to motions shown in Figure 20 to manifest in the lifetime distribution of hydrogen bonds. Hence, the timescales related to the main peaks and secondary peaks, shown in Figure 23, must be related to the motions presented in Figure 20, which cause breaking of hydrogen bond. Since we know that bonds can break either due to (1) stretching vibrations of O atoms (Figure 20a) or (2) librations of H atom (Figure 20b), the total lifetime distribution for any r_C value, $L(t)$, can be written as given by equation (131), where L_1 and L_2 correspond to lifetime distributions of bonds which break due to motions (1) and (2) respectively. To further clarify the meaning of L_1 and L_2, let us assume that a lifetime distribution, for a selected r_C, is calculated based on totally N lifetimes, with N being sufficiently large, such that the obtained distribution is smooth. For arbitrary value of t, $L(t)$ is obtained with relation (129),

$$L(t)\mathrm{d}t = \frac{N(t)}{N} \tag{129}$$

where $N(t)$ represents number of hydrogen bonds with the lifetime between t and $t + \mathrm{d}t$. $N(t)$ is

the sum of hydrogen bonds which broke due to violating distance criterion, $N_1(t)$, and hydrogen bonds which break due to violating angular criterion, $N_2(t)$. Therefore, one can write:

$$L(t)\mathrm{d}t = \frac{N_1(t)+N_2(t)}{N} \tag{130}$$

or, equivalently:

$$L = L_1 + L_2 \tag{131}$$

Hence, the total distribution $L(t)$ can be decomposed in two contributions, L_1 and L_2. L_1 is the contribution of bonds which break due to (1), while L_2 is the contribution of bonds which break due to (2). Distributions L_1 and L_2 for different values of r_C for ethanol are shown in the left and right panels of Figure 24 respectively.

Figure 24 helps to clarify the origins of the main peaks and secondary peaks in distributions presented in Figure 23. Figure 24 (left panel) shows that, when only breaking events due to violating distance criterion are accounted for, the distributions are dominated with the main peak, with the absence of secondary peaks. Hence, the main peaks represent the lifetime distributions of hydrogen bonds which break due to violating distance criterion between O atoms, imposed by choosing specific value of r_C. Therefore, the main peaks represent temporal description of stretching vibrations of O atoms, since particularly this type of dynamics causes breaking occurences. For small values of r_C, the main peak is centered at small values of t. Particularly, for $r_C = 2.5$ Å, the distribution is centered at $t \approx 0.01$ ps. We recall, from the analysis of static properties of ethanol, that $g_{OO}(r) \approx 0$ around $r \approx 2.5$ Å, meaning that the density at this separation from the reference particle is very low in average. This means that the occurences when two O atoms approach each other at this distance are highly unlikely. An additional information which we can extract from the lifetime distribution, particularly when $r_C = 2.5$ Å, (black curve in the left panel of Figure 24) is that those occurences, apart from being rare, also last very shortly. According to this lifetime distribution, two O atoms typically spend about 0.01 ps around this particular separation. The brevity of the time spent at this separation is induced by strong repulsive forces between O atoms, which make this bonding state unstable, leading to the two atoms being mutually repelled at larger distances within several femptoseconds. In this context, lifetime distribution provides complementary temporal information to already known static properties extracted from $g_{OO}(r)$.

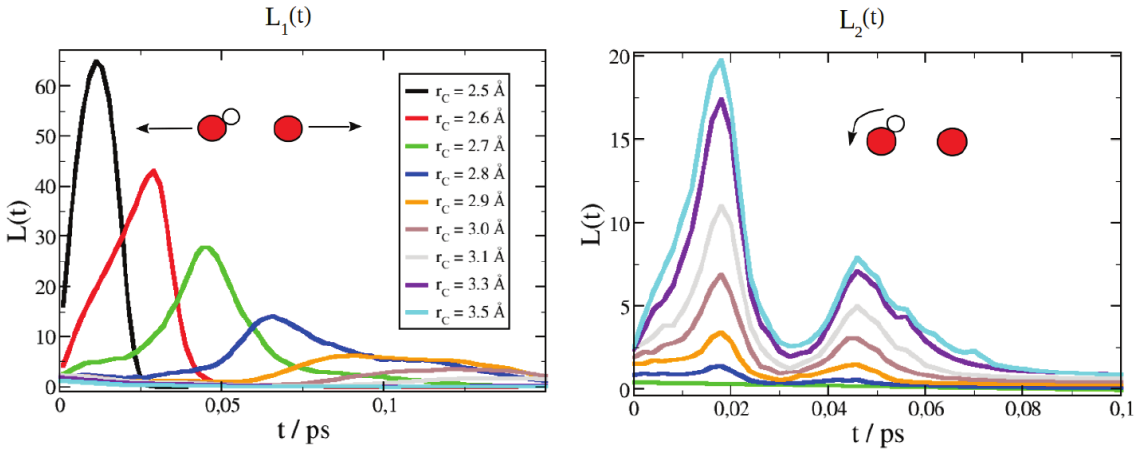

Figure 24: Decomposition of the total lifetime distributions, presented in Figure 23, into component $L_1(t)$, which correspsonds to the distribution of lifetime disruptions due to violating distance criterion (left panel), and component $L_2(t)$, which corresponds to the distribution of lifetime disruptions due to violating angular criterion (right panel). Distributions in the panels are normalized such that, for a given r_C value, equation $\int_0^\infty L_1(t)\mathrm{d}t + \int_0^\infty L_2(t)\mathrm{d}t = 1$ holds.

Furthermore, as r_C is gradually increased, the main peak shifts towards larger time values. In the context of $g_{OO}(r)$, we know that separations higher than 2.5 Å, particularly around $r \approx 2.8$ Å, correspond to the r-positions around the first maximum, meaning that particularly those separations between O atoms are statistically the most probable. They are the most probable due to enhanced stability of hydrogen bond which occurs particularly around this O - O separation. Hence, sampling higher values of r_C corresponds to sampling more stable O - O distances. However, we do not know what this *stability* implies in temporal context by looking at solely $g_{OO}(r)$. Conversely, by looking at lifetime distribution of hydrogen bonds, particularly for $r_C = 2.8$ Å (blue curve in the left panel of Figure 24), we can say that a pair of O atoms typically stays around 0.07 ps within separation of 2.8 Å. Therefore, the lifetime distribution provides information about the O - O pair stability in temporal context. This information is not accessible from static density correlations $g(r)$.

Next, in addition to the shift of the main peak, we observe that $L_1^{(r_C)}(t) \approx 0$ over whole time domain when r_C is sufficiently big (i.e. around 3.5 Å). This is the consequence of the fact that, when r_C is sufficiently large, hydrogen bonds break dominantly due to violating angular criterion, instead of distance criterion. This is obvious from the right panel of Figure 24, where, for $r_C = 3.5$ Å. one can observe $L_2^{(r_C)}$ in form of two peaks centered at $t \approx 0.02$ ps and $t \approx 0.05$ ps, while $L_1^{(r_C)}$ being nearly zero over the entire time domain in the left panel. The two peaks are centered at the same time values (0.02 ps and 0.05 ps) independently of the choice of r_C. The two-peak distribution suggests that there are two characteristic lifetimes associated to breakings of hydrogen bonds due to violating angular criterion. Since violation of angular criterion is caused by librational motions of H atoms, the two peaks could mean the existence of two characteristic times related to such motions, namely 0.02 ps and 0.05 ps. The amplitudes of the two peaks decrease with decreasing r_C simply because the impact of hydrogen bonds which

break due to violating angular criterion is smaller for lower r_C values. For those values of r_C, majority of hydrogen bonds is broken due to violating distance criterion.
To further clarify this, we can consider a hydrogen bonding interaction as superposition of OO repulsion superposed with OH attraction. OH attraction is the highest when the bonding angle θ is low ($\theta \approx 0$). If this is the case, OH attraction compensates for OO repulsion at very short binding distances, leading to formation of hydrogen bonds even when selected r_C is very low. However, those bonds will be unstable. Even small librational motions of H atoms, which are far from causing the violation of angular criterion, will lead to breakage of hydrogen bond because OH attraction cannot compensate for OO repulsion if binding angle is not nearly zero. Therefore, dominant OO repulsion will rapidly cause the increment of donor - acceptor separation at distance above critical distance r_C in this case, leading to breaking of hydrogen bond due to violating distance criterion. Conversely, at larger distances, both OO repulsion and OH attraction are lower than at short O - O separations. Weaker OH attraction will case H atom to move more freely, leading to enhancement of librational motions of the same atom. Consequently, hydrogen bonds will break dominantly due to violating angular criterion when r_C is large.

We remind that, for specific value of r_C, the total distribution $L^{(r_C)}(t)$ is given by the sum of distributions from the left and right panels. Since, $L^{(r_C)}(t)$ is a probability *density*, the equation $\int_0^\infty L^{(r_C)}(t)\mathrm{d}t = 1$ must hold. Obviously, this does not imply that $\int_0^\infty L_1^{(r_C)}(t)\mathrm{d}t = 1$ or $\int_0^\infty L_2^{(r_C)}(t)\mathrm{d}t = 1$, since $L^{(r_C)}(t)$ is given by the sum of $L_1^{(r_C)}$ and $L_2^{(r_C)}$. The separation of $L^{(r_C)}(t)$ into the two components was neccessary in order to clarify the origins of peaks in lifetime distributions. Since these origins have now been determined, only the total lifetime distribution, $L^{(r_C)}(t)$, will be shown in the upcoming chapters.

3.2.5 Universalities of hydrogen bonding dynamics in water and alcohols

The lifetimes related to primary and secondary peaks, discussed in section 3.2.4, represent the lifetimes of classical hydrogen bonds between *pairs* of molecules. However, as discussed in the Introduction, molecules in associative liquids are organized in form of clusters, due to directional hydrogen bonding. Statistically, the number of isolated dimers which are not part of bigger cluster is very small in any of these systems. This conclusion can be easily deduced from the analysis of the cluster size distribution, which has been performed in various works for various associative liquids [187, 190, 145, 140]. For example, in one of the recent works [187], authors have reported number of clusters per 1000 molecules (y - axis) as the function of cluster size (x - axis) at various temperatures of 2-propanol. At temperature of 280 K, there are around 15 clusters composed of only 1 molecule (i.e. monomers) and around 6 clusters composed of 2 molecules (i.e. dimers). Hence, in this example, totally 27 molecules out of 1000 are not part of cluster composed of at least 3 molecules. This results demonstrates that the microstructure of alcohols is highly dominated by clusters, where monomers and dimers make statistically insignificant contribution. Therefore, the lifetimes previously discussed are directly related to the lifetimes of clusters in hydrogen bonding liquids.
Of course, a precise definition of the lifetime of a n-sized cluster would be a time interval between the moment when all n molecules grouped in a single hydrogen bonding asscoiate untill the moment of breaking of at least one hydrogen bond which formed this associate. Lifetime distributions reported herein do not represent these lifetimes, but the lifetimes of hydrogen bonds between *pairs* of molecules. However, since all clusters obviously consist of these pairs, lifetime distributions discussed herein can serve as a fairly good representative of cluster lifetimes.

Previously, the distribution of hydrogen bonding lifetimes for ethanol has been shown and discussed, where we adressed the origin of specific peaks in the distribution. The origin of the primary peak is shown to be directly related to vibrational dynamics of O atoms, while the secondary peaks are manifestation of fast librational motions of H atoms. In this section, we will discuss the properties of hydrogen bonding dynamics for other associative systems (i.e. water, methanol, propanol, propylamine) and put them in comparison in order to appreciate for possible differences in O and H dynamics across different molecular species.

In order to put hydrogen bonding dynamics in the context of static properties (i.e. $g(r)$ correlations) discussed earlier, it is convenient to start the analysis with probability distribution of hydrogen bonding distances, $D_{\mathrm{HB}}(r)$, which represents the probability density that the distance between donor and acceptor atoms, forming a hydrogen bond (which satisfies both distance

and angular criteria), is r. Since $D_{\mathrm{HB}}(r)$ is a probability density, equation (132)

$$\int_0^{3.5\ \text{Å}} D_{HB}(r)\mathrm{d}r = 1 \tag{132}$$

must hold. The value of 3.5 Å is taken as the upper limit of the integral because this corresponds to maximum possible distance between donor and acceptor atoms. Left panel of Figure 25 shows the $D_{\mathrm{HB}}(r)$ functions for different models of different associative systems, whereas the right panel shows radial distribution functions of the same systems. We note that the distributions shown in the laft panel are broad and centered at $r = 2.7$ Å, which corresponds exactly to the center of the first maximum of $g_{OO}(r)$ functions shown in the right panel of Figure 25. While functions from the right panel exhibit differences in terms of the amplitudes of the first peaks, which have been discussed in previous chapters, functions in the left panel are nearly superimposed across different associative species and different models. The origin of this difference is related to different definitions of the two functions. Given a sample of N hydrogen bonds, function $D_{\mathrm{HB}}(r)$ can be expressed with equation (133),

$$D_{\mathrm{HB}}(r)\mathrm{d}r = \frac{N_D(r)}{N} \tag{133}$$

where $N_D(r)$ represents the number of hydrogen bonds with the O - O distance being between r and $r + \mathrm{d}r$. However, $g(r)$ is defined with (134),

$$g(r) = \frac{N_g(r)}{4\pi\rho r^2\mathrm{d}r} \tag{134}$$

where $N_g(r)$ represents the average number of O neighbours at distance between r and $r + \mathrm{d}r$ from the reference O atom, whereas ρ is the density of particles in bulk. Hence, although $N_D(r)$ and $N_g(r)$ from equations (133) and (134) are almost equivalent, both being directly proportional to the density of neighbouring particles at separation r from the reference particle, the height of the first peak of $g(r)$ differs across different associative species (see the right panel of Figure 25), while this feature is absent from $D_{\mathrm{HB}}(r)$ (see the left panel of Figure 25), where all the functions are nearly superimposed. Variation of amplitudes of the first maximum of $g(r)$ across different associative species is caused by the bulk density ρ (in equation 133), which differs across different associative species. Variation of amplitudes is absent from $D_{\mathrm{HB}}(r)$, because its definition is independent of ρ. The near superposition of all the distributions in the left panel clearly indicates that spatial hydrogen bonding properties are *universal* across different associative systems. This universality, which is in agreement with static properties presented in the right panel of Figure 25, will now be examined in temporal context as well, by the analysis of probability distributions of hydrogen bonding lifetimes for different associative systems. We note that small variations in the amplitudes of $D_{\mathrm{HB}}(r)$ are attributable to the differences in partial charges and Lennard-Jones parameters of different classical force fields.

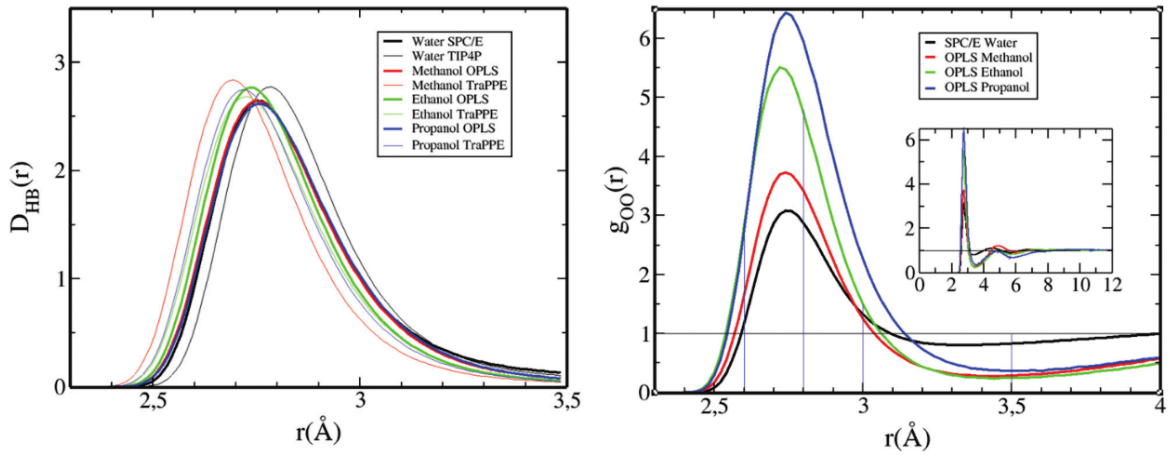

Figure 25: Probability distribution of donor - acceptor distances for various associative systems and different models (left panel) versus radial distribution functions of the same systems (right panel). The inset in the right panel shows the same functions at larger spatial scale.

Probability distribution of hydrogen bonding lifetimes for SPC/E model of water is shown in the left panel of Figure 26, while the right panel shows the same distributions in larger r-scale. The general pattern in the left panel is similar to the one already discussed for ethanol, namely the main peak (marked with filled circles) shifts to the right as r_C distance is increased, followed by the appearance of secondary peaks at $t = 20$ fs and $t = 50$ fs, marked with filled squares and diamonds respectively. We note that the positions of maxima do not differ when compared to the maxima of lifetime distributions of ethanol, shown in Figures 23 and 24, which indicates that dynamics of O and H atoms in the two liquids appears to be universal. Right panel shows the same distributions in kinetic timescale. We note that the t-decay of functions obtained with large values of r_C is significantly slower than the decay of functions obtained for small r_C. Fast decay obtained when r_C is very small reflects simply the fact that hydrogen bonds in this case break very quickly because of the strong repulsion forces between donor and acceptor atoms at short distances.

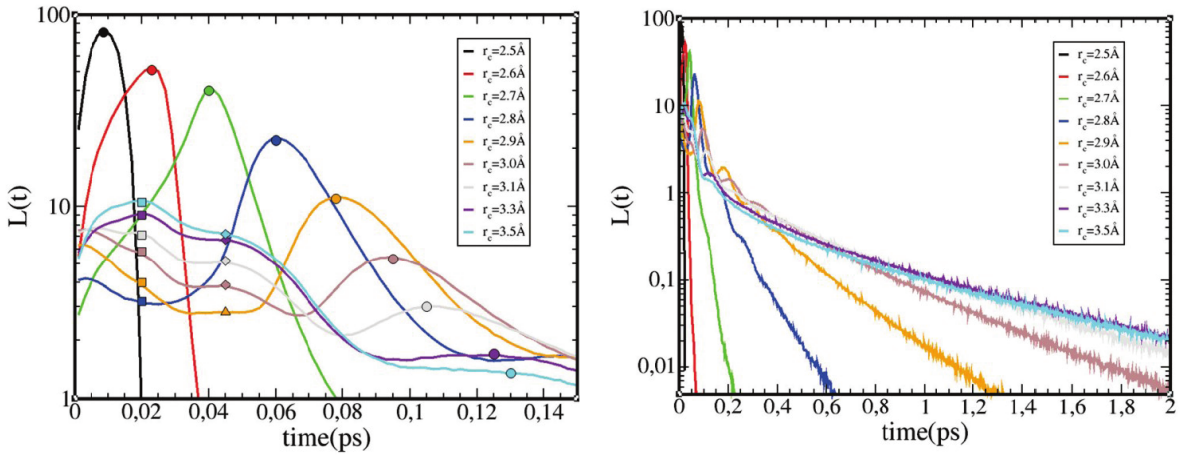

Figure 26: Probability distributions of hydrogen bonding lifetimes for various selected r_C values, listed in the legend box. Results are obtained by molecular dynamics simulations of SPC/E model of water at ambient conditions. Left panel shows the distributions at smaller timescale (transient regime), while right panel shows the same functions in log scale, at larger timescale (kinetic regime).

This universality is further supported with the lifetime distributions of hydrogen bonds in methanol and propanol, presented in the left and right panels of Figure 27 respectively, which exhibit the same features already discussed above.

As already stated, lifetimes related to the main peaks and secondary peaks are directly related to clusters. The main peaks contain the details of the O atom dynamics inside clusters, whereas the secondary peaks describe the timescale related to librations of H atoms inside the same clusters. The main question which naturally rises at this point is: why are there exactly two secondary peaks and what do they correspond to? In our interpretation, these peaks could correspond to different cluster topologies. It is well-known that linear monols are characterized by linearity of molecular aggregates, which can appear in form of linear chains, loops or lassos for example [171, 177]. Therefore, two distinct secondary peaks could be attributed to two different cluster topologies.

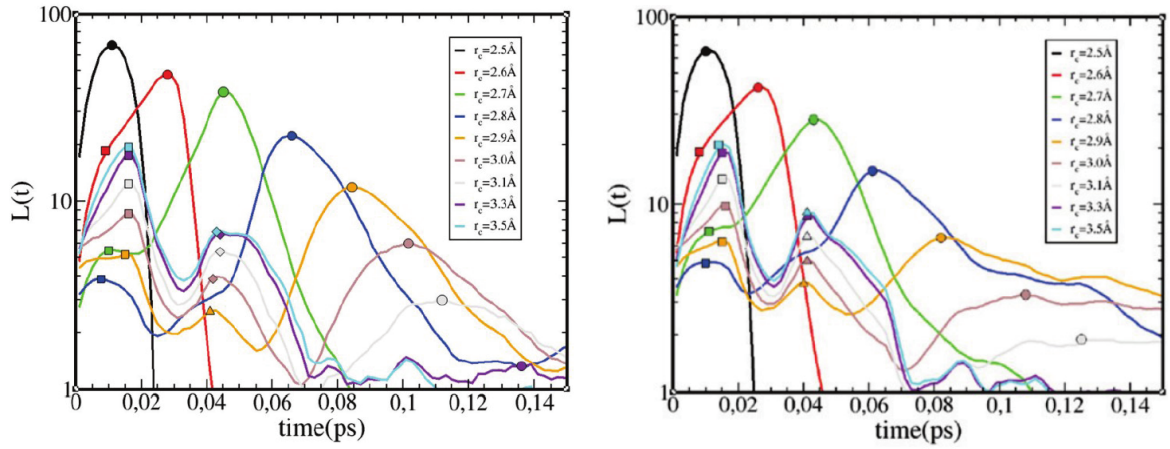

Figure 27: Probability distributions of hydrogen bonding lifetimes of methanol (left panel) and propanol (right panel), for various selected r_C values, listed in the legend box. Results are obtained by molecular dynamics simulations of OPLS models of methanol and propanol at ambient conditions. Both panels show the distributions at the timescale of transient temporal regime. Results in the kinetic timescale are omitted because they show the same trends as the one presented in the right panel of Figure 26 for SPC/E model of water.

It is important to note that the lifetimes discussed herein are not inside kinetic temporal regime. This means that these lifetimes are not representatives of the timescales related to structural relaxation processes at level of aggregates. This statement may sound contradictory, since earlier we related the maxima of lifetime distribution of hydrogen bonded pairs to cluster lifetimes. However, the timescales of *cluster lifetimes* and *structural relaxation processes at level of clusters* are not the same. Cluster lifetimes are influenced by fast dynamics of hydrogen bonding O and H atoms. This dynamics causes the same hydrogen bond to constantly break and reform while being part of the same aggregate. The timescale related to these breaking and reforming occurences are described with characteristic peaks of the lifetime distribution of hydrogen bonds (i.e. main peaks and secondary peaks). Although hydrogen bonds which form specific aggregate constantly break and reform within short period of time (~ 0.1 ps), the structure imposed by specific arrangement of molecules within the aggregate changes much slower, within the timescale much bigger than 0.1 ps. This is illustrated in Figure 28, which shows time evolution of an aggregate composed of ethanol molecules, obtained with molecular dynamics simulations with OPLS model of ethanol. We observe that the arrangement of molecules which form the aggregate remains similar to the initial arrangement (which corresponds to $t = 0$ case in Figure 28) even at $t = 40$ ps. Therefore, although hydrogen bond breaking and reforming occurences happen within very short period of time, the structural relaxation processes at the scale of aggregates, illustrated in Figure 28, occur at much slower timescale. We refer to this timescale as *kinetic* timescale. Structural relaxation processes inside kinetic temporal regime will be discussed in upcoming chapters, within the formalism of correlations functions.

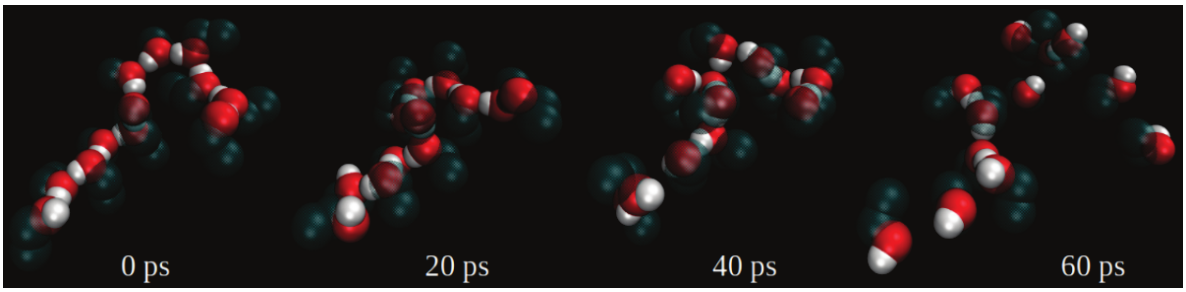

Figure 28: Time evolution of ethanol cluster composed of 12 molecules of ethanol. Oxygen atoms are shown in red, hydrogen atoms in white and alkyl groups in transparent grey color convention. Results are obtained by molecular dynamics simulations of OPLS model of ethanol at ambient conditions.

While previous works were mainly concerned about the properties of kinetic relaxation of hydrogen bonding network, our work shows that the relaxation within transient time interval also exhibits interesting and unexpected features, particularly from the context of dynamics. The analysis of the lifetime distribution of hydrogen bonds for various associative systems, within transient temporal regime, shows that hydrogen bonding dynamics appears to be universal across different molecular species in this timescale. This universality is manifested through the appearance of peaks centered at identical t-values of the lifetime distribution of hydrogen bonds, regardless of which system is considered. The differences between the system become more apparent in kinetic timescale (see Figure 29), where, for $r_C = 3.5$ Å, one can observe different (nearly-exponential) decays of water, methanol and ethanol. Water exhibits faster decay in comparison with methanol and ethanol, which suggests that kinetic relaxation of hydrogen bonding network in water is faster than in alcohols. This conclusion is in alignment with the conclusion reported by Padro, Saiz and Guardia [122], who came up with the same conclusion, based on the analysis of $C(t)$ for water, methanol and ethanol in kinetic regime. In context of both $C(t)$ or $L(t)$, slower decay of the function implies greater percentage of long - living hydrogen bonds, with the lifetime within kinetic timescale.

However, we note that the differences in kinetics of water, methanol and ethanol can be considered as negligible if put in the same context with propylamine (see Figure 29), whose kinetics differs significantly when compared to kinetics of the three systems previously mentioned. The origin of this large gap in kinetics of propylamine when compared with water or alcohols may be hidden in the fact that kinetics of systems with different functional groups (amino group in propylamine versus hydroxil group in alcohols) differs significantly. Hydrogen bonding relaxation of propylamine differs significantly from the rest of systems studied herein also in transient regime (not shown here), indicating that universality proposed herein could be restricted only to systems containing OH functional groups. This would imply that hydrogen bonding dynamics essentially depends only of donor and acceptor atomic species, and is less sensitive on the existence of neutral groups. Interestingly, the differences in kinetic relaxation

of water, methanol and ethanol become negligible for small values of r_C, as demonstrated in Figure 29 for $r_C = 2.7$ Å.

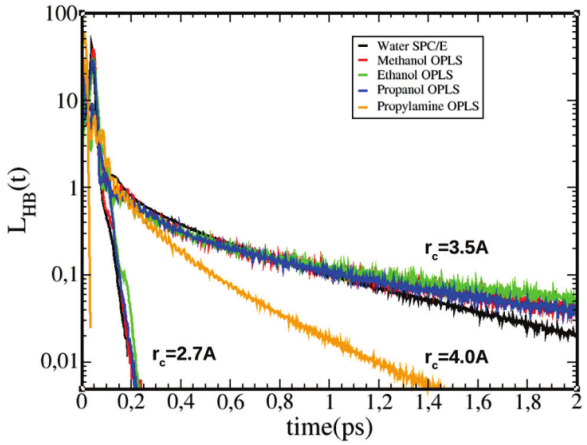

Figure 29: Long timescale behavior of probability distributions of hydrogen bonding lifetimes for SPC/E model of water and OPLS models of methanol, ethanol, propanol and propylamine. Two cut-off values are accounted for, $r_C = 2.7$ Å and $r_C = 3.5$ Å, corresponding to the r-range within the first peak of radial distribution functions of water, methanol, ethanol and propanol. In case of propylamine, $r_C = 4.0$ Å is accounted for, since this value corresponds to the center of the first minimum of radial distribution function in this case.

3.2.6 Weak water model - test of the impact of Coulomb association on atomic dynamics in associative liquids

We have previously discussed atomic dynamics of O and H atoms in the context of classical hydrogen bonding model. In classical models, hydrogen bonding is mimicked by Coulomb association, where the attractive force between donor and acceptor atoms is caused by Coulomb interaction between positively charged H atom and negatively charged acceptor atom. Since the basic properties of the dynamics of O and H atoms were herein discussed by the analysis of lifetime distributions of classical hydrogen bonds, based on electrostatic interaction, it would be instructive to examine how big is the impact of Coulomb association on the total lifetime distribution of hydrogen bonds or, equivalently, on the dynamics of O and H atoms.

The question posed above can be conveniently addressed by the analysis of previously introduced "weak-water" model [79]. This model is based on the SPC/E model of water, where the partial charges on the oxygen and hydrogen atoms are scaled by a parameter λ ($0 \leq \lambda \leq 1$), allowing tuning of the hydrogen bonding from the original model (with $\lambda = 1$) to a simple Lennard-Jonesium (with $\lambda = 0$). It was found that. for $\lambda \leq 0.6$, the influence of partial charges and hydrogen bonding were not relevant and the model was structurally similar to a simple Lennard-Jones liquid. Here, this model appears to be a useful way to measure the impact of Coulomb force on hydrogen bonding dynamics.

In the order to preserve the liquid state for small λ values and under ambient conditions, it was found necessary to increase the Lennard-Jones energy parameter $\varepsilon = \varepsilon(\lambda)$ according to the decrease in λ. In the present test, we have bypassed this procedure by doing the test simulations in the NVT canonical ensemble, hence keeping the volume fixed at that of the real liquid water.

Since the structure of the weak-water liquid is strongly affected by the decrease of the partial charges, the binding distance criteria must be adjusted appropriately. Figure 30.a shows the various $g_{OO}(r)$ data for different λ values we have used here, namely $\lambda = 0.8$, 0.5 and 0.2. The selected binding distances depend on the position of the maximum and differ quite a bit from that of the initial SPC/E water, ranging from 2.7 to 4.5 Å. It is important to note that, while we vary the binding-distance criteria, we keep the angular criterion the same as that for pure water, which is that the angle $\theta_C \leq 30^o$. Therefore, even though the weaker water model has weaker hydrogen bonding tendencies, we are keeping angular criterion fixed in order to examine how significant angular bias becomes when λ decreases.

For $\lambda = 0.8$ (Figure 30.d), the general behavior is similar to the original $\lambda = 1$ case, with the main difference being the fact that there is only *one* secondary peak (at $t \approx 0.02$ ps), instead

of two, which were observed for original $\lambda = 1$ case. Since secondary peaks are related to librational motions of H atoms, this result shows that even small decrement of λ causes significant changes in the stability of O-H...O alignment. For $\lambda = 1$, attractive forces between positively charged H atom and negatively charged O atom cause H atom to be, in average, more aligned along OO line. However, as λ decreases, H atom rotates more freely, which causes hydrogen bonds to break more easily when $\lambda = 0.8$ than for $\lambda = 1$. This effect of weakened OH attraction manifests as the appearance of a single secondary peak (for $\lambda = 0.8$) instead of two secondary peaks (for $\lambda = 1$). Weakening of OH attraction is even more pronounced for smaller values of λ, where we note that the contribution of the main peak (attributed to the breaking of bonds due to violating distance criterion) gradually decreases as λ decreases. For $\lambda = 0.2$, the main peak is almost invisible, meaning that lifetime distributions in this case (for all values of r_C) are completely governed by dynamics of H atoms. We remind that this was not the case for $\lambda = 1$, where these distributions were completely governed by O dynamics for small values of r_C, while H dynamics governed the shape of distribution only for larger values of r_C. Therefore, in weak water with significantly weakened Coulomb interaction, hydrogen bonding lifetime is principally determined by dynamics of H atoms, which rotate more freely in the system with weakened Coulomb force.

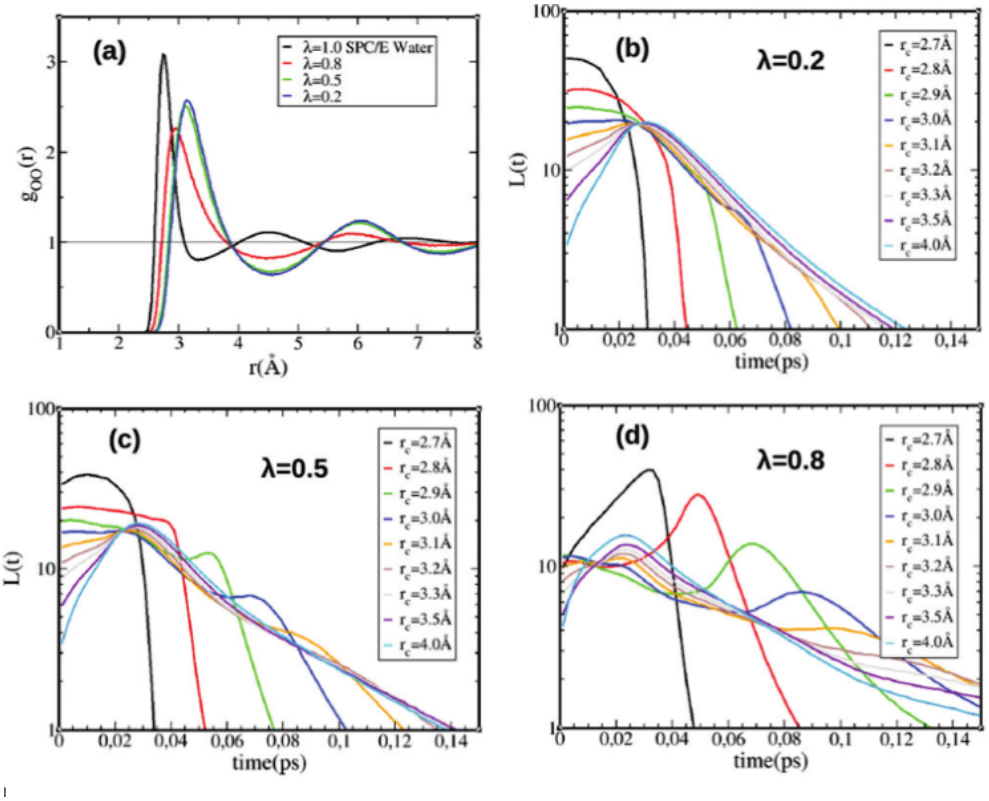

Figure 30: Probability distributions of hydrogen bonding lifetimes of weak SPC/E model of water, with $\lambda = 0.2$ (b), $\lambda = 0.5$ (c) and $\lambda = 0.8$ (d). Radial distribution functions of the weak-water model with different values of λ are shown in panel (a).

The analysis discussed above demonstrates the influence of Coulomb association on the lifetime

distributions of hydrogen bonds. Secondary peaks at $t = 20$ fs and $t = 50$ fs appear only for $\lambda = 1$, when Coulomb interaction is not weakened. Conversely, for smaller values of λ, double-peak feature is absent from lifetime distribution, which exhibits only one peak at $t \approx 0.02$ ps. This indicates that the double-peak feature of lifetime distribution is a direct signature of associative systems *only,* where Coulomb interaction is dominant. Since it is well-known that associative systems are, on molecular level, organized in form of clusters, this analysis indicates that the appearance of two secondary peaks in lifetime distribution of hydrogen bonds could be interpreted as a direct signature of aggregation in these systems. Conversely, in systems with weak Coulomb interaction, these aggregates are not well-defined, which is manifested with the absence of double-peak feature in lifetime distribution.

3.3 Dynamics of associative mixtures by classical hydrogen bonding model

3.3.1 Universalities of hydrogen bonding dynamics

It has been confirmed experimentally that molecular dynamics in the mixtures of alcohols with water differs from the dynamics in neat systems. Infrared and Raman spectroscopies [112, 85, 118, 18, 39, 44, 116, 115] have been used to study vibrational modes of ethanol molecules and clusters in water. Kuttenberg, Scheiber and Gutmann [85] performed an infrared spectroscopic study on several different alcohol–water mixtures and discovered that the addition of water causes significant changes in the absorption bands of the IR alcohol spectra due to the changes in OH stretching and bending. In addition, dielectric relaxation experiments are used to study the orientational dynamics of molecules [139, 154, 155] and provide results for dielectric relaxation time, which is the interval for the reorientation of a single molecule. These times were evaluated for mixtures of monohydroxyl alcohols with water by Dzida and Kaatze [42], where it was shown that reorientational motion of water molecules becomes slower in the mixtures with alcohols. The differences related to dynamics of mixtures in comparison with neat systems have been reported also in the case of mixtures of alcohols with non-polar solvents, where it has been observed a marked distinction in methanol vibration by the evolution of the OH stretching band in methanol–hexane and methanol–acetone mixtures [107, 108]. These reportings indicate that dynamics of O and H atoms in mixtures differ compared to their dynamics in neat liquids.

So far in this work, this dynamics has been discussed in the context of classical hydrogen bonding model, where the main features of probability distributions of hydrogen bonding lifetimes have been addressed for neat systems. In this chapter, we will extend this study to different types of mixtures of alcohols with polar and non-polar solvents in order to account for possible differences in dynamics which occur upon mixing. These results have also been previously published in one of our recent works [76].

Water - methanol (WM) mixtures:

Figure 31 shows probability distributions of hydrogen bonding lifetimes for the water–methanol (WM) mixtures, and for several r_C cutoff values, corresponding to different color codes (displayed in the legend box). Upper panels (a, b and c) show the distributions of lifetimes for r_C values in range 2.5 - 3.0 Å, while the lower panels (a', b' and c') show the distributions for r_C values in range 3.0 - 3.5 Å. The 3 hydrogen bonding possibilities between the oxygen atoms are shown in 3 separate columns, namely those involving the oxygens of water ($O_W - O_W$) in panels (a) and (a'), the cross oxygens bonds ($O_W - O_M$) in panels (b) and (b') and those between methanol oxygens ($O_M - O_M$) in panels (c) and (c'). For each r_C specifically colored curve, 3 methanol concentrations are shown with thick line ($x = 0.2$), thin line ($x = 0.5$) and dotted line

($x = 0.8$). The upper panels (a,b and c) highlight primary peaks, while the lower panels (a', b' and c') highlight the secondary peaks.

The first interesting feature is unmistakable similarity between all 3 columns of panels, highly suggesting that that the $L(t)$ features are nearly insensitive to the type ($O_M - O_M$, $O_W - O_M$ or $O_W - O_W$) of hydrogen bond. The second interesting feature is that there is a very small concentration dependence of the lifetimes $L(t)$, as can be seen by the proximity of different line types (thick, thin or dotted) for a given color.

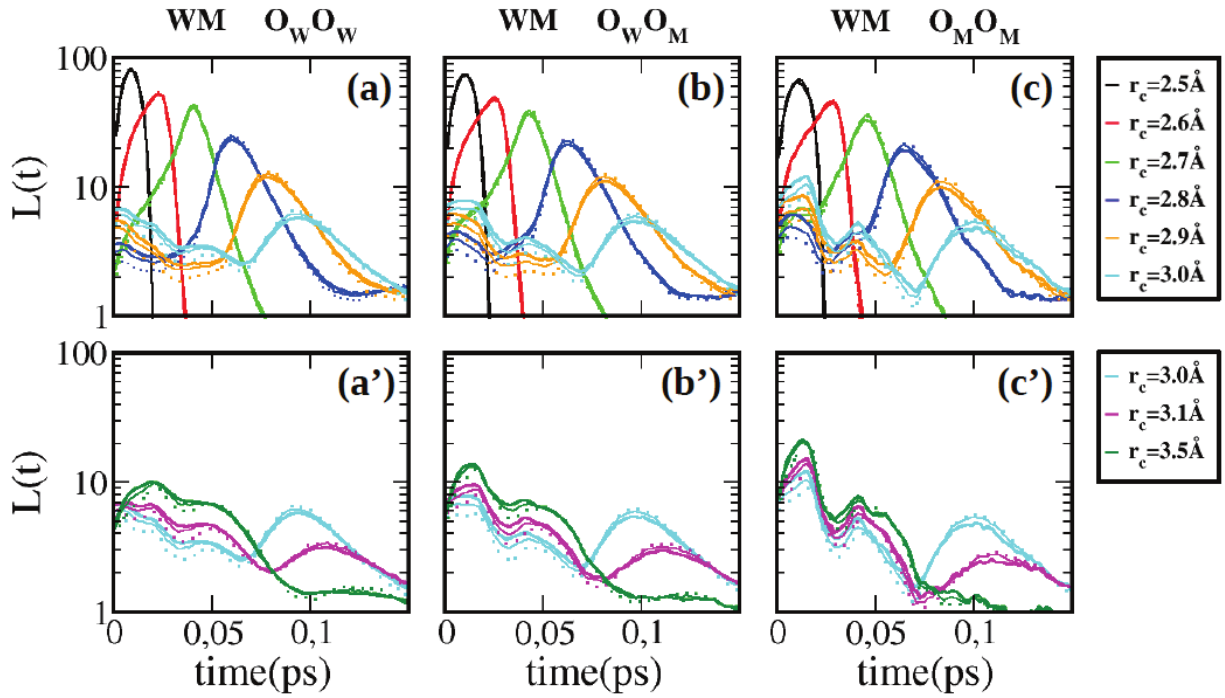

Figure 31: Probability distributions of lifetimes of hydrogen bonds in water - methanol (WM) mixtures for various selected r_C values, listed in the legend box. Dotted lines are obtained with $x_M = 0.8$, thin lines with $x_M = 0.5$ and thick lines with $x_M = 0.2$, where x_M represents concentration of methanol in the mixture. Upper panels show the distributions for r_C values in the range 2.5 - 3.0 Å, while lower panels show the same results for r_C being in the range 3.0 - 3.5 Å.

Regarding observed concentration dependence of peak amplitudes, we remind that, for any value of r_C, equation $\int_0^\infty L(t)dt = 1$ holds, since $L(t)$ is a probability density. The increment of primary peak amplitude represents the growth of probability of bond breaking due to O - O stretching vibrations. Similarly, the increment of secondary peaks amplitudes represents the growth of probability of bond breaking due to librations of H atom. From Figure 31, we note that the variation of the concentration dependence of the primary peaks for water–water clusters (O_WO_W) is opposite of that for methanol–methanol clusters (O_MO_M). This is highlighted in Figure 32, which shows zoomed view on panels (a') and (c') from Figure 31. Namely, in Figure 32, primary peaks (marked with letter P), for O_MO_M case, exhibit the increment of

the amplitude with the increment of methanol concentration. Conversely, in O_WO_W case, the amplitude of the primary peak is the highest at low water concentrations. Higher amplitude of O_WO_W primary peaks upon low concentrations of water, followed by lower amplitude of secondary peaks (marked with S), shows that the lifetime of water - water bonds is more affected by oxygen stretching vibrations in mixtures with low water content than in mixtures with high water content. Equivalently, it can be said that, upon low water concentrations, water bonds break less often due to fast librations of H_W atom than in the case when water concentration is high. Therefore, reorientational (or librational) dynamics of water molecules is faster when concentration of water in the mixture is high. Upon the addition of alcohol, reorientational dynamics of water slows down. Conversely, reorientational dynamics of methanol slows down upon high methanol concentrations, which is manifested by lower amplitudes of O_MO_M secondary peaks upon high methanol concentration. Upon low methanol concentrations, water imposes fast reorientational dynamics on methanol, which manifests as the increment of O_MO_M secondary peaks and decrement of O_MO_M primary peaks in the lifetime distribution of methanol - methanol hydrogen bonds.

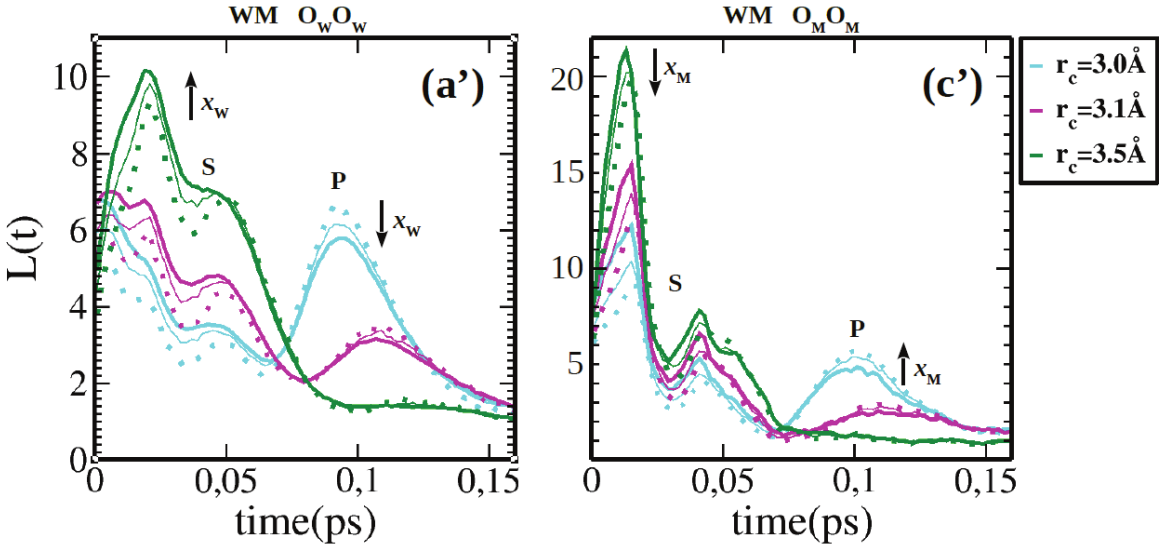

Figure 32: Enlarged view on panels (a') and (c') presented in Figure 31, in linear y - scale. Arrows marked with x_W and x_M indicate the direction of growing water and methanol concentrations respectively. Primary peaks are marked with the letter "P", while secondary peaks are marked with letter "S".

Water - ethanol mixtures (WE):

Next, we examine water–ethanol (WE) mixtures. We expect here to see how the extension of the alkyl tail influences the data observed in Figure 31 for methanol. The equivalent of Figure 31 is shown in Figure 33 for the case of water ethanol mixtures. Figure 33 show trends very similar to Figure 31, indicating that there are very little lifetime distribution differences, if we neglect the small $L(t)$ curve shapes differences between methanol and ethanol. It tends to

further confirm the idea of universal features introduced for pure liquids.

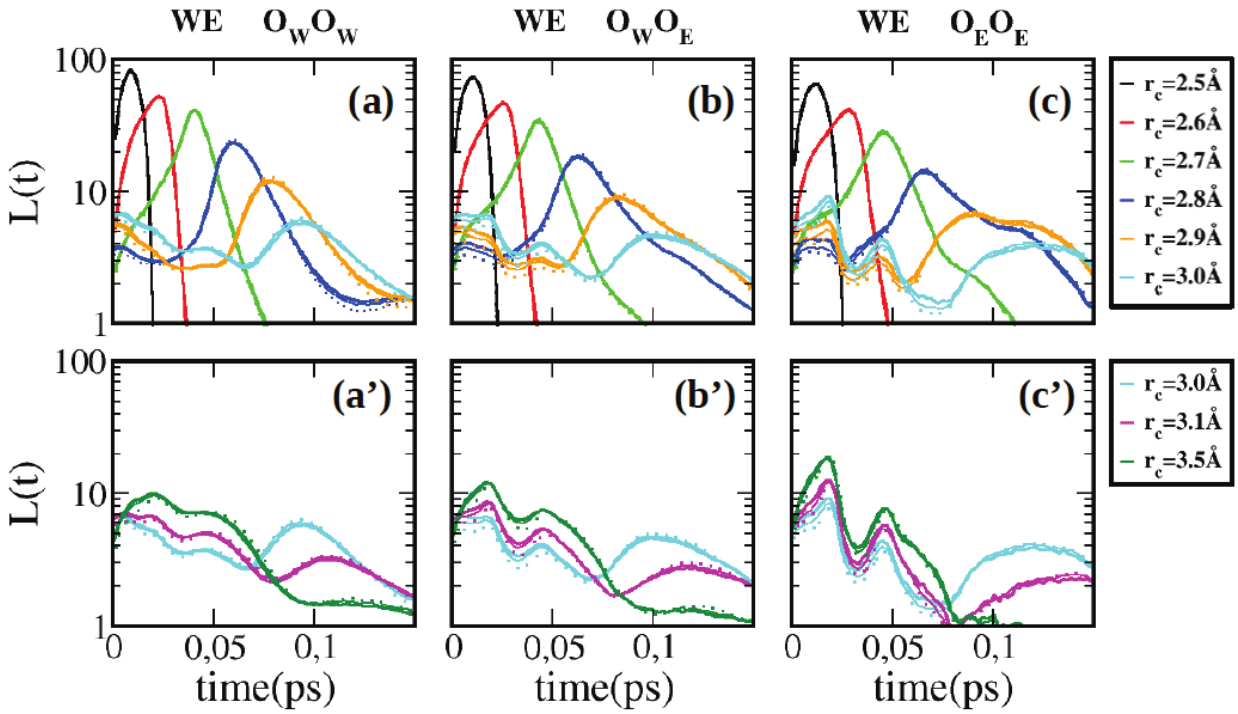

Figure 33: Probability distributions of lifetimes of hydrogen bonds in water - ethanol (WE) mixtures for various selected r_C values, listed in the legend box. Dotted lines are obtained with $x_E = 0.8$, thin lines with $x_E = 0.5$ and thick lines with $x_E = 0.2$, where x_E represents concentration of ethanol in the mixture. Upper panels show the distributions for r_C values in the range 2.5 - 3.0 Å, while lower panels show the same results for r_C being in the range 3.0 - 3.5 Å.

Water - DMSO (WD) mixtures:

While both water-methanol and water-ethanol mixtures show very similar features, water-DMSO mixture shows a feature absent previous aqueous mixtures. Lifetime distributions of hydrogen bonds between water molecules (O_WO_W) and between water and DMSO molecules (O_WO_D) are presented in Figure 34. The case of mixture with high water concentration ($x = 0.8$) is represented with dotted lines, while the case intermediate concentration ($x = 0.5$) and low concentration ($x = 0.2$) is shown in thin and thick lines respectively. Indeed, while water oxygen–oxgen (O_WO_W) dimer lifetimes appear to follow patterns similar to that observed in previous aqueous mixtures, the cross oxygen dimers (O_WO_D) exhibit a split - peak feature of the primary lifetimes (see the black curve on panel (b) of Figure 34, corresponding to r_C =2.5 Å). This split - peak feature is absent from the primary lifetimes shown for previous mixtures. From previous studies of aqueous–DMSO mixtures [136, 135], we assume that this duality of primary lifetimes could be directly related to the large positively charged sulfur atom of DMSO, which is known to have strong impact on the microstructure of the mixture. This impact is vis-

ible through the appearance of the double - peak feature of the first maximum of various atom - atom density correlations in the mixture (see Figure 35). In addition, we note, from Figure 34, that there is a more noticeable concentrational dependence of the secondary peaks amplitudes, while the t - positions seem to obey the same universality as that observed in previous mixtures, with the peaks centered at $t_1 \approx 0.02$ ps and $t_2 \approx 0.05$ ps.

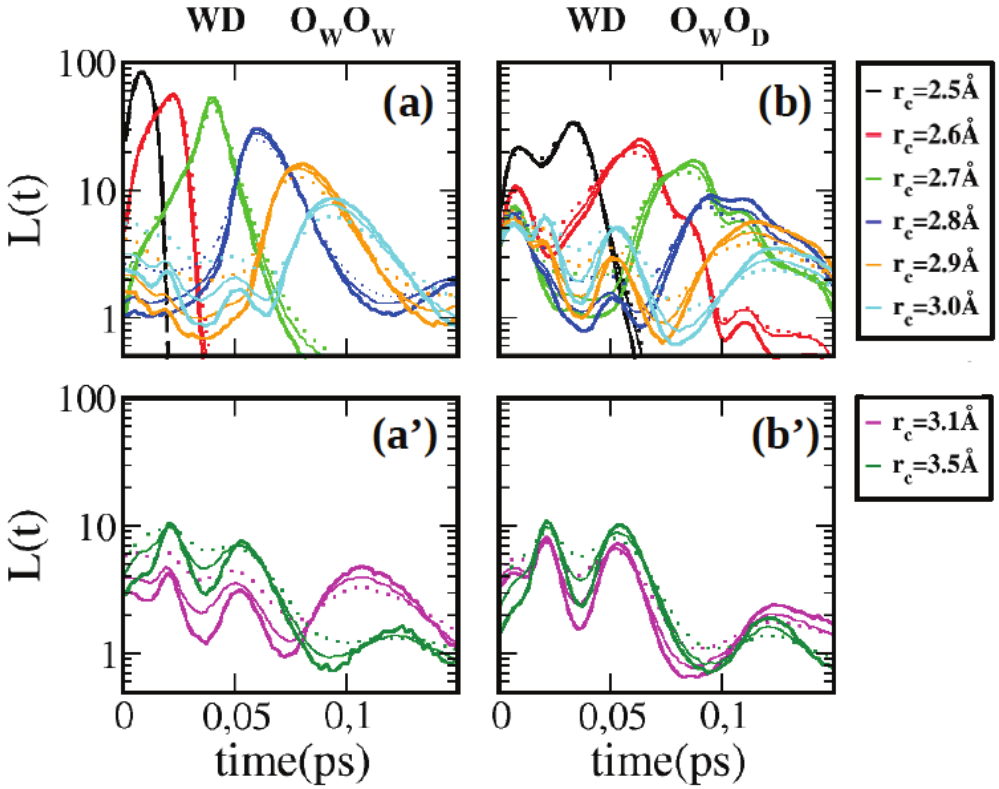

Figure 34: Probability distributions of lifetimes of hydrogen bonds in water - DMSO (WD) mixtures for various selected r_C values, listed in the legend box. Dotted lines are obtained with $x_W = 0.8$, thin lines with $x_W = 0.5$ and thick lines with $x_W = 0.2$, where x_W represents concentration of water in the mixture. Upper panels show the distributions for r_C values in the range 2.5 - 3.0 Å, while lower panels show the same results for r_C being in the range 3.3 - 3.5 Å.

Figure 35 shows SO_W(S - sulfur atom of DMSO, O_W−oxygen atom of water) and OO density correlations (O - oxygen atom of DMSO) for various concentrations of water in aqueous DMSO mixture. Both types of correlations exhibit the first maximum which is split into two, as indicated by black and red arrows in Figure 35. In the case of SO_W correlations, the maximum at $r \approx 4$ Å is the indication of hydrogen bonding between water and DMSO. As marked with black arrows in the left cartoon inset of Figure 35, up to two water molecules are hydrogen bonded to O atom of DMSO. The oxygen atom of these water molecules is typically located at 4 Å separation from the reference sulfur atom, denoted with S in the left panel of Figure 35. In contrast, non - hydrogen bonded water molecules (marked with red arrows) are distributed around the S atom at larger distances, leading to marked peak at $r \approx 5$ Å in SO_W correlations.

These molecules are distributed around the S atom at larger distances than hydrogen bonded water molecules, with their distribution being significantly governed by the size and charge of the sulfur atom. In the context of O_WO_D hydrogen bonding lifetimes presented in Figure 34, we assume that precisely the positive charge of the sulfur atom is at the origin of the double - peak feature of O_WO_D curve for $r_C = 2.5$ Å. When the two oxygen atoms (O_W and O_D) of hydrogen bonded water and DMSO molecules approach at small separations (as 2.5 or 2.6 Å), the hydrogen bonding dynamics of O_W and H_W atoms of the water molecule is governed by interactions with both O and S atoms of DMSO. While the impact of the sulfur atom on O_W and H_W dynamics is strong at short O_W - O_D separations, it weakens as the O_W - O_D distance increases, which could explain why O_WO_D curves in Figure 34 look similar to O_WO_W curves when r_C is sufficiently large.

Regarding the split of the first maximum of OO correlations presented in the right panel of Figure 35, the first peak ($r \approx 4$ Å) is the result of DMSO neighbours being hydrogen bonded to the same water molecule, as illustrated in the cartoon inset of the right panel. Reference O atom of DMSO (marked with O in the cartoon inset) is hydrogen bonded to the water molecule (marked with W), which simultaneously forms hydrogen bond to another DMSO molecule (marked with black arrow). Hence, water molecule W forms the bridge between two DMSO molecules. The distribution of distances between O first neighbours bridged by water molecules is described with the peak centered at $r \approx 4$ Å of OO density correlations. Similarly, the distribution of non - bridged O first neighbours is described with the peak centered at $r \approx 6$ Å.

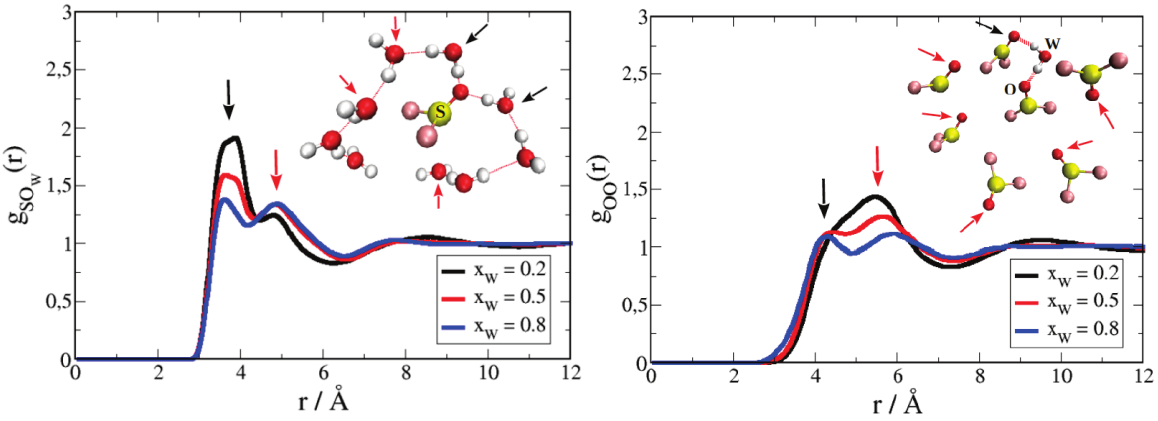

Figure 35: Radial distribution functions g_{SO_W}(left panel) and g_{OO} (right panel), for water - DMSO mixtures with different concentrations of water, listed in the legend boxes. Cartoon insets illustrate the distribution of water molecules around reference S atom of DMSO (left panel) and the distribution of DMSO molecules around reference O atom of DMSO (right panel).

Ethanol - hexane (EH) and methanol - acetone (MA) mixtures:

Finally, we examine the case of mixing alcohols with non-polar solutes. Figure 36 shows the distributions of lifetimes of hydrogen bonds in methanol–acetone (MA) mixture and ethanol–hexane (EH) mixtures. In the case of MA mixture, both hydrogen bonds between methanol molecules (O_MO_M), and those between methanol and acetone (O_MO_A) can be accounted for, since acetone is an acceptor of hydrogen bonds. However, for the EH mixtures, ethanol is the only hydrogen bonding specie (O_EO_E). Once again, all three panels of Figure 36 show the same 3 peak characteristics observed for the 2 previous mixtures.

However, it is interesting to account for methanol (O_MO_M) and ethanol (O_EO_E) self-bonding in presence of the solutes. We note that secondary peaks do not show any noticeable concentrational dependence, while the primary peaks show concentrational dependence similar to the one found in WM and WE mixtures. The same conclusions are also valid for O_MO_A case. But the most important point here is that, even the hydrogen bonding between an associating and non-associating species obeys the universality of lifetime distribution. This finding confirms once more that these distributions are really about atomic species involved in hydrogen bonding interaction (i.e. oxygen and hydrogen atoms), which are a permanent feature of the mixtures examined here. Finally, we note that ethanol (O_EO_E) hydrogen bonding lifetime distribution is nearly the same in water as in hexane, despite the very different properties of the two latter liquids.

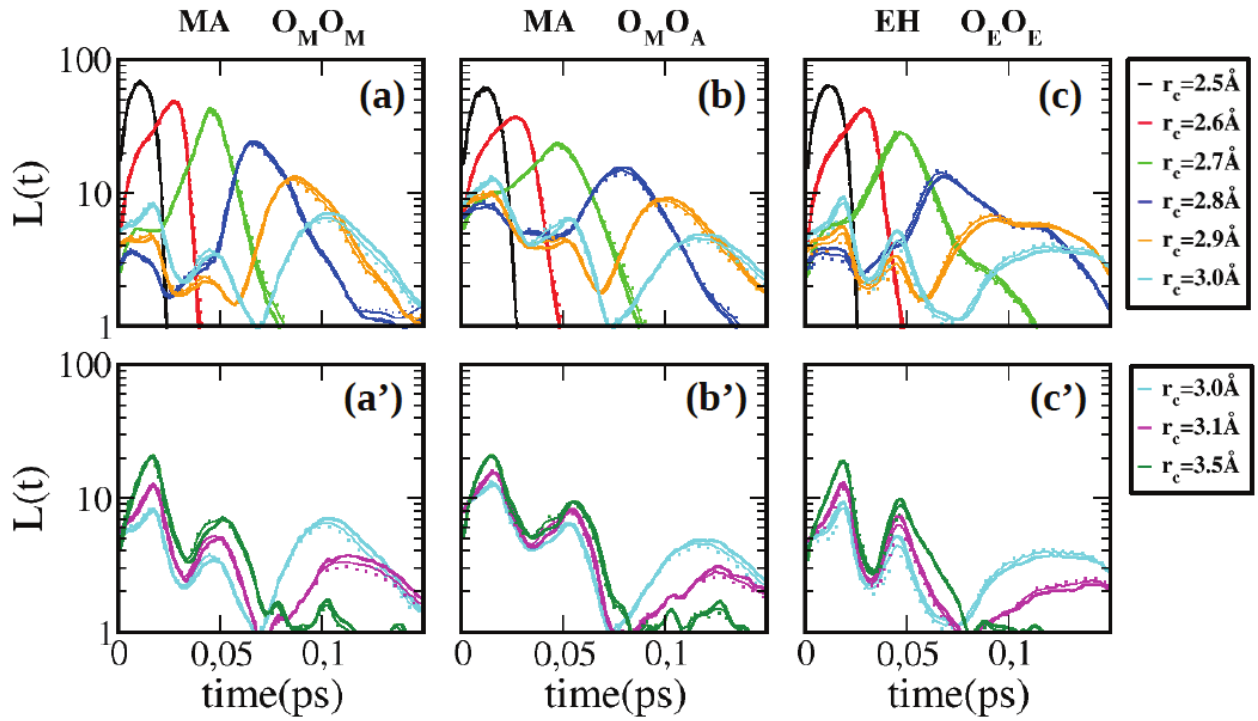

Figure 36: Probability distributions of lifetimes of hydrogen bonds in methanol - acetone (MA) mixtures and ethanol - hexane mixtures (EH) for various selected r_C values, listed in the legend box. Dotted lines are obtained with $x = 0.8$, thin lines with $x = 0.5$ and thick lines with $x = 0.2$, where x represents concentration of alcohol in the mixture. Upper panels show the distributions for r_C values in the range 2.5 - 3.0 Å, while lower panels show the same results for r_C being in the range 3.0 - 3.5 Å.

Hydrogen bonding dynamics in kinetic regime

Since earlier works have put emphasis mainly on long-t properties of the distribution of hydrogen bonding lifetimes, considering that this temporal regime should be more relevant to the kinetic relaxation of hydrogen bonding network, it would be instructive to examine the features of the lifetime distribution in terms of both cutoff r_C and concentrational dependence inside this time regime. This analysis is presented in Figure 37, where we show lifetime distributions ethanol - ethanol bonds (O_EO_E) for different concentrations of water in the mixture, listed in the legend box. For reference, lifetime distribution of water - water bonds (O_WO_W) in pure water ($x_E = 0$) is shown in black color. Left panel shows lifetime distributions for $r_C = 2.5$ Å, while the right panel shows the same distributions when $r_C = 3.5$ Å

We note that, for $r_C = 2.5$ Å (see left panel of Figure 37), there is negligible concentrational dependence of O_EO_E lifetime distributions, since all the curves seem to be nearly superposed. Lifetime distribution of O_WO_W bonds is slightly shifted towards smaller t values, which is the consequence of the difference between partial charges of oxygen and hydrogen sites of ethanol

when compared with partial charges of the same sites in water case. However, for $r_C = 3.5$ Å, we notice differences in the t - decay of O_EO_E lifetime distributions across different ethanol concentrations in the mixture. The decay is the fastest when concentration of water is high, which indicates that hydrogen bonding network of ethanol has the fastest kinetics in aqueous mixtures with high water content. However, as concentration of water decreases, kinetics of ethanol - ethanol bonds slows down. In the case when there is no water in the mixture ($x_E = 1$), ethanol - ethanol bonds exhibit slowest kinetics. Therefore, results presented in the right panel indicate that the addition of more water in WE mixture causes faster kinetics of ethanol - ethanol bonds.

Comparison of results from the left and right panel of Figure 37 shows that concentrational dependence of O_EO_E lifetime distributions grows with the increment of r_C cut - off distance. We remind that, for low values of r_C, lifetime distributions are governed by stretching vibrations of hydrogen bonded oxygen atoms of ethanol. Conversely, for large values of r_C, lifetime distributions are mostly governed by librations of hydrogen atoms of ethanol involved in hydrogen bonding. Therefore, we conclude that the addition of water in ethanol mostly affects reorientational (librational) dynamics of H atoms of ethanol, while O dynamics is not significantly affected.

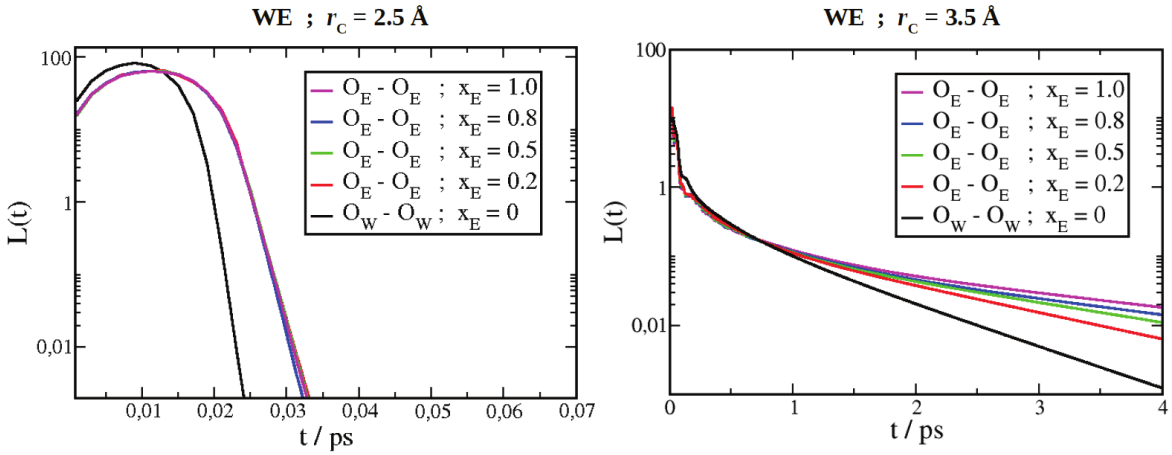

Figure 37: Long - t decay of lifetime distributions of ethanol - ethanol hydrogen bonds in ethanol - water mixture, for two selected r_C values (2.5 Å and 3.5 Å) and different concentrations of ethanol (x_E) in the mixture. Pure water case ($x_E = 0$) is shown in black color and pure ethanol case ($x_E = 1$) in magenta color. Left panel shows the distributions for $r_C = 2.5$ Å, while the right panel shows the distributions for $r_C = 3.5$ Å.

We note that the results shown in Figure 37 are in agreement with work by Cardona et al. [21], who discussed the kinetic properties of the probability distribution of hydrogen bonding lifetimes in ethanol-water mixtures in the context of dielectric relaxation. Namely, a dipole relaxation in these mixtures is described by dominant relaxation times τ_1 (8 - 200 ps) and τ_2 (0 - 2 ps). Time τ_1 represents the time needed for the reorganization of the hydrogen bonded net-

work in the system. Time τ_2 describes the processes related to fast formations and breakages of individual hydrogen bonds. In the context of the discussion within this work, time τ_1 would be related to the long - t decay of lifetime distributions, while time τ_2 is related to the disruptions of hydrogen bond within transient regime. While relaxation time τ_2 is nearly independent of concentrations changes in these mixtures (similarly like t - positions of primary and secondary peaks are unaffected), time τ_1 changes significantly upon changing concentration (similarly like long - t decay in the right panel of Figure 37 changes upon changing concentration). Since higher concentration of water in the system increases the number of hydrogen bonding possibilities, time τ_1 decreases upon increasing water concentration. This happens due to the fact that molecules "switch" hydrogen bonding partners more often when there is more water in the system. This affects reorientational dynamics of hydrogen bonding molecules, making it faster in systems with high water concentration. This effect is manifested as faster t - decay of the lifetime distributions in kinetic regime presented in Figure 37 and in work reported by Cardona et al [21] for mixtures with higher concentration of water.

To conclude, we note that the invariance of the characteristic time τ_2 to concentration changes, demonstrated by Cardona et al. [21], is in agreement with the idea of universality inside transient temporal regime which is proposed herein. Within this work, this invariance is supported by the concentrational independence of t - positions of primary and secondary peaks within transient temporal regime.

3.3.2 Power spectrum of atomic vibrations in associative mixtures

Dynamics in liquids can be examined by the analysis of the power spectrum, $Z_{\mathrm{PS}}(\omega)$, which is related to the velocity autocorrelation function, $Z(t)$, by simple Fourier transform, as given by equation (135) [56]:

$$Z_{\mathrm{PS}}(\omega) = \int_0^\infty Z(t)\exp(-i\omega t)dt \tag{135}$$

The definition of normalized velocity autocorrelation function is given by equation (136).

$$Z(t) = \frac{< v\,(t)v(0) >}{< v(0)v(0) >} \tag{136}$$

Function $Z(t)$ describes relaxation of particle's velocity in time. Brackets $<>$ represent statistical average, which can be conveniently described with $<>=\sum_i\sum_j$, where $\sum_i$ represents summation over the ensemble of different microstates, while $\sum_j$ represents summation over all particles in a given microstate. Therefore, function $Z(t)$ describes how correlated is, in average, a particle's velocity at time t with the particle's velocity at time 0. Velocity relaxation in time domain, described with $Z(t)$, occurs with specific frequencies, which are characteristic of every

system. These frequencies are given by vibrational power spectrum, $Z_{PS}(\omega)$, introduced earlier by equation (135). This physical quantity is measurable also in spectroscopic experiments, providing a direct comparison between results obtained by experiments versus computer simulations.

Figure 38 presents vibrational power spectrum of oxygen (O) and hydrogen (H) atoms of ethanol in water - methanol mixtures (panel (a)), water - ethanol mixtures (panel (b)) and ethanol - hexane mixtures (panel (c)), for various concentrations of alcohols (x_{ALC}), obtained by computer simulations. These results have been also published in the recent works of our group [75, 92].

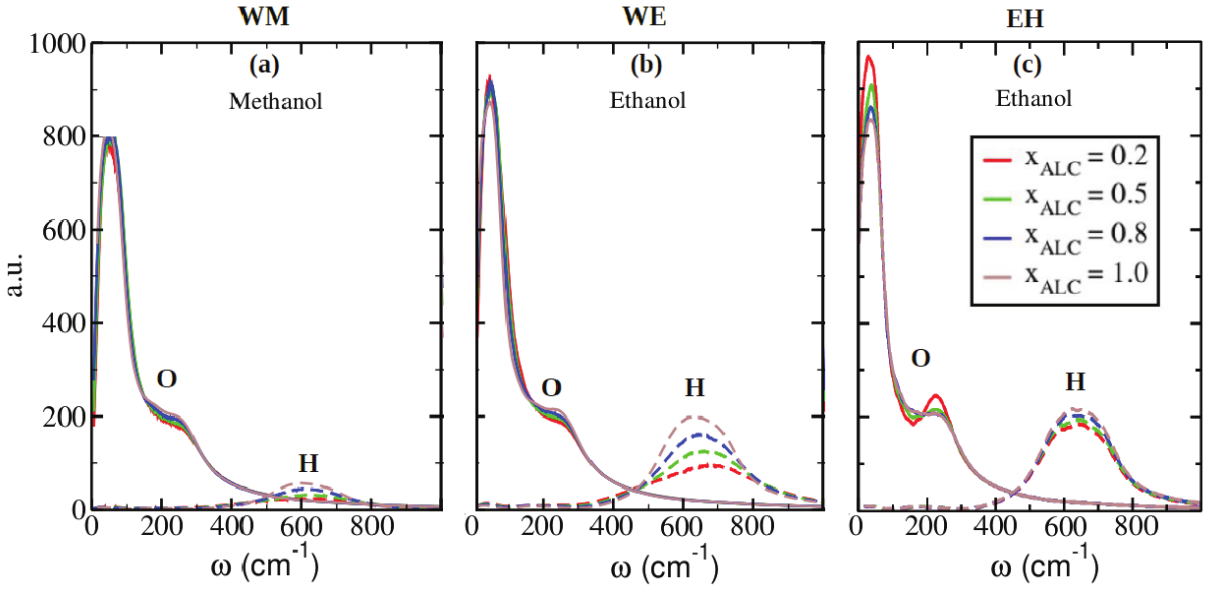

Figure 38: Power spectrum of oxygen (O) and hydrogen (H) vibrations in methanol - water (a), ethanol - water (b) and ethanol - hexane (c) mixtures. Alcohol concentrations (x_{ALC}) are listed in the legend box. Results are obtained by molecular dynamics simulations, with OPLS models of methanol and ethanol, OPLS model of hexane and SPC/E model of water, at ambient conditions.

As shown in Figure 38, the power spectrum of O atoms has a distinct first peak at 30 cm^{-1} in all three systems. This peak is attributed to the cage effect of neighbouring molecules on reference O atom [53, 54] and is observed also in the spectrum of non - associative liquids [148]. Next, we observe a shoulder between 200 cm^{-1} and 250 cm^{-1} in all three spectra, which has previously been associated with the existence of hydrogen bonds [122, 102, 152]. This vibrational mode is usually attributed to the stretching vibration of an oxygen atom along the hydrogen bond with another oxygen atom (already introduced earlier in the context of primary lifetimes in lifetime distribution of hydrogen bonds). Spectroscopic measurements found this peak at 110 cm^{-1} in pure ethanol [44, 174], at 130 cm^{-1} in pure methanol [174]. We note that the amplitude of this peak in power spectrum is nearly independent of the alcohol concentration in both methanol -

water (see panel (a)) and ethanol-water (see panel (b)) mixture. However, we observe that this is not the case for ethanol-hexane mixture (see panel (b)), where shoulder-peak around 200 - 250 cm^{-1} gradually evolves into a distinct peak as ethanol concentration decreases.
Results obtained by molecular dynamics simulations by Guardia et al. [53] have shown that the amplitude of the peak at $\omega \approx$200 cm^{-1}in the power spectrum increases as the mean number of hydrogen bonds per ethanol molecule increases. In the case when calculations were performed exclusively over ethanol molecules which participate in only 1 hydrogen bond, power spectrum with shoulder - peak was obtained. However, when only ethanol molecules with 2 hydrogen bonds were accounted for, a well – defined distinct peak at $\omega \approx$200 cm^{-1} instead of shoulder - peak was observed. This indicates that the amplitude of this peak is strongly correlated with the degree of ethanol - ethanol self bonding in the mixture. In ethanol - hexane mixture, ethanol self bonding is more pronounced than in pure ethanol, leading to larger the number of molecules with 2 hydrogen bonds and smaller number of molecules with only 1 hydrogen bond, resulting in the appearance of a marked distinct peak around 200 - 250 cm^{-1} in the power spectrum.

We note that the frequencies around 200 - 250 cm^{-1} correspond to the frequencies of 6 - 7.5 ps^{-1}. These frequencies describe vibrations with the period 1.33 - 1.67 ps. It is interesting to note that this time period matches with the t - position of the main peak in lifetime distribution of ethanol - ethanol hydrogen bonds in ethanol - water mixture, for $r_C \approx 3.5$ Å, as demonstrated in Figure 33. This is another indication that the main peaks in lifetime distribution of hydrogen bonds are directly related to stretching vibrations of O atoms involved in hydrogen bonding, which further supports our previous arguments. The fact that the same shoulder peak (200 cm^{-1} and 250 cm^{-1}) appears also in power spectra of other associative liquids (water and methanol, as also shown in ref [103]and [53]), supports the idea of universality of hydrogen bonding lifetimes across different associative species within transient temporal regime.

Let us now consider the power spectra of hydrogen (H) atoms in the three mixtures. As seen on the left panel of Figure 38, the hydrogen power spectra have a broad peak centered at around 600 cm^{-1}, which is attributed to the librations of ethanol molecules [53]. We note that this frequency describes vibrations with the time period of about 0.05 ps, which corresponds to the t - position of the right secondary peak in all lifetime distributions of hydrogen bonds presented earlier. This is another indication that secondary peaks in the lifetime distribution of hydrogen bonds are directly related to librations of H atoms.
As alcohol concentration decreases, we observe a small shift of the librational peak to higher frequencies in aqueous mixtures (see panels (a) and (b) in Figure 38), while this shift does not occur in the mixture with hexane (see panel (c)). This suggests that, upon the addition of water, librations of alcohol molecules becomes faster than in neat alcohols. This trend has also been observed in the results published by Hazra and Bagchi [59] for the case of ethanol - water mixture. Vibrational changes induced by the addition of water in ethanol have been also observed

experimentally in the infrared spectrum of ethanol [85]. It has been shown that water modifies the spectra of monohydric alcohols causing an extension of the OH intramolecular bond and a reduction of the OO intermolecular bond. Our results for the hydrogen spectra of both alcohols clearly indicate that the addition of water speeds up the hydrogen libration. However, as seen from the right panel of Figure 38, the librational band for ethanol hydrogen remains at about the same position for all ethanol concentrations in hexane, which, as expected, suggests that hexane does not alter the local molecular vibrations of ethanol as much as water.

Figure 39 shows the vibrational spectra of water oxygen (O_W) and hydrogen (H_W) atoms in methanol - water (a) and ethanol - water (b) mixtures. We observe a sharp peak at about 50 cm^{-1} and a shoulder at about 200 cm^{-1} in the oxygen spectra for all concentrations, similarly like in the oxygen spectra of alcohols presented in Figure 38. These peaks have been previously found for pure water by several authors [179, 68, 53]. The trends observed in Figure 39 are in agreement with results published by Palinkas, Bako and Heinzinger [123], who showed that that the peak positions in the vibrational O spectra of both methanol and water do not change greatly as concentrations are varied. In addition, they observe that the water librational band at 400 cm^{-1} becomes more pronounced with the decrease of the water concentration, which is also supported by our results for the hydrogen spectra in both water - methanol and water - ethanol mixtures.

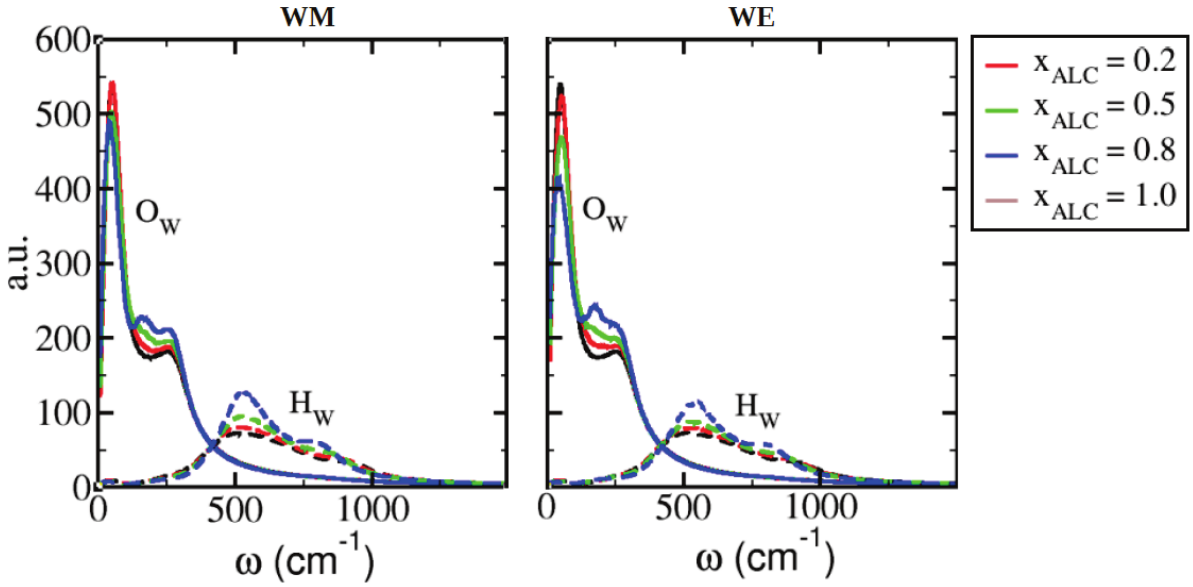

Figure 39: Power spectrum of water oxygen (O_W) and water hydrogen (H_W) vibrations in methanol - water (a), ethanol - water (b) and ethanol - hexane (c) mixtures. Alcohol concentrations (x_{ALC}) are listed in the legend box.

To conclude, dynamics of both water and alcohols modifies upon mixing conditions, as indicated by various experimental works mentioned earlier. For example, the differences in reorientational dynamics of aqueous alcohols versus neat alcohols are manifested by differences in

characteristic relaxation times obtained by dielectric relaxation experiments [139, 154, 155]. In this chapter, we showed that these differences are also manifested through the shape of the probability distribution of hydrogen bonding lifetimes, when these distributions are compared for mixtures with varying concentration of the solute. As demonstrated earlier, these distributions contain signatures of both stretching vibrations of O atoms and librations of H atoms, through the appearance of the primary peaks and secondary peaks respectively. The changes in O and H dynamics, which occur upon mixing conditions, manifest through variation of amplitudes of primary peaks and secondary peaks in lifetime distributions of hydrogen bonds over transient temporal regime. While the universality of peak positions in transient regime indicates that, in terms of vibrational frequencies, O and H dynamics is universal across different mixtures and different concentrations, the variation of amplitudes implies the differences in speed of reorientational dynamics across different concentrations of a solute in a mixture. Faster reorientational dynamics manifests through the increment of the amplitudes of secondary peaks, indicating higher percentage of short - living hydrogen bonds which break within characteristic librational period (0.05 ps). For example, considering the distribution of alcohol - alcohol hydrogen bonding lifetimes in aqueous alcohol mixtures, the amplitude of secondary peaks is higher at higher concentrations of water, implying that, in mixture with high water content, the percentage of short - living bonds (~0.05 ps) is larger. In this context, the analysis of the distribution of hydrogen bonding lifetimes leads to the conclusions which are in qualitative agreement with experimental findings. In addition, results are in quantitative agreement with the results obtained by power spectrum analysis (see Figure 38).

3.3.3 Rotational dynamics in associative mixtures

Reorientational dynamics of molecules in liquids can be described with reorientational correlation function $C_l(t)$, defined with [56]:

$$C_l(t) = \frac{< P_l(e(t) \cdot e(0))) >}{< P_l(e(0) \cdot e(0))) >} \tag{137}$$

where P_l is the Legendre polynomial of rank l, while $e(t)$ is the unit vector parallel to the inter-nuclear axis of the molecule at time t. Functions $C_1(t)$ can be experimentally obtained by dielectric relaxation experiments, while $C_2(t)$ can be obtained with NMR and Raman measurements [12]. In this work, we will consider $C_2(t)$ functions, with $e(t)$ being paraller to the OH vector of either alcohol or water molecule.

In the large - t limit, $C_2(t)$ has a Debye - like behavior, $C_2(t) \sim \exp(-t/\tau_2)$, where τ_2 is the reorientational correlation time. Integral reoreintational correlation time $< \tau_2 >$ is the average

time measured in NMR experiments. It is defined with:

$$< \tau_2 >= \int_0^\infty C_2(t)\mathrm{d}t \tag{138}$$

The calculated $C_2(t)$ functions are usually fitted to double - exponential function of the form $f(t)$:

$$f(t) = a \cdot \exp(-t/\tau_1) + (1-a) \cdot \exp(-t/\tau_2) \tag{139}$$

where the shorter time τ_1 corresponds to fast librational motions, whereas the larger time τ_2 corresponds to the relaxation (rearrangement) time of collective hydrogen bonding network.

Functions $C_2(t)$, obtained by molecular dynamics simulations, when $e(t)$ is taken to be parallel to the alcohol OH vector, are presented in Figure 40, for methanol - water (left panel), ethanol - water (middle panel) and ethanol - hexane (right panel) mixtures. Concentrations of alcohol in the mixtures are listed in the legend boxes. Results related to reorientational dynamics of water and alcohols in these mixtures have also been published in recent works of our group [92, 75].

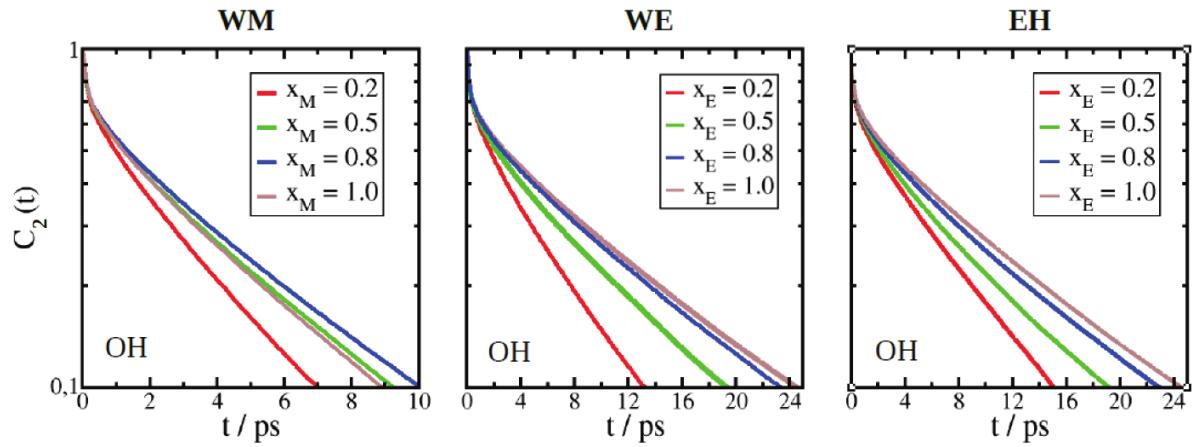

Figure 40: Reorientational correlation functions, $C_2(t)$, of the alcohol OH vector in water - methanol (left panel), water - ethanol (middle panel) and ethanol - hexane (right panel) mixtures. Concentrations of alcohol in the mixtures are listed in legend boxes.

All three panels presented in Figure 40 show similar trends, with $C_2(t)$ exhibiting slower t - decay as concentration of alcohol increases. We conclude that reorientational dynamics of alcohols speeds up with the addition of both water or hexane in the liquid. This conclusion is in agreement with the analysis of Skarmoutsos and Guardia [164], who analyzed the rotational dynamics in supercritical ethanol and discovered that reorientational correlation functions $C_2(t)$ decay faster in time if the molecules are less hydrogen bonded. If we focus particularly on $x_{\mathrm{ALC}} = 0.2$ alcohol concentrations (shown in red), we conclude that in methanol - water, alcohol molecules rotate faster than in ethanol - water, as expected, since it is known that in pure liquids, molecular reorientation of methanol is faster than that of ethanol [152].

In Table 1 we show the reorientational correlation times τ_1 , τ_2 and $< \tau_2 >$ for all three concentrations and mixtures. The trend for all three mixtures is the same: time constants related to the reorientation of the OH alcohol vector increases as alcohol concentration increases, as expected from the results seen in Figure 40. NMR experiments for pure alcohols have shown that the rotational correlation times of methanol is smaller than that of ethanol [94], which is consistent with our results where the methanol time constants are smaller.

System	Value (ps)	$x_{ALC} = 0.2$	$x_{ALC} = 0.5$	$x_{ALC} = 0.8$
Meth - Wat	τ_1	0.131 (+/- 0.006)	0.170 (+/- 0.005)	0.176 (+/- 0.006)
	τ_2	3.476 (+/- 0.069)	4.880 (+/- 0.089)	5.167 (+/- 0.058)
	$\langle\tau_2\rangle$	2.45 (+/- 0.05)	3.36 (+/- 0.07)	3.61 (+/- 0.09)
Eth - Wat	τ_1	0.219 (+/- 0.011)	0.274 (+/- 0.002)	0.295 (+/- 0.007)
	τ_2	6.272 (+/- 0.078)	9.012 (+/- 0.049)	10.921 (+/- 0.098)
	$\langle\tau_2\rangle$	4.41 (+/- 0.15)	6.05 (+/- 0.02)	7.22 (+/- 0.16)
Eth - Hex	τ_1	0.381 (+/- 0.021)	0.379 (+/- 0.045)	0.375 (+/- 0.032)
	τ_2	7.622 (+/- 0.019)	9.328 (+/- 0.018)	10.09 (+/- 0.01)
	$\langle\tau_2\rangle$	5.282 (+/- 0.027)	6.926 (+/- 0.015)	7.124 (+/- 0.025)

Table 1: Short reorientational correlation times τ_1, long reorientational correlation times τ_2 and integral reorientational correlation times $< \tau_2 >$ of the alcohol OH vector in methanol - water, ethanol - water and ethanol - hexane mixtures, for different concentrations of alcohol x_{ALC}.

Reorientational correlation functions $C_2(t)$ with $e(t)$ taken to be parallel to water OH vector are shown in Figure 41, whereas the time constants are given in Table 2. We observe in Figure 41 that, in both water - methanol and water - ethanol mixtures, $C_2(t)$ decays faster as alcohol concentration decreases, meaning that reorientation of water is faster when there is more water in the mixture. NMR relaxation study of alcohol-water mixtures by Ludwig [93] found that a small addition of alcohols (methanol. ethanol and 1-propanol) causes an increase in the rotational correlation times of water. Previous computer simulation studies of methanol-water [45] (with OPLS methanol [73] model and TIP4P water model [72]) found that, for $x_{ALC} = 0.5$, $< \tau_2 >= 5$ ps, which is comparable to our value of 3.686 ps.

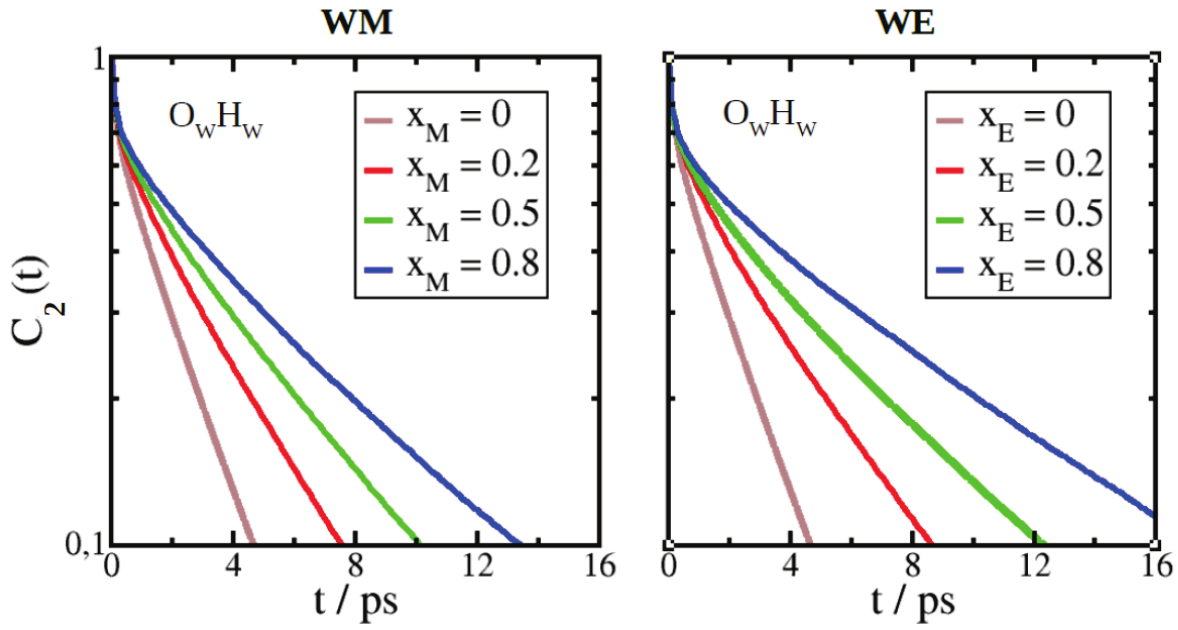

Figure 41: Reorientational correlation functions, $C_2(t)$, of the water O_WH_W vector in water - methanol (left panel) and water - ethanol (right panel) mixtures. Concentrations of alcohol in the mixtures are listed in legend boxes.

System	Value (ps)	$x_{ALC} = 0.2$	$x_{ALC} = 0.5$	$x_{ALC} = 0.8$
Meth-Wat	τ_1	0.129 (+/- 0.001)	0.157 (+/- 0.007)	0.175 (+/- 0.007)
	τ_2	3.764 (+/- 0.034)	5.195 (+/- 0.140)	6.281 (+/- 0.185)
	$\langle\tau_2\rangle$	2.745 (+/- 0.063)	3.686 (+/- 0.086)	4.505 (+/- 0.264)
Eth-Wat	τ_1	0.143 (+/- 0.003)	0.189 (+/- 0.007)	0.228 (+/- 0.013)
	τ_2	4.332 (+/- 0.081)	6.392 (+/- 0.093)	9.265 (+/- 0.328)
	$\langle\tau_2\rangle$	3.161 (+/- 0.042)	4.456 (+/- 0.056)	6.144 (+/- 0.135)

Table 2: Short reorientational correlation times τ_1, long reorientational correlation times τ_2 and integral reorientational correlation times $< \tau_2 >$ of the water O_WH_W vector in methanol - water and ethanol - water mixtures, for different concentrations of alcohol x_{ALC}.

To conclude, we note that reorientational trends observed in Figure 40 and Figure 41 can be also confirmed by the analysis of the lifetime distribution of hydrogen bonds in transient regime. This is illustrated in Figure 42, which shows the lifetime distributions of OO, OO_W and O_WO_W bonds in methanol - water mixture, for concentrations listed in the legend box. The distributions are calculated with the choice $r_C = 3.5$ Å.

Figure 42 shows that, in the context of the lifetime distribution of hydrogen bonds, faster reorientational dynamics manifests through the growth of the amplitudes of secondary peaks in the distribution of hydrogen bonding lifetimes. Taken methanol as an example, slower reorientational dynamics of methanol in pure liquid, compared to the same dynamics in acqueous mixture, is visible through lower amplitudes of secondary OO peaks in $x_M = 1$ case, compared to $x_M < 1$ cases (see left panel of Figure 42). Lower amplitudes indicate lower probability of the

lifetimes within librational period, which is expected for a system with slower reorientational dynamics.

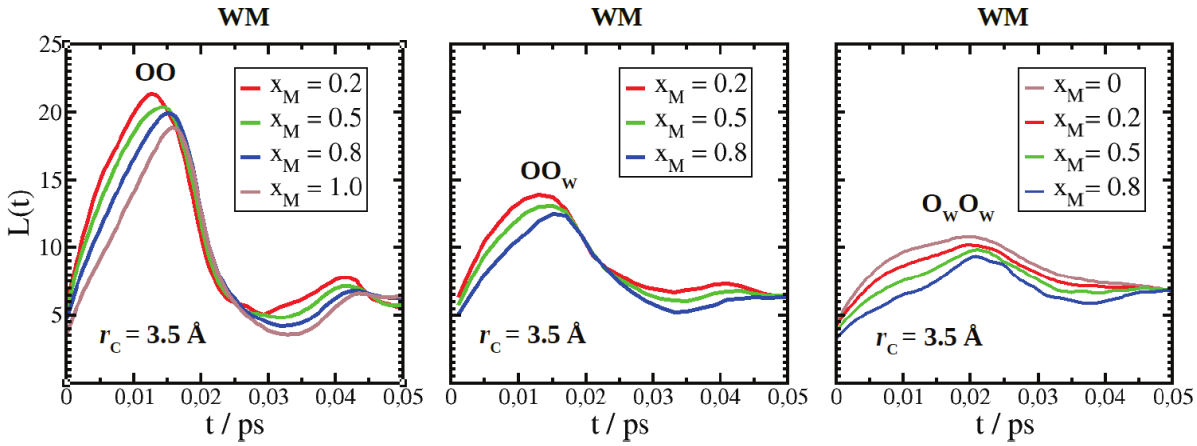

Figure 42: Lifetime distributions of OO (left panel), OO_W and O_WO_W hydrogen bonds in water - methanol mixtures. Alcohol concentrations are listed in the legend boxes for each panel. All distributions are calculated with the choice $r_C = 3.5$ Å.

3.4 Correlations in simple and complex disordered liquids

Previously, in section 3.2.1, dynamic density correlation functions have been discussed in the context of hydrogen bonding dynamics in associative liquids, while formal mathematical definition has been given in the section Theory. In this chapter, the detailed comparative analysis of time - dependent density correlations for different types of simple and associative liquids will be presented and discussed.

3.4.1 Simple Lennard - Jones liquid

Before considering more complex systems, it is convenient to start the analysis with time - dependent density correlations of simple Lennard - Jones liquid, since this system is a good representative of ordinary, simple disordered liquids. Hence, comparison of these functions for simple liquids versus complex liquids is expected to highlight specificities in dynamics of associative systems when compared with simple ones. Self and distinct Van Hove functions, $G^{(s)}(r,t)$ and $G^{(d)}(r,t)$, for several selected t values, listed in the legend box, are presented in Figure 43.

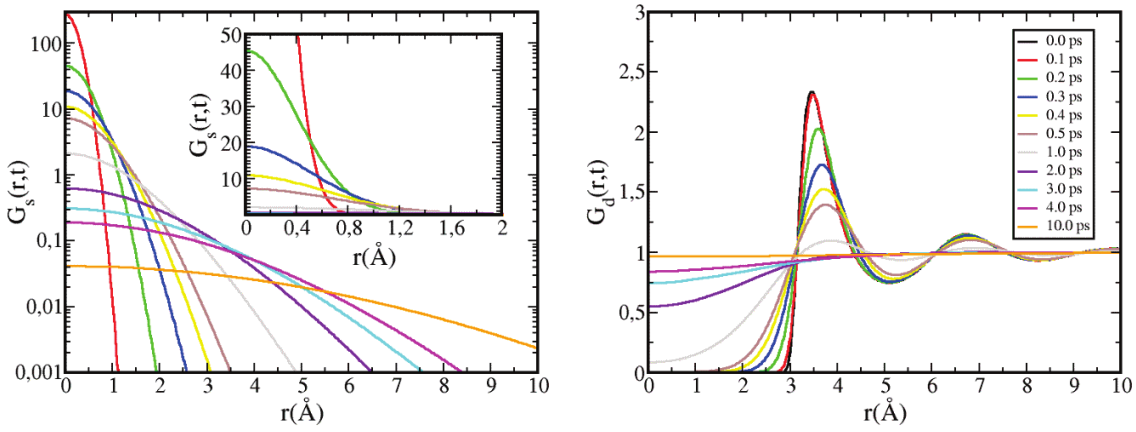

Figure 43: Time dependent self (left panel) and distinct (right panel) density correlations, $G_s(r,t)$ and $G_d(r,t)$ of simple LJ liquid. The y - axis of the main left panel is shown in log scale, while the inset shows the same functions in linear scale. Functions are shown for several selected t values, listed in the legend box in the right panel.

Left panel of Figure 43 shows $G^{(s)}(r,t)$ functions for different time values t in logarithmic y - scale (main panel) and linear scale (inset). In linear scale, $G^{(s)}(r,t)$, for fixed t, has a gaussian - like shape, centered at $r = 0$. At short times, the distribution is very narrow, with the high amplitude around $r = 0$. At larger times, the distribution is broader, with the amplitude around $r = 0$ monotonically decreasing with time.
We recall that $G^{(s)}(r,t)$ represents a probability that a particle diffuses the distance between r

and $r + \mathrm{d}r$ within time interval t. For short time values, narrow distribution of $G^{(s)}(r,t)$ around the origin reflects the fact that particles do not diffuse large distances within very short time intervals. However, at large times, broadening of the distribution around the origin indicates that the probability of diffusing at larger distances increases with increasing time.

Right panel of Figure 43 shows $G^{(d)}(r,t)$ functions for the same time values. One can see that all peaks in the distribution are becoming less defined as time increases, ultimately leading to perfectly homogenous distribution at large times, when $G^{(d)}(r,t) \approx 1$ over entire r - domain. The decay of peak amplitudes with increasing time describes the loss of density correlations at specific r distances as t increases. For instance, the first peak of $G^{(d)}(r,t=0)$ (see the black curve in the right panel of Figure 43), centered at $r \approx 3.5$ Å, describes the spatial distribution of first neighbours around a reference particle, located at the origin. As time increases, the reference particle diffuses from the origin, as implied by broadening of $G^{(s)}(r,t)$ as time increases. The diffusion of the reference particle induces the weakening of density correlations around the first peak, since the neighbouring particles will be more and more randomly distributed around the origin as the reference particle diffuses away. In the limit $t \to \infty$, neighbouring particles are perfectly randomly distributed around the origin, meaning that the average local density in the vicinity of the origin is equal to the density in bulk.

Another interesting feature visible from the right panel of Figure 43 is that the second peak of $G^{(d)}(r,t=0)$, centered at $r \approx 7$ Å, clearly decays slower in time than the first peak. Also, second peak of $G^{(d)}(r,t=0)$ is characterized by lower amplitude, relative to the first peak. Lower amplitude of the second peak indicates that the density within second coordination shell is much less correlated with the density at the origin, than the density within first coordination shell is. In addition, slower t - decay of the second peak implies that the density around second coordination shell is much less affected by the diffusion of the reference particle from the origin.

3.4.2 Simple liquids - acetone and carbon tetrachloride

We start this section by discussing dynamical correlations in acetone and carbon tetrachloride (CCl_4), which are good represntatives of simple disordered liquids. Both acetone and CCl_4 are modeled with OPLS models [41, 74]. Although both liquids are polar, they do not exhibit micro-heterogeneities, as the ones seen for alcohols. This is the reason why these liquids are not considered as complex liquids, but simple liquids. For each liquid, we present the self and distinct Van Hove functions $G^{(s)}(r,t)$ and $G^{(d)}(r,t)$, together with the self and total intermediate scattering functions $F^{(s)}(k,t)$ and $F^{(t)}(k,t)$, and the self and total dynamical structure factors $S^{(s)}(k,\omega)$ and $S^{(t)}(k,\omega)$. Time - dependent functions will be shown in r - space or k - space, for 29 selected time values (0 ps, 0.1 ps, 0.2 ps, ..., 1 ps, 2 ps, ..., 10 ps, 20 ps, ..., 100 ps). Since the decay of the curves is monotonic, we will not label all the curves, but merely few selected ones for reference (typically 0 ps, 0.1 ps, 1 ps, 10 ps and 100 ps).

Self Van Hove functions for acetone, $G^{(s)}_{\mathrm{OO}}$ and $G^{(s)}_{\mathrm{OC}}$, are presented in the left and right panels of Figure 44 respectively, while corresponding functions in k - space, $F^{(s)}_{\mathrm{OO}}$ and $F^{(s)}_{\mathrm{OC}}$, are shown in the insets. For reference, functions corresponding to the time values 0 ps, 0.1 ps, 1 ps, 10 ps and 100 ps are shown in thick lines, with black, red, green, blue and orange colors respectively. First, we observe the delta functions (thick black vertical lines), centered at $r = 0$ for OO correlations, and at $r \approx 1$ Å for OC correlations. Generally, if atoms a and b form the same molecule, $\rho G^{(s)}_{ab}(r,t)\mathrm{d}\mathbf{r}$, represents the probability at time t of finding atom b at separation r from where atom a was located at $t = 0$. At $t = 0$, this probability will be zero everywhere except at $r = d_{ab}$, with d_{ab} representing intramolecular distance between atoms a and b. This explains why the delta function is centered at the origin for OO correlations, while it is shifted at larger r for OC correlations.

For $t > 0$, $G^{(s)}$ functions have parabolic appearance in log-scale, which would correspond to gaussian form in linear scale. Formally, in the textbooks, we can find: [56]

$$G^{(s)}(r,t) = \frac{1}{\rho\,(4\pi Dt)^{\frac{3}{2}}}\exp(-\frac{r^2}{4Dt}) \tag{140}$$

with D representing the diffusion constant, and normalization factor $\rho^{-1}\,(4\pi Dt)^{-\frac{3}{2}}$ being determined with normalization condition:

$$\int G^{(s)}(r,t)\mathrm{d}\mathbf{r} = \frac{1}{\rho} \tag{141}$$

,where molar volume is equal to ρ^{-1}. However, our tests have shown that $G^{(s)}$ exhibits gaussian form (from equation 140) only for large t values (~ 10 ps), while, for lower t - values, it deviates significantly from the gaussian form. More details about the agreement between D from

equation (140) and the diffusion obtained by experiments will be discussed later on. For now, we return to the insets presented in Figure 44. From the left inset we note that $F_{\mathrm{OO}}^{(s)}(k,0)=1$ for all k - values (thick black line), which is the mathematical consequence of performing spatial Fourier transform of the delta function $\delta(r)$ from the main panel. In addition, the oscillating $F_{\mathrm{OC}}^{(s)}(k,0)$ function from the right inset is obtained from the Fourier transform of $\delta(r-d_{\mathrm{OC}})$, with d_{OC} denoting intramolecular OC distance.

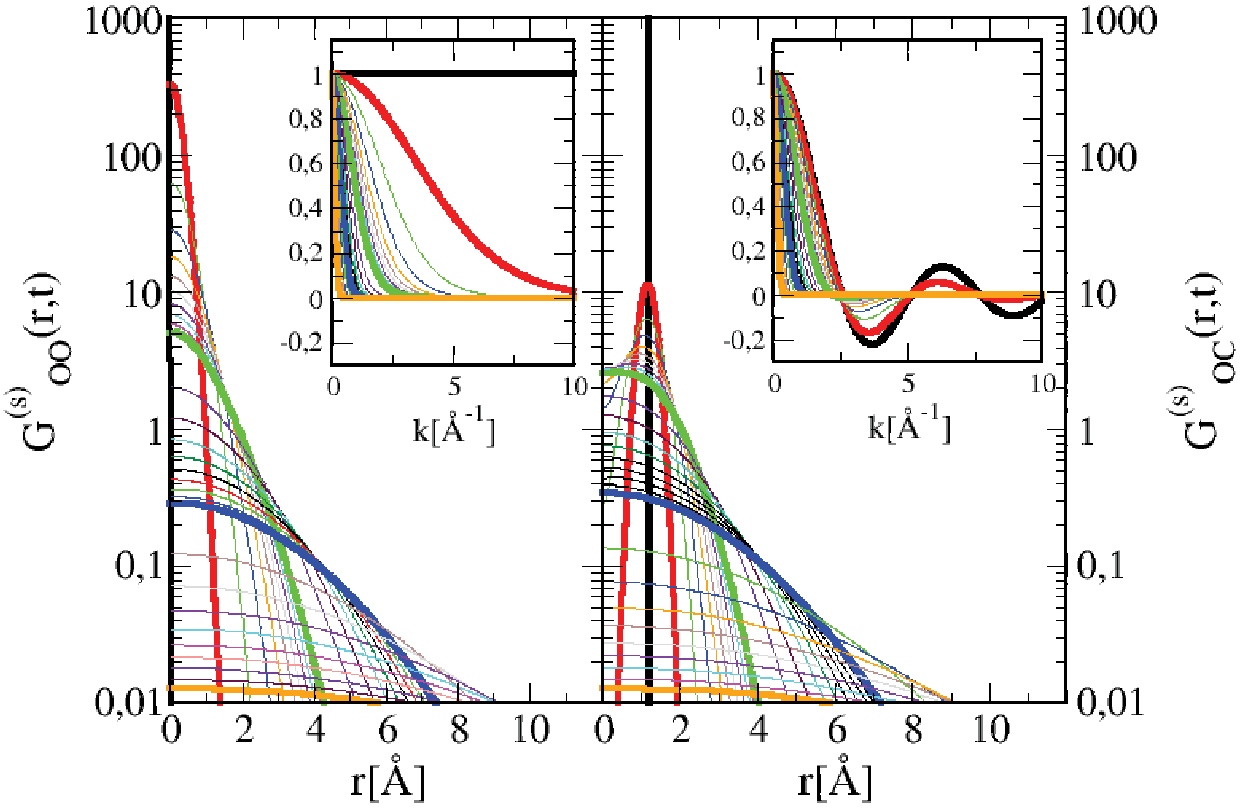

Figure 44: **acetone:** Main panels show self Van Hove functions, $G_{\mathrm{OO}}^{(s)}(r,t)$ and $G_{\mathrm{OC}}^{(s)}(r,t)$, in the left and right panels respectively. Corresponding scattering functions are shown in the insets. All plots are shown in logarithmic y-scale, for the visibility purpose. Time values of 0 ps, 0.1 ps, 1 ps, 10 ps and 100 ps are highlighted and presented with thick black, red, green, blue and orange lines respectively.

Figure 45 presents self CC and CCl correlations for CCl_4 in the same manner they are presented in Figure 44 for acetone. General trends appear to be similar to the ones observed in Figure 44. However, we note that the loss of self - correlations in time is faster for acetone than for CCl_4, which is visible through lower values of $G_{\mathrm{OO}}^{(s)}(r=0,t)$ and $G_{\mathrm{OC}}^{(s)}(r=0,t)$ of acetone when compared with correlations in CCl_4, $G_{\mathrm{CC}}^{(s)}(r=0,t)$ and $G_{\mathrm{CCl}}^{(s)}(r=0,t)$ respectively. Faster decay of acetone correlations, compared to correlations in CCl_4, could be attributed to larger

dipole moment of acetone molecule. Namely, the magnitude of partial charges on O and C sites of acetone, within the OPLS (united-atom) model [74], is 0.47, while the same magnitude in the case of CCl_4, within the OPLS (all-atom) model [41], is 0.248. Larger values of charges on acetone lead to stronger intermolecular interactions of the central molecule with the surrounding, which could lead to faster decay of self - correlations in time. In addition, we note that functions in k - space (see insets of Figures 44 and 45) confirm the trends observed in r - space.

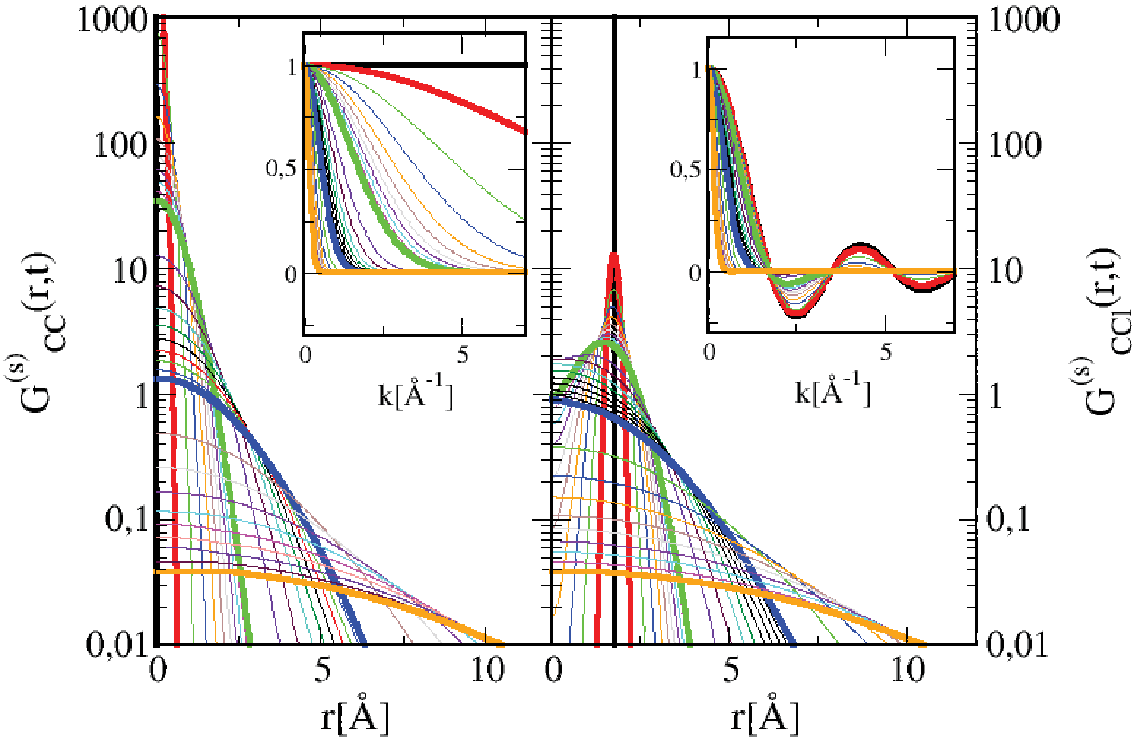

Figure 45: **CCl_4:** Main panels show self Van Hove functions, $G^{(s)}_{CC}(r,t)$ and $G^{(s)}_{CCl}(r,t)$, in the left and right panels respectively, while corresponding scattering functions are shown in the insets. We use the same conventions as in Figure 44.

Now we turn our attention to distinct Van Hove functions of acetone and CCl_4. Figure 46 shows $G^{(d)}_{OO}$ and $G^{(d)}_{OC}$ correlations in acetone in the left and right panels respectively, while $G^{(d)}_{CC}$ and $G^{(d)}_{CCl}$ correlations of CCl_4 are presented in Figure 47. The main differences between the two figures are related to the peak amplitudes of $G^{(d)}(r,t=0)$ correlations in acetone versus CCl_4, followed by the different decorrelation trends. For example, lower first peak of $G^{(d)}_{OO}$ correlations in acetone, compared to $G^{(d)}_{CC}$ correlations in CCl_4, indicates that correlations between the first neighbours are more pronounced in CCl_4 than in acetone. In addition, we observe faster decorrelation of acetone in time, compared to CCl_4. This is in agreement with the trend observed when $G^{(s)}$ correlations between the two liquids were compared, where we equally found that acetone decorrelates sooner than CCl_4 .

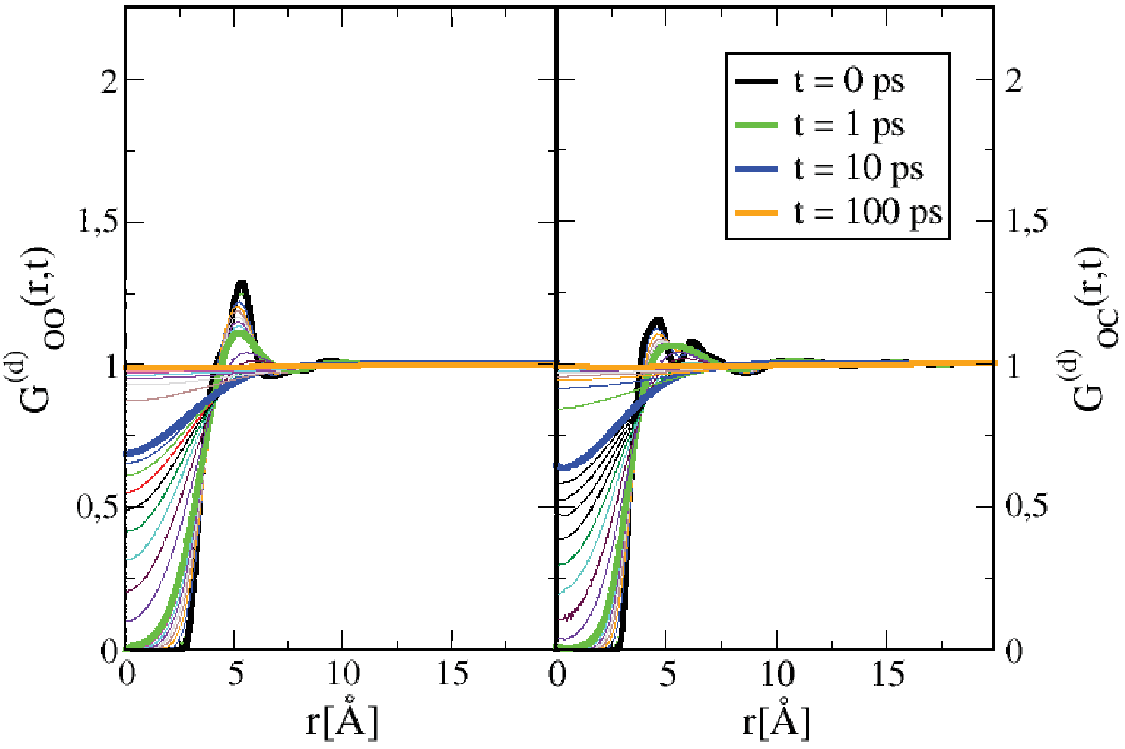

Figure 46: **acetone:** Distinct Van Hove functions, $G^{(d)}_{\mathrm{OO}}(r,t)$ and $G^{(d)}_{\mathrm{OC}}(r,t)$, are shown in the left and right panels respectively. Higlighted time values are presented with thick lines, with the color convention shown in the legend box.

Total intermediate scattering functions $F^{(t)}(k,t)$, corresponding to correlations discussed above, are shown in Figure 48 for acetone and Figure 49 for CCl_4. From Figure 48, we note that $F^{(t)}_{\mathrm{OO}}(k,t=0)$ function (left panel) goes asymptotically to 1, while $F^{(t)}_{\mathrm{OC}}(k,t=0)$ goes asymptotically to 0 in large r limit. This asymptotic difference is caused by the difference between the self parts, $F^{(s)}_{\mathrm{OO}}(k,t=0)$ versus $F^{(s)}_{\mathrm{OC}}(k,t=0)$, as demonstrated in the insets of Figure 44.

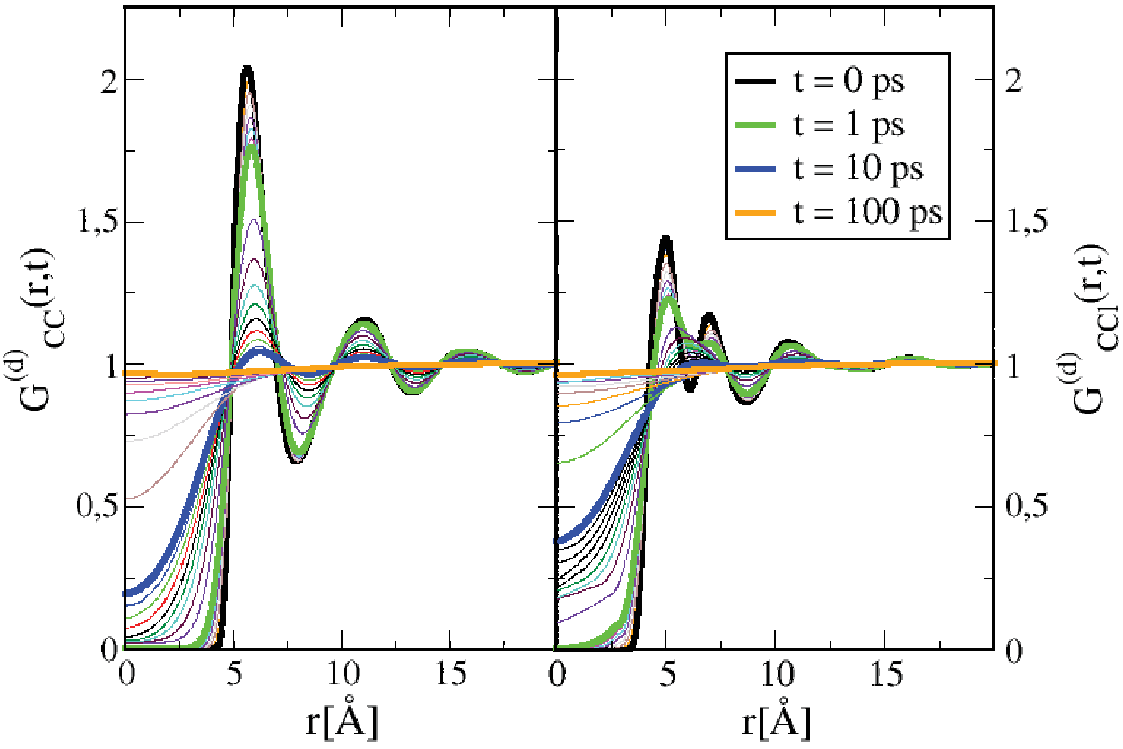

Figure 47: **CCl_4:** Distinct Van Hove functions, $G^{(d)}_{CC}(r,t)$ and $G^{(d)}_{CCl}(r,t)$, are shown in the left and right panels respectively. Highlighted time values are presented with thick lines, with the color convention shown in the legend box.

In addition, from Figure 48, the main peaks of $F^{(t)}_{OO}(k,t=0)$ and $F^{(t)}_{OC}(k,t=0)$ are observed at $k \approx 1.2$ Å^{-1} in both cases. This value corresponds to $r \approx 5$ Å in real space, which nearly corresponds to the first peaks of $G^{(d)}_{OO}(r,t=0)$ and $G^{(d)}_{OC}(r,t=0)$, as seen from Figure 46. Similar observations can be found also in the case of CCl_4 (see Figure 49).

Comparative analysis of Figures 48 and 49 leads to similar conclusions obtained from the analysis of correlations in r - space, where we found that acetone decorrelates faster than CCl_4.

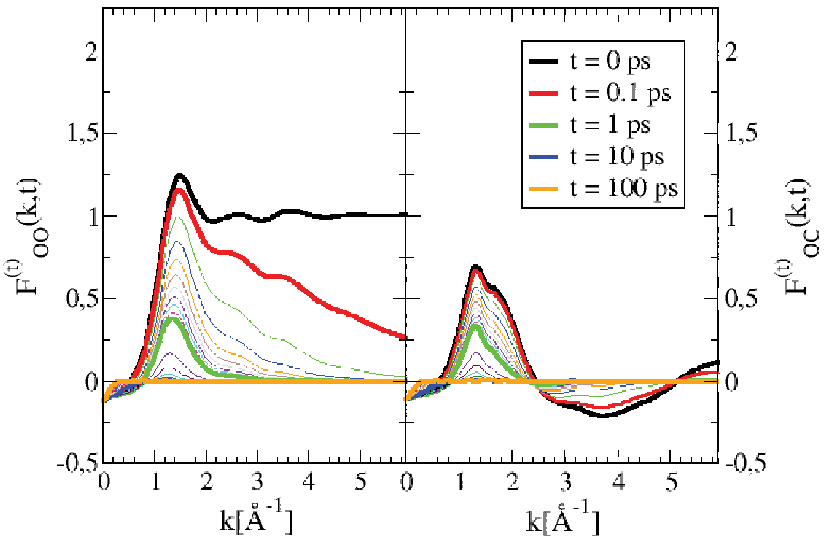

Figure 48: **acetone:** Total intermediate scattering functions, $F^{(t)}_{\mathrm{OO}}(k,t)$ and $F^{(t)}_{\mathrm{OC}}(k,t)$, are shown in the left and right panels respectively. Higlighted time values are presented with thick lines, with the color convention shown in the legend box.

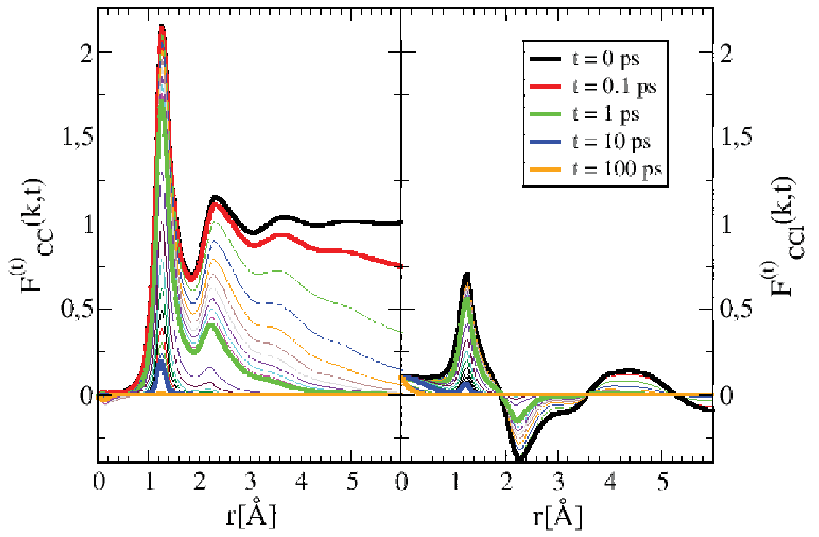

Figure 49: **CCl_4:** Total intermediate scattering functions, $F^{(t)}_{\mathrm{CC}}(k,t)$ and $F^{(t)}_{\mathrm{CCl}}(k,t)$, are shown in the left and right panels respectively. Higlighted time values are presented with thick lines, with the color convention shown in the legend box.

Finally, we show the total dynamic structure factors $S^{(t)}(k,\omega)$ in the main panels and its self parts $S^{(s)}(k,\omega)$ in the insets of Figures 50 and 51, for acetone and CCl_4 respectively. Functions are shown in k - space, for various ω values. For reference, we highlight particularly $\omega =$

0.05 ps^{-1} (thick black line), $\omega = 1$ ps^{-1} (thick red line), $\omega = 10$ ps^{-1} (thick green line) and $\omega = 30$ ps^{-1} (thick blue line).

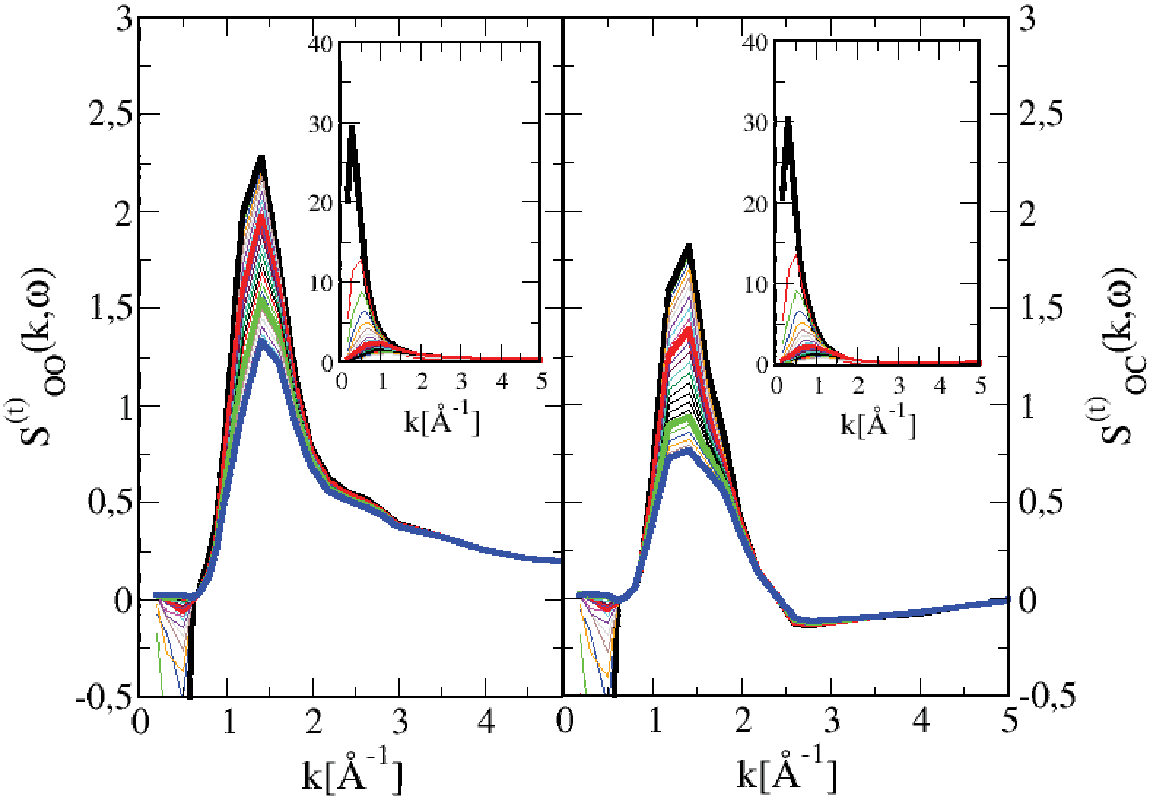

Figure 50: **acetone:** Main panels show total dynamical structure factors, $S^{(t)}_{\mathrm{OO}}(k,\omega)$ and $S^{(t)}_{\mathrm{OC}}(k,\omega)$, in the left and right panels respectively. Corresponding self parts, $S^{(s)}_{\mathrm{OO}}(k,\omega)$ and $S^{(s)}_{\mathrm{OC}}(k,\omega)$, are shown in the insets. Frequency values of 0.05 ps^{-1}, 1 ps^{-1}, 10 ps^{-1} and 30 ps^{-1} are highlighted and presented with thick black, red, green and blue lines respectively.

First, we note that the main peaks of all $S^{(t)}(k,\omega)$ functions coincide with the main peaks from corresponding $F^{(t)}(k,t)$ functions. Secondly, the negative parts of $S^{(t)}_{\mathrm{OO}}(k,\omega)$ and $S^{(t)}_{\mathrm{OC}}(k,\omega)$ around $k \approx 0$ are attributed to numerical artifacts, coming from the fact that $F^{(t)}_{\mathrm{OO}}(k,t)$ and $F^{(t)}_{\mathrm{OC}}(k,t)$ are negative around $k \approx 0$ (see Figures 48 and 49). This is caused by the well-known problem when $g(r)$ is calculated in simulations. Namely, the asymptote of $g(r)$ slightly differs from 1, tending to value below 1 [86]. This is also a known problem in the evaluation of KBI integrals from computer simulations [34, 111, 129, 82, 50].

By comparing the structure factors of acetone and CCl_4, we see that the biggest difference is the absence of the peak at $k \approx 2.5$ A$^{\circ -1}$of acetone $S^{(t)}_{\mathrm{OO}}(k,\omega)$, compared to $S^{(t)}_{\mathrm{CC}}(k,\omega)$ dynamical structure factor of CCl_4 . Apart from this, the dynamical structure factors between the two liquids look very similar.

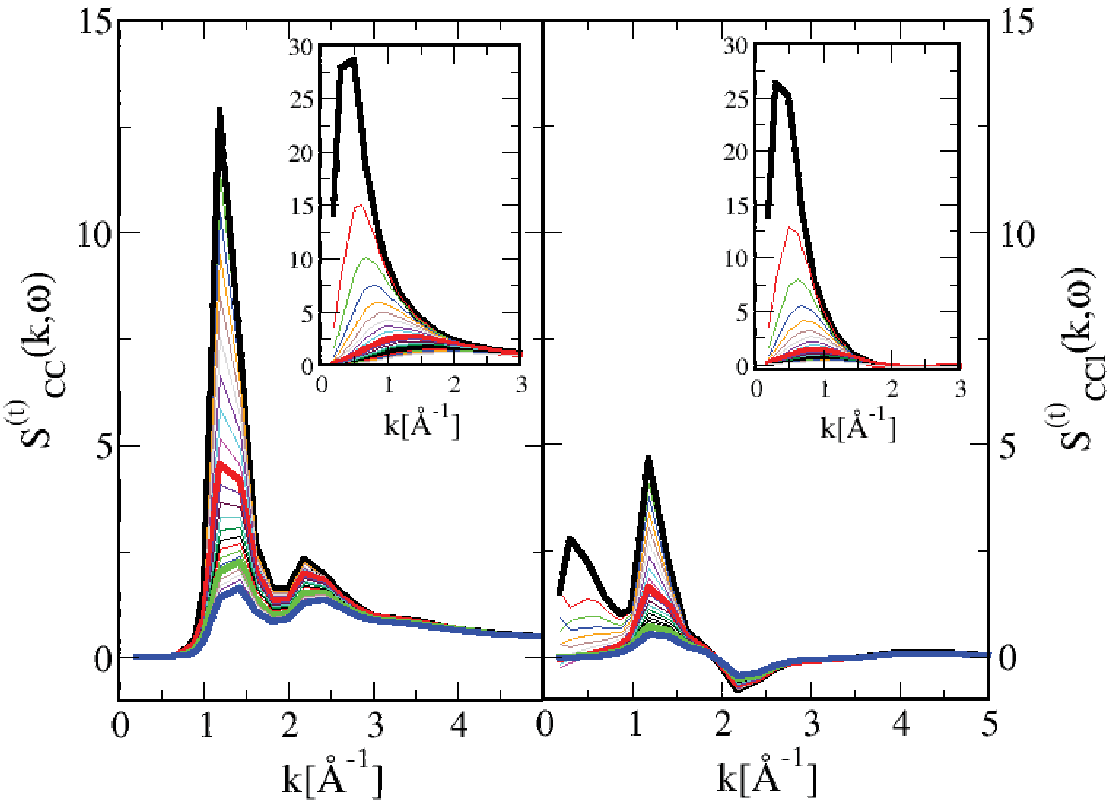

Figure 51: **CCl_4:** Main panels show total dynamical structure factors, $S^{(t)}_{CC}(k,\omega)$ and $S^{(t)}_{CCl}(k,\omega)$, in the left and right panels respectively. Corresponding self parts, $S^{(s)}_{CC}(k,\omega)$ and $S^{(s)}_{CCl}(k,\omega)$, are shown in the insets. Frequency values of 0.05 ps^{-1}, 1 ps^{-1}, 10 ps^{-1} and 30 ps^{-1} are highlighted and presented with thick black, red, green and blue lines respectively.

3.4.3 Complex liquids - water and ethanol

We will examine correlations in water and ethanol, taken as representatives of complex disordered liquids. Comparison of these results with the previous ones, related to acetone and CCl_4, is expected to reveal the differences between correlations in simple liquids versus complex disordered liquids. Recently, dynamic correlations functions of various models of water have been compared with experimental data [106]. We note that our data obtained for SPC/E model of water quantitatively matches with functions obtained in reference [106].

Self Van Hove functions, corresponding to OO and OH correlations in water, are presented in Figure 52. We can note immediately that correlations in r - space vanish faster in water than in both acetone and CCl_4. However, in k - space, decorrelation in acetone and water seem to be very similar. This difference between the trends observed in r - space versus k - space can be explained with the following arguments. As given by equation (140), the self Van Hove function, for a fixed value of t, is determined with the slope of the function, $(4Dt)^{-1}$ and the normalization factor $G_s(r=0,t)$, which depends of both molar volume of the liquid and the diffusion properties of the liquid:

$$G^{(s)}(r=0,t) = \frac{1}{\rho\,(4\pi Dt)^{\frac{3}{2}}} \tag{142}$$

Hence, the loss of correlations around $r=0$ in time, aside being dependent of diffusion, also depends of molar volume ρ^{-1}. This is important to keep in mind when comparing the loss of self - correlations between two different liquids in r - space, as it has been done in this section for OO correlations between water and acetone. The ratio of values obtained for the two liquids is:

$$\frac{G^{(s)}_{A;\mathrm{OO}}(r=0,t)}{G^{(s)}_{W;\mathrm{OO}}(r=0,t)} = \frac{\rho_W}{\rho_A}\left(\frac{D_{W;\mathrm{OO}}}{D_{A;\mathrm{OO}}}\right)^{\frac{3}{2}} \tag{143}$$

,where $G^{(s)}_{A;\mathrm{OO}}(r=0,t)$ and $G^{(s)}_{W;\mathrm{OO}}(r=0,t)$ denote OO self Van Hove functions of acetone and water respectively. This implies that condition $D_A = D_W$ does not necessarily imply identical loss of correlations in both liquids (i.e. it does not imply $G^{(s)}_{A;\mathrm{OO}}(r=0,t) = G^{(s)}_{W;\mathrm{OO}}(r=0,t)$). It is possible that acetone decorrelates slower than water, even if diffusion D in both liquids is the same. This will occur if the molar density of acetone is smaller than the molar density of water, as it is the case in reality.

In textbooks, the corresponding scattering function related to the self Van Hove function is: **[56]**

$$F^{(s)}(k,t) = \exp(-Dtk^2) \tag{144}$$

,implying that, for fixed value of t, gaussian given in the last equation depends only of diffusion D. Hence, the decay of $F^{(s)}(k,t)$ correlations in k - space is governed purely by diffusion. Since, at short times (~ 0.1 ps), $F^{(s)}_{\mathrm{OO}}(k,t)$ functions look nearly the same for both liquids (see thick red curves in the insets of Figures 44 and 52), we conclude that diffusion in both liquids is nearly the same at this short timescale. The differences in speed of decorrelation of the two liquids, which we observed in r - space at short times, are caused by different molar densities of the two liquids.

Next, we show OO and OH self correlations of ethanol in Figure 53. We observe that correlations in r - space are lost significantly slower than for water. In addition, comparison of the insets from Figures 52 and 53 indicates that the diffusion of ethanol and water is nearly similar at short timescales (~ 0.1 ps - thick red curves in the insets).

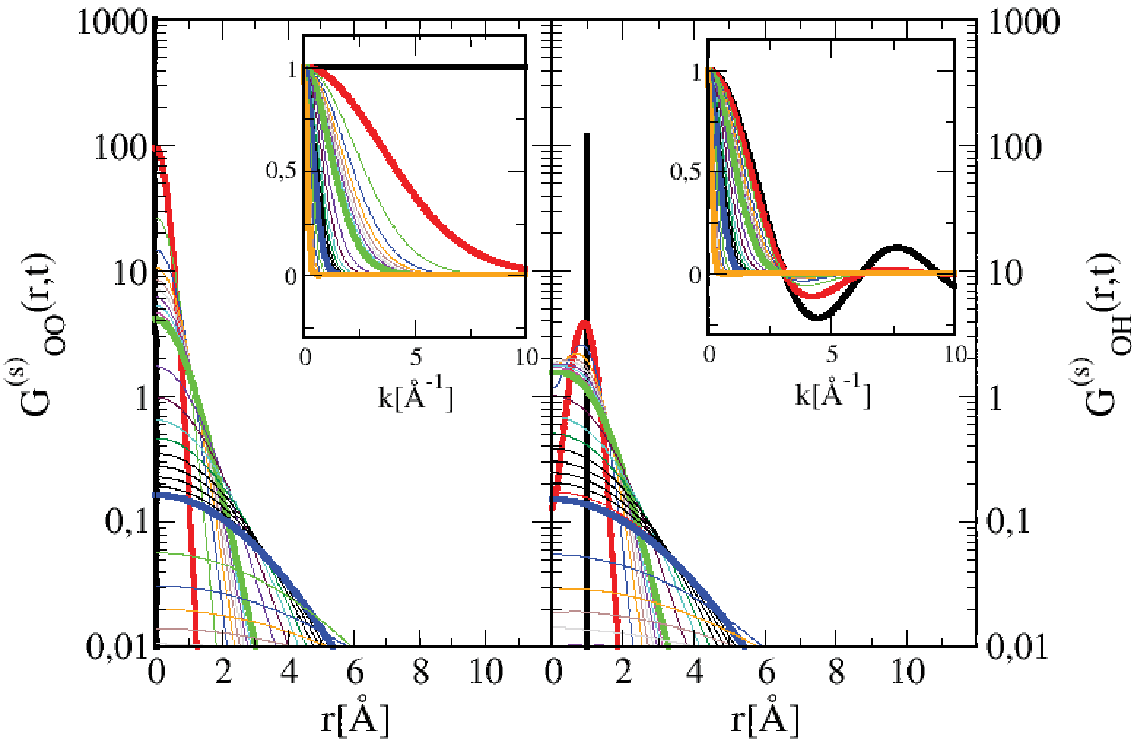

Figure 52: **water:** Main panels show self Van Hove functions, $G^{(s)}_{\mathrm{OO}}(r,t)$ and $G^{(s)}_{\mathrm{OH}}(r,t)$, in the left and right panels respectively. Corresponding scattering functions are shown in the insets. All plots are shown in logarithmic y-scale, for the visibility purpose. Time values of 0 ps, 0.1 ps, 1 ps, 10 ps and 100 ps are highlighted and presented with thick black, red, green, blue and orange lines respectively.

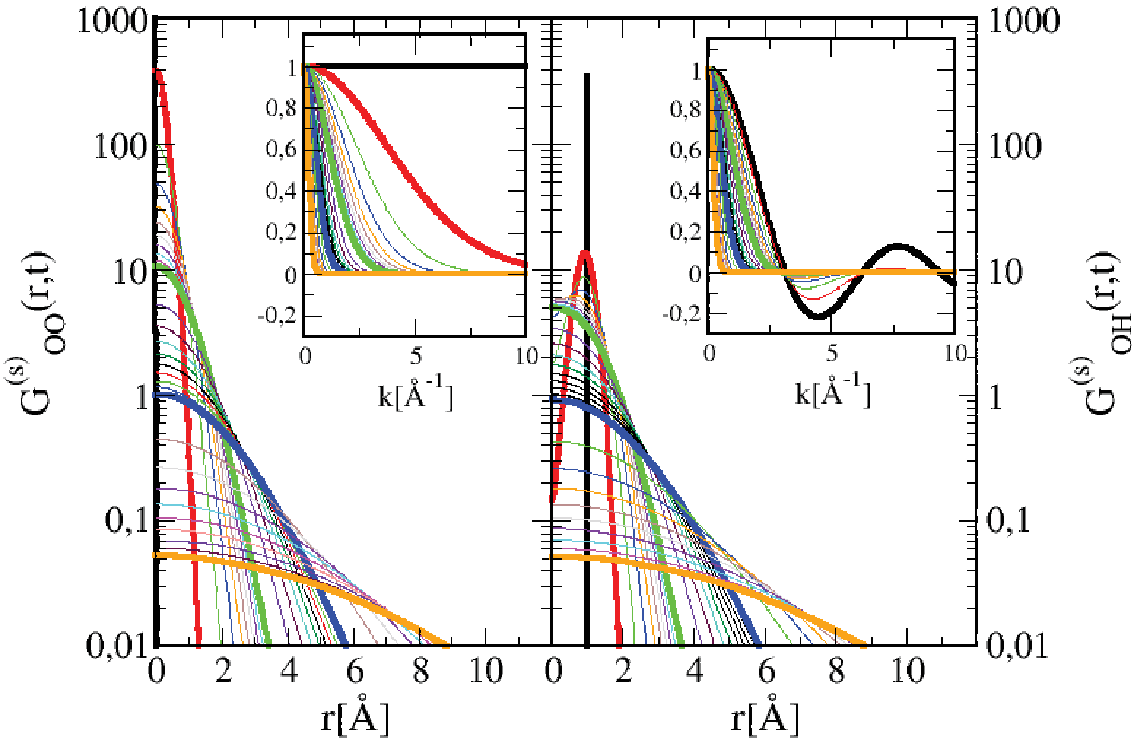

Figure 53: **ethanol:** Main panels show self Van Hove functions, $G_{\mathrm{OO}}^{(s)}(r,t)$ and $G_{\mathrm{OH}}^{(s)}(r,t)$, in the left and right panels respectively, while corresponding scattering functions are shown in the insets. We use the same conventions as in Figure 52.

Distinct OO and OH Van Hove correlations are presented in Figures 54 and 55 for water and acetone respectively. We observe similar trends as in the case of self correlations shown above: water decorrelates faster than ethanol. For example, for $t = 1$ ps (thick green curves), correlations around the first peak ($r \approx 2.8$ Å) are dead in the case of water, while they are still preserved in the case of ethanol. In addition, both water and ethanol decorrelate faster than CCl_4.

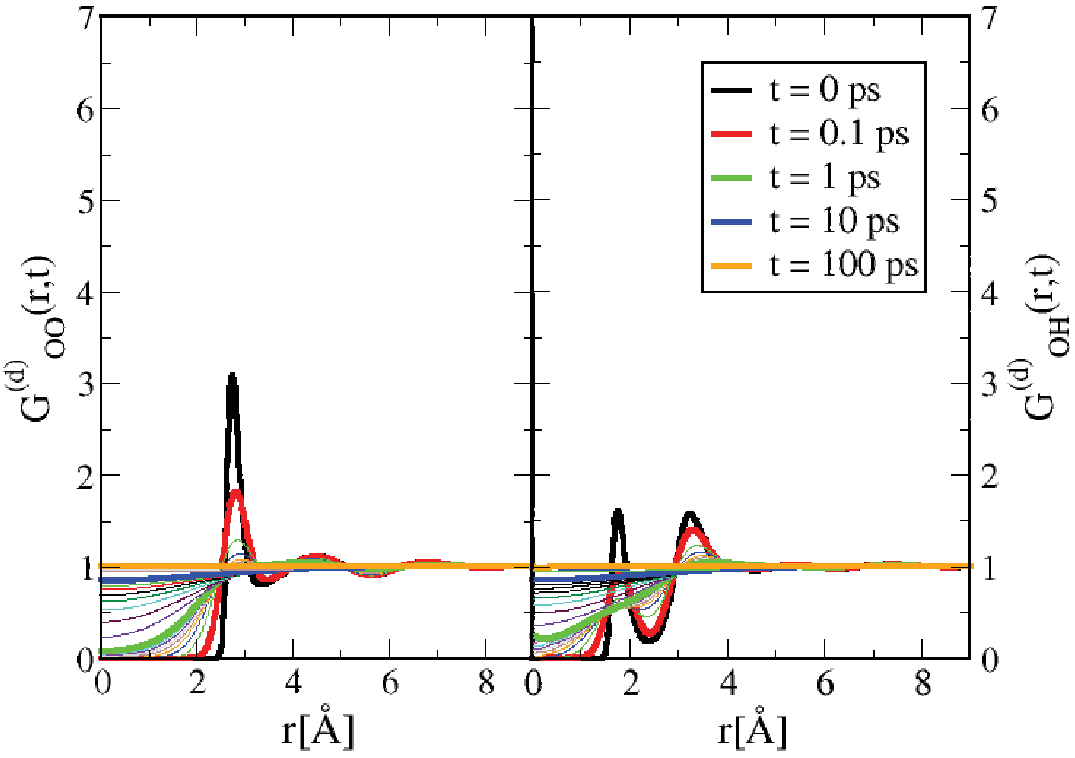

Figure 54: **water:** Distinct Van Hove functions, $G_{\mathrm{OO}}^{(d)}(r,t)$ and $G_{\mathrm{OH}}^{(d)}(r,t)$, are shown in the left and right panels respectively. Higlighted time values are presented with thick lines, with the color convention shown in the legend box.

Faster decorrelation between the first neighbours in associative liquids, compared to simple liquids, might seem counter-intuitive at first, since the attractive interaction between first neighbours in associative liquid is expected to be stronger than in simple liquids, potentially leading to longer lasting correlations between the first neighbours in time. However, strong attractive interaction between first neighbours has the opposite effect in reality. Since the attractive interaction between first neighbours in associative liquid is stronger than attractive interaction between first neighbours in simple liquid, atoms within the first shell of associative system are more affected by the diffusion of the reference atom from the origin, than it is the case in simple liquid, since the mutual attraction between first neighbours is weaker in latter case. Therefore, as the reference atom in associative system diffuses from the origin in time, it simultaneously drags the first neighbours out of the first coordination shell, with attractive electrostatic force. This effect is much weaker in the case of simple liquids, since the attractive interaction between neighbours is weaker. Consequently, first neighbours are less affected by the diffusion of the reference atom from the origin in time, leading to slower t - decay of density correlations.

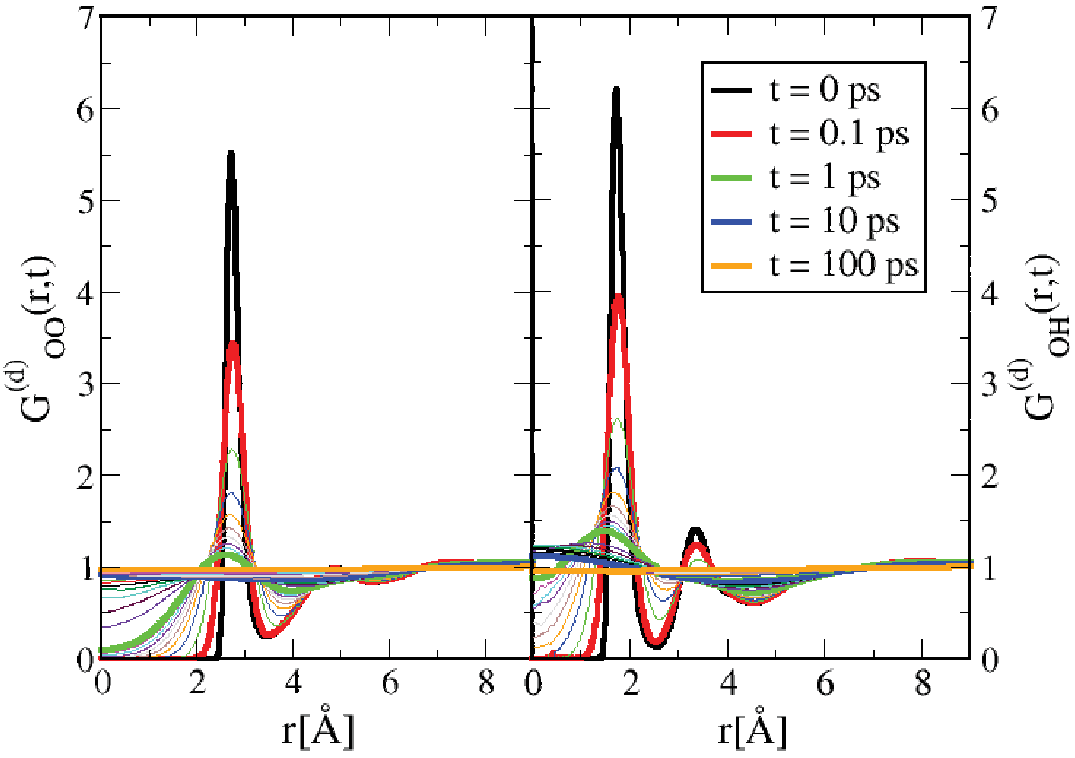

Figure 55: **ethanol:** Distinct Van Hove functions, $G^{(d)}_{\mathrm{OO}}(r,t)$ and $G^{(d)}_{\mathrm{OH}}(r,t)$, are shown in the left and right panels respectively. Higlighted time values are presented with thick lines, with the color convention shown in the legend box.

We show total intermediate scattering functions, $F^{(t)}_{\mathrm{OO}}$ and $F^{(t)}_{\mathrm{OH}}$ in Figures 56 and 57, for water and ethanol respectively. The origin of peaks at $k \approx 2$ A$^{\mathring{-}1}$ and $k \approx 3$ A$^{\mathring{-}1}$ of $F^{(t)}_{\mathrm{OO}}(k,t=0)$ function for both water and ethanol (left panels of Figures 56 and 57) has been discussed in section 3.1. Here, we note that the time decay of both peaks appears to be similar in both liquids. This indicates that the structural features associated to the two k - values relax similarly in time. In addition, the pre - peak of $F^{(t)}_{\mathrm{OO}}$ correlations of ethanol, located at $k \approx 1$ A$^{\mathring{-}1}$, decays significantly slower in time. The same conclusion is valid also for $F^{(t)}_{\mathrm{OH}}$ correlations in ethanol, where the pre - peak is centered around the same k - value as for $F^{(t)}_{\mathrm{OO}}$ case. This is expected, since the formation of the pre - peak in the structure factor is related to the formation of supra-molecular aggregates in associative liquids, as discussed in section 3.1. The time - decay of the pre - peak describes the timescale at which correlations between aggregates are lost. Our results show that these long - ranged correlations decay much slower in time than short - ranged correlations, attributed to larger k - values.

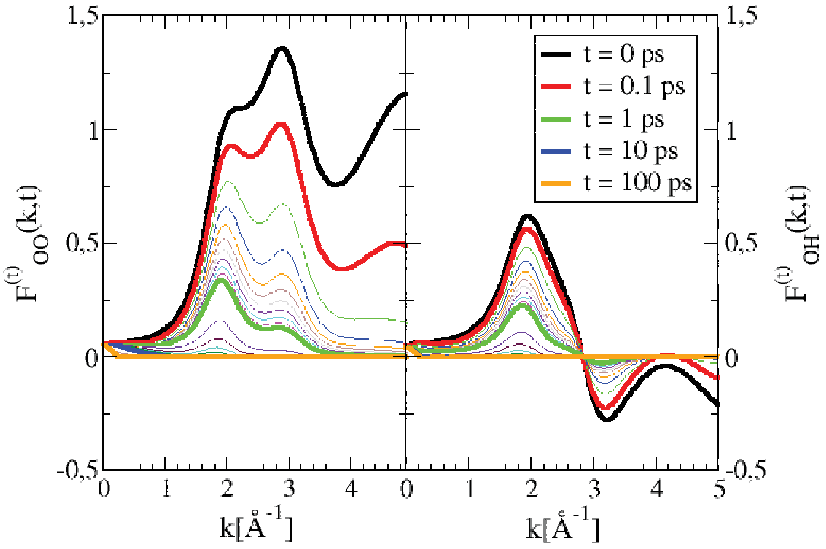

Figure 56: **water:** Total intermediate scattering functions, $F^{(t)}_{\mathrm{OO}}(k,t)$ and $F^{(t)}_{\mathrm{OH}}(k,t)$, are shown in the left and right panels respectively. Higlighted time values are presented with thick lines, with the color convention shown in the legend box.

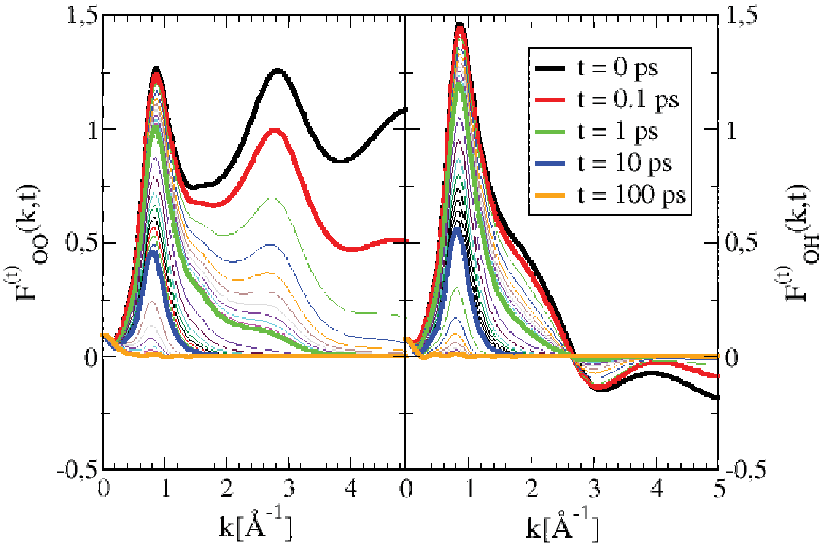

Figure 57: **ethanol:** Total intermediate scattering functions, $F^{(t)}_{\mathrm{OO}}(k,t)$ and $F^{(t)}_{\mathrm{OH}}(k,t)$, are shown in the left and right panels respectively. Higlighted time values are presented with thick lines, with the color convention shown in the legend box.

Finally, we show dynamic structure factors $S^{(t)}_{\mathrm{OO}}(k,\omega)$ and $S^{(t)}_{\mathrm{OH}}(k,\omega)$ in Figures 58 and 59. We note that the k- values at which peaks appear in $S^{(t)}(k,\omega)$ coincide with the peak positions in $F^{(t)}(k,t)$, for each type of correlations. However, in the case of $S^{(t)}_{\mathrm{OO}}(k,\omega)$ of water (left panel

of Figure 58), we observe an additional peak at $k \approx 0.5$ A$^{\circ -1}$, which we do not observe in the case of $F_{\mathrm{OO}}^{(t)}(k,t)$ for the same liquid. This peak could imply the existence of the structure at the lengthscale of ~ 10 Å in the microstructure of water. The peak appears only at low frequencies, namely for $\omega = 0.05$ ps^{-1} (thick black curve), but already disappears at $\omega = 1$ ps^{-1} (thick red curve). This suggests the slow relaxation process attributed to this structure. Interestingly, at the distance $r \approx 10$ Å, the periodicity of $g_{OO}(r)$ correlations in water shifts from ~ 2 Å (earlier denoted with $0.6\,\sigma$) to ~ 3 Å (earlier denoted with σ). This could imply that the peak at $k \approx 0.5$ A$^{\circ -1}$ of $S_{\mathrm{OO}}^{(t)}(k,\omega)$ corresponds to charge ordered local structure of water, characterized by periodicity of ~ 2 Å, which relaxes slowly in time. In addition, this peak could be interpreted as dynamical equivalent of the static pre - peak, observed earlier in the structure factors of alcohols.

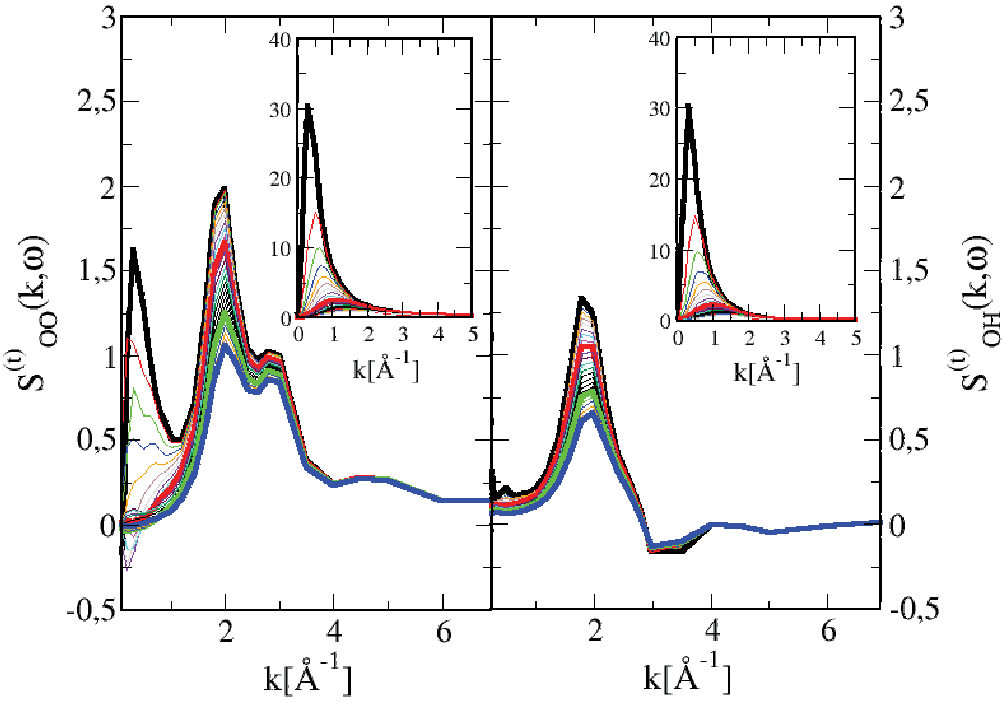

Figure 58: **water:** Main panels show total dynamical structure factors, $S_{\mathrm{OO}}^{(t)}(k,\omega)$ and $S_{\mathrm{OH}}^{(t)}(k,\omega)$, in the left and right panels respectively. Corresponding self parts, $S_{\mathrm{OO}}^{(s)}(k,\omega)$ and $S_{\mathrm{OH}}^{(s)}(k,\omega)$, are shown in the insets. Frequency values of 0.05 ps^{-1}, 1 ps^{-1}, 10 ps^{-1} and 30 ps^{-1} are highlighted and presented with thick black, red, green and blue lines respectively.

In the case of ethanol (see Figure 59), the equivalent peak appears at $k \approx 1$ A$^{\circ -1}$, which coincides with the position of the pre - peak of the structure factor of ethanol. However, the height of the peak is significantly larger in the case of ethanol, implying that slow relaxation processes (i.e. low ω) are mainly associated with relaxation of correlations between supramolecular aggregates in the alcohol. Conversely, in water, low frequencies are almost equally associated

with both short - ranged and long - ranged correlations (both small k and large k wavevectors).

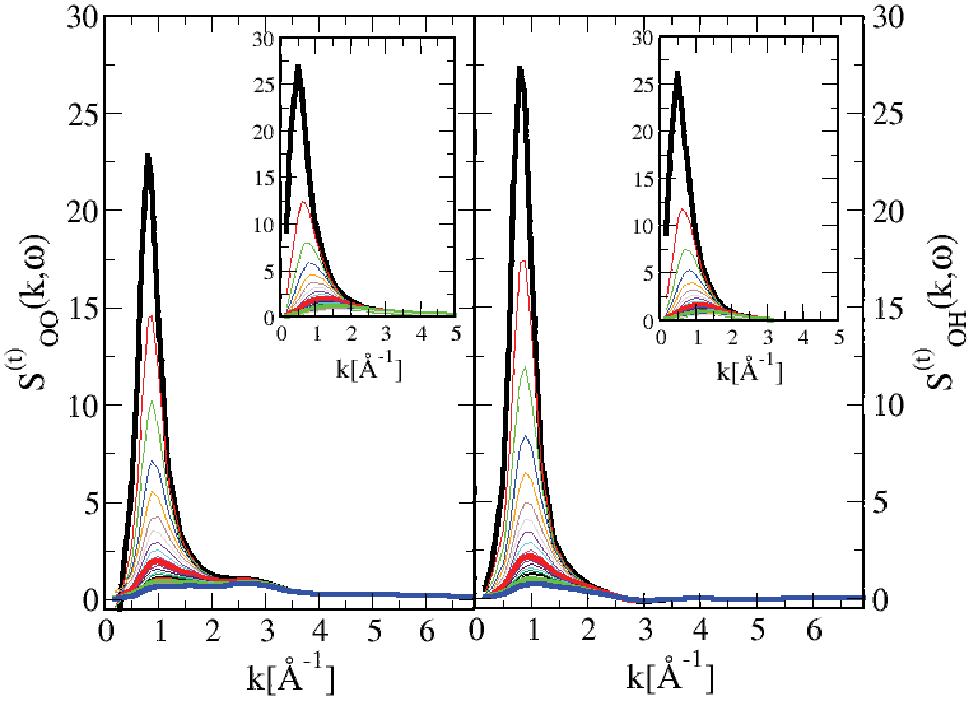

Figure 59: **ethanol:** Main panels show total dynamical structure factors, $S^{(t)}_{\mathrm{OO}}(k,\omega)$ and $S^{(t)}_{\mathrm{OH}}(k,\omega)$, in the left and right panels respectively. Corresponding self parts, $S^{(s)}_{\mathrm{OO}}(k,\omega)$ and $S^{(s)}_{\mathrm{OH}}(k,\omega)$, are shown in the insets. Frequency values of 0.05 ps^{-1}, 1 ps^{-1}, 10 ps^{-1} and 30 ps^{-1} are highlighted and presented with thick black, red, green and blue lines respectively.

3.4.4 Self Van Hove function and diffusion

In this section, we put focus on the diffusion properties of simple and complex liquids, which can be extracted from self part of Van Hove correlation function. Previously, we compared $G^{(s)}(r,t)$ functions for different liquids, highlighting the differences in the speed of decorrelation between different systems. We noted that faster diffusion does not imply faster decorrelation, since decorrelation depends also of molar density of each system. This is why we observed somewhat different trends when we accounted for $G^{(s)}(r,t)$ self - correlations, compared to trends observed for $F^{(s)}(k,t)$. While the loss of $G^{(s)}(r,t)$ correlations depends strongly of both diffusion and molar density, loss of $F^{(s)}(k,t)$ correlations is governed only by diffusion.

In this section we wish to examine the differences in diffusion, instead of correlations, between different types of liquids. Again, we take acetone and CCl_4 as representatives of simple liquids, together with water and ethanol, as representatives of complex liquids. We plot the self Van Hove functions weighted by molar density ρ, since the decay of this form is not affected by the density of the liquid. Hence, the decay of this function is governed solely by diffusion. Therefore, the equation:

$$4\pi \int \rho G^{(s)}(r,t) r^2 \mathrm{d}r = 1 \tag{145}$$

is valid for every $\rho G^{(s)}(r,t)$ function which we show below. Figure 60 shows $\rho G^{(s)}(r,t)$ functions for water (thick lines), ethanol (dotted thick lines), acetone (dashed thick lines) and CCl_4 (thin full lines) in the main panel. Functions are shown for different values of t, where each time value corresponds to specific color: 0.1 ps (black), 1 ps (green), 10 ps (blue) and 100 ps (orange). The inset shows corresponding scattering functions $F^{(s)}(k,t)$ with the same color conventions. In the cases of water, ethanol and acetone, we consider OO correlations, while CC correlations are considered in the case of CCl_4.

When weighted $\rho G^{(s)}(r,t)$ are considered instead of non - weighted $G^{(s)}(r,t)$, we notice that the trends observed in r - space (main panel) match perfectly with the trends in k - space (inset). We remind that this was not the case in the previous section. At short times (black curves - 0.1 ps), CCl_4 (thin black line) exhibits slowest diffusion than the other liquids, which diffuse very similarly in this short timescale. Namely, water, ethanol and acetone show similar behavior, which is visible by near superposition of thick full, dotted and dashed black curves, in both panels.

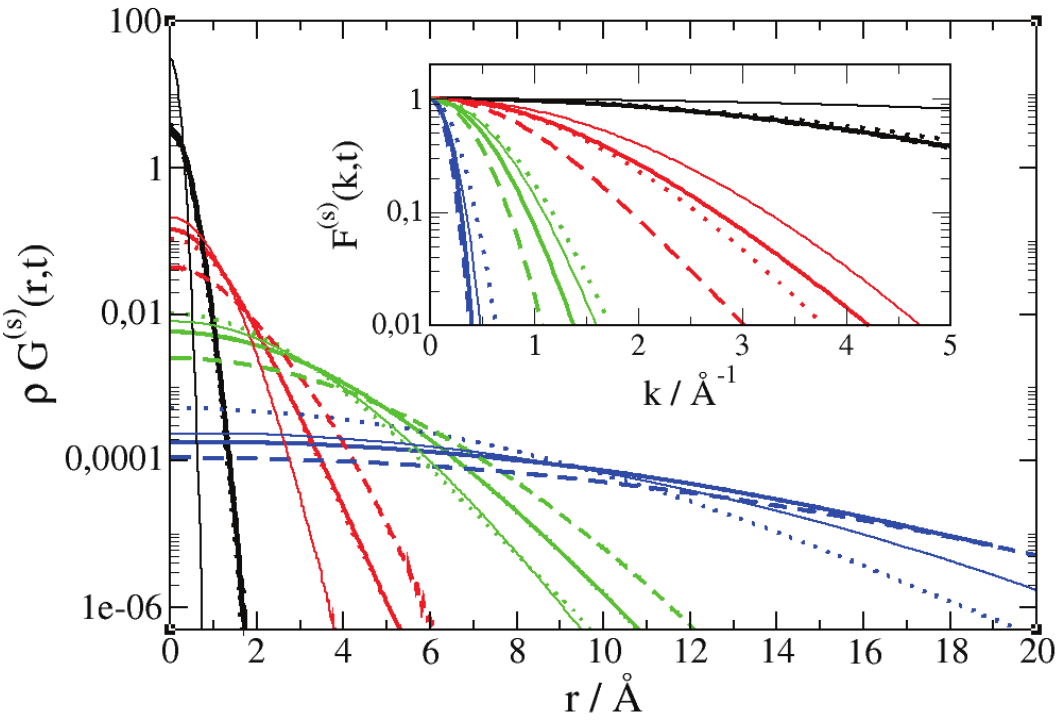

Figure 60: Self Van Hove correlations of water (thick full lines), ethanol (thick dotted lines), acetone (thick dashed lines) and CCl_4 (thin full lines). Each color corresponds to different time value: black - 0.1 ps, red - 1 ps, green - 10 ps, blue - 100 ps. Main panel shows correlations in *r* - space, while the inset shows the same correlations in *k* - space.

At larger times, the curves differentiate more clearly, highlighting the differences between self - diffusion close to diffusive temporal regime across different types of liquids. Our results suggest that acetone (thick dashed curve) exhibits fastest diffusion, while the diffusion of ethanol is the slowest at large times (100 ps - blue lines).

It is also instructive to examine the differences in diffusion of different atoms *within the same liquid*. For example, in the case of ethanol, we can compare OO, HH, C_1C_1 and C_2C_2 self - correlations, in order to account for possible differences between different atomic sites. Self Van Hove correlations for acetone and CCl_4 are presented in Figure 61, while those corresponding to methanol and ethanol are shown in Figure 62. Types of correlations are specified in the legend boxes of each panel. In case of ethanol, C_1 represents the carbon site covalently bound to the O atom, while C_2 represents the carbon site at the edge of the molecule, according to the OPLS model. For acetone, C_1 represents one of the two methyl groups bound to the central C atom. Every color in the plot corresponds to specific time value: 0.1 ps - black, 1 ps - green, 10 ps - blue, 50 ps - orange.

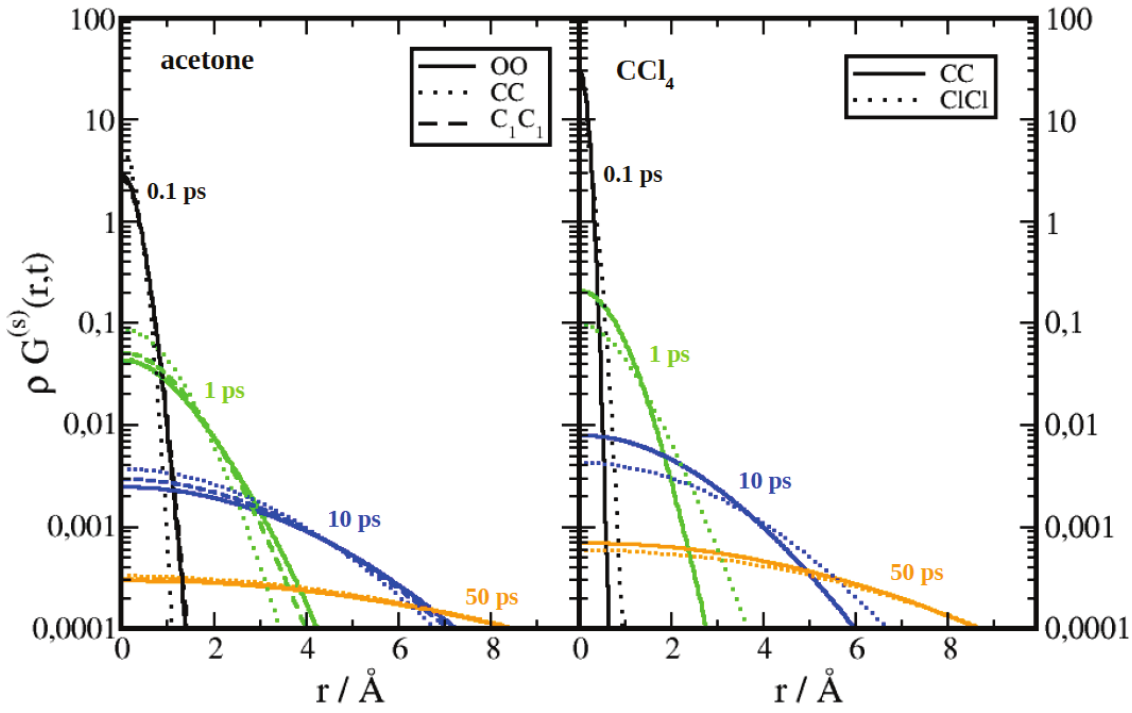

Figure 61: Self Van Hove correlations of acetone (left panel) and CCl_4(right panel), for different atomic sites (see the legend boxes). Each color corresponds to different time value: black - 0.1 ps, red - 1 ps, green - 10 ps, blue - 100 ps.

For simple liquids (see Figure 61), we observe that the differences in diffusion are more enhanced at short times (0.1 ps, 1 ps and 10 ps) than at large times (50 ps), implying that these differences vanish in diffusive temporal regime. In addition, at short times, atoms at the center of molecules (i.e. C atoms in both acetone and CCl_4) exhibit slower diffusion than the atoms at the edge of molecules. Similar trends are observed also for methanol (see Figure 62). However, for ethanol, the differences between curves are visible even at large times ($t = 50$ ps - orange color). This indicates that larger amount of time is required for ethanol to reach diffusive regime than it is required for other liquids shown here. Slower relaxation of ethanol into diffusive regime is the consequence of slower kinetics of ethanol, when compared with kinetics of simple liquids or methanol, which is simpler alcohol. Slower kinetics is the consequence of the formation of microheterogeneities, which grow with the size of alkyl tails in alcohols. The enhancement of microheterogeneity with the growth of alkyl tails is proved by the shift of the pre - peak of the structure factor towards smaller k - values when shifting from lower to higher alcohols, as shown in section 3.1.2. In addition, slower kinetics of higher alcohols, compared to lower ones, will be demonstrated in section 3.4.6.

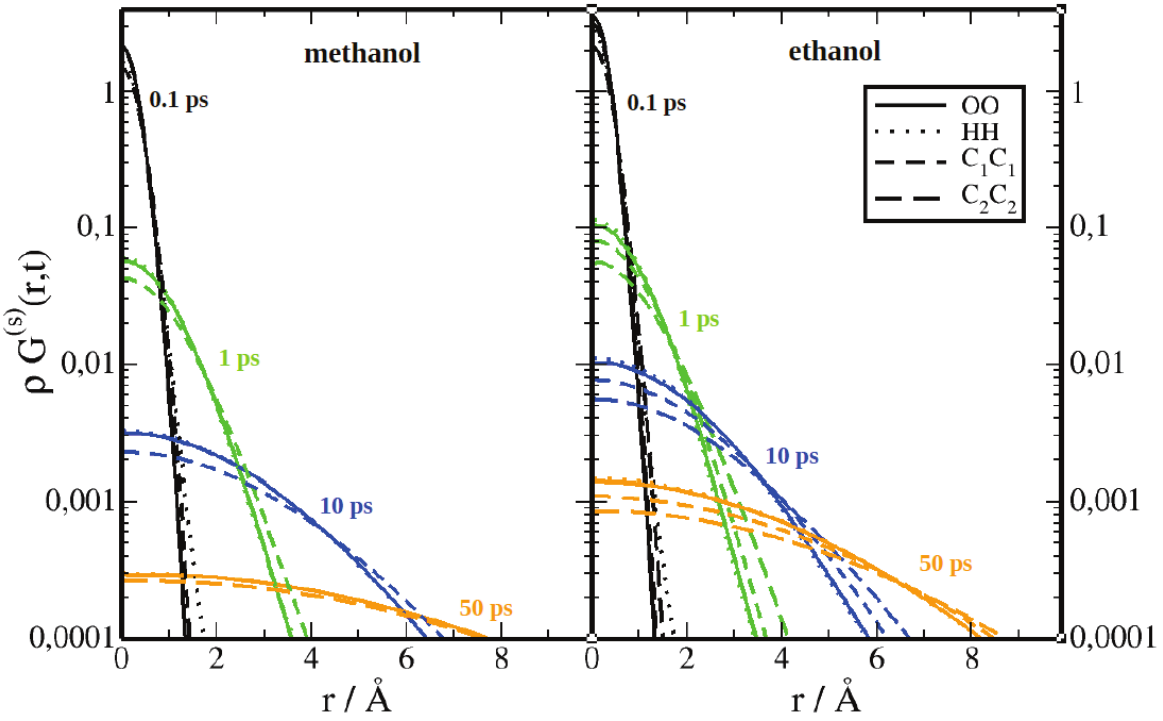

Figure 62: Self Van Hove correlations of methanol (left panel) and ethanol (right panel), for different atomic sites (see the legend boxes). Each color corresponds to different time value: black - 0.1 ps, red - 1 ps, green - 10 ps, blue - 100 ps.

To confirm quantitatively the trends discussed above, we list in Table 3 the diffusion coefficients obtained by fitting of self Van Hove functions ($t = 100$ ps) to gaussian from equation (140). With $D(G_s^X)$ we denote the diffusion constant obtained by gaussian fitting of $G_{\mathrm{XX}}^{(s)}(r,t = 100\,\mathrm{ps})$ function to the equation (140), with X denoting the atomic specie for which correlations are accounted for. With D_{EXP} we denote the experimental value of self - diffusion constant from references [43, 78, 52, 110] for water, reference [83] for methanol and ethanol, reference [29] in the case of CCl_4 and reference [58] for acetone. Blank fields, denoted with *, indicate non - existing correlations.

Table 3 shows that the obtained diffusion coefficients qualitatively match with corresponding experimental values. We note that our results are in good agreement with previously reported values of self - diffusion coefficients of SPC/E model of water [87, 100] and OPLS models of methanol [83] and ethanol [83], at room temperature, obtained by the application of Einstein relation [56]. However, in these works, diffusion coefficients have not been calculated for each atomic sites individually, like it is done in this work. Although quantitative experimental values, are not reproduced perfectly, qualitative trends are preserved, as shown in table 3,. For example, ethanol shows the slowest diffusion both from experiments and from our data, while acetone has the largest diffusion coefficient in both cases. Also, we observe that the differences between different types of ethanol self - correlations (OO, HH, C_1C_1 and C_2C_2) are much more

enhanced than the differences between different acetone correlations (OO, C_1C_1 and CC) for example, which is in accordance with qualitative analysis written above, where we attributed this effect to slower relaxation of ethanol to diffusive regime, due to microheterogenous structure.

SYSTEM	$D(G_s^{O})$ / 10^{-3} nm^2 ps^{-1}	$D(G_s^{H/Cl})$ / 10^{-3} nm^2 ps^{-1}	$D(G_s^{C1})$ / 10^{-3} nm^2 ps^{-1}	$D(G_s^{C2/C})$ / 10^{-3} nm^2 ps^{-1}	D_{EXP} / 10^{-3} nm^2 ps^{-1}
WATER	2.711 ± 0.002	2.7094 ± 0.0008	*	*	2.3
METHANOL	2.714 ± 0.002	2.717 ± 0.001	2.8245 ± 0.002	*	2.4
ETHANOL	1.1175 ± 0.0015	1.165 ± 0.001	1.344 ± 0.001	1.4932 ± 0.0004	1.0
ACETONE	3.2547 ± 0.0014	*	3.219 ± 0.002	3.181 ± 0.003	4.7
CCl_4	*	2.107 ± 0.001	*	2.031 ± 0.003	1.4

Table 3: Diffusion constants obtained by gaussian fitting of $G^{(s)}(r,t = 100\text{ ps})$ functions to gaussian of the form $G^{(s)}(r,t) \sim \exp(-\frac{r^2}{4Dt})$. Self correlations for specific atomic specie X is denoted with G_s^X. With D_{EXP} we denote the experimental value of self - diffusion constant from the literature.

3.4.5 Time decay of $G_d(r,t)$ correlations at the first peak

In the last section we observed that the loss of correlations around the first peak of $G^{(d)}(r,t)$ occurs slower for simple liquids (i.e. acetone and CCl_4) than for complex associative liquids (i.e. water and ethanol). Here, we demonstrate this in more details by showing $G^{(d)}(R,t)$ functions in time domain, instead of space domain (i.e. we put t instead of r on the x - axis), with keeping R fixed. We choose the value of R such that it corresponds to the position of the first peak for each case.

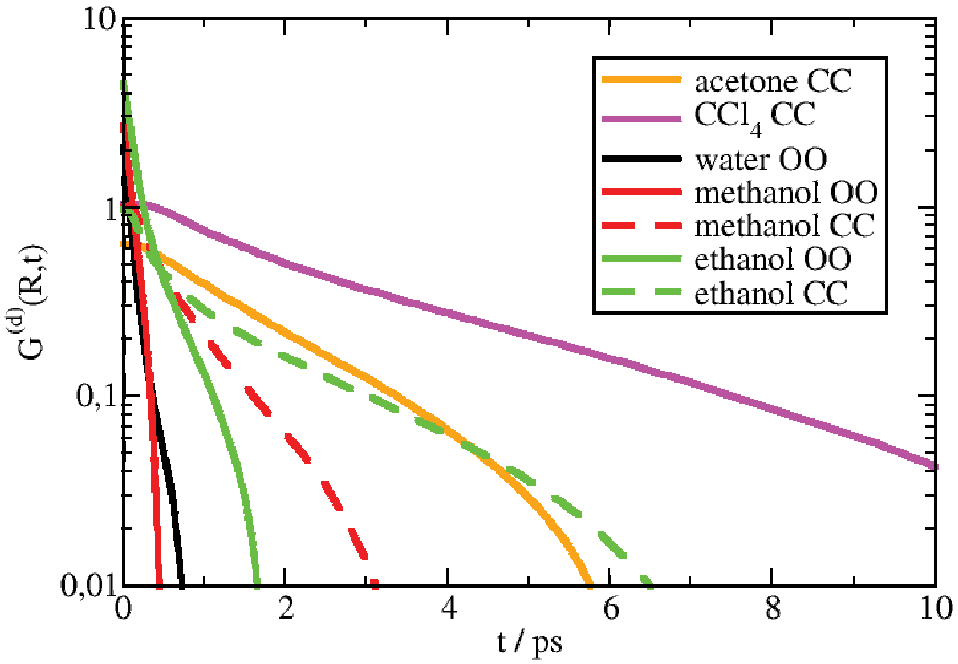

Figure 63: Time decay of various $G^{(d)}(R,t)$ functions, with R corresponding to the position of the first peak of $G^{(d)}(r,t)$ in each case.

Figure 63 shows the time decays of various $G^{(d)}(R,t)$ functions of water, methanol, ethanol, acetone and CCl_4. Particularly, we show CC correlations for all four liquids, including also OO correlations in case of water, methanol and ethanol. We can immediately confirm the trends observed in previous section: OO correlations of associative liquids decay significantly faster than correlations corresponding to simple liquids. While OO correlations in associative liquids fall below 0.1 already within nearly 1 ps, those in simple liquids are more persistent. Namely, correlations fall below 0.1 within 4 ps in case of acetone and around 8 ps in case of CCl_4. Also, we observe that CC correlations of the two alcohols decay slower than OO correlations. In fact, the decay of CC correlations in ethanol is similar to the decay of CC correlations in acetone. This suggests that the dynamics of alkyl groups of alcohols reminds of dynamics observed in simple liquids, and differs from the dynamics of atoms within hydroxil groups, which are

influenced by charge order. In addition, we observe that OO correlations exhibit higher initial values $G^{(d)}(r,t=0)$, which is in alignment with the high first peak of static $g_{OO}(r)$ correlations observed earlier.

3.4.6 Dynamic and kinetic aspect of correlations in (k,t) space

Now we will put focus on the time decay of density correlations in k - space, namely the decay of $F(k,t)$ function. Prior to performing similar analysis as the one from the previous section, we will discuss the physical meaning of the time evolution of $F(k,t)$ and its relationship with the trends observed in $G_d(r,t)$. Figure 64 shows $G_d(r,t)$ correlations between OO intermolecular pairs in water (left panel), together with corresponding $F_d(k,t)$ functions (right panel). Functions are calculated for selected t - values, which are listed in the legend box. The inset in the left panel shows the zoomed view on $G_d(r,t)$ functions shown in the main panel.

As shown in Figure 64, $G_d(r,t=0)$ functions (shown in black color in the left panel) exhibit oscillatory behaviour, with oscillations being characterized by two dominant spatial periods: 0.6 σ and σ (see the inset of the left panel). The distance 0.6 σ corresponds to the typical separation between first and second shell of $G_d(r,t=0)$ function, while the distance σ represents spatial period of long - ranged oscillations (see $r > \sigma$ interval in the left panel). These two spatial periods give rise to the diffraction pattern of water being characterized by the split - peak feature (see $F_d(k,t=0)$ function in the right panel), with the two dominant peaks found at $k \approx 2\pi\sigma^{-1}$(marked with red arrow) and $k \approx 3\pi\sigma^{-1}$(marked with black arrow). The former peak is related to σ spatial period of $G_d(r,t=0)$, while the latter is related to 0.6 σ.

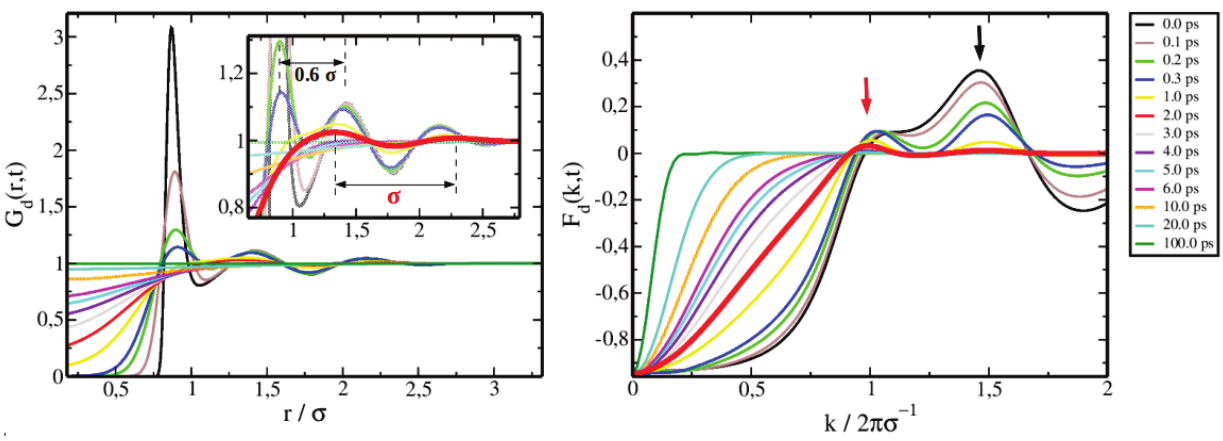

Figure 64: Left panel shows $G^{(d)}_{\mathrm{OO}}(r,t)$ correlations for water, while corresponding $F^{(d)}_{\mathrm{OO}}(k,t)$ functions are shown in the right panel.

Larger times ($t > 0$) are characterized by weakening of density correlations, as visible from the left panel, where we note lowering of the peak amplitudes as time increases. At sufficiently large times ($t \sim 1$ ps), the first and second peak of $G_d(r,t)$ merge into one single peak (see

the red curve in the left inset, corresponding to $G_d(r,t = 2\text{ ps})$), with correlations now being characterized by one single dominant spatial period - σ, over whole r - domain. In k - space (see the right panel), this is visible through disappearance of the peak at $k \approx 3\pi\sigma^{-1}$ (marked with black arrow), leaving $F_d(k,t)$ being dominated by single peak centered at $k \approx 2\pi\sigma^{-1}$ (see the red curve in the right panel).

Previously, we related the existence of two spatial frequencies in the microstructure of water to previously suggested picture of water by other authors, where water is considered to be a mixture of tetrahedrally ordered liquid and ordinary disordered liquid [131, 160]. In this context, the existence of σ periodicity in the microstructure of water reflects the disordered nature of water, while the existence of shorter 0.6 σ periodicity reflects its charge ordered nature. The right panel of Figure 64 suggests that charge ordered component of water microstructure relaxes faster than its disordered component. This is visible through the fact that the outer peak of the structure factor of water (marked with black arrow) decays faster in time than the inner peak (marked with red arrow). Before focusing on the differences in time decay more thoroughly, it would be instructive to make similar analysis, as the one presented in Figure 64 for water, as well for ethanol, since the structure factor of the alcohol is characterized by the pre - peak.

Figure 65 shows $G_d(r,t)$ functions for OO intermolecular correlations in ethanol (left panel), together with corresponding $F_d(k,t)$ functions (right panel). Left panel shows that short time ($t < 1$ ps) correlations, similarly like in the case of water, exhibit shorter 0.6 σ periodicity over small - r domain ($r < 2\ \sigma$). However, larger r separations are characterized by 2.5 σ periodicity, the value which is larger than periodicity (σ) of long ranged correlations in water (see the left panel of Figure 64). In the right panel of Figure 65, shorter periodicity of ethanol microstructure is visible through the peak at $k \approx 3\pi\sigma^{-1}$ (marked with black arrow in the right panel), as in the water case. Larger 2.5 σ periodicity manifests through the pre - peak at $k \approx \pi\sigma^{-1}$ (marked with red arrow). Right panel indicates that the component of ethanol microstructure, attributed to larger periodicity, decays significantly slower in time than the component attributed to shorter periodicity. Similarly like in the case of water, peak at $k \approx 3\pi\sigma^{-1}$ is attributed to charge ordered nature of ethanol microstructure, while the peak at $k \approx \pi\sigma^{-1}$ is the pre - peak.

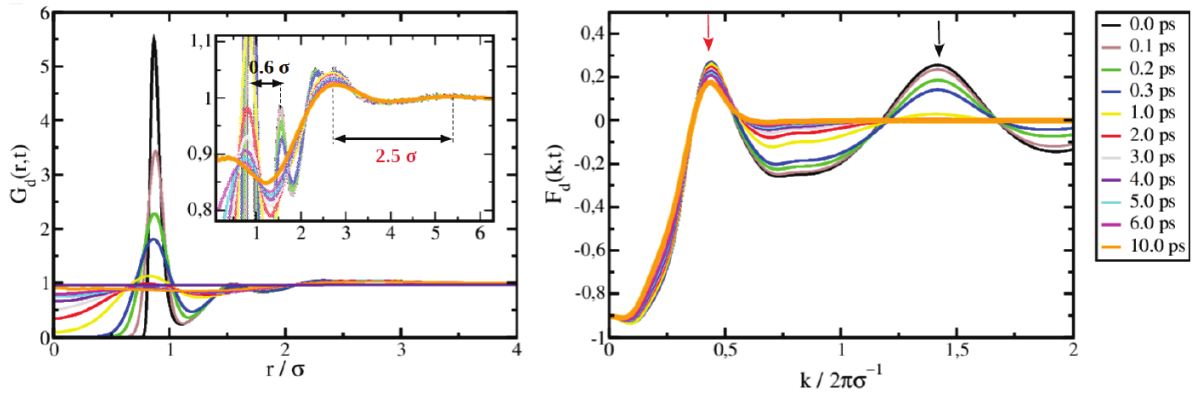

Figure 65: Left panel shows $G_{\mathrm{OO}}^{(d)}(r,t)$ correlations for ethanol, while corresponding $F_{\mathrm{OO}}^{(d)}(k,t)$ functions are shown in the right panel.

In chapter 3.1.2, we addressed the relationship between k - position of the pre - peak with the characteristic separation between nearest OH aggregates in alcohols. Namely, a pre - peak centered at $k = \frac{2\pi}{D}$ implies that a characteristic separation between two such aggregates is equal to D. In the context of OO dynamic structure factor of ethanol, presented in the right panel of Figure 65, the pre – peak (marked with red arrow) represents a typical separation between two O atoms forming two such aggregates. The average separation between two such atoms will clearly be governed by by the size of alkyl tails, which form hydrophobic barriers between OH aggregates in the liquid. This explains why the position of the pre - peak shifts to lower k - values (indicating larger inter - aggregate separations) when moving from lower to higher alcohols [143, 16, 185, 171]. However, the main peak of the structure factor (marked with black arrow) is related to characteristic separation between first and second shells of OO correlations in r - space (see the left panel of Figure 65) and is, therefore, a signature of charge order in the liquid. This characteristic separation is universal for both water and alcohols studied herein, which explains why the peak centered at $k \approx 3\pi\sigma^{-1}$ is common feature of all associative systems considered in this work. In addition, the bump in correlations at $k \approx 2\pi\sigma^{-1}$ is related to characteristic contact distance between first hydrogen bonded O neighbours, as already explained.

Prior to the comparative analysis of the t - decay of OO, OH and HH correlations in k - space for water, methanol and ethanol, we show total OO, OH and HH structure factors of water, methanol and ethanol in Figure 66. Left panel shows OO structure factors of the selected systems (water in black, methanol in red and ethanol in green lines), while OH and HH structure factors are shown in the central and right panels respectively, with the same color convention as for the left panel. All structure factors are in agreement with previously published OO, OH and HH partial structure factors by other authors [185, 166, 131, 165].

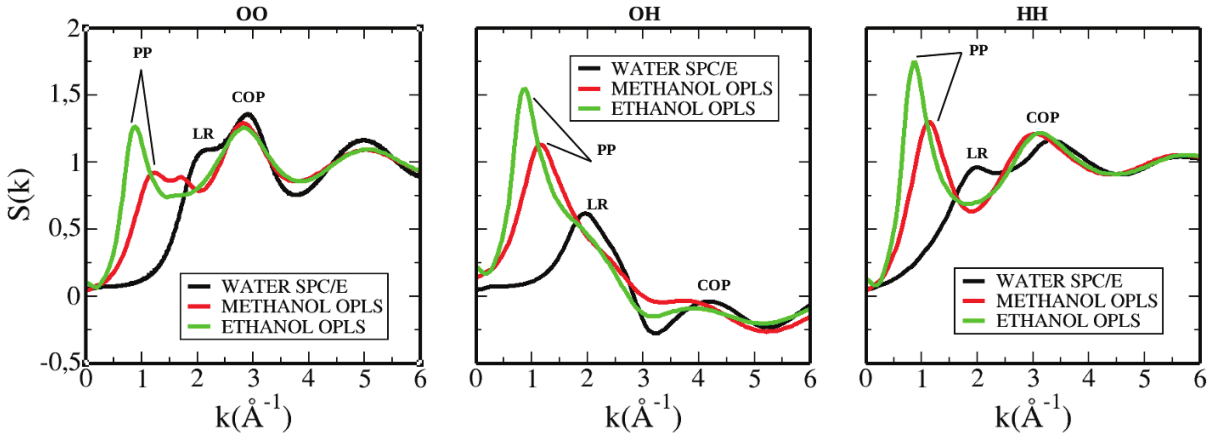

Figure 66: Static structure factors OO (left panel), OH (central panel) and HH (right panel) of water (black lines), methanol (red lines) and ethanol (green lines). Pre - peaks are marked with PP, charge ordering peaks with COP and peaks corresponding to long - ranged correlations in r - space with LR.

Structure factors (OO) presented in the left panel have been already discussed. Here, we shortly remind of the main features. In the case of water (black line), the peak at $k \approx 2$ Å^{-1} (marked with "LR") is the manifestation of characteristic periodicity of $g_{OO}(r)$ correlations over large - r interval ("LR" stands for "long - ranged" correlations). In methanol and ethanol, this peak is shifted to lower k - values, forming a pre - peak, marked with "PP". This shift is the consequence of the increment of spatial period of $g_{OO}(r)$ over large - r domain, when moving from water to the alcohols. Both LR peak and PP peaks reveal the details of long - ranged OO correlations in the liquid. In addition, similar shift of LR peak to PP peak is observed also in the case of OH (central panel) and HH (right panel) structure factors of the three liquids.

Peak marked with "COP" (where "COP" stands for "charge - ordering peak") is caused by the distribution of atoms in close vicinity of the reference atom, and is the signature of charge ordering. Particularly, in the case of OO correlations (left panel), this peak represents characteristic separation between first and second shell of $g_{OO}(r)$, as previously discussed. In the case of OH structure factor (central panel), COP peak represents a characteristic contact distance between nearest OH intermolecular pair. The peak is centered at $k \approx 4$ Å^{-1}, indicating that the characteristic separation between OH intermolecular pairs should be around $r \approx 1.6$ Å. This separation can be confirmed from Figures 54 and 55 (see the case of OH correlations). In the case of HH structure factor (right panel), COP peak represents nearest intermolecular HH separation.

Let us now consider the time relaxation of OO, OH and HH correlations in k - space through the t - decay of $F(k,t)$ functions. Particularly, we will examine the decay of PP peaks for alcohols, LR peaks for water and COP peaks for all the three liquids and all three types of correlations. In Figure 67, the decay of OO (full lines), OH (dotted lines) and HH (dashed lines) correlations

is shown in black color for water, red for methanol and green for ethanol. Thin lines show the decay of COP peaks, while thick lines show the decay of PP peaks for alcohols and LR peaks for water. Left panel shows the t - decay of correlations in linear y - scale, while the right panel shows the same decay in log y - scale.

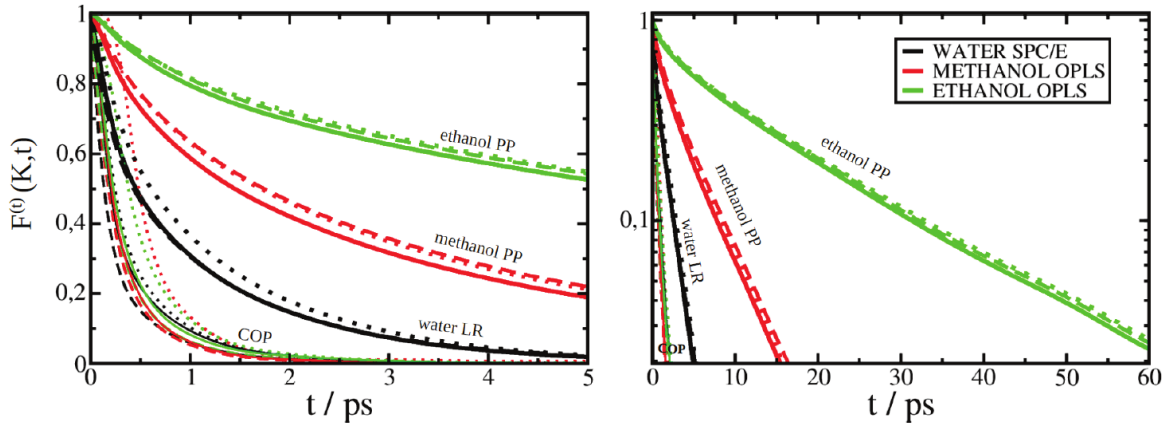

Figure 67: Time decay of marked peaks from Figure 66 in linear scale (left panel) and logarithmic scale (right panel).

First feature visible from Figure 67 is that all COP peaks (for all three types of intermolecular correlations and all three liquids) decay very similarly in time. This feature indicates that small - r correlations, governed by charge order, decays similarly in all three selected liquids. Hence, time relaxation of charge ordered component of microstructure is similar for all selected liquids.

However, more noticeable differences are present when PP peaks of alcohols and LR peaks of water are considered. We remind that the meaning of the LR peak of water is essentially equivalent to PP peak of any of the two alcohols, since both peaks describe the periodicity characteristic for large - r correlations. In this context, LR peak can be considered as the pre - peak of water, although, in the literature, pre - peaks are commonly attributed exclusively to other types of liquids, such as alcohols [188, 161, 162, 133, 146, 138, 51, 142] or ionic liquids [30, 161, 186, 20, 151]. These liquids contain neutral groups of atoms (i.e. alkyl tails) attached to charged groups. In alcohols, the existence of neutral groups induces the increment of the spatial period of OO large - r correlations, when compared with OO correlations of water, which does not have these groups. The increment of the spatial period increases as the size of alkyl tails increases. Hence, the LR peak of water describes the periodicity of large - r correlations in special case when there are no neutral groups attached to charged groups. In this sense, LR peak could be considered as pre - peak of water.

Results presented in Figure 67 show that the t - decay of long - ranged correlations (represented with the LR peak of water and PP peaks of the alcohols) slows down as the size of alkyl tails increases. Earlier, in the context of alcohols, we explained that PP peaks represent cluster

- cluster correlations (where the term cluster refers to OH aggregates). Hence, the temporal relaxation of cluster - cluster correlations becomes slower with the increment of alkyl chain legth. We note that the decay of PP peaks is nearly independent of the choice of intermolecular correlations (OO, OH or HH) for specific liquid, which is visible from the superposition of different thick lines (full, dotted or dashed) for a given color. This indicates that the t - decay of PP peak describes the structural relaxation at the spatial scale of aggregates, where the choice of the atomic species (O or H) does not have significant impact. The characteristic time attributed to the decay of PP peak for each liquid is what we call kinetic time. Therefore, we conclude, from Figure 67, that kinetics of the three liquids differs significantly, while the dynamics of charge order is nearly the same in all three systems.

In experiments, structural relaxation at PP and COP can be probed by QuasiElastic Neutron Scattering (QENS). Total scattering functions $F(k,t)$ at the PP and COP have been measured and it was found that the dynamics at the PP is slower than that at the COP [162, 14, 13, 184], which is in agreement with our findings. Similar findings have also been observed for room - temperature ionic liquids [81].

The study of kinetic aspect of water and monohydroxy alcohols is shown to have significant importance in understanding the relationship between microscopic and macroscopic properties of these liquid [188, 186]. Particularly, neutron scattering experiments of 1-propanol have shown that the temperature dependence of characteristic decay times at the pre - peak exhibit Arrhenius dependence ($\tau(T) \sim \exp(-E_A/RT)$) over the tested temperature range 170 - 280 K, with the activation energy E_A being similar to the activation energy of viscosity [188]. This result highlights the influence of mesoscopic cluster dynamics on rheological properties of liquids. The coupling between viscosity and clustering has also been confirmed by molecular dynamics simulations of methanol and ethanol performed by Yamaguchi [185].

3.4.7 Memory function - simple approximation

In section 2.3.3 we introduced the simplest approximation of the memory function:

$$M(k,t) = M(k) \cdot \delta(t) \tag{146}$$

We have shown that, within this approximation, the solution of Mori - Zwanzig equation for the time evolution of $F(k,t)$ is given with:

$$F(k,t) = S(k) \cdot \exp\left[-t \cdot M(k)\right] \tag{147}$$

with $S(k)$ representing the static structure factor, while $M(k)$ is the memory function, which is independent of time. The last equation implies that, for fixed k, $F(k,t)$ decays as single exponential in time, with the decay rate being dependent of k through $M(k)$.

However, we have shown in section 3.4.6 (see Figure 67) that the time decay of $F(k,t)$ does not decay as single exponential, which already indicates that approximation (146) is not good enough for describing the dynamics of realistic liquids. However, it would be instructive to examine how close one can get towards realistic description of liquids within this simple approximation. First, we note that, within approximation (146), the dynamical structure factor is given with the time Fourier transform of equation (147):

$$S(k,\omega) = S(k) \int_{-\infty}^{+\infty} \exp\left[-t \cdot M(k)\right] \cdot \exp\left[-i\omega t\right] \mathrm{d}t \tag{148}$$

which ultimately leads to:

$$S(k,\omega) = \frac{2M(k)S(k)}{\omega^2 + M^2(k)} \tag{149}$$

Therefore, in order to test the quality of approximation (146), one can compare the $S(k,\omega)$ from equation (149) with $S(k,\omega)$ obtained from simulations. In order to obtain $S(k,\omega)$ from equation (149), one needs to know $M(k)$ and $S(k)$. We obtain $M(k)$ by performing exponential fit of $F(k,t)$ in the time interval 0 - 1 ps for large series of k-values. We note that 1 ps is approximately the time by which correlations around the charge ordering peak of $F(k,t)$ decay to 0 (see Figure 67).

The main panel of Figure 68 shows the inverse of $M(k)$ functions, obtained by exponential fitting of $F_{\mathrm{OO}}(k,t)$ correlations for simple LJ liquid, water, methanol and ethanol. The inset shows the same figure in logarithmic y-scale. We first observe that positions of peaks of $M^{-1}(k)$ coincide with the ones of dynamical structure factor $S(k,\omega)$ for each system (see section 3.4.6). In addition, we observe the divergence of $M^{-1}(k)$ in $k \to 0$ limit, which is the consequence of the slow time decay of $F_{\mathrm{OO}}(k,t)$ for small k-values.

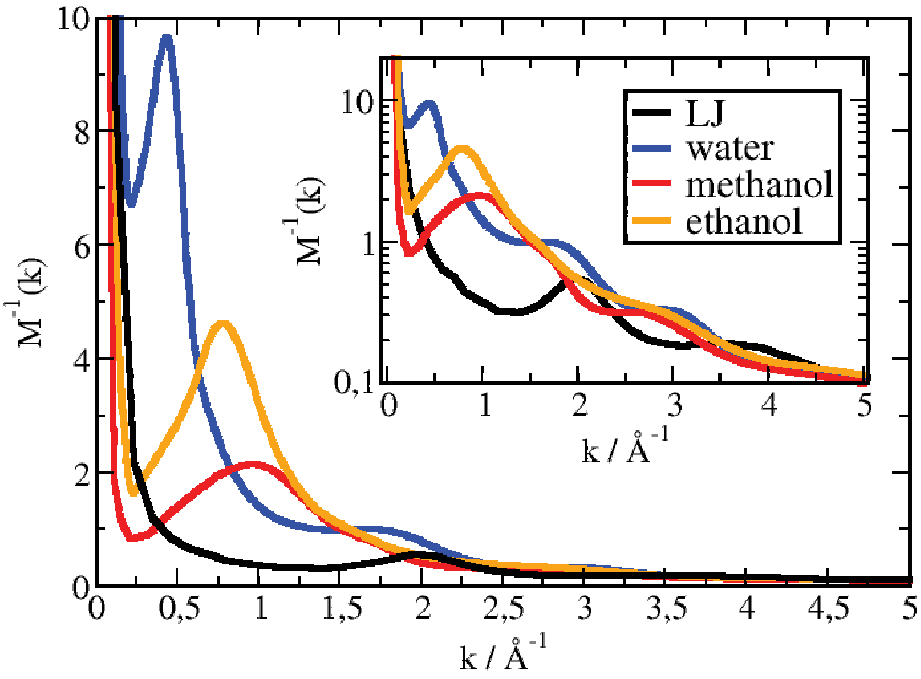

Figure 68: Main panel shows time - independent approximations of memory functions $M(k)$, corresponding too OO correlations in simple LJ liquid (black line), water (blue line), methanol (red line) and ethanol (orange line). The inset shows the same plot in logarithmic y-scale.

In order to obtain the approximation of $S(k,\omega)$, we insert the memory functions from Figure 68 into equation (149). Figures 69 and 70 show the comparison of $S(k,\omega)$ obtained from simulations (left panel) with the $S(k,\omega)$ obtained from approximation (right panel), for water and methanol respectively.

We observe that $S(k,\omega)$ from the left and right panels differ quite significantly. However, we note the best agreement between the approximative and realistic structure factors for very small ω values. Overall, the speed of decay in ω space is significantly overestimated when approximation (146) is used. This is the consequence of the fact that the time evolution of $F(k,t)$ is not well described with equation 147 in reality. Therefore, in order to obtain the memory function of realistic liquids, one has to rely on Mori - Zwanzig formalism.

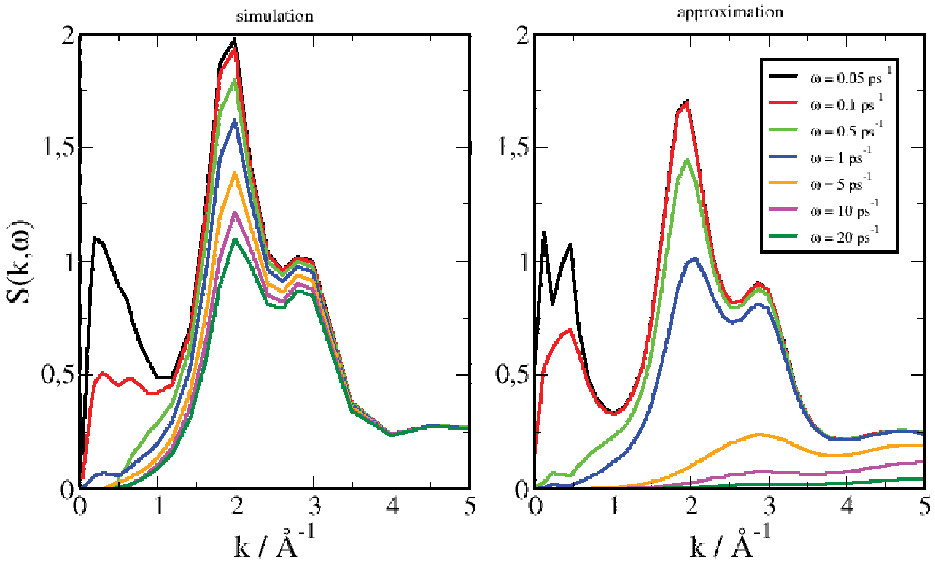

Figure 69: Comparison of $S(k,\omega)$ structure factor of water (OO correlations), obtained with simulations (left panel) versus $S(k,\omega)$ obtained from equation (149) (right panel), when the Markovian approximation of memory function is applied.

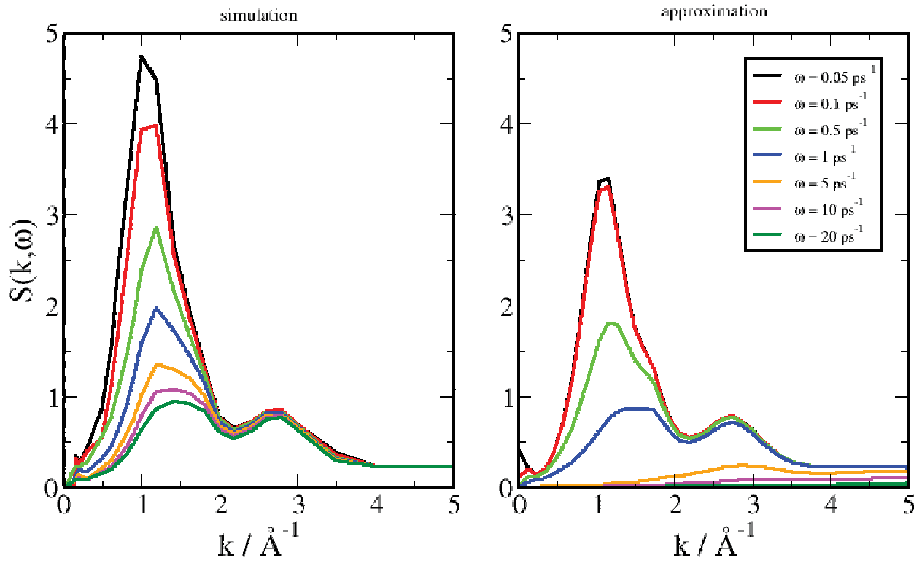

Figure 70: Comparison of $S(k,\omega)$ structure factor of methanol (OO correlations), obtained with simulations (left panel) versus $S(k,\omega)$ obtained from equation (149) (right panel), when the Markovian approximation of memory function is applied.

To conclude, approximation (146) is a type of Markovian approximation [56], where the state of the system at time t is assumed to be independent of the past. This type of approximation can be applied when the timescale of random force fluctuations (i.e. the timescale of atomic collisions in the liquid) is significantly faster than the timescale at which the momentum of the reference particle changes. For example, this is the case with the dynamics of large brownian particle in a bath consisting of much smaller particles. In this case, the dynamics of such particle is described with Langevin equation (64), where the memory function (here equivalent to the friction coefficient ξ) is assumed to be independent of the past, $\xi(t) = \xi_0\delta(t)$. This type of Markovian approximation is used widely in soft matter, specifically in Coarse Graining [70, 80, 88, 89, 97, 32, 31], where one attempts to solve the Mori - Zwanzig equation in order to solve for the dynamics of mesoscopic coarse - grained system, and is not interested in the details of microscopic dynamics, which occurs at much smaller timescale than mesoscopic dynamics. However, we demonstrate here that simple Markovian approximation is not useful for describing the dynamics of molecular liquids. Our tests, presented in Figures 69 and 70, demonstrated this for the cases of water and methanol. In addition, even exponential approximation of the memory function, developed by Chong and Hirata [25, 26, 27], does not suffice to reproduce various dynamical observables obtained by experiments, specifically time - dependent correlations in a liquid. Therefore, in order to obtain the memory function capable of describing the dynamics of realistic liquids, one needs to rely on Mori - Zwanzig formalism.

Conclusion

4

4 Conclusion

The main goal of this thesis was to study the specificities in the dynamics of micro - heterogeneous liquids [145, 128, 142, 134], when compared with other types of liquids which do not exhibit this type of micro - structure. The formation of micro - heterogeneity is realized through formation of supramolecular aggregates [145, 142, 134, 138] on the scale of several molecular sizes. In associative liquids, such as alcohols, aggregation is the consequence of hydrogen bonding between OH hydroxil groups [14, 13, 138, 16, 76, 118, 126]. Hence, in addition to regular molecular dynamics, characteristic for any liquid, micro - heterogeneous liquids have kinetic aspect of dynamics, which is related to dynamics of molecular aggregates, instead of individual molecules. In general, micro - heterogeneous liquids belong to class of complex liquids [134]. The division of liquids into simple versus complex is inspired by significant differences in static and dynamic properties of these two types of systems, which are caused by different intermolecular interactions which each type exhibits.

In typical simple liquids, like liquid argon for example, interactions are governed by weak Van der Waals forces, characteristic for non – polar species, which are typically modeled by Lennard – Jones potential in classical simulations [56]. The micro - structure of this type of liquid, or any other type, can be described with radial distribution function $g(r)$, which describes the mean radial distribution of density around particle in the system, obtained as an average over all particles and all microstates (ensemble average) [56]. It has been shown that $g(r)$ of typical simple liquid oscillates around the asymptote $g(r) = 1$, with characteristic period of oscillations being equal to σ, denoting atomic diameter, and the first peak positioned at $r \approx \sigma$. The structure factor $S(k)$ of such liquid, mathematically equal to the spatial Fourier transform of $g(r)$, is characterized by the main diffraction peak at the wave-vector $k = 2\pi\sigma^{-1}$ [56], indicating that the liquid disorder of this system is fully governed by σ inter-particle separation. This is the simplest form of liquid disorder, which is the reason why we refer to these liquids as simple disordered liquids.

In the case when liquid is composed of globally non-neutral species, interactions become more complex, due to the addition of Coulomb interaction to the existing Lennard – Jones interaction. If we take an example of simple ionic liquid, composed of positively charged atomic species A and negatively charged atomic species B, with both species having the same atomic diameter, the micro-structure of this liquid is shown to differ from the previous case. Namely, the disorder in this type of system is characterized by the formation of charge order [133], with positively and negatively charged species being arranged in $+-+-+-$ sequence, governed by Coulomb interaction. Charge order is shown to leave trace in radial distribution functions of these liquids, by observed anti-phase oscillations of cross $g_{AB}(r)$ correlations, compared to $g_{AA}(r)$ or $g_{BB}(r)$ [133]. Similar anti-phase behavior can be observed also in k–space. If the

species A and B are not charged, all distribution functions are equivalent, leading to simple case when $g_{AA}(r) = g_{BB}(r) = g_{AB}(r)$. Hence, the structure of simple ionic liquids is obviously characterized by higher level of complexity, compared to regular simple liquids. However, although being more complex, the micro - structure of this type of system is not heterogeneous.

Situation with ionic liquids becomes more interesting as neutral groups of atoms are bound to positively and negatively charged groups. Building units of such systems are molecules, composed of neutral groups, covalently bound to charged groups. These types of liquids are called complex ionic liquids [133, 137]. In this type of system, Coulomb interactions between charged groups again induce charge ordering. However, charge - ordered chains are now mutually separated by neutral groups, which act as barriers between them. This leads to the formation of heterogeneities, with the density of charged groups not being homogeneously distributed across space. The formation of these heterogeneities, which we call micro - heterogeneities, significantly affects the global microstructure of the liquid and, consequently, leaves marked trace in both radial distribution functions and corresponding structure factors.

Before discussing the effect of micro - heterogeneity on static observables $g(r)$ and $S(k)$, it is important to adress the similarity of complex ionic liquids with alcohols [133], which are also considered as complex liquids. Although molecules of alcohols are globally neutral and molecules of complex ionic liquids are not, the micro - structure of the two systems is similar, both exhibiting charge order in similar fashion. Although positively charged O and negatively charged H atoms in alcohols are bound in one single molecule, charge order is realized in similar fashion like for complex ionic liquids, with formation of O-H...O-H...O-H alternating chains, ultimately leading to alternation of positive and negative charges along the chain. Alkyl groups of alcohols play similar role as neutral groups in complex ionic liquids, causing the formation of micro - heterogeneities, where neighbouring OH chains are mutually separated by alkyl domains. The formation of OH aggregates in this way is visible in both $g(r)$ and $S(k)$, meaning that the formation of micro - heterogeneities can clearly be observed from these two static quantities.

The most apparent difference between $g_{\mathrm{OO}}(r)$ correlations of alcohols versus simple liquids is in the first peak, which is narrowed and shifted to lower r for alcohols, indicating strong association between OO intermolecular pairs, due to charge ordering. In addition, the first peak is followed by the depletion of correlations [138, 143], which reflects the formation of linear OH aggregates in alcohols, which reduces the number of neighbours in second coordination shell from the central atom . We have shown that the characteristic separation between first and second shell of $g_{\mathrm{OO}}(r)$ is fixed for water and all alcohols examined herein, being nearly equal to $0.6\,\sigma$ (with σ being the diameter of O atom), indicating that the mechanism of charge ordering is similar in both water and alcohols. This characteristic separation is manifested in k-space

through the main peak of the OO structure factor, centered at $k = 3\pi\sigma^{-1}$ for all three systems, which we conveniently refer to as charge ordering peak. Less apparent differences between $g_{OO}(r)$ of alcohols, compared to simple liquids, are related to long – ranged features, where we observed that the periodicity of $g_{OO}(r)$ increases with the size of alkyl tails. In the case of water, this periodicity was found to be equal to σ, while it is equal to 1.5 σ and 2.5 σ in the case of methanol and ethanol. We demonstrated that this long – ranged periodicity in r – space manifests in k – space through the appearance of the pre – peak of the structure factor at low k–region. The pre-peak is centered at $k = 2\pi D^{-1}$, with D being equal to the periodicity of long – ranged correlations in r-space (i.e. σ for water, 1.5 σ for methanol and 2.5 σ for ethanol). Physical meaning of D is the average distance between neighbouring OH clusters [185]. In the case of water, this periodicity manifests as the "inner-peak" or the "shoulder-peak" of the OO structure factor, centered at slightly lower k than the charge ordering peak. Shoulder - peak of water could be seen as special case of pre-peak, realized in scenario when there are no neutral groups attached to charged groups. In this context, shoulder - peak of water can be seen as pre - peak of water, which has not been proposed in the literature yet. In case of OH or HH structure factors, pre - peaks appear at the same k-value as for the OO case, which further confirms the fact that this k-value represents the average distance between OH clusters. The average OO distance between two atoms belonging to neighbouring clusters will be the same as the OH or HH distance. However, the position of charge ordering peak is not the same for OO, OH and HH structure factors. This is because charge order represents local ordering of atoms in close vicinity of the central atom. Clearly, nearest intermolecular OO distance will not be the same as the OH or HH distance (as visible when comparing g_{OO}, g_{OH} and g_{HH} distribution functions), which explains why the position of charge ordering peak varies with the choice of correlations. Moreover, we note that the effects of micro - heterogeneity are less apparent in CC correlations, where we observed that correlations between atoms behave similarly as in simple liquids, both in r-space and in k-space.

In order to study the time evolution of static $g(r)$ and $S(k)$, we analyzed time – dependent correlation functions in both r-space and k-space. Dynamic equivalents to static $g(r)$ and $S(k)$ are given with Van Hove correlation function $G(r,t)$ and intermediate scattering function $F(k,t)$ respectively [56]. In addition, the power spectrum of $F(k,t)$ is given with dynamic structure factor $S(k,\omega)$ [56]. Our results have shown that dynamic correlation functions allow to clearly distinguish between dynamics and kinetics in micro - heterogenous liquids, as discussed below.

The analysis of time – dependent density correlations in r-space has shown that the characteristic decorrelation time is significantly larger in the case of simple liquids, than it is for selected associative liquids. Particularly, when correlations between first neighbours are considered, faster decorrelation of associative systems is the consequence of charge ordering, where nearest neighbours interact with strong Coulomb attractive interaction. Due to this interaction,

particles within first coordination shell are strongly affected by the diffusion of the central particle from the origin, leading to faster decorrelation of the density around first shell, compared to simple liquids. Generally, the speed of decorrelation is observed to grow with the increment of partial charges on molecules, indicating that stronger intermolecular interactions lead to faster decorrelation of the density around central particle. However, although this aspect of correlations is instructive, it does not directly allow to distinguish between dynamic versus kinetic aspect of liquids. This differentiation becomes more straighforward in k-space.

As explained above, k-dependent structure factors reflect both short -ranged and long - ranged features of density correlations in r-space. For example, structure factors of methanol and ethanol are shown to exhibit two main features: charge ordering peak (i.e. manifestation of short-ranged correlations between nearest atoms) and the pre-peak (i.e. manifestation of long-ranged correlations between OH aggregates). This means that time - dependent structure factors, $F(k,t)$, represent convenient observable for the differentiation between dynamics versus kinetics in micro - heterogeneous liquids. While dynamics can be conveniently accessed by the time evolution of $F(K,t)$, with K being fixed to the k-position of charge ordering peak, kinetics can be similarly accessed by the time evolution of the same function, but with K corresponding to the position of the pre - peak. Our results have shown that the t-decay of charge ordering peak is universal for both water and alcohols considered herein, regardless of OO, OH or HH correlations being considered. This means that the dynamics of charge order appears to be universal across different associative species. However, when the time evolution of the pre - peak has been considered, significant differences between kinetics of different associative species were found. Namely, we found that kinetics depends on the size of alkyl groups, such that it slows down as the size of alkyl tail increases. Therefore, structural relaxation of heterogeneous microstructure is governed by the size of neutral groups.

The universality of the dynamics of charge order has been further supported with the analysis of the probability distribution of hydrogen bonding lifetimes for different associative liquids presented herein. Although classical hydrogen bonding model is known to have limited value for studying hydrogen bonding interaction, which is essentially quantum - mechanical phenomenon, it serves as useful tool for studying the dynamics of charge order. Particularly, by considering a classical hydrogen bonding lifetime of bonded O-H...O intermolecular pair, one essentially accounts for the vibrations of charge - ordered microstructure. Our results [75, 76] have found the universality of these vibrational modes across different associative species, suggesting that the dynamics of charge order could be universal across different associative systems containing OH groups. This universality is then confirmed more rigorously by the analysis of correlation functions.

One can also account for k-dependent correlations in frequency space, instead of time space,

by considering dynamical structure factor $S(k,\omega)$. We have shown that $S(k,\omega)$ of water and alcohols, for fixed value of ω, has marked peaks at k-positions corresponding to the pre-peak and charge ordering peak of static structure factor $S(k)$. For small values of ω, the amplitude of $S(k,\omega)$ is significantly higher at the pre - peak, compared to charge ordering peak, implying that slow relaxation in time ($\omega \approx 0$) is mainly related to the kinetics and much less for dynamics of the liquid. For larger ω frequencies, the amplitude of $S(k,\omega)$ at the pre - peak is close to 0, showing marked amplitudes only around charge ordering peak at higher k-values. This shows that larger frequencies (i.e. faster relaxation in time) are mainly related to the dynamics of charge ordered microstructure, and are not related to the kinetics of the liquid, which relaxes significantly slower.

In addition, our analysis of $S(k,\omega)$ of water has led to surprising result. We found that dynamical structure factor of water, for small ω, has an additional marked peak which is absent from static structure factor, namely around 0.5 Å^{-1}, which is lower than the position of the shoulder-peak (2 Å^{-1}). This peak could imply slow relaxation mode related to the microstructure of water of the lengthscale of $\sim$ 10 Å. Interestingly, 10 Å is precisely the distance where the shift of periodicity from 0.6 σ to σ occurs in $g_{\text{OO}}(r)$ of water. This means that this additional peak in the dynamical structure factor of water could also be related to the relaxation of charge order in the microstructure of the liquid. This topic requires more investigation in order to be developed further.

In order to study the time evolution of dynamical correlations by the application of Mori-Zwanzig formalism [62, 56, 89, 191], which puts the memory function in the center of investigation, one needs to perform the inversion of the $\mathbf{S}(k,\omega)$ matrix, in order to obtain the memory matrix. Our research revealed that the memory matrix is characterized by ambiguous divergence over small - k region, whose origin appears to be related to irregularities related with the $\mathbf{S}(k,\omega)$ matrix, particularly by the manner in which $\mathbf{S}(k,\omega)$ converges to 0 in small - k limit, when ω is fixed. These irregularities cause big numerical problems when the inversion of this matrix is supposed to be performed, in order to obtain the memory matrix. Since the origin of these unexpected anomalies is still unknown, it stopped us from further progress in obtaining the memory function. At precise moment, it seems that further development of the theory is essential step in order to overpass current obstacles. Then, these obstacles are expected to be treated and overpassed analytically. Nevertheless, significant progress has been made, particularly in sense that dynamic structure factors have been extracted "by hand" for several selected ω-values, which enabled us to observe interesting trends in frequency domain, and show part of interesting features. Particularly, we have demonstrated how close to the description of realistic liquids one can get by applying simple Markovian approximation of the memory function to realistic liquids. Our results show that, although these approximations are widely used in soft matter for solving Mori - Zwanzig equation for mesoscopic dynamics of coarse - grained sys-

tems [70, 80, 97, 98, 88, 89], they are unuseful for describing the time - dependent properties of realistic molecular liquids, such as dynamic correlations. This was desmonstrated by comparing simple Markovian $S(k,\omega)$ with $S(k,\omega)$ obtained directly from simulations, where we observed that Markovian approximation undoubtedly fails to reproduce realistic correlations in the liquid. In addition, we highlight the discovery of unexpected peak of dynamical structure factor of water at $k = 0.5$ Å^{-1}, both in the case of OO and OH correlations, which is expected to represent important starting point of future research works. Interestingly, this peak shows up also within Markovian approximation. Furthermore, the importance of the observed universality of the probability distribution of hydrogen bonding lifetimes [75, 76], within transient temporal regime, should not be left out. While previous research works were mainly focused on the kinetic aspect of this distribution [96, 95, 105, 122], we have shown here that the properties within transient regime have important connection with the dynamics of charge order, suggesting its universality across different associative species with OH functional groups. This universality has been confirmed both in the context of classical hydrogen bonding model and in the context of correlation functions. Finally, we demonstrated how k-dependent correlation functions allow to differentiate between dynamics and kinetics in micro - heterogeneous liquids, which was also one of the main aims of this thesis.

Curriculum vitae: Ivo Jukić

Education:

M.Sc. in Computational Physics (2017. - 2019.)
Faculty of Science, University of Split, Croatia

B.Sc. in Physics (2014. - 2017.)
Faculty of Science, University of Split, Croatia

Employment:

2019. - 2023. Research assistant on the scientific project "Dynamics in micro - segregated systems" (Ass. Prof. Bernarda Lovrinčević) , financed by Croatian Science Foundation (HRZZ), under the code UIP-2017-05-1863:

2019. - 2023. Student of Doctoral School of Biophysics at Faculty of Science, University of Split

Grants & Awards:

French Government Grant (2020. - 2022.)
Dean's Award for great GPA after finishing Masters study
Dean's Award for great GPA after finishing Bachelor study

List of publications:

1) M. Požar, I. Jukić, B. Lovrinčević: Thermodynamic, structural and dynamic properties of selected non-associative neat liquids; *Journal of Physics: Condensed Matter* 32 (40), 405101, 2020.

2) I. Jukić, M. Požar, B. Lovrinčević: Comparative analysis of ethanol dynamics in aqueous and non-aqueous solutions; *Physical Chemistry Chemical Physics* 22 (41), 23856-23868, 2020.

3) B. Lovrinčević, I. Jukić, M. Požar: An Overview on the Dynamics in Aqueous Mixtures of Lower Alcohols; Molecular Basics of Liquids and Liquid-Based Materials, 169-193, Springer Nature Singapore, 2021.

4) I. Jukić, M. Požar, B. Lovrinčević, A. Perera: Universal features in the lifetime distribution of clusters in hydrogen-bonding liquids; *Physical Chemistry Chemical Physics* 23 (35), 19537-19546, 2021.

5) I. Jukić, M. Požar, B. Lovrinčević, A. Perera: Lifetime distribution of clusters in binary mixtures involving hydrogen bonding liquids; *Scientific Reports* 12 (1), 1-9, 2022.

6) B. Lovrinčević, M. Požar, I. Jukić, A. Perera: Role of charge ordering in the dynamics of cluster formation in associated liquids, *Journal of Physical Chemistry B,* 2023.

References

[1] M.J. Abraham, D. Van Der Spoel, E. Lindahl, B. Hess, et al. Gromacs user manual version 5.0. 4. *The GROMACS Development Team at the Royal Instituta of Technology and Uppsala University, Sweden*, 2014.

[2] A. Ziya Akcasu and James J. Duderstadt. Derivation of kinetic equations from the generalized langevin equation. *Physical Review*, 188(1):479, 1969.

[3] Michael P. Allen and Dominic J. Tildesley. *Computer simulation of liquids*. Oxford university press, 2017.

[4] Dimitri Antoniou and Steven D. Schwartz. Langevin equation in momentum space. *The Journal of chemical physics*, 119(21):11329–11334, 2003.

[5] Imre Bakó, Tünde Megyes, Szabolcs Bálint, Tamás Grósz, and Viorel Chihaia. Water–methanol mixtures: topology of hydrogen bonded network. *Physical Chemistry Chemical Physics*, 10(32):5004–5011, 2008.

[6] Saikat Banerjee, Jonathan Furtado, and Biman Bagchi. Fluctuating micro-heterogeneity in water–tert-butyl alcohol mixtures and lambda-type divergence of the mean cluster size with phase transition-like multiple anomalies. *The Journal of chemical physics*, 140(19):194502, 2014.

[7] David Beeman. Some multistep methods for use in molecular dynamics calculations. *Journal of computational physics*, 20(2):130–139, 1976.

[8] Arieh Ben-Naim. *Molecular theory of solutions*. OUP Oxford, 2006.

[9] Arieh Ben-Naim. The kirkwood–buff integrals for one-component liquids. *The Journal of chemical physics*, 128(23):234501, 2008.

[10] Herman J.C. Berendsen, J.P.M. van Postma, Wilfred F. Van Gunsteren, A.R.H.J. DiNola, and Jan R. Haak. Molecular dynamics with coupling to an external bath. *The Journal of chemical physics*, 81(8):3684–3690, 1984.

[11] F.J. Bermejo, E. Enciso, J. Alonso, N. Garcia, and W.S. Howells. How well do we know the structure of simple molecular liquids? ccl4 revisited. *Molecular Physics*, 64(6):1169–1184, 1988.

[12] Bruce J. Berne and Robert Pecora. *Dynamic light scattering: with applications to chemistry, biology, and physics*. Courier Corporation, 2000.

[13] C.E. Bertrand, J.L. Self, J.R.D. Copley, and Antonio Faraone. Nanoscopic length scale dependence of hydrogen bonded molecular associates dynamics in methanol. *The Journal of Chemical Physics*, 146(19):194501, 2017.

[14] Christopher E. Bertrand, Jeffrey L. Self, J.R.D. Copley, and Antonio Faraone. Dynamic signature of molecular association in methanol. *The Journal of Chemical Physics*, 145(1):014502, 2016.

[15] L Blum and AJ Torruella. Invariant expansion for two-body correlations: Thermodynamic functions, scattering, and the ornsteinâzernike equation. *The Journal of Chemical Physics*, 56(1):303–310, 1972.

[16] Roland Bohmer, Catalin Gainaru, and Ranko Richert. Structure and dynamics of monohydroxy alcohols - milestones towards their microscopic understanding, 100 years after debye. *Physics Reports*, 545(4):125–195, 2014.

[17] Jean Pierre Boon and Sidney Yip. *Molecular hydrodynamics*. Courier Corporation, 1991.

[18] Sergey Burikov, Tatiana Dolenko, Svetlana Patsaeva, Yuriy Starokurov, and Viktor Yuzhakov. Raman and ir spectroscopy research on hydrogen bonding in water–ethanol systems. *Molecular physics*, 108(18):2427–2436, 2010.

[19] Gaia Camisasca, Nuno Galamba, Kjartan Thor Wikfeldt, and Lars G.M. Pettersson. Translational and rotational dynamics of high and low density tip4p/2005 water. *The Journal of chemical physics*, 150(22):224507, 2019.

[20] José NA Canongia Lopes and Agílio AH Pádua. Nanostructural organization in ionic liquids. *The Journal of Physical Chemistry B*, 110(7):3330–3335, 2006.

[21] Javier Cardona, Martin B. Sweatman, and Leo Lue. Molecular dynamics investigation of the influence of the hydrogen bond networks in ethanol/water mixtures on dielectric spectra. *The Journal of Physical Chemistry B*, 122(4):1505–1515, 2018.

[22] David Chandler. Derivation of an integral equation for pair correlation functions in molecular fluids. *The Journal of Chemical Physics*, 59(5):2742–2746, 1973.

[23] David Chandler. Structures of molecular liquids. *Annual Review of Physical Chemistry*, 29(1):441–471, 1978.

[24] David Chelazzi, Rodorico Giorgi, and Piero Baglioni. Microemulsions, micelles, and functional gels: how colloids and soft matter preserve works of art. *Angewandte Chemie International Edition*, 57(25):7296–7303, 2018.

[25] Song-Ho Chong and Fumio Hirata. Interaction-site-model description of collective excitations in classical molecular fluids. *Physical Review E*, 57(2):1691, 1998.

[26] Song-Ho Chong and Fumio Hirata. Mode-coupling theory for molecular liquids based on the interaction-site model. *Physical Review E*, 58(5):6188, 1998.

[27] Song-Ho Chong and Fumio Hirata. Interaction-site-model description of collective excitations in liquid water. i: Theoretical study. *The Journal of chemical physics*, 111(7):3083–3094, 1999.

[28] Zonglin Chu, Cécile A Dreiss, and Yujun Feng. Smart wormlike micelles. *Chemical Society Reviews*, 42(17):7174–7203, 2013.

[29] AF Collings and R Mills. Temperature-dependence of self-diffusion for benzene and carbon tetrachloride. *Transactions of the Faraday Society*, 66:2761–2766, 1970.

[30] Tyler Cosby, Utkarsh Kapoor, Jindal K Shah, and Joshua Sangoro. Mesoscale organization and dynamics in binary ionic liquid mixtures. *The journal of physical chemistry letters*, 10(20):6274–6280, 2019.

[31] Vincent Dahirel, Marie Jardat, Jean-François Dufreche, Ivan Lucas, Serge Durand-Vidal, and Pierre Turq. Coarse-graining in suspensions of charged nanoparticles. *Pure and Applied Chemistry*, 80(6):1229–1238, 2008.

[32] Vincent Dahirel, Marie Jardat, Jean-François Dufrêche, and Pierre Turq. New coarse-graining procedure for the dynamics of charged spherical nanoparticles in solution. *The Journal of chemical physics*, 126(11):114108, 2007.

[33] Krishnendu Das, Luca Gabrielli, and Leonard J. Prins. Chemically fueled self-assembly in biology and chemistry. *Angewandte Chemie International Edition*, 60(37):20120–20143, 2021.

[34] N. Dawass, P. Krüger, S.K. Schnell, D. Bedeaux, S. Kjelstrup, J.M. Simon, and T.J.H. Vlugt. Finite-size effects of kirkwood-buff integrals from molecular simulations. *Molecular Simulation*, 44:599, 2018.

[35] Noura Dawass, Peter Krüger, Sondre K. Schnell, Jean-Marc Simon, and Thijs J.H. Vlugt. Kirkwood-buff integrals from molecular simulation. *Fluid Phase Equilibria*, 486:21–36, 2019.

[36] P.G. de Gennes. An analogy between superconductors and smectics a. *Solid State Communications*, 10(9):753–756, 1972.

[37] I.M. De Schepper and M.H. Ernst. Self-diffusion beyond fick's law. *Physica A: Statistical Mechanics and its Applications*, 98(1-2):189–214, 1979.

[38] R. Dengler. Another derivation of generalized langevin equations. *arXiv preprint arXiv:1506.02650*, 2015.

[39] Qin Dong, Chen Yu, Lian Li, Lei Nie, Danyang Li, and Hengchang Zang. Near-infrared spectroscopic study of molecular interaction in ethanol-water mixtures. *Spectrochimica Acta Part A: Molecular and Biomolecular Spectroscopy*, 222:117183, 2019.

[40] J.P. Donley. Liquids in equilibrium: Beyond the hypernetted chain. *The European Physical Journal E*, 16:273–282, 2005.

[41] E.M. Duffy, D.L. Severance, and W.L. Jorgensen. Solvent effects on the barrier to isomerization for a tertiary amide from ab initio and monte carlo calculations. *Journal of the American Chemical Society*, 114(19):7535, 1992.

[42] Marzena Dzida and Udo Kaatze. Compressibility and dielectric relaxation of mixtures of water with monohydroxy alcohols. *The Journal of Physical Chemistry B*, 119(38):12480–12489, 2015.

[43] Allan J. Easteal, William E. Price, and Lawrence A. Woolf. Diaphragm cell for high-temperature diffusion measurements. tracer diffusion coefficients for water to 363 k. *Journal of the Chemical Society, Faraday Transactions 1: Physical Chemistry in Condensed Phases*, 85(5):1091–1097, 1989.

[44] K. Egashira and N. Nishi. Low-frequency raman spectroscopy of ethanol- water binary solution: evidence for self-association of solute and solvent molecules. *The Journal of Physical Chemistry B*, 102(21):4054–4057, 1998.

[45] Mauro Ferrario, Michael Haughney, Ian R. McDonald, and Michael L. Klein. Molecular-dynamics simulation of aqueous mixtures: methanol, acetone, and ammonia. *The Journal of chemical physics*, 93(7):5156–5166, 1990.

[46] Rana A. Fine and Frank J. Millero. Compressibility of water as a function of temperature and pressure. *The Journal of Chemical Physics*, 59(10):5529–5536, 1973.

[47] Riccardo Foffi and Francesco Sciortino. Correlated fluctuations of structural indicators close to the liquid–liquid transition in supercooled water. *The Journal of Physical Chemistry B*, 2022.

[48] Daan Frenkel, Berend Smit, and Mark A. Ratner. *Understanding molecular simulation: from algorithms to applications*, volume 2. Academic press San Diego, 1996.

[49] Paola Gallo, Katrin Amann-Winkel, Charles Austen Angell, Mikhail Alexeevich Anisimov, Frédéric Caupin, Charusita Chakravarty, Erik Lascaris, Thomas Loerting, Athanassios Zois Panagiotopoulos, John Russo, et al. Water: A tale of two liquids. *Chemical reviews*, 116(13):7463–7500, 2016.

[50] P. Ganguly and N.F.A. van der Vegt. Convergence of sampling kirkwood-buff integrals of aqueous solutions with molecular dynamics simulations. *Journal of Chemical Theory and Computation*, 9(3):1347–1355, 2013. PMID: 26587597.

[51] Aziz Ghoufi. Molecular origin of the prepeak in the structure factor of alcohols. *The Journal of Physical Chemistry B*, 124(50):11501–11509, 2020.

[52] Kenneth T. Gillen, D.C. Douglass, and M.J.R. Hoch. Self-diffusion in liquid water to-31 c. *The Journal of Chemical Physics*, 57(12):5117–5119, 1972.

[53] E. Guardia, J. Marti, J.A. Padro, L. Saiz, and A.V. Komolkin. Dynamics in hydrogen bonded liquids: water and alcohols. *Journal of molecular liquids*, 96:3–17, 2002.

[54] Gabriela Guevara-Carrion, Jadran Vrabec, and Hans Hasse. Prediction of self-diffusion coefficient and shear viscosity of water and its binary mixtures with methanol and ethanol by molecular simulation. *The Journal of chemical physics*, 134(7):074508, 2011.

[55] Jean Pierre Hansen and Ian R. McDonald. Statistical mechanics of dense ionized matter. iv. density and charge fluctuations in a simple molten salt. *Physical Review A*, 11(6):2111, 1975.

[56] Jean-Pierre Hansen and Ian Ranald McDonald. *Theory of simple liquids: with applications to soft matter*. Academic press, 2013.

[57] J.P. Hansen and I.R. McDonald. Self-diffusion and electrical conductance in a simple molten salt. *Journal of Physics C: Solid State Physics*, 7(21):L384, 1974.

[58] AP Hardt, DK Anderson, R Rathbun, BW Mar, and AL Babb. Self-diffusion in liquids. ii. comparison between mutual and self-diffusion coefficients. *The Journal of Physical Chemistry*, 63(12):2059–2061, 1959.

[59] Milan K. Hazra and Biman Bagchi. Collective excitations and ultrafast dipolar solvation dynamics in water-ethanol binary mixture. *The Journal of Chemical Physics*, 148(11):114506, 2018.

[60] Daniel Herschlag and Margaux M. Pinney. Hydrogen bonds: Simple after all? *Biochemistry*, 57(24):3338–3352, 2018.

[61] Berk Hess, Carsten Kutzner, David Van Der Spoel, and Erik Lindahl. Gromacs 4: algorithms for highly efficient, load-balanced, and scalable molecular simulation. *Journal of chemical theory and computation*, 4(3):435–447, 2008.

[62] Carmen Hijón, Pep Espanol, Eric Vanden-Eijnden, and Rafael Delgado-Buscalioni. Mori–zwanzig formalism as a practical computational tool. *Faraday discussions*, 144:301–322, 2010.

[63] Fumio Hirata. Interaction-site representation of the smoluchowski–vlasov equation: The space–time correlation functions in a molecular liquid. *The Journal of chemical physics*, 96(6):4619–4624, 1992.

[64] Fumio Hirata. Theory of molecular liquids. *Molecular theory of solvation*, pages 1–60, 2003.

[65] R.W. Hockney. Potential calculation and some applications. *Methods Comput. Phys. 9: 135-211(1970).*

[66] William G. Hoover. Canonical dynamics: Equilibrium phase-space distributions. *Physical review A*, 31(3):1695, 1985.

[67] C.S. Hsu, David Chandler, and L-J_ Lowden. Applications of the rism equation to diatomic fluids: the liquids nitrogen, oxygen and bromine. *Chemical Physics*, 14(2):213–228, 1976.

[68] Abdenacer Idrissi, Franjo Sokolić, and Aurélien Perera. A molecular dynamics study of the urea/water mixture. *The Journal of Chemical Physics*, 112(21):9479–9488, 2000.

[69] Takuya Iwashita, Bin Wu, Wei-Ren Chen, Satoshi Tsutsui, Alfred Q. R. Baron, and Takeshi Egami. Seeing real-space dynamics of liquid water through inelastic x-ray scattering. *Science Advances*, 3(12):e1603079, 2017.

[70] Sergei Izvekov. Mori-zwanzig projection operator formalism: Particle-based coarse-grained dynamics of open classical systems far from equilibrium. *Physical Review E*, 104(2):024121, 2021.

[71] William L. Jorgensen. Optimized intermolecular potential functions for liquid alcohols. *The Journal of Physical Chemistry*, 90(7):1276–1284, 1986.

[72] William L Jorgensen, Jayaraman Chandrasekhar, Jeffry D. Madura, Roger W. Impey, and Michael L. Klein. Comparison of simple potential functions for simulating liquid water. *The Journal of chemical physics*, 79(2):926–935, 1983.

[73] William L Jorgensen, Jeffry D. Madura, and Carol J. Swenson. Optimized intermolecular potential functions for liquid hydrocarbons. *Journal of the American Chemical Society*, 106(22):6638–6646, 1984.

[74] W.L. Jorgensen, J.M. Briggs, and M.L. Contreras. Relative partition coefficients for organic solutes from fluid simulations. *The Journal of Physical Chemistry*, 94(4):1683, 1990.

[75] Ivo Jukić, Martina Požar, and Bernarda Lovrinčević. Comparative analysis of ethanol dynamics in aqueous and non-aqueous solutions. *Physical Chemistry Chemical Physics*, 22(41):23856–23868, 2020.

[76] Ivo Jukić, Martina Požar, Bernarda Lovrinčević, and Aurélien Perera. Lifetime distribution of clusters in binary mixtures involving hydrogen bonding liquids. *Scientific Reports*, 12(1):9120, 2022.

[77] Hemant K. Kashyap, Cherry S. Santos, Harsha V.R. Annapureddy, N. Sanjeeva Murthy, Claudio J. Margulis, and Edward W. Castner Jr. Temperature-dependent structure of ionic liquids: X-ray scattering and simulations. *Faraday discussions*, 154:133–143, 2012.

[78] George S. Kell. Effects of isotopic composition, temperature, pressure, and dissolved gases on the density of liquid water. *Journal of Physical and Chemical Reference Data*, 6(4):1109–1131, 1977.

[79] B. Kezic, R. Mazighi, and A. Perera. A model for molecular emulsions: Water and weak water mixtures. *Physica A: Statistical Mechanics and its Applications*, 392(4):567–582, 2013.

[80] Viktor Klippenstein, Madhusmita Tripathy, Gerhard Jung, Friederike Schmid, and Nico FA van der Vegt. Introducing memory in coarse-grained molecular simulations. *The Journal of Physical Chemistry B*, 125(19):4931–4954, 2021.

[81] Maiko Kofu, Michihiro Nagao, Takeshi Ueki, Yuzo Kitazawa, Yutaro Nakamura, Syota Sawamura, Masayoshi Watanabe, and Osamu Yamamuro. Heterogeneous slow dynamics of imidazolium-based ionic liquids studied by neutron spin echo. *The Journal of Physical Chemistry B*, 117(9):2773–2781, 2013.

[82] P. Krüger, S.K. Schnell, D. Bedeaux, S. Kjelstrup, T.J.H. Vlugt, and J.-M. Simon. Kirkwood-buff integrals for finite volumes. *The Journal of Physical Chemistry Letters*, 4(2):235–238, 2013. PMID: 26283427.

[83] Tobias Kulschewski and Jürgen Pleiss. A molecular dynamics study of liquid aliphatic alcohols: simulation of density and self-diffusion coefficient using a modified opls force field. *Molecular Simulation*, 39(9):754–767, 2013.

[84] R. Kumar, J.R. Schmidt, and J.L. Skinner. Hydrogen bonding definitions and dynamics in liquid water. *The Journal of chemical physics*, 126(20):05B611, 2007.

[85] C. Kuttenberg, E. Scheiber, and V. Gutmann. An infrared spectroscopic study on the influence of water on alcohols. *Monatshefte für Chemie/Chemical Monthly*, 126(8):889–895, 1995.

[86] J.L. Lebowitz and J.K. Percus. Long-range correlations in a closed system with applications to nonuniform fluids. *Physical Review*, 122(6):1675, 1961.

[87] Song Hi Lee and Jahun Kim. Transport properties of bulk water at 243–550 k: a comparative molecular dynamics simulation study using spc/e, tip4p, and tip4p/2005 water models. *Molecular physics*, 117(14):1926–1933, 2019.

[88] Zhen Li, Xin Bian, Bruce Caswell, and George Em Karniadakis. Construction of dissipative particle dynamics models for complex fluids via the mori–zwanzig formulation. *Soft Matter*, 10(43):8659–8672, 2014.

[89] Zhen Li, Xin Bian, Xiantao Li, and George Em Karniadakis. Incorporation of memory effects in coarse-grained modeling via the mori-zwanzig formalism. *The Journal of chemical physics*, 143(24):243128, 2015.

[90] André Liemert, Trifce Sandev, and Holger Kantz. Generalized langevin equation with tempered memory kernel. *Physica A: Statistical Mechanics and its Applications*, 466:356–369, 2017.

[91] Chuanlong Lin, Jesse S Smith, Stanislav V Sinogeikin, and Guoyin Shen. Experimental evidence of low-density liquid water upon rapid decompression. *Proceedings of the National Academy of Sciences*, 115(9):2010–2015, 2018.

[92] Bernarda Lovrinčević, Ivo Jukić, and Martina Požar. An overview on the dynamics in aqueous mixtures of lower alcohols. *Molecular Basics of Liquids and Liquid-Based Materials*, pages 169–193, 2021.

[93] R. Ludwig. Nmr relaxation studies in water-alcohol mixtures: the water-rich region. *Chemical physics*, 195(1-3):329–337, 1995.

[94] R. Ludwig, M.D. Zeidler, and T.C. Farrar. Molecular dynamics in lower alcohols. *Zeitschrift für physikalische Chemie*, 189(1):19–27, 1995.

[95] Alenka Luzar. Resolving the hydrogen bond dynamics conundrum. *The Journal of Chemical Physics*, 113(23):10663–10675, 2000.

[96] Alenka Luzar and David Chandler. Hydrogen-bond kinetics in liquid water. *Nature*, 379(6560):55–57, 1996.

[97] Zhan Ma, Shu Wang, Minhee Kim, Kaibo Liu, Chun-Long Chen, and Wenxiao Pan. Transfer learning of memory kernels for transferable coarse-graining of polymer dynamics. *Soft Matter*, 17(24):5864–5877, 2021.

[98] Zhan Ma, Shu Wang, Minhee Kim, Kaibo Liu, Chun-Long Chen, and Wenxiao Pan. Transfer learning of memory kernels in coarse-grained modeling. *arXiv preprint arXiv:2103.10578*, 2021.

[99] Fabio Marchesoni. A nonlinear langevin equation for fluid relaxation. *Progress of theoretical physics*, 74(6):1339–1342, 1985.

[100] Pekka Mark and Lennart Nilsson. Structure and dynamics of the tip3p, spc, and spc/e water models at 298 k. *The Journal of Physical Chemistry A*, 105(43):9954–9960, 2001.

[101] Omer Markovitch and Noam Agmon. Reversible geminate recombination of hydrogen-bonded water molecule pair. *The Journal of chemical physics*, 129(8):084505, 2008.

[102] J. Martí, J.A. Padró, and E. Guardia. Hydrogen bonding influence on the intermolecular vibrational spectra of liquid methanol. *Journal of molecular liquids*, 64(1-2):1–12, 1995.

[103] J. Marti, J.A. Padro, and E. Guardia. Molecular dynamics simulation of liquid water along the coexistence curve: Hydrogen bonds and vibrational spectra. *The Journal of chemical physics*, 105(2):639–649, 1996.

[104] Marcus G. Martin and J. Ilja Siepmann. Transferable potentials for phase equilibria. 1. united-atom description of n-alkanes. *The Journal of Physical Chemistry B*, 102(14):2569–2577, 1998.

[105] H.F.M.C. Martiniano and N. Galamba. Insights on hydrogen-bond lifetimes in liquid and supercooled water. *The Journal of Physical Chemistry B*, 117(50):16188–16195, 2013.

[106] Ray A Matsumoto, Matthew W Thompson, Van Quan Vuong, Weiwei Zhang, Yuya Shinohara, Adri CT van Duin, Paul RC Kent, Stephan Irle, Takeshi Egami, and Peter T Cummings. Investigating the accuracy of water models through the van hove correlation function. *Journal of Chemical Theory and Computation*, 17(10):5992–6005, 2021.

[107] Jean-Joseph Max and Camille Chapados. Infrared spectroscopy of acetone-methanol liquid mixtures: Hydrogen bond network. *The Journal of chemical physics*, 122(1):014504, 2005.

[108] Jean-Joseph Max and Camille Chapados. Infrared spectroscopy of methanol-hexane liquid mixtures. ii. the strength of hydrogen bonding. *The Journal of chemical physics*, 130(12):124513, 2009.

[109] Hugues Meyer, Thomas Voigtmann, and Tanja Schilling. On the" generalized generalized langevin equation". *arXiv preprint arXiv:1706.00658*, 2017.

[110] R. Mills. Self-diffusion in normal and heavy water in the range 1-45. deg. *The Journal of Physical Chemistry*, 77(5):685–688, 1973.

[111] J. Milzetti, D. Nayar, and N.F.A. van der Vegt. Convergence of kirkwood-buff integrals of ideal and nonideal aqueous solutions using molecular dynamics simulations. *The Journal of Physical Chemistry B*, 122(21):5515–5526, 2018. PMID: 29342355.

[112] Kazuko Mizuno, Yasue Miyashita, Yohji Shindo, and Hideo Ogawa. Nmr and ft-ir studies of hydrogen bonds in ethanol-water mixtures. *The Journal of Physical Chemistry*, 99(10):3225–3228, 1995.

[113] Anatolii V. Mokshin, Renat M. Yulmetyev, and Peter Hänggi. Simple measure of memory for dynamical processes described by a generalized langevin equation. *Physical review letters*, 95(20):200601, 2005.

[114] Hazime Mori. Transport, collective motion, and brownian motion. *Progress of theoretical physics*, 33(3):423–455, 1965.

[115] Marija Nedić, Tobias N. Wassermann, Rene Wugt Larsen, and Martin A. Suhm. A combined raman-and infrared jet study of mixed methanol–water and ethanol–water clusters. *Physical Chemistry Chemical Physics*, 13(31):14050–14063, 2011.

[116] Marija Nedić, Tobias N. Wassermann, Zhifeng Xue, Philipp Zielke, and Martin A. Suhm. Raman spectroscopic evidence for the most stable water/ethanol dimer and for the negative mixing energy in cold water/ethanol trimers. *Physical Chemistry Chemical Physics*, 10(39):5953–5956, 2008.

[117] A. Nilsson, S. Schreck, F. Perakis, and L. G. M. Pettersson. Probing water with x-ray lasers. *Advances in Physics: X*, 1(2):226–245, 2016.

[118] Nobuyuki Nishi, Satoru Takahashi, Masaki Matsumoto, Aki Tanaka, Keisuke Muraya, Toshiyuki Takamuku, and Toshio Yamaguchi. Hydrogen-bonded cluster formation and hydrophobic solute association in aqueous solutions of ethanol. *The Journal of Physical Chemistry*, 99(1):462–468, 1995.

[119] Sture Nordholm and Robert Zwanzig. A systematic derivation of exact generalized brownian motion theory. *Journal of Statistical Physics*, 13(4):347–371, 1975.

[120] Shūichi Nosé. A molecular dynamics method for simulations in the canonical ensemble. *Molecular physics*, 52(2):255–268, 1984.

[121] Adu Offei-Danso, Ali Hassanali, and Alex Rodriguez. High-dimensional fluctuations in liquid water: Combining chemical intuition with unsupervised learning. *Journal of Chemical Theory and Computation*, 18(5):3136–3150, 2022.

[122] J.A. Padró, L. Saiz, and E. Guardia. Hydrogen bonding in liquid alcohols: a computer simulation study. *Journal of Molecular Structure*, 416(1-3):243–248, 1997.

[123] G. Pálinkás, I. Bakó, K. Heinzinger, and Ph. Bopp. Molecular dynamics investigation of the inter-and intramolecular motions in liquid methanol and methanol-water mixtures. *Molecular Physics*, 73(4):897–915, 1991.

[124] Michele Parrinello and Aneesur Rahman. Crystal structure and pair potentials: A molecular-dynamics study. *Physical review letters*, 45(14):1196, 1980.

[125] Michele Parrinello and Aneesur Rahman. Polymorphic transitions in single crystals: A new molecular dynamics method. *Journal of Applied physics*, 52(12):7182–7190, 1981.

[126] K.N. Pathak. Langevin equationâapplication to liquid state dynamics. In *Stochastic Processes Formalism and Applications: Proceedings of the Winter School Held at the University of Hyderabad, India December 15–24, 1982*, pages 197–219. Springer, 2005.

[127] Fivos Perakis, Gaia Camisasca, Thomas J Lane, Alexander Späh, Kjartan Thor Wikfeldt, Jonas A Sellberg, Felix Lehmkühler, Harshad Pathak, Kyung Hwan Kim, Katrin Amann-Winkel, et al. Coherent x-rays reveal the influence of cage effects on ultrafast water dynamics. *Nature communications*, 9(1):1–10, 2018.

[128] A. Perera, R. Mazighi, and B. Kežić. Fluctuations and micro-heterogeneity in aqueous mixtures. *The Journal of Chemical Physics*, 136(17):174516, 2012.

[129] A. Perera and F. Sokolić. Modeling nonionic aqueous solutions: The acetone-water mixture. *The Journal of Chemical Physics*, 121:11272, 2004.

[130] A Perera, F. Sokolić, L. Almasy, and Y. Koga. Kirkwood-buff integrals of aqueous alcohol binary mixtures. *The Journal of chemical physics*, 124(12):124515, 2006.

[131] Aurélien Perera. On the microscopic structure of liquid water. *Molecular Physics*, 109(20):2433–2441, 2011.

[132] Aurélien Perera. Charge ordering and scattering pre-peaks in ionic liquids and alcohols. *Physical Chemistry Chemical Physics*, 19(2):1062–1073, 2017.

[133] Aurélien Perera. Charge ordering and scattering pre-peaks in ionic liquids and alcohols. *Physical Chemistry Chemical Physics*, 19(2):1062–1073, 2017.

[134] Aurélien Perera, Bernarda Kežic, Franjo Sokolic, and Larisa Zoranic. Micro-heterogeneity in complex liquids. In *Molecular Dynamics-Studies of Synthetic and Biological Macromolecules*. IntechOpen, 2012.

[135] Aurélien Perera and Bernarda Lovrinčević. A comparative study of aqueous dmso mixtures by computer simulations and integral equation theories. *Molecular Physics*, 116(21-22):3311–3322, 2018.

[136] Aurélien Perera and Redha Mazighi. On the nature of the molecular ordering of water in aqueous dmso mixtures. *The Journal of Chemical Physics*, 143(15):154502, 2015.

[137] Aurélien Perera and Redha Mazighi. Simple and complex forms of disorder in ionic liquids. *Journal of Molecular Liquids*, 210:243–251, 2015.

[138] Aurélien Perera, Franjo Sokolić, and Larisa Zoranić. Microstructure of neat alcohols. *Physical Review E*, 75(6):060502, 2007.

[139] P. Petong, R. Pottel, and UJTJoPCA Kaatze. Water- ethanol mixtures at different compositions and temperatures. a dieletric relaxation study. *The Journal of Physical Chemistry A*, 104(32):7420–7428, 2000.

[140] Szilvia Pothoczki, Ildikó Pethes, László Pusztai, László Temleitner, Koji Ohara, and Imre Bakó. Properties of hydrogen-bonded networks in ethanol–water liquid mixtures as a function of temperature: Diffraction experiments and computer simulations. *The Journal of Physical Chemistry B*, 125(23):6272–6279, 2021.

[141] Szilvia Pothoczki, László Pusztai, and Imre Bakó. Variations of the hydrogen bonding and hydrogen-bonded network in ethanol–water mixtures on cooling. *The Journal of Physical Chemistry B*, 122(26):6790–6800, 2018.

[142] Martina Požar. *On the nature of structural fluctuations in complex liquids*. PhD thesis, University of Split. University of Split, Faculty of science. Department of Physics, 2018.

[143] Martina Požar, Jennifer Bolle, Christian Sternemann, and Aurélien Perera. On the x-ray scattering pre-peak of linear mono-ols and the related microstructure from computer simulations. *The Journal of Physical Chemistry B*, 124(38):8358–8371, 2020.

[144] Martina Požar, Bernarda Lovrinčević, Larisa Zoranić, Tomislav Primorać, Franjo Sokolić, and Aurélien Perera. Micro-heterogeneity versus clustering in binary mixtures of ethanol with water or alkanes. *Physical Chemistry Chemical Physics*, 18(34):23971–23979, 2016.

[145] Martina Požar, Bernarda Lovrinčević, Larisa Zoranić, Tomislav Primorać, Franjo Sokolić, and Aurélien Perera. Micro-heterogeneity versus clustering in binary mixtures of ethanol with water or alkanes. *Physical Chemistry Chemical Physics*, 18(34):23971–23979, 2016.

[146] Martina Požar and Aurélien Perera. On the existence of a scattering pre-peak in the mono-ols and diols. *Chemical Physics Letters*, 671:37–43, 2017.

[147] Sander Pronk, Szilárd Páll, Roland Schulz, Per Larsson, Pär Bjelkmar, Rossen Apostolov, Michael R Shirts, Jeremy C Smith, Peter M Kasson, David Van Der Spoel, et al. Gromacs 4.5: a high-throughput and highly parallel open source molecular simulation toolkit. *Bioinformatics*, 29(7):845–854, 2013.

[148] Aneesur Rahman. Correlations in the motion of atoms in liquid argon. *Physical review*, 136(2A):A405, 1964.

[149] Miha Ravnik and Slobodan Žumer. Landau–de gennes modelling of nematic liquid crystal colloids. *Liquid Crystals*, 36(10-11):1201–1214, 2009.

[150] Robert C. Rizzo and William L. Jorgensen. Opls all-atom model for amines: resolution of the amine hydration problem. *Journal of the American Chemical Society*, 121(20):4827–4836, 1999.

[151] Olga Russina and Alessandro Triolo. New experimental evidence supporting the mesoscopic segregation model in room temperature ionic liquids. *Faraday Discussions*, 154:97–109, 2012.

[152] L. Saiz, J.A. Padro, and E. Guardia. Structure and dynamics of liquid ethanol. *The Journal of Physical Chemistry B*, 101(1):78–86, 1997.

[153] Cherry S. Santos, Harsha V.R. Annapureddy, N. Sanjeeva Murthy, Hemant K. Kashyap, Edward W. Castner, and Claudio J. Margulis. Temperature-dependent structure of methyltributylammonium bis (trifluoromethylsulfonyl) amide: X ray scattering and simulations. *The Journal of chemical physics*, 134(6), 2011.

[154] Takaaki Sato and Richard Buchner. Dielectric relaxation processes in ethanol/water mixtures. *The Journal of Physical Chemistry A*, 108(23):5007–5015, 2004.

[155] Takaaki Sato and Richard Buchner. Cooperative and molecular dynamics of alcohol/water mixtures: the view of dielectric spectroscopy. *Journal of molecular liquids*, 117(1-3):23–31, 2005.

[156] Daniel Schlesinger, K. Thor Wikfeldt, Lawrie B. Skinner, Chris J. Benmore, Anders Nilsson, and Lars G.M. Pettersson. The temperature dependence of intermediate range oxygen-oxygen correlations in liquid water. *The Journal of Chemical Physics*, 145(8):084503, 2016.

[157] P. Schuster, G. Zundel, and C. Sandorfy. *The Hydrogen Bond: Recent Developments in Theory and Experiments*. Number s. 1 in The Hydrogen Bond: Recent Developments in Theory and Experiments. North-Holland Publishing Company, 1976.

[158] Jonas Sellberg, C. Huang, T. McQueen, N. Loh, Hartawan Laksmono, Daniel Schlesinger, R. Sierra, Dennis Nordlund, Christina Hampton, Dmitri Starodub, D. DePonte, Martin Beye, C. Chen, Andrew Martin, A. Barty, Kjartan Wikfeldt, T. Weiss, C. Caronna, Jan Feldkamp, and A. Nilsson. Ultrafast x-ray probing of water structure below the homogeneous ice nucleation temperature. *Nature*, 510:381–4, 06 2014.

[159] Jonas A. Sellberg, C. Huang, Trevor A. McQueen, N.D. Loh, Hartawan Laksmono, Daniel Schlesinger, R.G. Sierra, Dennis Nordlund, C.Y. Hampton, Dmitri Starodub, et al. Ultrafast x-ray probing of water structure below the homogeneous ice nucleation temperature. *Nature*, 510(7505):381–384, 2014.

[160] Rui Shi and Hajime Tanaka. Direct evidence in the scattering function for the coexistence of two types of local structures in liquid water. *Journal of the American Chemical Society*, 142(6):2868–2875, 2020.

[161] Gourav Shrivastav, Aditya Gupta, Aman Rastogi, Debdas Dhabal, and Hemant K. Kashyap. Molecular dynamics study of nanoscale organization and hydrogen bonding in binary mixtures of butylammonium nitrate ionic liquid and primary alcohols. *The Journal of Chemical Physics*, 146(6):064503, 2017.

[162] Per Sillrén, Aleksandar Matic, Maths Karlsson, M Koza, M Maccarini, P Fouquet, M Götz, Th Bauer, Rudolf Gulich, Peter Lunkenheimer, et al. Liquid 1-propanol studied by neutron scattering, near-infrared, and dielectric spectroscopy. *The Journal of chemical physics*, 140(12):124501, 2014.

[163] Leonardo JA Siqueira and Mauro C.C. Ribeiro. Charge ordering and intermediate range order in ammonium ionic liquids. *The Journal of chemical physics*, 135(20):204506, 2011.

[164] Ioannis Skarmoutsos and Elvira Guardia. Local structural effects and related dynamics in supercritical ethanol. 2. hydrogen-bonding network and its effect on single reorientational dynamics. *The Journal of Physical Chemistry B*, 113(26):8898–8910, 2009.

[165] Lawrie B. Skinner, Congcong Huang, Daniel Schlesinger, Lars G.M. Pettersson, Anders Nilsson, and Chris J. Benmore. Benchmark oxygen-oxygen pair-distribution function of ambient water from x-ray diffraction measurements with a wide q-range. *The Journal of chemical physics*, 138(7):074506, 2013.

[166] Jon M. Sorenson, Greg Hura, Robert M. Glaeser, and Teresa Head-Gordon. What can x-ray scattering tell us about the radial distribution functions of water? *The Journal of chemical physics*, 113(20):9149–9161, 2000.

[167] Masatake Sugita, Itaru Onishi, Masayuki Irisa, Norio Yoshida, and Fumio Hirata. Molecular recognition and self-organization in life phenomena studied by a statistical mechanics of molecular liquids, the rism/3d-rism theory. *Molecules*, 26(2):271, 2021.

[168] Dorota Swiatla-Wojcik. Evaluation of the criteria of hydrogen bonding in highly associated liquids. *Chemical Physics*, 342(1-3):260–266, 2007.

[169] William C. Swope, Hans C. Andersen, Peter H. Berens, and Kent R. Wilson. A computer simulation method for the calculation of equilibrium constants for the formation of physical clusters of molecules: Application to small water clusters. *The Journal of chemical physics*, 76(1):637–649, 1982.

[170] Sila Toksoz, Handan Acar, and Mustafa O Guler. Self-assembled one-dimensional soft nanostructures. *Soft Matter*, 6(23):5839–5849, 2010.

[171] Matija Tomsic, Andrej Jamnik, Gerhard Fritz-Popovski, Otto Glatter, and Lukas Vlcek. Structural properties of pure simple alcohols from ethanol, propanol, butanol, pentanol, to hexanol: Comparing monte carlo simulations with experimental saxs data. *The Journal of Physical Chemistry B*, 111(7):1738–1751, 2007.

[172] David Van Der Spoel, Erik Lindahl, Berk Hess, Gerrit Groenhof, Alan E. Mark, and Herman J.C. Berendsen. Gromacs: fast, flexible, and free. *Journal of computational chemistry*, 26(16):1701–1718, 2005.

[173] Loup Verlet. Computer" experiments" on classical fluids. i. thermodynamical properties of lennard-jones molecules. *Physical review*, 159(1):98, 1967.

[174] J.K. Vij, C.J. Reid, and M.W. Evans. Submillimetre laser and interferometric spectroscopy of the alkyl alcohols. *Chemical Physics Letters*, 92(5):528–532, 1982.

[175] Aleksey Vishnyakov, Alexander P. Lyubartsev, and Aatto Laaksonen. Molecular dynamics simulations of dimethyl sulfoxide and dimethyl sulfoxide- water mixture. *The Journal of Physical Chemistry A*, 105(10):1702–1710, 2001.

[176] V.P. Voloshin and Yu I. Naberukhin. Hydrogen bond lifetime distributions in computer-simulated water. *Journal of Structural Chemistry*, 50:78–89, 2009.

[177] Aleksander Vrhovsek, Orsolya Gereben, Andrej Jamnik, and László Pusztai. Hydrogen bonding and molecular aggregates in liquid methanol, ethanol, and 1-propanol. *The Journal of Physical Chemistry B*, 115(46):13473–13488, 2011.

[178] Akihiro Wakisaka and Kazuo Matsuura. Microheterogeneity of ethanol–water binary mixtures observed at the cluster level. *Journal of molecular liquids*, 129(1-2):25–32, 2006.

[179] G.E. Walrafen, M.R. Fisher, M.S. Hokmabadi, and W-H. Yang. Temperature dependence of the low-and high-frequency raman scattering from liquid water. *The Journal of chemical physics*, 85(12):6970–6982, 1986.

[180] Nathan P. Walter, Abhishek Jaiswal, Zhikun Cai, and Yang Zhang. Liquidlib: A comprehensive toolbox for analyzing classical and ab initio molecular dynamics simulations of liquids and liquid-like matter with applications to neutron scattering experiments. *Computer Physics Communications*, 228:209–218, 2018.

[181] Frank Weinhold and Roger A. Klein. What is a hydrogen bond? mutually consistent theoretical and experimental criteria for characterizing h-bonding interactions. *Molecular Physics*, 110(9-10):565–579, 2012.

[182] George M. Whitesides and Bartosz Grzybowski. Self-assembly at all scales. *Science*, 295(5564):2418–2421, 2002.

[183] Jianhua Xing. Mori-zwanzig projection formalism: from linear to nonlinear. *arXiv preprint arXiv:0904.2691*, 2009.

[184] Tsuyoshi Yamaguchi. Viscoelastic relaxations of high alcohols and alkanes: Effects of heterogeneous structure and translation-orientation coupling. *The Journal of Chemical Physics*, 146(9):094511, 2017.

[185] Tsuyoshi Yamaguchi. Coupling between structural and dielectric relaxations of methanol and ethanol studied by molecular dynamics simulation. *The Journal of Physical Chemistry B*, 124(32):7027–7036, 2020.

[186] Tsuyoshi Yamaguchi, Ken-ichi Mikawa, Shinobu Koda, Kenta Fujii, Hitoshi Endo, Mitsuhoro Shibayama, Hiroshi Hamano, and Yasuhiro Umebayashi. Relationship between mesoscale dynamics and shear relaxation of ionic liquids with long alkyl chain. *The Journal of Chemical Physics*, 137(10):104511, 2012.

[187] Yanqin Zhai, Peng Luo, Michihiro Nagao, Kenji Nakajima, Tatsuya Kikuchi, Yukinobu Kawakita, Paul A. Kienzle, Antonio Faraone, et al. Relevance of hydrogen bonded associates to the transport properties and nanoscale dynamics of liquid and supercooled 2-propanol. *Physical Chemistry Chemical Physics*, 23(12):7220–7232, 2021.

[188] Yanqin Zhai, Peng Luo, Michihiro Nagao, Kenji Nakajima, Tatsuya Kikuchi, Yukinobu Kawakita, Paul A Kienzle, Antonio Faraone, et al. Relevance of hydrogen bonded associates to the transport properties and nanoscale dynamics of liquid and supercooled 2-propanol. *Physical Chemistry Chemical Physics*, 23(12):7220–7232, 2021.

[189] Jan Zielkiewicz. Structural properties of water: Comparison of the spc, spce, tip4p, and tip5p models of water. *The Journal of chemical physics*, 123(10):104501, 2005.

[190] Larisa Zoranić, Franjo Sokolić, and Aurélien Perera. Microstructure of neat alcohols: a molecular dynamics study. *The Journal of chemical physics*, 127(2):07B604, 2007.

[191] Robert Zwanzig. *Nonequilibrium statistical mechanics*. Oxford university press, 2001.

Sažetak:

Mikro - heterogene tekućine karakterizira specifična heterogena mikro - struktura, koja sadrži labilne supra - molekularne agregate. Tipični primjeri takvih tekućina su alkoholi, ionske tekućine i razne tekućine meke tvari. Osim uobičajene molekularne dinamike, zajedničke svim tekućinama, dinamiku ovih sustava karakterizira i kinetički aspekt, koji je povezan s dinamikom labilnih supra - molekularnih agregata, uz uobičajenu dinamiku individualnih atoma i molekula. Cilj ovog rada je otkriti specifičnosti u dinamici mikro - heterogenih tekućina, vezane upravo uz spomenuti kinetički aspekt. Dinamika se proučava analizom različitih dinamičkih veličina dobivenih simulacijama molekularne dinamike, kao što je van Hove korelacijska funkcija $G(r,t)$, funkcija raspršenja $F(k,t)$ i dinamički strukturni faktor $S(k,\omega)$. Pokazat će se da heterogena mikro-struktura ostavlja trag u ovim dinamičkim veličinama, što omogućuje direktno razlikovanje dinamike i kinetike u istim sustavima. Pokazat će se i da je, za razliku od dinamike, kinetika pod jakim utjecajem prisustva neutralnih atomskih grupa i veličinom istih grupa. Istraživanje se provodi za različite vrste tekućina, uključujući jednostavne tekućine, kao što je aceton, te složene tekućine, kao što su voda i mali monoli. Svrha rada je razviti teorijski i računalni okvir za istraživanje složenosti u tekućinama.

Abstract:

Micro - heterogeneous liquids are characterized by particular heterogeneous micro - structure, which contains labile bonded supra - molecular aggregates. Typical examples of such liquids are alcohols, ionic liquids and various soft - matter liquids. In addition to the usual molecular dynamics, common to all liquids, the dynamics of these systems is characterized by kinetic aspect, which is related to the dynamics of labile supra - molecular aggregates, instead of individual atoms or molecules. The aim of the thesis is to reveal the specificities in the dynamics of micro - heterogeneous liquids, which are attributed precisely to this kinetic aspect. Particularly, dynamics will be studied by extraction of various dynamical quantities from computer simulations, such as the van Hove correlation function $G(r,t)$, the associated scattering function $F(k,t)$ and the dynamical structure factor $S(k,\omega)$. It will be shown that heterogeneous micro - structure leaves marked signature in these observables, which enables to directly distinguish between dynamics and kinetics in these systems. While dynamics is shown to be governed by the time evolution of charge order, which determines the arrangement of charged species in the system, kinetics is governed by the existence of neutral species and their size. Study is performed for several types of liquids, ranging from simple disordered liquids, such as carbon tetrachloride or acetone, and complex disordered liquids, such as water and small monols. The purpose of the thesis is to elaborate the theoretical and computational framework for exploring complexity in liquids.